TAMPEREEN TEKNILLINEN YLIOPISTO
TAMPERE UNIVERSITY OF TECHNOLOGY

Mulugeta Kiros Fikadu

Performance Analysis, Resource Allocation and Optimization of Cooperative Communication Systems under Generalized Fading Channels

Julkaisu 1393 • Publication 1393

Tampere 2016

Tampereen teknillinen yliopisto. Julkaisu 1393
Tampere University of Technology. Publication 1393

Mulugeta Kiros Fikadu

Performance Analysis, Resource Allocation and Optimization of Cooperative Communication Systems under Generalized Fading Channels

Thesis for the degree of Doctor of Science in Technology to be presented with due permission for public examination and criticism in Tietotalo Building, Auditorium TB109, at Tampere University of Technology, on the 29th of June 2016, at 12 noon.

Tampereen teknillinen yliopisto - Tampere University of Technology
Tampere 2016

Supervisor
Mikko Valkama, Dr. Tech., Professor
Department of Electronics and Communications Engineering
Tampere University of Technology
Tampere, Finland

Co-Supervisor
Paschalis C. Sofotasios, Ph. D
Department of Electronics and Communications Engineering
Tampere University of Technology
Tampere, Finland

Department of Electrical and Computer Engineering
Aristotle University
Thessaloniki, Greece

Pre-examiners
Daniel Benevides da Costa, Ph. D, Professor
Department of Computer Engineering
Federal University of Ceará
Fortaleza, CE, Brazil

Daniel K. C. So, Ph. D, Associate Professor
School of Electrical and Electronics Engineering
University of Manchester
Manchester, UK

Opponent
Jyri Hämäläinen, D.Sc. (Tech.), Dean, Professor
School of Electrical Engineering
Aalto University
Aalto, Finland

ISBN 978-952-15-3767-7 (printed)
ISBN 978-952-15-3776-9 (PDF)
ISSN 1459-2045

Performance Analysis, Resource Allocation and Optimization of Cooperative Communication Systems under Generalized Fading Channels

Mulugeta Kiros Fikadu

June 2, 2016

Abstract

The increasing demands for high-speed data transmission, efficient wireless access, high quality of service (QoS) and reliable network coverage with reduced power consumption impose demanding intensive research efforts on the design of novel wireless communication system architectures. A notable development in the area of communication theory is the introduction of cooperative communication systems. These technologies become promising solution for the next-generation wireless transmission systems due to their applicability in size, power, hardware and price constrained devices, such as cellular mobile devices, wireless sensors, ad-hoc networks and military communications, being able to provide, e.g., diversity gain against fading channels without the need for installing multiple antennas in a single terminal. The performance of the cooperative systems can in general be significantly increased by allocating the limited power efficiently. In this thesis, we address in detail the performance analysis, resource allocation and optimization of such cooperative communication systems under generalized fading channels. We focus first on energy-efficiency (EE) optimization and optimal power allocation (OPA) of regenerative cooperative network with spatial correlation effects under given power constraint and QoS requirement. The thesis also investigates the end-to-end performance and power allocation of a regenerative multi-relay cooperative network over non-homogeneous scattering environment, which is realistic case in practical wireless communication scenarios. Furthermore, the study investigates the end-to-end performance, OPA and energy optimization analysis under total power constraint and performance requirement of full-duplex (FD) relaying transmission scheme over asymmetric generalized fading models with relay self-interference (SI) effects.

The study first focuses on exact error analysis and EE optimization of regenerative relay systems under spatial correlation effects. It first derives novel exact and asymptotic expressions for the symbol-error-rates (SERs) of M-ary quadrature amplitude and M-ary phase-shift keying (M-QAM) and (M-PSK) modulations, respectively,

assuming a dual-hop decode-and-forward relay system, spatial correlation, path-loss effects and maximum-ratio-combing (MRC) at the destination. Based on this, EE-optimization and OPA are carried out under certain QoS requirement and transmit power constraints.

Furthermore, the second part of the study investigates the end-to-end performance and power allocation of MRC based regenerative multi-relay cooperative system over non-homogeneous scattering environment. Novel exact and asymptotic expressions are derived for the end-to-end average SER for M-QAM and M-PSK modulations. The offered results are employed in performance investigations and power allocation formulations under total transmit power constraints.

Finally, the thesis investigates outage performance, OPA and energy optimization analysis under certain system constraints for the FD and half-duplex (HD) relaying systems. Unlike the previous studies that considered the scenario of information transmission over symmetric fading conditions, in this study we considered the scenario of information transmission over the most generalized asymmetric fading environments.

The obtained results indicate that depending on the severity of multipath fading, the spatial correlation between the direct and relayed paths and the relay location, the direct transmission is more energy-efficient only for rather short transmission distances and until a certain threshold. Beyond this, the system benefits substantially from the cooperative transmission approach where the cooperation gain increases as the transmission distance increases. Furthermore, the investigations on the power allocation for the multi-relay system over the generalized small-scale fading model show that substantial performance gain can be achieved by the proposed power allocation scheme over the conventional equal power allocation (EPA) scheme when the source-relay and relay-destination paths are highly unbalanced. Extensive studies on the FD relay system also show that OPA provides significant performance gain over the EPA scheme when the relay SI level is relatively strong. In addition, it is shown that the FD relaying scheme is more energy-efficient than the reference HD relaying scheme at long transmission distances and for moderate relay SI levels.

In general, the investigations in this thesis provide tools, results and useful insights for implementing space-efficient, low-cost and energy-efficient cooperative networks, specifically, towards the future green communication era where the optimization of the scarce resources is critical.

Preface

This thesis is based on the research work carried out during the years 2013-2016 at the Department of Electronics and Communications Engineering, Tampere University of Technology, Tampere, Finland, together with some background studies carried out during the years 2011-2012, at the Department of Computer Science, University of Vaasa, Vaasa, Finland.

First, I feel incredibly fortunate to have Prof. Mikko Valkama as my thesis supervisor. His guidance and motivation based on his vast knowledge have been of great help for progressing my research smoothly. He not only has a profound understanding in this area but also can turn his knowledge into easily understandable words. I have been many times impressed by his way of approach in understanding and solving problems critically. Throughout these years, I tried to learn from him how to ask questions that lead to valuable research. Despite the amazing career that he has already established, his endless pursuit of perfection in his work and high standard of self-discipline set up a role model for me. I also greatly appreciate his skills and sincerity in developing personal relations. He is the key person in establishing conducive environment for research in our department for which I am thankful from the bottom of my heart.

I also would like to express my deepest gratitude to my co-supervisor Dr. Paschalis C. Sofotasios for his excellent thoughtful guidance, motivation and sharing his valuable experiences in many different matters for the successful realization of this thesis. I am additionally grateful to him for all friendly and constructive discussions throughout the compilation of this research work. For all of these things, I am extremely thankful.

I want to acknowledge the thesis pre-examiners, Prof. Daniel Benevides da Costa from Federal University of Ceará and Assoc. Prof. Daniel K. C. So from the University of Manchester for their valuable comments and suggestions for improving the dissertation. I also wish to thank Prof. Jyri Hämäläinen from Aalto University for agreeing to act as the opponent in my dissertation defense.

I would like to thank to Prof. Mohammed Elmusrati for his encouragement and constructive feed-backs during my stay at the University of Vaasa. Thanks also to M.Sc. Reino Virrankoski, D. Sc. Duan Ruifeng, M.Sc. Tobias Glocker. I am indebted to my office mate D. Sc. Adnan Kiayani for the good office atmosphere and being resourceful. I am happy for the friendly discussions with D. Sc. Syed Yunas, M.Sc. Beshah Mogesie, M.Sc. Gashaw Bekele and M. Sc. Birhanu Assefa.

The research work was financially supported by the Finnish Funding Agency for Technology and Innovations (Tekes) under the project entitled "Energy-Efficient Wireless Networks and Connectivity of Devices-Systems (EWINE-S)", by the Academy of Finland under the projects No. 251138 "Digitally-Enhanced RF for Cognitive Radio Devices " and No. 284694 " Fundamentals of Ultra Dense 5G Networks with Application to Machine Type Communication" all of which are gratefully acknowledged.

For all practical matters, I would like to extend my deepest gratitude to Ms. Tarja Erälaukko, Ms. Soile Lönnqvist and also Sari Kinnari. A big thank you to Ms. Ulla Siltaloppi for being helpful in numerous practical and administrative matters. My sincere appreciation also goes to Ms. Elina Orava for being nice and helpful in academic matters. Ms. Heli Ahlfors is also appreciated for sorting out financial matters related to official travels during the doctoral studies.

Thanks to the teams developing open-source softwares, such as MikTEX, TeXnic-Center and Open Office, which greatly helped in writing scientific papers as well as this thesis.

Special thanks to all Ethiopian friends living here in Finland and in Norway. I would just like to say; *'Thank you for your friendships, lovely memories and enjoyable time that we have had together.'*

Last but not least, I want to express my gratitude to my wonderful, sisters, brothers, friends at home and all members of my family. I have no way to say thank you for your unconditional love, endless inspiration and genuine support.

" In loving memory of my late father, mother, my Aunt and my sweet nephew-You will always be in my heart."

Tampere, Finland
Mulugeta Kiros Fikadu

Table of Contents

List of Abbreviations

3GPP	3rd Generation Partnership Project
ADC	Analog to Digital Converter
AF	Amplify-and-Forward
ANC	Analog Network Coding
ARQ	Automatic Repeat Request
ASER	Average Symbol-Error-Rate
AWGN	Additive White Gaussian Noise
BC	Broadcast Channel
BER	Bit-Error-Rate
BS	Base-Station
CC	Coded Cooperation
CDF	Cumulative Distribution Function
CDM	Code Division Multiplexing
CDMA	Code Division Multiple Access
CF	Compress-and-Forward
CG	Cooperation Gain
CRC	Cyclic Redundancy Check
CSI	Channel State Information
CT	Cooperative Transmission
D2D	Device-to-Device
DAC	Digital to Analog Converter
DF	Decode-and-Forward
DSP	Digital Signal Processing
DT	Direct Transmission
EE	Energy-Efficiency
EGC	Equal-Gain-Combining
EPA	Equal Power Allocation

FD	Full-Duplex
FDM	Frequency Division Multiplexing
FDMA	Frequency Division Multiple Access
FDR	Full-Duplex Relaying
GCD	Greater Common Divisor
HD	Half-Duplex
HDR	Half-Duplex Relaying
HF	High Frequency
i.i.d	independent and identically distributed
i.n.i.d	Independent and non-identical distribution
IC	Interference Cancellation
I-CSI	Instantaneous CSI
IG	Inverse Gaussian
IR	Incremental Relaying
KKT	Karush Kuhn Tucker
LNA	Low Noise Amplifier
LOS	Line-of-Sight
LTE	Long-Term Evolution
MAC	Multiple Access Channel
MGF	Moment Generating Function
MIMO	Multi-Input Multi-output
M-PSK	M-ary Phase Shift Keying
M-QAM	M-ary Quadrature Amplitude Modulation
MRC	Maximum-Ratio-Combining
MS	Mobile Station
NLOS	Non-Line-of-Sight
NLP	Non -Linear Programming
OP	Outage Probability
OPA	Optimal Power Allocation
PA	Power Amplifier
PDF	Probability Density Function
PL	Path-Loss
PLL	Phase Locked Loop
PNC	Physical-Layer Network Coding
QoS	Quality of Service
RF	Radio Frequency
RSI	Residual SI

RV	Random Variable
SC	Selection Combining
SE	Spectral-Efficiency
SER	Symbol-Error-Rate
SI	Self-Interference
SINR	Signal-to-Interference-and-Noise Ratio
SNR	Signal-to-Noise-Ratio
SR	Selective Relaying
TDBC	Time-Division Broadcast
TDMA	Time Division Multiple Access
UE	User Equipment
UHF	Ultra High Frequency
UL	UpLink
V2V	Vehicle-to-Vehicle
VGA	Variable Gain Amplifier
VHF	Very High Frequency
WiMAx	Worldwide Interoperability for Microwave Access

Chapter 1

Introduction

1.1 Background and Motivation

Emerging wireless communication systems are expected to provide high-speed data transmission, high quality of service (QoS), high network coverage as well as the widespread use of smart phones, mobile devices and other multimedia services. However, the scarcities of fundamental resources, such as power and bandwidth are serious challenges to achieve these demands. In addition, most energy constrained devices, such as terminals of mobile cellular, ad-hoc and wireless sensor networks, are typically powered by small batteries where replacement is a rather difficult and costly procedure. Moreover, wireless channel features like multipath fading, shadowing, interference and other impairments are degrading the quality of the information signals during the wireless propagation and make the channel unpredictable.

Multipath fading is one of the most severe impairments in wireless communications. This phenomenon occurs due to the fact that the transmitted signal reaches the receiver via multiple paths and these paths change with time due to the mobility of the users and/or the random scattering from reflectors in the environment. Generally, the transmitted signal arrives at the receiver with different gains, delays and phase shifts. Destructive interference results in fading which may cause temporary failure of communication as the amplitude of the received signal may be low to the extent that the receiver may not be able to distinguish it from thermal noise [1, 2, 68].

The effective technique to combat such diverse effects in a radio communications is to introduce diversity into the wireless communication system. Diversity is a technique by which multiple copies of a signal are sent to the receiver through independently fading channels [75, 76]. If one or more copies are highly degraded due to severe fading, then the receiver can still process and decode the signal from the other received copies. Diversity gain is related to the number of independent channels over which the signal is being received. Common forms of diversity that allows independent

channels are classified into three physical domains: time, frequency, and space. Time diversity is achieved by transmitting multiple versions of the same signal via different time slots. To avoid any correlation between the channels at the slots, the intervals between transmissions of the same symbol should be longer than the coherence time. Related shortcomings of the time diversity include loss in the system information rate and an increase in transmission delay. Frequency diversity is achieved by transmitting the same signal over several frequency channels. Such form of diversity is inefficient in bandwidth utilization. Spatial diversity, on the other hand, is achieved by sending and receiving the same signal using multiple transmitter antennas (transmit diversity) and/or multiple receiver antennas (reception diversity) that are physically separated from one another and where a diversity combining technique is required before handling further signal processing. Spatial diversity has gained significant considerations since it does not increase the bandwidth requirements or the transmission delay [5, 6, 8, 9, 31, 76].

The use of multiple transmit and multiple receive antennas in spatial diversity results in multiple-input multiple-output (MIMO) system. It has been shown that MIMO techniques constitute an effective method to enhance the spectral-efficiency (SE) as well as the diversity of the wireless system; however, this implementation typically comes at the cost of complex transceiver circuitry and in massive systems may lead to high-energy consumption requirements. Furthermore, it is not currently feasible to embody large multi-antenna systems at hand held terminals due to spatial restrictions. Another, efficient technique to overcome these kind of resource limitations of the MIMO system is engaging distributed wireless nodes (active terminals or fixed relays) in a cooperative fashion that emulates antenna diversity. This mode of transmit diversity is known as *cooperative transmission* (CT) also referred to as *virtual antenna arrays*, *cooperative diversity*, or *user cooperation* [5, 6, 9, 30, 42, 139].

CT schemes exploit the broadcast nature and the inherent spatial diversity of fading channels without the need to install multiple antennas in a single mobile radio terminal, as in the conventional MIMO systems. In cooperative systems, wireless terminals share and coordinate their resources for relaying messages to each other and for transmitting information signals over the numerous independent paths in the wireless network. A distinct feature of cooperative communications is that wireless agents share resources, instead of competing for them, which ultimately enhances performance of the wireless system [6,8,20,25,31,152,156]. The destination terminal in the cooperative diversity exploit the received signals often through different combining methods which have been extensively shown to provide efficient and robust operation in signal distortion by fading effects [2, 75, 76].

The performance and total average energy consumption of a cooperative system can be greatly improved by allocating the limited resources of the wireless network optimally to the source and relay nodes in the network. This can be carried out by optimizing certain performance metrics under given constraints, e.g., [24–26, 153, 155, 159, 184, 196, 220, 229]. However, the vast majority of the reported investigations in energy-efficient cooperative communications assume that the involved communication paths are statistically independent to each-other. Nevertheless, this assumption is rather simplistic as in realistic cooperative communication scenarios the wireless channels may often be spatially correlated, which should be taken into account particularly in the design and deployment of low-power and energy-efficient wireless networks. Hence, this important issue in the wireless communications is addressed in this thesis. To the best of the authors' knowledge, a comprehensive exact and asymptotic error-rate analysis for regenerative systems over spatially correlated channels, as well as a detailed energy-efficiency (EE) analysis and optimization of total energy consumption have not been reported in the open technical literature; thus, this thesis aims to contribute in this essential area of study. In addition to this, the majority of the existing works have dealt with performance analysis and power allocation strategy of the cooperative system on the scenario of information transmission over either Rayleigh fading channels or Nakagami-m fading channels. However, these fading distributions rely basically on the assumption of homogeneous scattering environment, which is not necessarily practical since the surfaces can be spatially correlated in most radio propagation environments [77, 78, 108, 109]. Motivated by these important observations, in this thesis, we present comprehensive power allocation strategies with respective exact expressions for analyzing the end-to-end performance of multi-relay cooperative networks over the most generalized and realistic fading models.

Energy optimization and optimal power allocation (OPA) in the full-duplex relaying (FDR) system with self-interference (SI) levels is the final study in this thesis. Most studies on the FDR scheme are limited to the information transmission over basic symmetric multipath fading models, e.g., [210–217]. However, in practice, asymmetric fading channels are frequently encountered due to terminal and relay locations. For example, the link between a fixed relay and the base-station (BS) might experience *line-of-sight* (LOS) radio propagation, whereas the link between a mobile terminal and a relay might experience *non-line-of-sight* (NLOS) fading scenarios. Considering this fact, this thesis addresses a comprehensive performance, power allocation as well as energy optimization of the full-duplex (FD) relay system over generalized LOS and NLOS fading conditions. For further insights, the FDR and the half-duplex relaying

(HDR) systems are compared under the same fading conditions.

1.2 Objective and Scope of the Thesis

The main objective of this thesis is to study and analyze certain important energy-optimized regenerative cooperative networks over realistic generalized fading environments that can be useful in the design and deployment of low-cost and energy-efficient cooperative communication systems in the next-generation networks, particularly towards the green communication era. Novel exact expressions for the end-to-end performance of the cooperative networks are provided to facilitate the study. Based on this, energy-optimization and OPA over practical fading conditions are investigated. However, the topic of resource allocation and energy-optimization of cooperative networks is too vast to be covered in a single thesis. The scope is thus limited to the power allocation and energy minimization for single and multi-relay nodes with HD relay system and single relay system with FDR scheme.

1.3 Author's Contribution and Thesis Outline

The research work for the thesis was carried out mainly at the Department of Electronics and communications Engineering, Tampere University of Technology, Finland under the supervision of Prof. Mikko Valkama and Dr. Paschalis C. Sofotasios. Furthermore, during the initial stage of the thesis work at the Department of Computer Science, University of Vaasa, Finland Prof. Mohammed Elmusrati has contributed through various technical discussions. Results obtained from the research work have been reported in nine academic publications in the form of conference papers and journal articles; [113–121] and one submitted for publication [122]. This thesis gathers the obtained results from the publications into a monograph form. It may be noted that for all the results presented in the following chapters, the author was solely responsible for formulations and numerical analysis, while the exact expressions of the results, analysis and discussions were done jointly with supervisors with detailed suggestions, discussions and comments from Prof. Qimei Cui, Prof. Sami Muhaidat, and Prof. George K. Karagiannidis. Chapters 2 and 3 are general review studies in the field of cooperative and wireless communications, whereas chapters 4, 5, 6 are based on the publications and describe the scientific contributions of this thesis. The outline of the thesis and the main corresponding contributions of the authors in each of the chapters can be summarized as follows:

1. Chapter 2 briefly discusses the fundamentals of cooperative communication systems, historical backgrounds and its pros and cons. This is followed by the general descriptions of the cooperative relaying protocols, and alternative transmission modes operated on the relay nodes. The chapter also describes bidirectional relaying technique, which has the potential to enhance the SE.

2. Chapter 3 introduces the basic channel characteristics of the wireless and mobile communications, including path-loss (PL), shadowing and multipath fading. Then, statistical characterizations of fading processes with respective distributions are introduced. Furthermore, common performance measures used in this study are presented. Finally, the chapter concludes with discussions on popular diversity combining techniques that are often used in wireless communication systems.

3. Chapter 4 first reviews EE and its optimization in direct and cooperative networks. Then, the exact and asymptotic symbol-error-rate (SER) expressions for $M-$ary Phase-Shift Keying ($M-$PSK) and $M-$ary Quadrature Amplitude ($M-$QAM) modulations are derived assuming a dual-hop regenerative relay system where the source-destination and relay-destination paths are spatially correlated and maximal-ratio-combining (MRC) scheme is adopted in the receiver. The total average power consumption models for the direct and cooperative systems are investigated. Based on the derived SER expressions and the power consumption models, energy-optimization with corresponding OPA under certain QoS requirements and total maximum transmit power constraints are formulated. Finally, the investigations are corroborated with numerical analysis and discussions using a relatively harsh PL model, which accounts for realistic device-to-device (D2D) communications. The results and analysis in this chapter are based on the publications [113, 114]. The author was responsible for analysis and formulations of the energy-optimization with numerical results. The energy formulations for the cooperative network, derivation of closed-form expressions and the post-analysis of the numerical results leading to the publications were jointly done with supervisor Prof. Mikko Valkama and co-supervisor Dr. Paschalis C. Sofotasios. Prof. Qimei Cui provided valuable suggestions and comments for the optimization models. Prof. George K. Karagiannidis provided many insightful comments and discussions that supports the contents of the articles.

4. Chapter 5 gives a brief review on the performance and OPA strategies of single and multi-relay systems over various basic fading channels. Then, novel exact

expressions are derived for the end-to-end SER for both $M-$PSK and $M-$QAM modulations over independent and non-identically distributed (i.n.i.d) generalized fading channels. The results are expressed in terms of Lauricella function, which can be readily evaluated with the aid of the proposed computational algorithm. Simple expressions are also derived for the corresponding SER at asymptotically high signal-to-noise-ratio (SNR) regimes. Based on these results, OPA strategy that enhances the performance of the regenerative cooperative systems is formulated and analyzed. Numerical investigations are performed for various fading conditions to acquire further insights on the OPA schemes. The results and analysis presented therein are mainly based on the publications reported in [117, 121]. The key ideas of the two scientific papers are based on the publications reported in [118–120] expanded into more comprehensive forms. The derivation of the exact expressions, formulations of the power optimization and post-analysis of the numerical results were jointly carried with supervisor Prof. Mikko Valkama and co-supervisor Dr. Paschalis C. Sofotasios. Prof. Qimei Cui, Prof. Sami Muhaidat and Prof. George K. Karagiannidis provided valuable suggestions, comments and discussions for supporting the contents of this chapter which are reported in [117,121]. Prof. Mohammed Elmusrati and M.Sc. Reino Virrankoski provided their valuable suggestions and discussions for the publication reported in [120].

5. Chapter 6 focuses on the FDR system over generalized LOS and NLOS asymmetric fading scenarios in the presence of different relay SI levels. Novel closed-form expressions are derived for the outage probabilities (OPs) of the FDR system. Based on these, performance, OPA and energy optimization for the considered system are investigated. The performance analyses presented therein are based on the publications reported in [115, 116]. Based on the results obtained in the reported publications, the chapter further extends the contents to OPA and energy optimization analysis as in [122]. The derivation of the exact expressions, formulations of the power optimization and discussions were jointly carried out with supervisor Prof. Mikko Valkama and co-supervisor Dr. Paschalis C. Sofotasios. Prof. Qimei Cui, Prof. Sami Muhaidat and Prof. George K. Karagiannidis provided insightful suggestions, comments and discussions for the publications reported in [115, 116].

6. Chapter 7 draws concluding remarks and discusses possible future work topics for extending the studies presented in this dissertation.

In summary, the thesis author has been the primary author of all reported works. He has carried out system model developments, mathematical formulations, numerical results and discussions, with natural supervision and guidance from the supervisors. Furthermore, the thesis author has written all the associated papers [113–122] as the first author, and composed majority of the text in the articles.

1.4 Basic Mathematical Notations

In this thesis, the mathematical notations are defined as follows. The probability density function (PDF) of a continuous random variable (RV) X is given by $f_X(x)$, whereas the cumulative distribution function (CDF) of the random variable is given by

$$F_X(x) = \int_0^x f_X(x)\mathrm{d}x.$$

The statistical average value or the expected value of the RV is defined and denoted as

$$\mathrm{E}(X) = \int x f_X(x)\mathrm{d}x.$$

The variance of the RV is also defined by

$$\mathrm{Var}(X) = \mathrm{E}[(X - \mathrm{E}(X))^2] = \mathrm{E}[X^2] - (\mathrm{E}[X])^2.$$

The conditional PDF of the RV X given the occurrence of Y is written as $f_X(x|Y = y)$. For complex random vector U the covariance is defined as

$$\mathrm{Cov}(U) = \mathrm{E}[(U - \mathrm{E}(U))(U - \mathrm{E}(U))^\dagger].$$

Also, the covariance of two complex random vectors U and V is given by

$$\mathrm{Cov}(U, V) = \mathrm{E}[(U - \mathrm{E}(U))(V - \mathrm{E}(V))^\dagger].$$

The Gamma function is described as

$$\Gamma(t) = \int_0^\infty x^{t-1} \exp(-x)\mathrm{d}x \qquad \text{for } t \in \mathbb{R}.$$

Also, for $t \in \mathbb{Z}^+$, $\Gamma(t) = (t-1)!$.
The Pochhammer symbol is denoted as

$$(x)_n \triangleq \frac{\Gamma(x+n)}{\Gamma(x)}.$$

The lower incomplete gamma function is defined by

$$\gamma(\alpha, x) = \int_0^x t^{\alpha-1} \exp(-t) \mathrm{d}t \qquad \mathrm{Re}\,(\alpha) > 0.$$

Formally, the Q-function is defined as

$$Q(x) = \frac{1}{\sqrt{2\pi}} \int_x^\infty \exp\left(-\frac{u^2}{2}\right) \mathrm{d}u.$$

An alternative form of the Q-function known as Craig's formula is expressed as

$$Q(x) = \frac{1}{\pi} \int_0^{\pi/2} \exp\left(-\frac{x^2}{2\sin^2\theta}\right) \mathrm{d}\theta.$$

The generalized Marcum Q-function in terms of the Bessel function $I_{m-1}(\cdot)$ is defined as

$$Q_m(\alpha, \beta) = \frac{1}{\alpha^{m-1}} \int_\beta^\infty x^m \exp\left(-\frac{x^2+\alpha^2}{2}\right) I_{m-1}(\alpha x) \mathrm{d}x.$$

The binomial coefficients are denoted by

$$\binom{n}{k} = \frac{n!}{k!(n-k)!}.$$

$(\cdot)^*$ represents the complex conjugate operator.
$(\cdot)^\dagger$ represents conjugate transpose operator.
$|a|$ represents the modulus of a complex scalar a.
$\mathcal{L}\{\cdot\}$ represents the Laplace transformation operator.
$\mathcal{L}^{-1}\{\cdot\}$ represents th inverse of the Laplace transformation.
$\max(\cdot)$ represents the maximization operator.
$\min(\cdot)$ represents the minimization operator.

Chapter 2

Cooperative Communications: Fundamentals

In this chapter, we address the general background and basics of cooperative communications. In particular, we first review the general aspect of cooperative communication and its essential background. This in turn leads us to the discussion of several cooperative relaying protocols that have been proposed to date, and alternative transmission modes operated on the cooperative users. Furthermore, bidirectional relaying systems are also introduced.

2.1 Overview of Cooperative Communications

Cooperative communication technologies have become notable candidate for the next-generation of wireless networks. For example, these technologies have been considered in some recent communication standards, such as in IEEE 802.16 Worldwide Interoperability for Microwave Access (WiMAX) standard and in Long Term Evolution (LTE)-Advanced standard specified by the 3rd Generation Partnership Project(3GPP). The cooperative schemes have been also incorporated into many modern wireless applications, such as cognitive radio and physical layer security [3,4]. Besides, without incurring additional costs for BS deployment, cooperative communications have the ability to expand cellular network coverage, increase channel capacity and reduce power consumption of wireless devices [8,9,21,25]. Cooperative communications can significantly improve the system performance and robustness of wireless networks, especially in severe fading scenarios. The fundamental principle in cooperative communications is that wireless terminals share and coordinate their resources for relaying messages to each other and for transmitting information signals over multiple independent paths in the wireless network [5, 6]. By doing so, users can effectively form a distributed virtual antenna array that emulates the inherent spatial diversity

gains without the need for installing co-located multiple antennas in a single mobile radio terminal, as in the case of centralized MIMO systems.

The two main features that differentiate cooperative transmission schemes from the conventional non-cooperative transmissions systems are: 1) the use of multiple user's resources to transmit the message of a single source; and 2) a proper combination of signals from multiple cooperating users at the destination. The transmission in cooperative network usually involves two phases of transmission: coordination phase, where users exchange their own source data and control messages with each other and/or the destination, and a cooperation phase, where the users cooperatively re-transmit their messages to the destination [2, 5, 8, 9]. Fig. 2.1 illustrates a typical cooperative network in the uplink (UL) of a mobile communication system that consists of two users transmitting their local messages to a common destination over independent fading channels. At some instant of time, one user may act as a source of information while the other user serves as a relay. The role between the source and the relay can be interchanged at any instant in time. In the coordination phase, in phase I, the source, (e.g., user 1), broadcasts its data to both the relay, (e.g., user 2), and destination. The relay is usually located between the source and destination to split the longer path into shorter segments in order to reduce the overall PL effects. In the cooperation phase, phase II, the relay forwards a processed version of the source's data to the destination. The destination then combines the signals received from the source and the relay using common combining techniques, such as MRC, Equal-Gain Combining (EGC) or Selection Combining (SC) to enhance reception at the destination. These methods have been shown to provide efficient and robust operations in signal distortion and fading effects [75, 76]. Using this way, spatial diversity is exploited as the two messages are received from potentially uncorrelated paths.

To enable cooperation among users, many cooperative relaying techniques have been proposed. Some of the relaying methods that are adopted in literature are amplify-and-forward (AF), decode-and-forward (DF), selective relaying (SR), incremental relaying (IR) [6], coded cooperation (CC) [7, 9], compress-and-forward (CF) [10, 11] and buffer-aided relaying with adaptive link selection [12, 13]. When the AF relaying scheme is employed, the relay node just amplifies the received signal before re-transmitting towards the destination. If the relay node uses the DF scheme, it will decode and regenerate the message towards the destination. When the generated message by the relay is re-encoded to provide additional error protection to the original message, it is also refereed to as CC. The SR scheme, on the other hand, is used based on the instantaneous channel information to decide between relay forwarding and source re-transmission. The IR scheme uses a feedback from the desti-

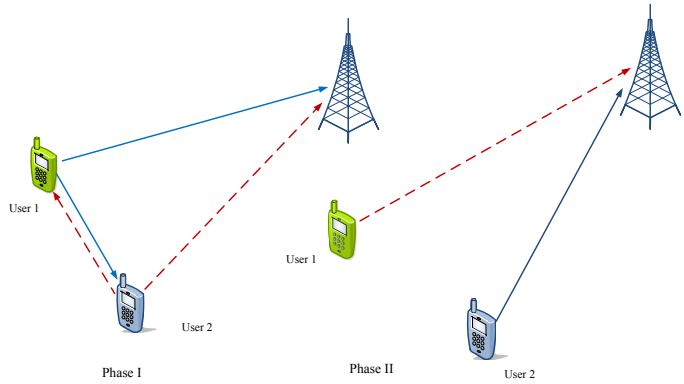

Figure 2.1 In cooperative communication each user is both a source and a relay.

nation to indicate the success or failure of the DT while in the CF scheme, the relay node re-transmits a quantized or compressed version of the received message. In the buffer-aided relaying protocol with adaptive link selection, the relay transmits when the relay-destination channel is comparatively stronger than the source-relay channel, and otherwise the relay receives and stores the received information in its buffer.

Furthermore, relay nodes can adopt either HDR or FDR modes. FDR allows the relay nodes to receive and transmit simultaneously in the same frequency band and hence achieves higher SE, whereas in the HDR mode the reception and transmission at the relay nodes are performed in time or frequency orthogonal channels. The cooperation communication schemes described here can be readily extended to a large cooperative network where one node acts as a source and intermediate users serve as relays. The relays form distributed or virtual antenna array to achieve high spatial diversity gain similar to that of the conventional MIMO systems.

2.2 Historical Background of Cooperative Communications

The basic ideas behind cooperative communications can be traced back to the seminal work of Van Der Meulen on the three-terminal communication channel [14] as shown in Fig. 2.2. The three-node network generalizes the notation of point-to-point channel that consists of a source (S), a destination (D), and a dedicated relay (R) whose sole purpose is to help the transfer of information from the source to the destination. Later in 1979, Cover and El Gamal [15] provided a significantly improved capacity of the physically degraded relay channel from information theoretic aspect. The authors

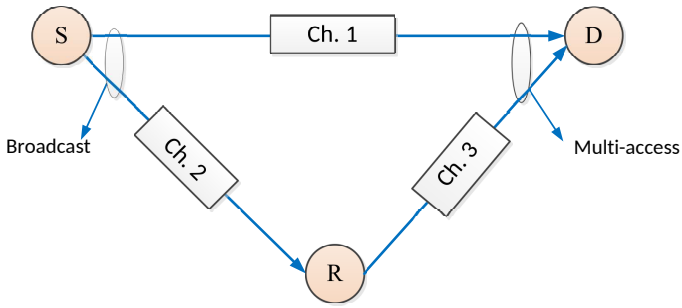

Figure 2.2 The relay channel.

analyzed the capacity of the relay channel by assuming all nodes operate in the same band. Under this assumption, the system can be decomposed into a broadcast channel (BC) from the view point of the source and multiple access channel (MAC) from the view point of the destination. The mathematical frameworks of these pioneering works have significantly contributed to the understanding of relay channels. For example, the authors in [16] derived some certain capacity theorems for multiple-access relay channels. In [17], the authors proposed capacity theorems for the fading interference channel with relay and feedback links. Likewise, the authors in [18] analyzed the capacity of discrete-memoryless relay channels with orthogonal components.

The idea of user cooperation was first addressed by Sendonaris *et al.* [5, 19] from the communication community. The authors proved that cooperative communications can improve the achievable rates of two users communication scenario, and it is a more robust system even when the inter-user channel is noisy. Later, this work was further extended by Laneman *et al.* [6] and the authors proposed and analyzed the outage behavior of several low-complexity cooperative diversity protocols that can combat fading induced by multipath propagation in wireless networks employing HD transmission building on time-division multiple access (TDMA). Also, from the signal processing community the works by Scaglione and Hong [20, 21] contributed to the efficient cooperative transmissions for wireless sensor networks and wireless multihop ad-hoc networks. The idea of CC, which was developed as the integration of cooperative communication and channel coding, was addressed by Hunter *et al.* in [7]. Besides the performance improvement of the cooperative communications compared to the conventional non-cooperative system, various efforts have been carried to further improve the performance of the cooperative network through efficient management of the available radio resources. One of the early works in this area includes the contribution in [22] on OPA. The author investigated the problem of

efficient power allocation in a wireless communication system with two cooperating sources and a destination where the source communicates with the destination via an orthogonal AF protocol with two time-slots. Also noteworthy are the contributions of [23–25] for studying the performance improvement of some practical resource constrained cooperative communication systems over fading environment. Yet another important set of contributions from the wireless communications perspective with significant insight into the performance enhancement of cooperative communication systems are reported in [26].

2.3 Pros and Cons of Cooperative Communications

The key advantages of cooperation in system deployment can be summarized as follows [2, 9, 27]:

- **Performance Gains.** Cooperative communications can provide large system-wide performance gains due to PL savings as well as diversity and multiplexing gains. These benefits of cooperation can be translated into reduced transmission power, higher throughput, better transmission reliability or larger network coverage.

- **Balanced Quality of Service.** In conventional systems, users at the edge of a network or in shadowed areas with poor channel conditions suffered from capacity and/or coverage limitations. However, cooperative relaying can be used to overcome such discrepancy by allowing more balanced QoS to all users.

- **Infrastructure-Less Deployment.** Cooperative communications ease the roll-out of a system that has minimal or no infrastructure available prior to deployment. For instance, in disaster-struck areas, relaying can be used to facilitate communications, even though cellular systems or other existing communication systems are out of order.

- **High Energy-Efficiency and Extended Network lifetime**. CT is utilized to improve EE and extend the lifetime of networks composed of battery-operated nodes, such as sensors in wireless sensor networks. It has been shown that CT schemes with multiple nodes can greatly improve network lifetimes by reducing the forwarding traffic loads of energy-depleting nodes.

- **Reduced Costs.** Cooperative communications provides more cost effective solutions in capital and operational expenditures. For example, in cellular net-

works, the cost of providing a given level of QoS for all users in the cell can be lower when relays are used.

Contrary to the above advantages, there also exist some major disadvantages in cooperative systems as listed below [2, 27].

- **Complex Schedulers.** In cooperative systems, relaying requires more sophisticated schedulers since not only traffic of different users and applications needs to be scheduled but also the relayed data flows. In such scenarios, the complexity of scheduling mechanisms increases significantly when there are more users with multiple participating relays in the network. Any gains due to cooperation at the physical layer dissipate rapidly if not handled properly at medium access and network layers.

- **Increased Overhead.** Fully functioning cooperative systems require handovers, synchronization, extra security, and other related issues. All these requirements certainly induce an increased overhead in comparison with traditional communication systems.

- **Partner Choice.** Determining the optimum relaying and cooperative partner(s) is a fairly sophisticated task. Also, the complexity of maintaining such cooperative partnership is higher with respect to non-cooperative relaying.

- **Extra Relay Traffic and Interference.** Extra resources in the form of timeslots, frequency channels or orthogonal codes need to be typically allocated for relaying traffic. In addition, without smart power allocation schemes, relaying will certainly generate extra intra-and inter-cell interference, which potentially causes the deterioration of system performance.

- **Increased End-to-End Latency.** Relaying typically involves the reception and decoding of entire data packet before it is re-transmitted. With regard to delay-sensitive services, such as voice and the increasingly popular multimedia services, the extra latency introduced by decoding may become detrimental. To circumvent this latency, either simple transparent relaying or some advanced decoding methods can be used.

- **More Channel Estimates.** The effective use of relays certainly increases the number of wireless channels. This requires the estimation of more channel coefficients if coherent modulation is used.

From the aforementioned discussions, the disadvantages of cooperative communications can be as significant as the advantages. Therefore, cooperative system

design needs to be performed carefully in order to achieve the full gains of cooperative communications and at the same time to ensure that cooperation does not cause deterioration of system performance.

2.4 Cooperative Relaying Protocols

In this section, we review different cooperative protocols or transmission techniques that are used in cooperative communication systems. Based on the signal processing employed at the relay terminal, the cooperative relaying methods are generally classified into fixed relaying schemes and adaptive relaying schemes. For fixed relaying, the relay can simply amplify its received signal subject to its power constraint, or decode, re-encode and re-transmit the message [6]. These cooperation schemes, as already mentioned, are referred to as AF and DF, respectively. Such approaches have the advantage of easy implementation. On the other hand, adaptive relaying schemes are building upon fixed relaying and adapt the channel state information (CSI) between the cooperating terminals (selective relaying) or upon limited feedback from the destination (incremental relaying). SR allows transmitting nodes to select either cooperative or non-cooperative transmissions based on the measured SNR between them [2, 6], while the IR scheme uses feedback from the destination about the success or failure of direct transmission (DT) [6, 39, 40]. Besides the fixed and adaptive schemes, other sophisticated techniques include CC and CF cooperation. In the following discussions, we assume HD transmission based cooperative network systems for understanding the various types of relaying protocols.

2.4.1 Amplify-and-Forward Relaying

AF also refereed to as the non-regenerative relaying scheme that works in the analog domain is conceptually the most simple of the cooperative relaying methods. In this protocol, the relay simply forwards an amplified version of the received message without explicitly decoding or demodulating the received message as shown in Fig. 2.3. Because of the noise added at the relay and as there is no error-checking mechanism, the forwarded message is a noisy version of the original message from the source. Although the noise is amplified along with the signal in this technique, a full spatial diversity gain can be achieved by transmitting the signal over spatially independent channels. In this scheme, the relay does not to have knowledge of the encoding or modulation schemes used at the source. This scheme is particularly desirable when the source-relay link is not sufficient to guarantee reliable decoding at the relay [2, 6].

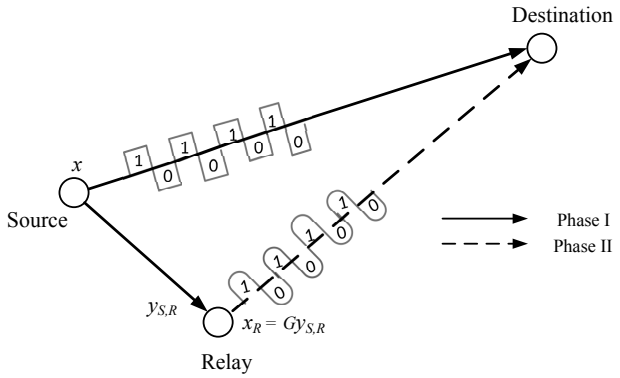

Figure 2.3 Illustration of amplify-and-forward relaying scheme.

This protocol was first proposed and analyzed by Laneman and Wornell in [28]. In the work, the bit-error-rate (BER) performance was analyzed and showed that despite the noise propagation from the relay the AF performs significantly better than the non-cooperative transmission. Furthermore, it was shown that this scheme achieves diversity gain of two in case of a single relay based cooperative system, i.e., the end-to-end average BER decreases twice as fast as that of DT or with the case without diversity combining.

The operation in the AF mode is done in two phases. In phase I, the source broadcasts its information to the relay and destination, where the received signals are given by

$$y_{S,R} = \sqrt{P_S}\alpha_{S,R}x + n_{S,R} \tag{2.1}$$

and

$$y_{S,D} = \sqrt{P_S}\alpha_{S,D}x + n_{S,D} \tag{2.2}$$

respectively, where P_S is the transmitted power at the source, x denotes the transmitted signal, whereas $\alpha_{S,R}$ and $\alpha_{S,D}$ are the fading coefficients from the source to the relay and destination. Moreover, $n_{S,R}$ and $n_{S,D}$ are the zero-mean additive white Gaussian noise (AWGN) terms with variance N_0, respectively. In phase II, the relay multiplies the received signal in (2.1) with a gain of [2]

$$G = \frac{1}{\sqrt{P_S \mid \alpha_{S,R} \mid^2 + N_0}}. \tag{2.3}$$

The gain G in (2.3) depends on the source-relay fading coefficient $\alpha_{S,R}$; thus, the scheme is often referred to as variable-gain AF relaying scheme. The received signal

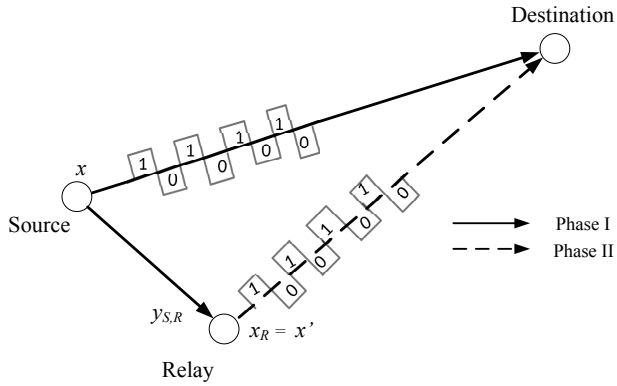

Figure 2.4 Illustration of decode-and-forward relaying scheme.

at the destination in Phase II is also given by

$$y_{R,D} = \frac{\sqrt{P_R}}{\sqrt{P_S \mid \alpha_{S,R} \mid^2 + N_0}} \alpha_{R,D} y_{S,R} + n_{R,D} \tag{2.4}$$

where P_R is the relay transmission power, $\alpha_{R,D}$ is the fading coefficient from the relay to the destination and $n_{R,D}$ is the AWGN term with zero-mean and variance N_0. Using the expression in (2.1), the above expression can be further expressed as

$$y_{R,D} = \frac{\sqrt{P_S P_R}}{\sqrt{P_S \mid \alpha_{S,R} \mid^2 + N_0}} \alpha_{S,R} \alpha_{R,D} x + \frac{\sqrt{P_R}}{\sqrt{P_S \mid \alpha_{S,R} \mid^2 + N_0}} \alpha_{R,D} n_{S,R} + n_{R,D}. \tag{2.5}$$

Different processing techniques, to combine the two received signals at the destination, namely $y_{S,D}$ and $y_{R,D}$, are described in Section 3.5.

2.4.2 Decode-and-Forward Relaying

In this protocol, the relay decodes the received message from the source, re-encodes it and then forwards it to the destination as illustrated in Fig. 2.4. This scheme is also known as regenerative relaying and requires correct decoding of the message at the relay in order for the forwarded message to be usable at the destination terminal; otherwise, the relayed message leads to error at the destination. Comparing with the AF scheme, the digital processing nature of the DF relaying makes more efficient than AF scheme, which requires radio frequency (RF) transceivers to scale up the analog signal and to mitigate coupling effects before relaying and forwarding the noisy version of the signal [33–37]. The DF protocol performs better when the inter user links are of high quality; on the other hand, the usage of AF is reasonable when the inter-user

links are of poor quality. The potential advantage of the DF approach is that the relay transmits a *clean copy* of the original message, i.e., a noise-free copy, if it can successfully decode the message from the source.

Similar to the AF mode, the operation of the DF mode is also done in two phases. The signal received at the relay and destination in the first phase are similar to the formulations in (2.1) and (2.2), whereas in phase II signal received at the destination can be expressed as

$$y_{R,D} = \sqrt{\bar{P}_R}\alpha_{R,D}x + n_{R,D}. \tag{2.6}$$

In the above expression if the relay decodes the signal from the source correctly, then the relay forwards the signal to the destination with power $\bar{P}_R = P_R$; otherwise, the relay does not send, i.e., $\bar{P}_R = 0$. Again, the destination can combine the two received signals as elaborate in more details in Section 3.5.

In [31], the performance of AF and DF relaying schemes are compared for three cases. We summarize the outcomes of the analysis here for the sake of completeness. **Case I** : If the source-relay channel link quality is the same as that of the relay-destination, the investigation shows that DF performs better than AF especially for small modulation sizes. However, as the modulation size increases the performance benefit of the DF cooperation protocol is not significant comparing with that of AF. **Case II** : If the channel link quality of the source-relay is much better than that between relay and destination, the result shows that despite the modulation size, the performance of the DF cooperation is almost the same as that of the AF cooperation scheme.
Case III : As a final scenario, when the channel link quality from the relay to destination is much better that that of the source-relay link, the analysis indicates that the performance of the DF scheme is better than of the AF system. Furthermore, it is shown in the same analysis that the advantage of the DF cooperation system is more significant if $M-$PSK is used instead of $M-$QAM modulation. From the three scenarios, it can be concluded that the performance of DF cooperation protocol is better than that of the AF scheme.

Furthermore, the AF scheme leads to thermal noise enhancement, which has a profound impact on the end-to-end performance. The amount of noise enhancement depends on the amplification factor, channel statistics in each path, the network topology, etc. [27]. So, non perfect separation of information signals and noise can cause detrimental effects in the overall system performance. In addition, it is recalled that DF provides a better performance than AF due to the involved decoding and re-encoding process. This is further enhanced by different protocols where relays

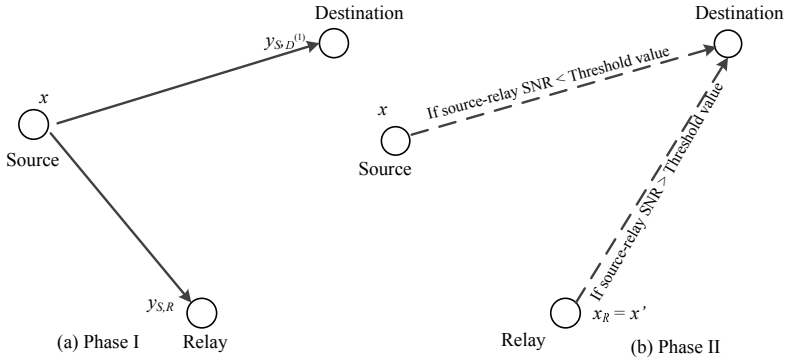

Figure 2.5 Example of of selective DF relaying scheme.

forward a re-encoded signal only if this has been decoded correctly. Thus, based on the discussions on AF and DF this thesis mainly focuses on the DF scheme to investigate the performance of the cooperative networks.

2.4.3 Selective DF Relaying

In this relaying scheme, if the instantaneous SNR at the relay terminal exceeds a certain threshold value, the relay will cooperate in transmitting the message by performing DF operation to achieve the diversity gain. On the other hand, if the channel between the source and relay suffers, such that the instantaneous SNR falls below the required threshold, the source simply continues its transmission to the destination in the form of repetition or more powerful codes without any help from the relay [2,6] to achieve full temporal diversity or coding gain. Fig. 2.5 illustrates an example of SR scheme based on DF decoding operated on two phases. The estimation of the threshold value depends on a number of factors, e.g., the source's transmission power, data rate, channel bandwidth and noise level at the receiving terminal. More details on the estimation of the threshold value can be found in [6]. It is recalled that this dual-hop diversity transmission requires knowledge of the instantaneous CSI (I-CSI) on the source-relay link; thus, the source can reasonably estimate if the relay successfully decodes the message and forwards to the destination. One possible drawback of this relaying scheme is the high overhead related to acquiring CSI, which may overwhelm the gain from cooperation.

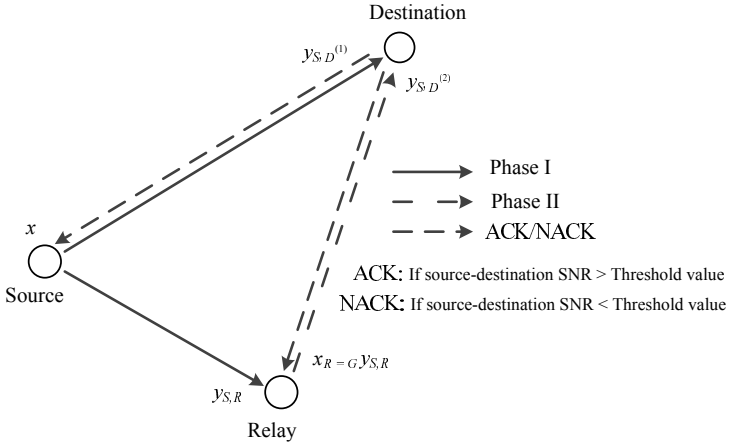

Figure 2.6 Example of of incremental AF relaying scheme.

2.4.4 Incremental Relaying

The IR protocol [6,39,40] utilizes the second transmission phase only when the source's transmission is unsuccessful in the first phase. This protocol has the best SE among the other techniques because the relay does not always need to transmit in the second phase, and this can be implemented with a feedback from the destination terminal. If the source-destination SNR is sufficiently high, the feedback indicates success of the DT, and the relay does nothing while the source continues to transmit the next message by reducing the time-slot resource from two to one. On the other hand, if the source-destination SNR is not sufficiently high for successful DT, the feedback requests the relay to re-transmit what it has received from the source in the first phase either using AF or DF scheme. In the latter case, the destination tries to combine the two transmissions using MRC technique or any other diversity combining techniques. Fig. 2.6 illustrates an example of IR scheme based on AF. The IR protocols can be viewed as extensions of incremental redundancy or hybrid automatic-repeat-request (ARQ) where in the context of a cooperation system the relay re-transmits in an attempt to achieve spatial diversity.

2.4.5 Coded Cooperation

CC [7, 9, 41] is a method that integrates cooperation into channel coding where diversity is achieved by partitioning a source's codeword. The basic idea of the CC is that the source's codeword of length N is divided into two segments of length N_1 and N_2, respectively, where $N_1 + N_2 = N$. The first portion of the data with N_1 bits is a

valid codeword by itself but weakly coded and the N_2 bits in the second part are the additional parity bits [7]. Similar to the previous cooperation protocols, the CC also operates into two phases. In the first phase, the source broadcasts a sub-codeword of length N_1 and is received by the destination as well as by the relay. The relay thus receives a noisy version of the coded message from the source. If the relay can correctly decode the source's message, it will regenerate the remaining N_2 bits of the codeword and transmit it to the destination in the second phase; otherwise, the source will transmit the remaining N_2 bits by itself in the second transmission phase.

The CC framework can be achieved with a wide variety of channel codes. For example, the overall code may be a block code, convolutional codes, or the combination of both. Furthermore, the symbols in the two portions of the codeword can be partitioned through puncturing, product codes, or other forms of concatenation. The repetition-based DF schemes can be considered as a special case of the CC where the two partitioned codewords are equal.

2.4.6 Compress-and-Forward

In this relaying protocol, the relay first samples, quantizes and compresses the received message. Second, the relay encodes the compressed message into a new message (as if they were information bits) and forwards it to the destination [42,43]. The destination jointly processes the observations from the source and relay. The quantization and compression process at the relay is a process of source encoding and it is realized using Wyner-Ziv source coding [44]. In contrast to the DF or CC schemes, the relay in CF may not decode perfectly the source's message but needs only to extract, from its observation, the information that is the most relevant to the decoding of the destination. This scheme has been shown to provide higher capacity than the DF or AF for some specific channel configurations. However, it is considerably more complicated than either of the two basic protocols. Further practical studies on CF relaying schemes can be found in [10, 11, 45, 46].

2.5 Half-Duplex and Full-Duplex Relaying

User cooperation can adopt either HDR or FDR operation modes depending on how the relay regulates the simultaneity of reception and transmission phases. In this context, if a relay cannot transmit and receive simultaneously in the same band, then it is said to be operated in HD mode. In this mode, the transmission and reception signals are orthogonal to each other. The orthogonality between the transmitted and received

signals can be in time-domain (i.e., reception and transmission occur in different time slots) or in a frequency domain (i.e., reception and transmission occur in different frequency bands). The HDR mode avoids relay SI at the cost of sacrificing the limited resources (e.g. time-slots and frequency). On the other hand, FD relaying [47–49] refers to the ability of the relay nodes to receive and transmit signals simultaneously on a single frequency band. Because of the single frequency operation, the FDR is sometimes descriptively referred to as single-frequency "*simultaneous transmit and receive*". This alternative efficiently uses the channel bandwidth, as it requires only one channel use for the end-to-end transmission, but suffers from unavoidable SI due to relay's output looping back to its input. This technology was first adopted for fixed infrastructure-based nodes due to huge difference of power levels (interference vs. the signal of interest) and later for small portable, or even hand-held, radios [47–49, 60].

Theoretically, FD can render up to double SE when compared to conventional HD operation. However, in practice this is possible only after tackling a significant technical challenge in minimizing the relay SI levels. Recently, there have been considerable and promising results in mitigating this SI for building practical FD radios [61, 62]. The main techniques used to cancel the SI are usually classified into passive and active suppression. In passive SI suppression, the SI signal power is attenuated due to the PL between the physically separated transmit and receive antennas on the same device. Active SI cancellation technique is used to reduce the dynamic range of the interference. This method includes: analog cancellation where RF processing is utilized to cancel the interference at the receiving antenna before the receiver low noise amplifier (LNA). Since this cancellation method is never perfect, the residual SI (RSI) after analog cancellation should be further reduced with the aid of digital cancellation, where the SI is removed in baseband after analog to digital conversion [60,63]. Further studies concluded that there is always RSI after taking all practical means of interference mitigation, e.g., due to channel estimation errors and non-ideal transceiver components introducing unknown transmit-side noise. However, these effects can still be minimized by proper *transmit power adaptation* [49].

2.6 Bidirectional Relaying Communication

In many applications of relay networks, two different sources may need to exchange information with the help of a relay. The relay enables a *bidirectional* (two-way) communication between the two sources, and hence, two traffic flows are supported by the same physical channels concurrently, which enhances SE of the system [50,51]. The two-way communication problem without the relay was first studied by Shannon [52],

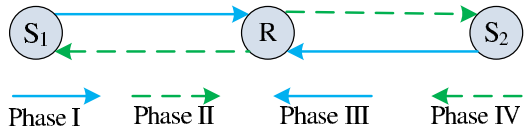

Figure 2.7 Four-phase one-way relaying for bidirectional cooperation.

which is considered as the first study of a network information theory problem. Later, in [53] the two-way relay system was exploited to mitigate the SE loss of cooperative protocols under HD relaying.

To elaborate more on efficient bidirectional relaying schemes, first, let us consider the conventional bidirectional communication shown in Fig. 2.7 where the two end-sources S_1 and S_2 intend to exchange information with the help of R. This can be accomplished by straightforwardly applying the unidirectional relaying in a two-way manner. That is, in the first time-slot S_1 transmits information to R; in the second time slot, R forwards the incoming signal to S_2 using, for instance, AF, DF or CF relaying schemes; in the third time slot, S_2 transmits information to R; and in the fourth time slot, R forwards the signal to S_1. One problem with this transmission scheme is that a total of four time-slots are needed to exchange the information in opposite directions, which obviously reduces the SE [51, 54].

The SE of the four time-slot based bidirectional communication system can be improved by exploiting the shared broadcast channel (BC) nature of the wireless medium through the network coding concept [55, 56]. In this regard, the well-known bidirectional relaying scheme adopted commonly is the *time-division broadcast* (TDBC) protocol [51, 57, 59] which reduces the number of time slots to three as shown in Fig. 2.8. In this protocol, S_1 and S_2 transmit their own signals in the first and second time-slots, respectively. In the third time-slot, R broadcast a superimposed signal to S_1 and S_2 using, for example, AF relaying scheme. Alternatively, R can decode the received signals first and performs an XOR operation over the two decoded message bits from S_1 and S_2; then re-encodes the XOR processed message to transmit a new symbol in the third time-slot [51, 58, 59]. Finally, each end source detects the signal from its counterpart through network coding techniques. This way, the TDBC protocol can accomplish the information exchange in three time-slots to increase the SE by 33% over unidirectional relaying [56].

The SE of TDBC protocol can be further improved by allowing the two end-sources to transmit simultaneously over a multiple-access channel (MAC). Such a protocol is widely known as physical-layer network coding (PNC) if the DF protocol is employed at the relay [54, 56] or analog network coding (ANC) if the AF protocol is employed

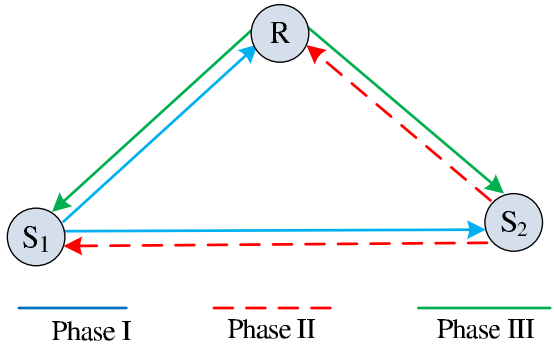

Figure 2.8 TDBC protocol in bidirectional networks.

at the relay [51, 57, 58]. The PNC and ANC protocols require only two time-slots to exchange the information between two sources. In this case, the two sources S_1 and S_2, as shown in Fig. 2.9, simultaneously transmit their signals at the first time-slot to the relay; at the second time-slot, the relay processes the incoming signals using either AF or DF schemes and retransmits to the two sources. Obviously, the PNC and ANC protocols achieve the highest SE since two-traffic flows are concurrently supported at each time-slot. However, due to the HD constraint the direct-link between the two sources can not be utilized even if such direct-link physically exists [51, 59], and hence, PNC and ANC achieve diversity order of one. On the other hand, the TDBC protocol can actually utilize the direct-link even if the terminals operate in a HD mode since the two end-sources transmit signals in two time-slots. As a result, the TDBC protocol can achieve diversity order of two [51, 54, 57].

Applications of the two-way relay system include: The communication between two wireless routers that communicate with each other through the help of a relay terminal. The communication between S_1 and S_2 where there is no reliable direct-link due to shadowing, the large separation between them, or use of low power signaling. This may occur in practice when the users are geographically separated and signals received from each other are very weak due to PL effects, or in the case of two mobile users located on the opposite sides of a building to communicate to each other.

Next, as an example, we discuss the mathematical descriptions of the two-way relay system when the relay uses AF relaying strategies to process the received signals. The source terminals S_1 and S_2 of Fig. 2.9 transmit their information to R during the MAC phase. Then, the relay receives an additive-Gaussian-noise-corrupted superposition of the two transmitted signals which can be expressed as

$$y_R = \sqrt{P_{S_1}}\alpha_{S_1,R}x_1 + \sqrt{P_{S_2}}\alpha_{S_2,R}x_2 + n_R \tag{2.7}$$

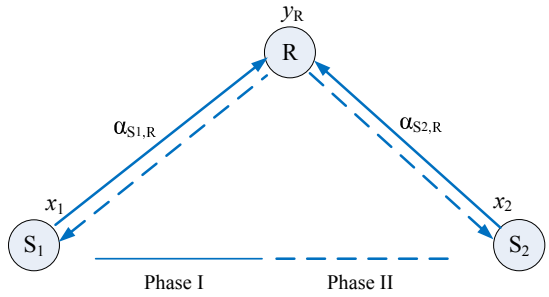

Figure 2.9 Two-phase two-way relaying for bidirectional cooperation.

where P_{S_1} and P_{S_2} denote the transmit powers of the source terminals S_1 and S_2, respectively, x_1 and x_2 denote the information symbols with normalized unit energy. Moreover, $\alpha_{S_1,R}$ and $\alpha_{S_2,R}$ represent the fading coefficients of $S_1 \rightarrow R$ and $S_2 \rightarrow R$ links, whereas n_R stands for the AWGN term. The relay then multiplies y_R with

$$G_{TW} = \frac{1}{\sqrt{P_{S_1} \mid \alpha_{S_1,R} \mid^2 + P_{S_2} \mid \alpha_{S_2,R} \mid^2 + 1}} \tag{2.8}$$

and forwards an amplified sum signal $x_R = G_{TW} y_R$ to users S_1 and S_2 during the broadcast phase. The channels in the forward direction can be assumed to be the same as in the backward directions, i.e., channel reciprocity is assumed [64, 65]. To this effect, users S_1 and S_2 receive Gaussian-noise-corrupted and fading distorted signals of $\sqrt{P_R}\alpha_{R,S_1} x_R + n_{R,S_1}$ and $\sqrt{P_R}\alpha_{R,S_2} x_R + n_{R,S_2}$, respectively. Since terminals S_1 and S_2 know their own transmitted symbols, they can subtract the back-propagating SI prior to decoding. Assuming perfect knowledge of the corresponding fading coefficients, the received instantaneous SNRs at the two user terminals can thus be expressed as [64]

$$\gamma_{S_1} = \frac{P_{S_2} P_R \mid \alpha_{S_1,R} \mid^2 \mid \alpha_{S_2,R} \mid^2}{(P_{S_1} + P_R) \mid \alpha_{S_1,R} \mid^2 + P_{S_2} \mid \alpha_{S_2,R} \mid^2 + 1} \tag{2.9}$$

and

$$\gamma_{S_2} = \frac{P_{S_1} P_R \mid \alpha_{S_1,R} \mid^2 \mid \alpha_{S_2,R} \mid^2}{(P_{S_2} + P_R) \mid \alpha_{S_2,R} \mid^2 + P_{S_1} \mid \alpha_{S_1,R} \mid^2 + 1}. \tag{2.10}$$

The mutual information that users S_1 and S_2 can achieve from the information exchange are depicted as [66]

$$I_{S_1} = \frac{1}{2} \log_2(1 + \gamma_{S_1}) \tag{2.11}$$

and

$$I_{S_2} = \frac{1}{2}\log_2(1+\gamma_{S_2}) \tag{2.12}$$

respectively. The pre-log factor 1/2 that appears in (2.11) and (2.12) is due to one-round information exchange, which takes place in two time-slots. Furthermore, the mutual information here is measured in bits/sec/Hz since it is normalized by the system's bandwidth. The mutual information between the source and destination for one-way AF relay system without the direct-link is given by [2]

$$I_D = \frac{1}{2}\log_2\left(1+\frac{P_S \mid \alpha_{S,R} \mid^2 P_R \mid \alpha_{R,D} \mid^2}{P_S \mid \alpha_{S,R} \mid^2 + P_R \mid \alpha_{R,D} \mid^2 + 1}\right). \tag{2.13}$$

Chapter 3

Fading Channels and Diversity Combining Techniques

In this chapter, we introduce some basic characteristics of the wireless environment, including path-loss, shadowing and multipath fading effects. Then, channel fading models with respective distributions and common performance measures used in this thesis are briefly presented. Finally, we conclude with discussions on popular diversity combining techniques that are often used for increasing the performance of wireless communication systems. More detailed discussions on these topics can be found, e.g., in [68], [75] and [76].

3.1 Channel Characteristics of Wireless and Mobile Communications

Wireless mobile communication systems have evolved remarkably since the last decades due to advances in wireless hardware technology and because of large demand for mobile access. Compared with the conventional wired communications, the radio wave propagation through wireless channels is highly dynamic. In addition, propagation characteristics change drastically from environment to environment because of the inherent nature of wave propagation mechanisms. This makes the radio wave propagation through wireless channels a complicated phenomenon, which is characterized by various effects, such as PL, shadowing and multipath fading. In this section, we briefly describe what these factors are and their effects on the performance of wireless communication systems.

3.1.1 Path-Loss

A fundamental property of the wireless signal is that when a transmitter communicates with a receiver by sending an electromagnetic signal through the wireless medium, the strength of the signal attenuates as it traverses the medium; thus, the received power becomes weaker as the propagation distance increases. To account this amount of degradation in signal strength, the ratio of transmit power P_t to receive power P_r in decibel (dB) scale is described by

$$PL(\text{dB}) = 10\log_{10}\left(\frac{P_t}{P_r}\right). \tag{3.1}$$

The above expression is used to quantify the PL and depends on certain radio properties, such as the transmission distance, radio wavelength, heights of the transmitter and receiver antennas, among many other factors. For radio propagation in free space, where there is unobstructed LOS path, the PL can be written as [67]

$$PL(\text{dB}) = -10\log_{10}\left(\frac{G_t G_r \lambda_c^2}{(4\pi)^2 d^2}\right) \tag{3.2}$$

where G_t and G_r are the gains of the transmitting and receiving antennas, respectively, d is the geographic distance between the transmitter and the receiver and λ_c is the radio wavelength in free space. Furthermore, to facilitate analytical studies on the wireless communication a simple PL model, which is based on experimental data, is adopted in practice as [67, 71, 75]

$$P_r = P_t K_c \left(\frac{d}{d_0}\right)^{-\beta} \tag{3.3}$$

The simplified PL model in the above expression can be re-written in dB scale as

$$P_r(\text{dB}) = P_t(\text{dB}) + K_c(\text{dB}) - 10\beta\log_{10}\left(\frac{d}{d_0}\right) \tag{3.4}$$

where d_0 is the reference distance, K_c is a unit-less constant which depends on the antenna characteristics and the average channel attenuation and β is the PL exponent. K_c can be obtained from the empirical average of the receive power at the reference distance d_0. The value of d_0 is usually $1-10$ meters for indoors and $10-100$ meters for outdoor environment. The value of the PL exponent, β, depends on the propagation environment and usually ranges between 2 and 6 [68]. Table 3.1 shows the summary of typical values of the PL exponent for different indoor and outdoor environments and

Table 3.1 Typical path-loss exponents for different environment.

Environment	Path-Loss exponents
Free Space	2
Urban macrocells	3.7–6.5
Urban microcells	2.7–3.5
Office Buildings (same floor)	1.6–3.5
Office Buildings (multiple floors)	2–6
Store	1.8–2.2
Factory	1.6–3.3
Home	3

antenna heights at 900 MHz and 1.9 GHz [67–70]. The wide range of empirical PL exponents for indoor propagation environment in the table may be due to attenuation caused by floors, objects, and partitions. The PL information is a major component in analysis and design of link budget of a wireless communication system [71]. More details of the modeling and effects of the PL phenomena in wireless communications can be found in [68].

3.1.2 Shadow Fading

In addition to the power loss caused by basic propagation described previously, the signal transmitted through the wireless channel may be obstructed by particular obstacles (e.g. buildings, trees, vehicles, or airplanes). Such obstacles attenuate the signal power through absorption, reflection, diffraction, and by causing random scattering; when the attenuation is very strong, the signal is blocked. This random variation in the received signal power is called *shadowing effect* and is considered as a type of large-scale (or macroscale) fading. To account for this effect, a statistical model must be used to characterize the random attenuation. The most common model for this additional attenuation is log-normal shadowing [67,68,74]. This model has been confirmed empirically to accurately model the variation in received power in both outdoor and indoor radio propagation environments [72,73]. In this log-normal shadowing model, the ratio of transmit-to-receive power $\psi = P_t/P_r$, when the basic PL is normalized away, is assumed to be random with log-normal distribution of PDF given by [68]

$$f_\psi(\psi) = \frac{\xi}{\sqrt{2\pi}\sigma_{\psi_{\text{dB}}}\psi} \exp\left(-\frac{(10\log_{10}\psi - \mu_{\psi_{\text{dB}}})^2}{2\sigma^2_{\psi_{\text{dB}}}}\right), \quad \psi > 0 \tag{3.5}$$

where $\xi = 10/\ln(10)$ is a constant. The received signal strength in decibel scale, i.e., $\psi_{\text{dB}} = 10\log_{10}\psi$ is a Gaussian random variable with mean $\mu_{\psi_{\text{dB}}}$ and variance $\sigma^2_{\psi_{\text{dB}}}$. The evaluation of the mean can be based either on an analytical model or empirical measurements. Furthermore, to jointly account for both PL and shadowing effects we may simply combine the log-normal distributed shadowing effect with the average PL [2, 68]

$$\frac{P_r}{P_t}(\text{dB}) = 10\log_{10} K_c - 10\beta\log_{10}\left(\frac{d}{d_0}\right) - \psi_{\text{dB}}. \tag{3.6}$$

3.1.3 Multipath Fading

In wireless mobile communication systems, a signal emitted from the transmitter arrives at the receiver over multiple paths. Multipath arises because the propagated signal is reflected, diffracted, and scattered by the objects in the channel environment. Example of such obstructions of the signal path includes, e.g., buildings, trees, and cars in outdoor settings, and walls, furniture, and people in indoor settings [1, 75, 76, 91]. The replicas of the signal arriving from different paths can add up either constructively or destructively at the receiver end; thus, the signal strength may fluctuate rapidly over time, frequency and space. This propagation phenomenon, which results in fast and small-scale (or microscale) amplitude and phase variation, is known as *multipath fading* [67, 71, 75]. This effect is experienced by both short-wave radio communications as well as by other forms of radio communications systems, including cellular telecommunications and many other users of the very-high frequency (VHF) and ultra-high frequency (UHF) spectrum. Fig.3.1 shows an example of multipath fading where the receiver is surrounded by objects and the replicas of the original signal arrives at the receiver from different paths with different delays and strengths. As the mobile station (MS) moves along the street, rapid variations of the signal are found to occur over distances of about one-half the wavelength. For $N(t)$ paths between the transmitter and receiver at time t the signal at the receiver can be modeled as [2, 75]

$$y(t) = \sum_{i=1}^{N(t)} \alpha_i(t)x(t - \tau_i(t)) + n(t) \tag{3.7}$$

where $x(t)$ represents the waveform from the transmitter and $\alpha_i(t)$ and $\tau_i(t)$ denote the relative amplitude and delay of the i^{th} path between the transmitter and the receiver at time t, respectively, and $n(t)$ represents the AWGN in the channel. Furthermore, the coherence bandwidth B_c of the channel is related to the maximum delay spread

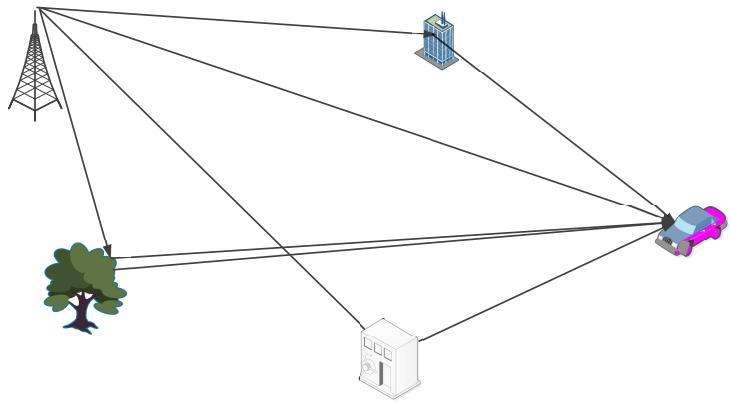

Figure 3.1 Example of multipath fading in urban environment.

$\tau_{\max}$ which is given by [76]

$$B_c \backsimeq \frac{1}{\tau_{\max}}. \tag{3.8}$$

Based on the channel variation characteristics in the frequency domain, the channel is said to be flat fading if the coherence bandwidth of the channel is much greater than the signal bandwidth B, i.e., $B_c \gg B$; otherwise, it is considered to be frequency selective [67, 76, 91]. If the signal is narrow with respect to the channel's coherence bandwidth, the flat fading channels are also known as narrow-band channels [76].

3.2 Statistical Characterization of Fading Processes

Due to the complex nature of the scattering environment, precise physical modeling of channels is practically intractable. For this reason, system designers frequently employ statistical models to characterize the channel effects. The statistics of the short-term signal variation can be described by a great number of distributions, such as Rayleigh, Rice (Nakagami$-n$), Nakagami$-m$, Hoyt (Nakagami$-q$), and Weibull distributions [32, 67, 76, 207]. The derivation of theses well-known distributions is based on the assumption of a homogeneous diffuse scattering field, resulting from randomly distributed scatterers. However, this assumption is not necessarily always realistic since surfaces in most radio propagation environments are spatially correlated [77, 78]. To address such non-homogeneous nature of the propagation medium more generic distributions have been proposed. This includes the $\alpha-\mu$, the $\kappa-\mu$ and the $\eta-\mu$ distributions [78,100,102,107]. In this section, we present an overview of the most popular distributions used for modeling and designing wireless communication

systems. Throughout this discussion, a narrow-band fading model is assumed. Furthermore, we note that the fading gain at the input of a receiver is a RV described by $R = |\alpha|$ with mean-square value $\Omega = E[R^2]$ and PDF of $f_R(r)$. Moreover, the instantaneous SNR per received symbol is described by $\gamma = (P/N_0)|\alpha|^2$, where P is the transmit power and N_0 is variance of the AWGN. The corresponding average SNR per symbol is described by $\overline{\gamma} = (P/N_0)\Omega$. Performing a simple RV transformation the PDF of γ can be expressed as

$$f_\gamma(\gamma) = \frac{f_R\left(\sqrt{\frac{\Omega\gamma}{\overline{\gamma}}}\right)}{2\sqrt{\frac{\overline{\gamma}\gamma}{\Omega}}}. \tag{3.9}$$

Finally, the moment generating function (MGF) $M_\gamma(s)$ of γ is defined by

$$M_\gamma(s) \triangleq E[\exp(-s\gamma)] = \int_0^\infty \exp(-s\gamma) f_\gamma(\gamma) \mathrm{d}\gamma \tag{3.10}$$

where s denotes the Laplace transform parameter with $s > 0$.

3.2.1 Rayleigh Fading Model

Rayleigh distribution is commonly used to model multipath fading where there are a large number of reflected paths and no direct LOS path. It is also used in analysis and prediction of radio waves propagation performance for areas, such as cellular communications in a well built-up urban environment where there are many reflections from the surrounding objects, in high frequency (HF) ionospheric radio waves propagation [79,80], in tropospheric radio waves propagation where signals may follow a variety of different paths [81] as well as in ship-to-ship radio links [82]. According to the central limit theorem, if there is sufficiently large amount of scatterers, the channel impulse response will be well-modeled as a zero mean complex , i.e., $E[\alpha] = 0$ Gaussian process. In this case, the envelope of the channel fading amplitude $R = |\alpha|$ can be statistically described by a Rayleigh distribution as [75]

$$f_R(r) = \frac{2r}{\Omega} \exp\left(-\frac{r^2}{\Omega}\right), \qquad r \geq 0. \tag{3.11}$$

Using (3.9), the PDF of the instantaneous SNR per symbol of the channel, γ is given by

$$f_\gamma(\gamma) = \frac{1}{\overline{\gamma}} \exp\left(-\frac{\gamma}{\overline{\gamma}}\right), \qquad \gamma \geq 0. \tag{3.12}$$

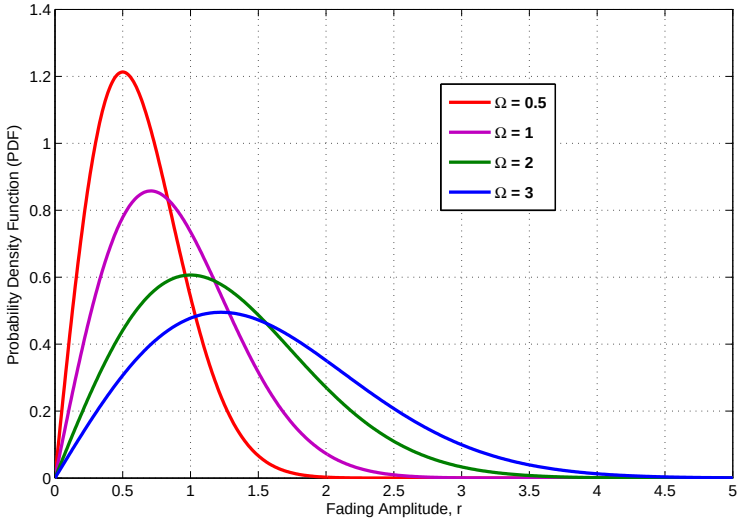

Figure 3.2 Rayleigh PDF for various values of Ω.

As can be observed from the PDF expression in (3.12), γ is distributed exponentially with parameter $1/\overline{\gamma}$. Finally, the MGF of γ is expressed in a simple form as

$$M_{\gamma}(s) = \frac{1}{1 + s\overline{\gamma}}. \tag{3.13}$$

3.2.2 The Rice Fading Model

The Rice distribution, also known as Nakagami$-n$, is often used to model paths consisting of a strong LOS component and weaker components in the received signal. This model is commonly observed in micro-cellular urban and suburban land-mobile systems [83], pico-cellular indoor [84], and factory environments [85]. It is also used in the dominant LOS path of satellite and ship-to-ship radio links [82]. In this case, the channel fading amplitude follows the distribution described as [76]

$$f_R(r) = \frac{2r(n^2+1)}{\Omega} \exp\left(-n^2 - \frac{(n^2+1)r^2}{\Omega}\right) I_0\left(2nr\sqrt{\frac{n^2+1}{\Omega}}\right), \qquad r \geq 0 \tag{3.14}$$

where n is the Nakagami$-n$ parameter that lies in $0 \leq n \leq \infty$, $I_0(\cdot)$ is the modified Bessel function of the first kind of order zero [86]. The fading parameter n is related

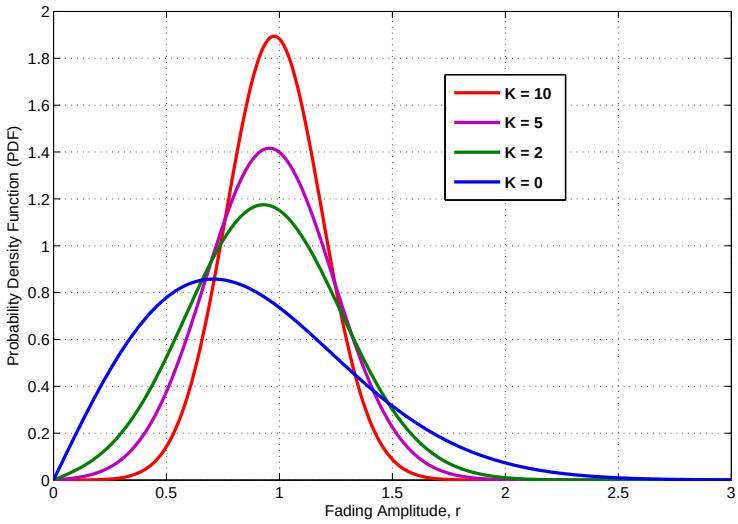

Figure 3.3 Rice PDF for several values of K with $\Omega = 1$.

to the Rice factor K by $K = n^2$. K is defined as the ratio of the LOS (specular) to the scattered power component. When $K = 0$, there is no LOS or specular component and the fading becomes Rayleigh distributed. When $K = \infty$, there is no scattered component and the channel does not exhibit any fading, i.e., it transforms to non-fading AWGN model. Fig. 3.3 illustrates the Rice PDF for several values of K with $\Omega = 1$. The case with $K = 0$ corresponds to the Rayleigh PDF. Applying (3.9), the PDF of the instantaneous SNR , γ, can be expressed as

$$f_\gamma(\gamma) = \frac{(n^2+1)}{\overline{\gamma}} \exp\left(-n^2 - \frac{(n^2+1)\gamma}{\overline{\gamma}}\right) I_0\left(2n\sqrt{\frac{(n^2+1)\gamma}{\overline{\gamma}}}\right), \qquad \gamma \geq 0. \quad (3.15)$$

As it can be observed from the above expression, γ follows a non-central chi-square distribution. The corresponding MGF of this fading model is expressed in a closed-form as

$$M_\gamma(s) = \frac{1+n^2}{1+n^2+s\overline{\gamma}} \exp\left(-\frac{n^2 s\overline{\gamma}}{1+n^2+s\overline{\gamma}}\right). \quad (3.16)$$

3.2.3 The Hoyt Fading Model

The Hoyt distribution, also referred to as the Nakagami$-q$ distribution, is commonly used to describe the short-term signal variations in satellite links subject to strong

ionospheric scintillation [87,88], in multipath wireless links with heavy shadowing [89] or in general in those fading conditions which are more severe than the Rayleigh. Physically, it accounts for case of enriched multipath fading with the absence of a dominant component. The distribution considers the in-phase and quadrature signal components as zero-mean Gaussian with arbitrary variances. The probability distribution for the envelope of the received signal is given by [76]

$$f_R(r) = \frac{(q^2+1)r}{q\Omega} \exp\left(-\frac{(q^2+1)^2 r^2}{4q^2\Omega}\right) I_0\left(\frac{(1-q^4)r^2}{4q^2\Omega}\right) \qquad r \geq 0 \tag{3.17}$$

where q is the Nakagami$-q$ fading parameter which ranges from 0 to 1. The distribution spans from the worst case scenario of the one-sided Gaussian fading with $q = 0$ to the Rayleigh fading case with $q = 1$. With the aid of (3.9), it can be shown that the SNR is distributed according to

$$f_\gamma(\gamma) = \frac{q^2+1}{2q\overline{\gamma}} \exp\left(-\frac{(q^2+1)^2\gamma}{4q^2\overline{\gamma}}\right) I_0\left(\frac{(1-q^4)\gamma}{4q^2\overline{\gamma}}\right), \qquad \gamma \geq 0. \tag{3.18}$$

Furthermore, the MGF of γ is expressed in a closed-form as

$$M_\gamma(s) = \left[1 + 2s\overline{\gamma} + \frac{(2s\overline{\gamma})^2 q^2}{(1+q^2)^2}\right]^{-\frac{1}{2}}. \tag{3.19}$$

3.2.4 Nakagami$-m$ Fading Model

The Nakagami$-m$ fading model is a more general model that better fits to experimental measurements of different environments. Specifically, it gives the best fit to land-mobile and indoor mobile multipath propagation environment [77, 91], in scintillating ionospheric radio links [80, 92], in satellite-to-indoor and satellite-to-outdoor radio waves propagation [93, 94]. Moreover, it is mathematically tractable since it leads to convenient closed-form analytical expressions when investigating the performance of some important wireless communication systems. In this fading model, the PDF of the fading envelope is given by [90]

$$f_R(r) = \frac{2m^m r^{2m-1}}{\Omega^m \Gamma(m)} \exp\left(-\frac{mr^2}{\Omega}\right), \qquad r \geq 0 \tag{3.20}$$

where m is the Nakagami$-m$ fading parameter that ranges from 1/2 to ∞. Fig. 3.4 shows the Nakagami$-m$ PDF for $\Omega = 1$ and different values of the fading parameter. The PDF of the SNR per symbol γ is distributed according to a gamma distribution

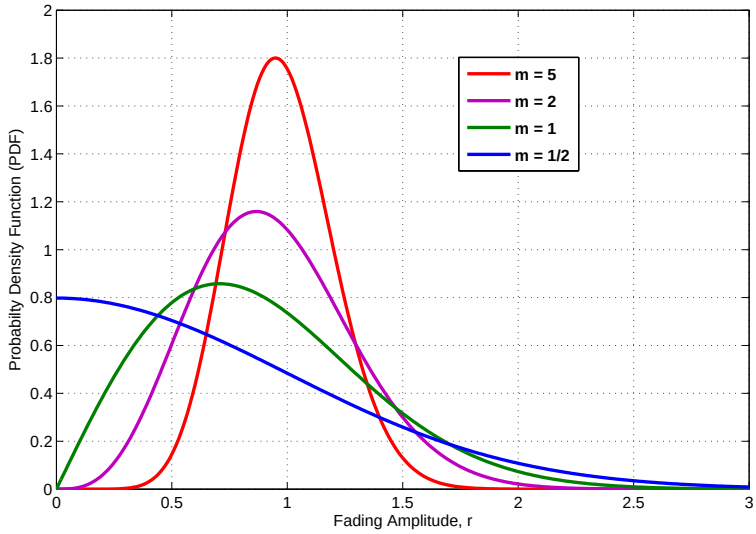

Figure 3.4 Nakagami$-m$ PDF for different values of the fading parameter m with $\Omega = 1$.

given by

$$f_\gamma(\gamma) = \frac{m^m \gamma^{m-1}}{\overline{\gamma}^m \Gamma(m)} \exp\left(-\frac{m\gamma}{\overline{\gamma}}\right), \qquad \gamma \geq 0. \tag{3.21}$$

Moreover, it can be easily shown that the MGF of γ is given by

$$M_\gamma(s) = \left(1 + \frac{s\overline{\gamma}}{m}\right)^{-m}. \tag{3.22}$$

The Nakagami$-m$ distribution can model fading conditions that are either more or less severe than Rayleigh fading. When $m = 1$, the Nakagami$-m$ distribution becomes the Rayleigh distribution, while when $m = 1/2$ it becomes a one-sided Gaussian distribution. In the limit as $m \to \infty$, the distribution converges to nonfading AWGN channel [76]. By one-to-one mapping between the Hoyt fading parameter q and the Nakagami$-m$ fading parameter m the model closely approximates Hoyt (Nakagami$-q$) for $m < 1$ as

$$m \approx \frac{(1+q^2)^2}{2(1+2q^4)}, \qquad m \leq 1. \tag{3.23}$$

Similarly, when $m > 1$ the Rice distribution can be closely approximated using the

following mapping between the Rice factor K and the Nakagami shape factor m [76] as

$$K \approx \sqrt{m^2 - m} + m - 1, \quad m \geq 1 \tag{3.24}$$

$$m \approx \frac{(K+1)^2}{2K+1}, \qquad K \geq 0. \tag{3.25}$$

3.2.5 The Weibull Fading Model

Weibull is a simple and flexible statistical model that effectively describes multipath fading for both indoor and outdoor propagation environment [95,96]. It also provides a better fit to the empirical measurement data for 900MHz-band mobile radio channels, ultrawide-band fading channels [97], and 5GHz-band vehicle-to-vehicle (V2V) channels [98]. In this fading model, the PDF of the fading envelope is given by [76]

$$f_R(r) = \frac{b}{(\Lambda\Omega)^{b/2}} r^{b-1} \exp\left(-\left(\frac{r^2}{\Lambda\Omega}\right)^{b/2}\right), \qquad r \geq 0 \tag{3.26}$$

where $b > 0$ is the fading parameter and $\Lambda = 1/\Gamma(1 + 2/b)$. This model reduces to the Rayleigh fading model when $b = 2$ and when $b = 1$, it reduces to an exponential distribution with parameter $1/\sqrt{\Lambda\Omega}$. Fig. 3.5 shows the Weibull PDF for $\Omega = 1$ and different values of the fading parameter b. The corresponding SNR per symbol has PDF given by

$$f_\gamma(\gamma) = \frac{b}{2(\Lambda\overline{\gamma})^{b/2}} \gamma^{b/2-1} \exp\left(-\left(\frac{\gamma}{\Lambda\overline{\gamma}}\right)^{b/2}\right), \qquad \gamma \geq 0. \tag{3.27}$$

One can observe that γ also follows a Weibull distribution, but with parameter $b/2$ instead of b. For $b > 0$, the MGF of γ can be expressed in a closed-form as [99]

$$M_\gamma(s) = \frac{b}{2} \frac{l^{\,b/2}\sqrt{k/l}}{(\Lambda\bar{\gamma}s)^{b/2}(\sqrt{2\pi})^{k+l-2}} \mathrm{G}_{l,k}^{k,l}\left(\frac{l^{\,l}/k^{\,k}}{(\Lambda\bar{\gamma}s)^{kb/2}} \middle| \begin{matrix} I(l, 1-b/2) \\ I(k,0) \end{matrix}\right). \tag{3.28}$$

In the above expression, $\mathrm{G}_{l,k}^{k,l}(\cdot)$ is the Meijer G-function [104], $I(n,\xi) = \xi/n, (\xi + 1)/n, \cdots, (\xi + n - 1)/n$ and k and l are positive integers such that $l/k = b/2$ with GCD $(l, k) = 1$ (greater common divisor). It is also noted that the Meijer's G-function is available as a built-in function in many mathematical software packages, such as MATHEMATICA, MAPLE and MATLAB.

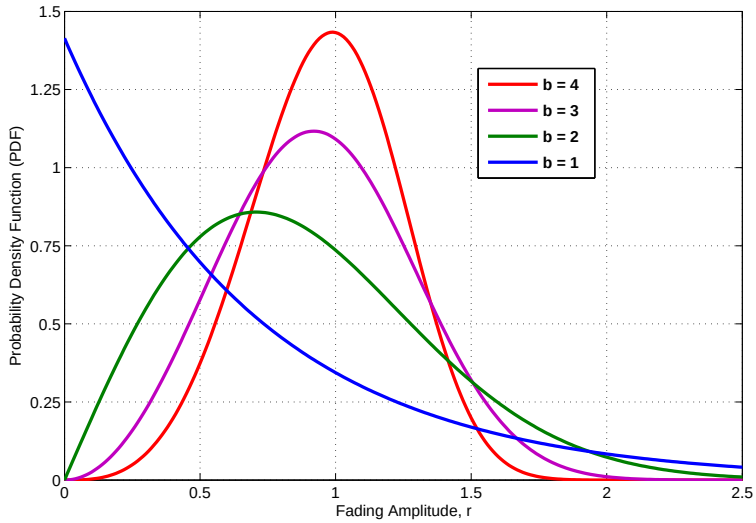

Figure 3.5 Weibull PDF for different values of the fading parameter b with $\Omega = 1$.

3.3 Generalized Fading Models

In many practical cases, situations are encountered for which no distributions seem to adequately fit experimental data, though one or another may yield a moderate fitting. For example, the well-known Nakagami$-m$ distribution does not seem to yield a good fitting to experimental data at its tail, while better fitting is being observed around the mean or median [105]. As already mentioned previously, the well-known distributions have been derived by assuming a homogeneous diffuse scattering field, resulting from randomly distributed point scatterers. With such an assumption, the central-limit theorem leads to complex Gaussian processes, with in-phase and quadrature Gaussian-distributed variables having zero means and equal standard deviations [78]. To account for the non-homogeneous nature of the surfaces, recently alternative generic fading models, such as $\alpha-\mu$, $\kappa-\mu$ and $\eta-\mu$ distributions have been proposed [78, 100, 107]. These distributions fit well to experimental data and include as special cases the well-known distributions presented above.

3.3.1 $\alpha-\mu$ Fading

The $\alpha-\mu$, also known as the Stacy fading model, is a general, flexible and mathematically tractable distribution that accounts for the non-linearity of a propagation

medium as well as for the multipath clustering of the radio waves by rewriting the Stacy distribution in terms of two physical fading parameters, namely, α and μ [100]. The usefulness of the model has recently been verified in practice [102] through field measurements in both isotropic and anisotropic environments. In this fading model, the PDF of the fading envelope is given by [100, 101]

$$f_R(r) = \frac{\alpha r^{\alpha\mu-1}}{(\Omega\tau)^{\alpha\mu/2}\Gamma(\mu)} \exp\left(-\left(\frac{r^2}{\Omega\tau}\right)^{\alpha/2}\right), \qquad r \geq 0 \tag{3.29}$$

where $\tau = \Gamma(\mu)/\Gamma(\mu + 2/\alpha)$, $\alpha > 0$ denotes the non-linearity parameter and $\mu > 0$ is related to the number of multipath clusters. Under some special cases, the fading model can reduce to other distributions, such as Rayleigh ($\alpha = 2, \mu = 1$), Nakagami$-m$ ($\alpha = 2, \mu = m$) and Weibull ($\alpha = b, \mu = 1$). The PDF of γ for this distribution can be expressed as

$$f_\gamma(\gamma) = \frac{\alpha\gamma^{\alpha\mu/2-1}}{2\,\Gamma(\mu)\,(\tau\overline{\gamma})^{\alpha\mu/2}} \exp\left(-\left(\frac{\gamma}{\tau\overline{\gamma}}\right)^{\alpha/2}\right), \qquad \gamma \geq 0. \tag{3.30}$$

The MGF of γ can be expressed in a closed-form as [103]

$$M_\gamma(s) = \frac{\alpha}{2\Gamma(\mu)(\tau\overline{\gamma}s)^{\alpha\mu/2}} \frac{k^{1/2} l^{\frac{\alpha\mu-1}{2}}}{(2\pi)^{\frac{l+k-2}{2}}} \mathrm{G}_{l,k}^{k,l}\left(\left(\frac{l^l/k^k}{(\tau\overline{\gamma}s)^{k\alpha/2}}\right)\middle| \begin{matrix} I(l, 1-\alpha\mu/2) \\ I(k, 0) \end{matrix}\right). \tag{3.31}$$

Here, $\alpha/2 = l/k$, where l and k are positive integers with GCD $(l, k) = 1$. This MGF result is a general result that can reduce easily into other MGF expressions for different channel models, such as Rayleigh, Nakagami$-m$ and Weibull as special cases.

3.3.2 $\kappa-\mu$ Fading Model

The $\kappa-\mu$ fading model is a generic and flexible fading model that represents the small-scale variations of the signal fading under a LOS propagation scenario. This model considers a signal composed of clusters of multipath waves propagating in a non-homogeneous environment [78, 107, 206, 207]. The phases of the scattered waves within any one cluster are random and they have similar delay times. It is also assumed that the delay-time spreads of different clusters are relatively large. The clusters of multipath waves are assumed to have scattered waves with identical powers, but within each cluster a dominant component is found, which presents an arbitrary power [78]. The flexibility of the model renders it to be suitable and to better fit to field

Table 3.2 Common fading distributions obtained from the $\kappa-\mu$ distribution.

Fading Distributions	Parametrs of $\kappa-\mu$ Distribution
One-Sided Gaussian	$\mu = 0.5, \kappa \to 0$
Rayleigh	$\mu = 1, \kappa \to 0$
Nakagami$-m$ (with shapping parametr m)	$\mu = m, \kappa \to 0$
Rice (with shapping parametr K)	$\mu = 1, \kappa = K$

measurements data in variety of scenarios, both for low and high-order statistics [106]. As implied by its name, the distribution is controlled by two physical parameters, namely, κ and μ. The parameter κ is defined as the ratio between the total power of the dominant components and the total power of the scattered waves, whereas the parameter μ is related to the multipath clustering. In this fading model, the PDF of the fading envelope is given by [78]

$$f_R(r) = \frac{2\mu(1+\kappa)^{\frac{\mu+1}{2}} r^{\mu}}{\kappa^{\frac{\mu-1}{2}} \exp(\mu\kappa)\Omega^{\frac{\mu+1}{2}}} \exp\left(-\frac{\mu(1+\kappa)r^2}{\Omega}\right) I_{\mu-1}\left(2\mu r\sqrt{\frac{\kappa(1+\kappa)}{\Omega}}\right), \qquad r \geq 0 \tag{3.32}$$

where $\kappa > 0$, $\mu > 0$ given by $\mu = E^2[R^2](1+2\kappa)/(V[R^2](1+\kappa)^2)$, I_ν is the modified Bessel function of the first kind of order ν [86]. The $\kappa-\mu$ distribution is an extremely versatile fading model which contains other important distributions as special cases. Table 3.2 reflects the parameter specializations that allow us to obtain the One-Sided Gaussian, Rice (Nakagami$-n$), Nakagami$-m$ and Rayleigh distributions from the two shaping parameters κ and μ. The PDFs for different parameter combinations are plotted in Fig. 3.6 and Fig. 3.7, respectively. Fig. 3.6 represents the PDF of the distribution for fixed μ and different values of κ, whereas Fig. 3.7 illustrates for fixed κ and various values of μ. The PDF of the instantaneous SNR γ can be expressed as

$$f_\gamma(\gamma) = \frac{\mu(\kappa+1)^{\frac{(\mu+1)}{2}} \gamma^{\frac{(\mu-1)}{2}}}{\kappa^{\frac{(\mu-1)}{2}} \exp{(\mu\kappa)}\bar{\gamma}^{\frac{(\mu+1)}{2}}} \exp\left(-\frac{\mu(\kappa+1)\gamma}{\bar{\gamma}}\right) I_{\mu-1}\left(2\mu\sqrt{\frac{\kappa(\kappa+1)\gamma}{\bar{\gamma}}}\right), \quad \gamma \geq 0. \tag{3.33}$$

Furthermore, the MGF of γ is expressed in closed-form as [107]

$$M_\gamma(s) = \frac{(1+\kappa)^{\mu}\mu^{\mu}}{[s\overline{\gamma} + (1+\kappa)\mu]^{\mu}} \exp\left(\frac{\mu^2\kappa(1+\kappa)}{s\overline{\gamma} + \mu(1+\kappa)} - \mu\kappa\right). \tag{3.34}$$

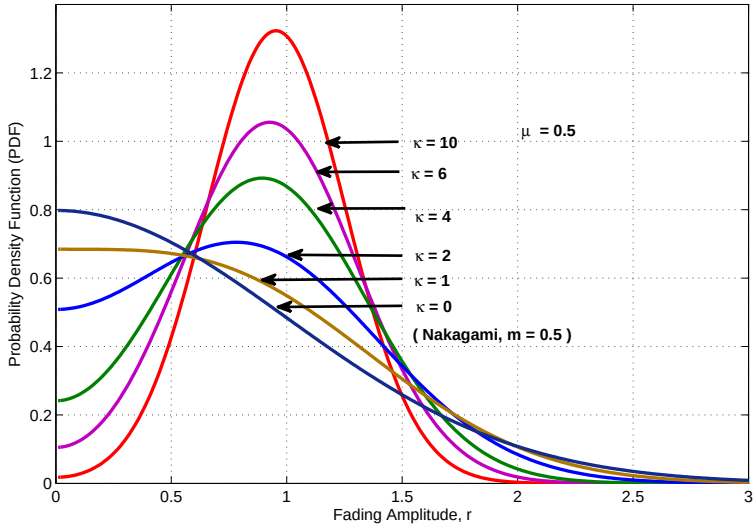

Figure 3.6 $\kappa-\mu$ PDF for various values of κ and fixed μ with $\Omega = 1$.

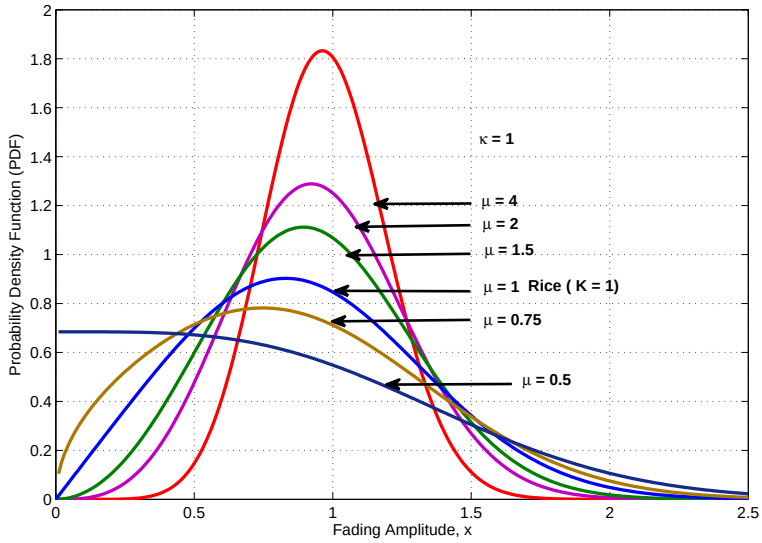

Figure 3.7 $\kappa-\mu$ PDF for various values of μ and fixed κ with $\Omega = 1$.

3.3.3 $\eta-\mu$ Fading Model

The $\eta-\mu$ fading model is a general fading model that can be used to better represent the small-scale variations of the fading signal in NLOS communication scenarios. Similar to the $\kappa-\mu$ case, this model also considers a signal composed of clusters of multipath waves propagating in non-homogeneous environment. The phases of the scattered waves within any one cluster are random and they have similar delay times. It is also assumed that the delay-time spreads of different clusters are relatively large. This fading model is described by the two named parameters, η and μ, and it is valid for two different formats that correspond to two physical models. In both formats, the parameter μ is related to the number of multipath clusters in the environment, whereas the parameter η is related to the ratio of the powers in Format-1 or correlation in Format-2 between the multipath waves in the in-phase and quadrature components [78, 108]. In this fading model, the PDF of the fading envelope is given by [78]

$$f_R(r) = \frac{4\sqrt{\pi}\,\mu^{\mu+\frac{1}{2}}\,h^{\mu}r^{2\mu}}{\Gamma(\mu)H^{\mu-\frac{1}{2}}\,\Omega^{\mu+\frac{1}{2}}}\exp\left(-\frac{2\mu h r^2}{\Omega}\right)I_{\mu-\frac{1}{2}}\left(\frac{2\mu H r^2}{\Omega}\right), \qquad r \geq 0 \qquad (3.35)$$

where $\mu > 0$ which is given by $\mu = E^2[R^2]\,(1+(H/h)^2)/2V[R^2]$ and h and H are given in terms of η in two formats. In Format-1, the in-phase and quadrature components of the fading signal within each cluster are assumed to be independent from each other and to have different powers where the parameter $0 < \eta < \infty$ is the scattered waves power ratio between the in-phase and quadrature components of each cluster. In this case, $h = (2+\eta^{-1}+\eta)/4$ and $H = (\eta^{-1}-\eta)/4$. It can be easily shown that within this format, $H/h = (1-\eta)/(1+\eta)$. On the other hand, in Format-2 the in-phase and quadrature components of the fading signal within each cluster are assumed to have identical powers and to be correlated with each other where $-1 < \eta < 1$ is the correlation coefficient between the in-phase and quadrature components. In this case, $h = 1/(1-\eta^2)$ and $H = \eta/(1-\eta^2)$, then $H/h = \eta$. With the aid of bilinear transformation, the parameter of one format can be obtained from the other. In this regard, $\eta_1 = (1-\eta_2)/(1+\eta_2)$ or, equivalently, $\eta_2 = (1-\eta_1)/(1+\eta_1)$ where η_1 and η_2 corresponds to the parameters of Format-1 and Format-2, respectively. The PDFs of the envelope for different parameter combinations are plotted in Fig. 3.8 and Fig.3.9. Specifically, Fig. 3.8 represents the PDF of the distribution for fixed η and different values of μ, whereas Fig. 3.9 illustrates for fixed μ and various values of η. The PDF of instantaneous SNR per symbol γ is distributed as

$$f_\gamma(\gamma) = \frac{2\sqrt{\pi}\,\mu^{\mu+\frac{1}{2}}\,h^{\mu}\gamma^{\mu-\frac{1}{2}}}{\Gamma(\mu)H^{\mu-\frac{1}{2}}\,\overline{\gamma}^{\mu+\frac{1}{2}}}\exp\left(-\frac{2\mu\gamma h}{\overline{\gamma}}\right)I_{\mu-\frac{1}{2}}\left(\frac{2\mu H\gamma}{\overline{\gamma}}\right), \qquad \gamma \geq 0. \qquad (3.36)$$

Table 3.3 Relation between $\eta-\mu$ distribution and other common fading distributions.

Fading Distribution	Format-1	Format-2
$\eta-\mu$	$h=(1+\eta^{-1}+\eta)/4$	$h=1/(1-\eta^2)$
	$H=(\eta^{-1}-\eta)/4$	$H=\eta/(1-\eta^2)$
Nakagami$-m$	$\mu=m, \eta\to 0$ or $\eta\to\infty$	$\eta\to\pm 1$
	$\mu=m/2, \eta\to 1$	$\eta\to 0$
Nakagami$-q$ (Hoyt)	$\mu=0.5, \eta=q^2$	$q^2=(1-\eta)/(1+\eta)$
Rayleigh	$\mu=0.5, \eta=1$	$\mu=0.5, \eta=0$
One-Sided Gaussian	$\mu=0.5, \eta\to 0$ or $\eta\to\infty$	$\mu=0.5, \eta\to\pm 1$

By varying the values of η and μ, the $\eta-\mu$ distribution can cover the whole range of conditions that are typically encountered in modeling fading scenarios. For example, considering the case where the in-phase and quadrature components are identically distributed, i.e., $\eta=1$ the $\eta-\mu$ PDF reduces to the Nakagami$-m$ PDF with fading parameter of $m=2\mu$ [78]. Table 3.3 depicts the reduction of the $\eta-\mu$ distribution to the other important distributions, such as One-Sided Gaussian, Hoyt (Nakagami$-q$), Nakagami$-m$ and Rayleigh distributions under some typical special cases. Furthermore, it has been shown in [109] that the model accurately approximates the sum of independent non-identical Hoyt envelopes having arbitrary mean powers and arbitrary fading degrees. Finally, the MGF of γ in a closed-form is given as [107]

$$M_\gamma(s)=\left(\frac{4\mu^2 h}{(2(h-H)\mu+s\bar{\gamma})(2(h+H)\mu+s\bar{\gamma})}\right)^{\mu}. \tag{3.37}$$

3.3.4 Inverse Gaussian Distribution

The inverse Gaussian (IG) distribution (also known as the Wald distribution) is a two-parameter family of continuous probability distribution that better models shadowing effects in wireless communications. As mentioned previously, shadowing phenomenon are also modeled by the log-normal distribution. However, there exist real situations for which the log-normal distribution seems not to adequately fit the experimental data, although one or another may yield a moderate fitting. In the IG model, the instantaneous SNR has the following PDF [110]

$$f_\gamma(\gamma)=\sqrt{\frac{\lambda}{2\pi\gamma^3}}\ \exp\left(-\frac{\lambda(\gamma-\theta)^2}{2\theta^2\gamma}\right). \tag{3.38}$$

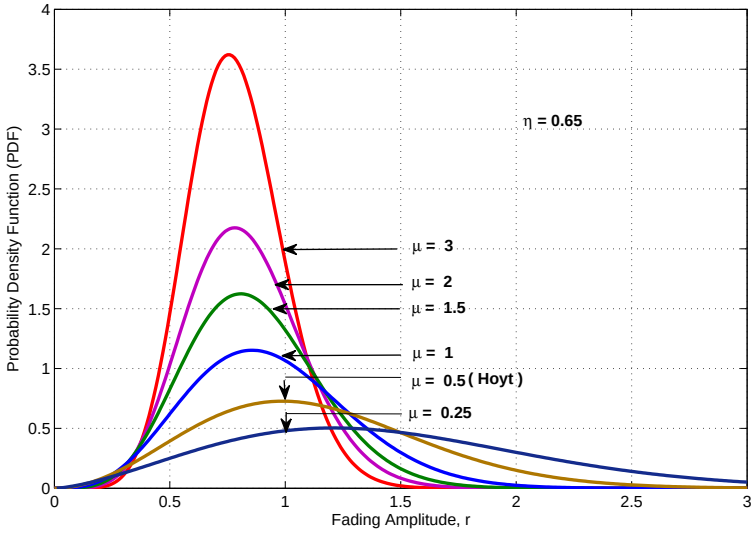

Figure 3.8 $\eta-\mu$ PDF for various values of μ and fixed η with $\Omega = 1$ in Format-1.

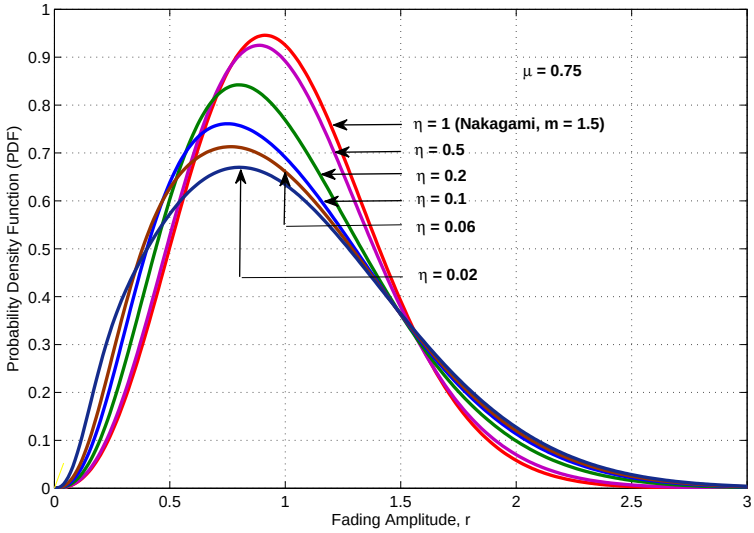

Figure 3.9 $\eta-\mu$ PDF for various values of η and fixed μ with $\Omega = 1$ in Format-1.

The previous expression is valid for $\gamma > 0$, whereas $\lambda > 0$ is the shape parameter of the distribution and $\theta > 0$ relates to the mean value of the corresponding fluctuations with $\overline{\gamma} = E(\gamma) = \theta$.

3.3.5 Composite Fading Models

It has been widely shown in the literature that multipath and shadowing effects typically occur simultaneously. Based on this, several composite models have been proposed for providing a holistic treatment of fading and are typically based on the superposition of multipath and shadowing distributions that ultimately lead to the desired PDF. Such distributions are employed in cases where the MSs are slowly moving or stationary [67,91] and also observed in land-mobile satellite systems subject to vegetative and/or urban shadowing [67,76]. In this fading environment, the receiver does not average out the envelope fading due to multipath but rather reacts to the instantaneous composite multipath/shadowed signal [75]. There are different approaches and various combinations suggested in literature for deriving composite distributions of interest. To this end, the authors in [111] formulated and derived the $\kappa-\mu$/gamma and $\eta-\mu$/gamma distributions, respectively. Furthermore, $\alpha-\kappa-\mu$/gamma composite distribution is proposed in [112], and is composed by the flexible $\alpha-\kappa-\mu$ non-linear generalized multipath model and the gamma shadowing model. More detailed discussions on various composite statistical distributions and their applications in digital communications over fading channels can be found, e.g., in [207] [1]

3.4 Performance Metrics of Fading channels

The digital communication systems use several performance metrics to evaluate the performance of wireless communications. In this discussion, we mention only the performance measures that are used in this thesis as outlined below.

3.4.1 Average-Signal-to-Noise Ratio

Signal-to-noise-ratio, often written as S/N or SNR, is a measure of signal strength relative to the background noise. SNR is usually expressed in dBs, i.e., SNR (dB) $= 10\log_{10}(\text{SNR})$. For instantaneous SNR γ at the output of a receiver with fading effects, the average SNR is defined as

[1] it is noted that the present dissertation does not consider composite fading conditions. However, the investigated topics can be also extended in this case and constitutes an interesting topic of future research.

$$\overline{\gamma} = \int_0^{\infty} \gamma f_{\gamma}(\gamma) \mathrm{d}\gamma. \tag{3.39}$$

The average SNR can also be obtained by taking the first derivative of the MGF expression in (3.10) with respect to s and evaluating the result at $s = 0$

$$\overline{\gamma} = \frac{\mathrm{d}M_{\gamma}(s)}{\mathrm{d}s}\Big|_{s=0}. \tag{3.40}$$

3.4.2 Outage Probability

Another important performance metric for wireless communications operated over fading channels is the so-called OP denoted by P_{out}. It is defined as the probability that the instantaneous SNR at the receiver output, γ, falls below a predefined outage threshold γ_{th}. Using this definition, the OP can be expressed mathematically as

$$P_{\text{out}} = \Pr\{\gamma < \gamma_{\text{th}}\} = \int_0^{\gamma_{\text{th}}} f_{\gamma}(\gamma) \mathrm{d}\gamma \ = F_{\gamma}(\gamma_{\text{th}}). \tag{3.41}$$

For many of the well-known fading distributions, the OP can be analytically evaluated using (3.41). Furthermore, P_{out} can be evaluated using the MGF of γ. More specifically, using the well-known Laplace transform property, $M_{\gamma}(s) = s\mathcal{L}\{F_{\gamma}(\gamma_{\text{th}})\}$, P_{out} can be obtained as

$$P_{\text{out}} = \mathcal{L}^{-1}\left\{\frac{M_{\gamma}(s)}{s}; s; t\right\}\Big|_{t=\gamma_{\text{th}}}. \tag{3.42}$$

Importantly, the inverse Laplace transform can be performed by restoring to the efficient Euler summation-based technique [123] or using the standard mathematical software packages, such as MAPLE, MATHEMATICA and MATLAB.

3.4.3 Average Symbol Error Rate

This performance measure is one of the most revealing regarding the wireless system behavior and the one most often illustrated in technical documents containing performance evaluation of wireless communication systems. In general, evaluation of the ASER is one of the most challenging tasks in digital communication systems. This is because, the conditional SER on fading channels is a nonlinear function of the instantaneous SNR, as the nature of the nonlinearity is a function of the modulation/detection scheme used by the system [76]. When the end-to-end γ in a system randomly varies, the ASER can be obtained by averaging the conditional symbol error rate for the desired M-ary signaling schemes in an AWGN channel, $P(e|\gamma)$, over the

PDF of γ, namely

$$P_{\text{SER}} = \int_0^\infty P(e|\gamma) f_\gamma(\gamma) \mathrm{d}\gamma. \tag{3.43}$$

For our purpose, we will also use some well-known results on the MGF-based approach to evaluate the ASER for $M-$PSK and $M-$QAM schemes. However, we note here that at sufficiently high SNR regime the above expression can be written as [124]

$$P_{\text{SER}} \approx (G_c \text{SNR})^{-G_d} \tag{3.44}$$

where the exponent G_d is related to the diversity gain (diversity order) and the constant G_c which multiplies the average SNR denotes the coding gain. The diversity gain determines the slope of the ASER versus average SNR curve, at high SNR, in a log-log scale, whereas G_c (expressed in dBs) represents the horizontal shift of the curve in SNR relative to the benchmark ASER curve of SNR^{-G_d} [124]. Due to transmit power constraints and/or regulatory requirements, increasing the diversity gain of the system is often the only way of reducing the error probability in systems with fading channels. Furthermore, for Rayleigh fading channels the diversity order is at most the number of independent fading coefficients [124]. In general, the higher diversity order of the system is the better is the performance of the system. The diversity order can also be defined in terms of OP at high SNR regime [6].

3.5 Diversity Combining Techniques

As mentioned previously, diversity reception is an efficient technique for mitigating the detrimental effects of fading in wireless communication systems at relatively low cost. The diversity techniques are classified as microdiversity, which is the focus of this section, and macrodiversity. Microdiversity techniques are designed to combat short-term multipath fading effects, whereas macrodiversity techniques are designed to mitigate long-term shadowing effects caused by obstructions, such as buildings, trees, and hills and are generally implemented by combining signals received by several base stations or access points [68]. The microdiversity techniques include time, frequency or space diversity methods. In this section, we focus our discussion on the concept of spatial diversity since it is a fundamental aspect in the cooperative diversity systems which is the main topic of this thesis. Spatial diversity gain can be achieved by employing diversity combining techniques at the receiver. Basically, these combining techniques are used to combine the multiple received copies of the same information bearing signal into an enhanced signal. As a result, the overall

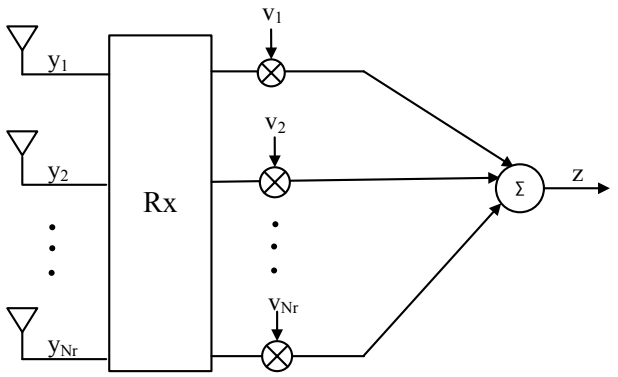

Figure 3.10 Example of a linear combiner.

SNR is increased which thus improves the radio link performance. The most popular diversity combining methods are EGC, SC and MRC [32, 68, 75, 76].

To study the performance of each diversity combining techniques, we consider an N_r-branch diversity receiver, as shown in Fig. 3.10, operated over independent Rayleigh flat fading environment with x denoting the transmitted symbol assuming that $E[|x|^2] = 1$. The signal received at the l-th, $l = 1, 2, \ldots, N_r$, diversity branch can be expressed as

$$y_l = \sqrt{P}|\alpha_l| \exp(j\theta_l)x + n_l. \tag{3.45}$$

In the above expression, the term $\alpha_l = |\alpha_l| \exp(j\theta_l)$ describes the fading coefficient in each branch with phase-angle θ_l. Assuming the I-CSI, i.e., the set of fading coefficients $\{\alpha_1, \alpha_2, \ldots, \alpha_{N_r}\}$ is known at the receiver, the receiver linearly combines the received signals before performing signal detection to obtain a combined signal of the form

$$z = \sum_{l=1}^{N_r} v_l y_l. \tag{3.46}$$

The weighting factors, v_l, can be determined according to the diversity combining technique used. Notice that while the basic diversity combining discussion is here focusing on a classical multiantenna receiver, the diversity combining processing in the receiver of the cooperation communication system is addressed in Subsection 3.5.4.

3.5.1 Equal-Gain Combining

In this scheme, the signals received on the N_r diversity branches are co-phased and then combined with equal weighting factor of $v_l = \exp(-j\theta_l)$. This scheme

achieves phase coherence at the receiver; thus, increases considerably the received signal strength. The SNR of the combiner output, assuming equal N_0 in each branch, is given by [2, 68]

$$\gamma_{\text{EGC}} = \frac{P\left(\sum_{l=1}^{N_r} |\alpha_l|\right)^2}{N_r N_0} \tag{3.47}$$

The CDF and PDF of γ_{EGC} for $N_r > 2$ do not exist in a closed-forms. However, for the independently identically distributed (i.i.d) Rayleigh fading with two-branch diversity ($N_r = 2$), the CDF in terms of the well-known Q function is given by [68, 75]

$$F_{\gamma_{\text{EGC}}}(\gamma) = 1 - e^{-2\frac{\gamma}{\overline{\gamma}}} - \sqrt{\frac{\pi\gamma}{\overline{\gamma}}} e^{-\frac{\gamma}{\overline{\gamma}}} \left(1 - 2Q\left(\sqrt{\frac{2\gamma}{\overline{\gamma}}}\right)\right). \tag{3.48}$$

The resulting OP can be expressed as

$$P_{\text{out}} = 1 - e^{-2\frac{\gamma_{\text{th}}}{\overline{\gamma}}} - \sqrt{\frac{\pi\gamma_{\text{th}}}{\overline{\gamma}}} e^{-\frac{\gamma_{\text{th}}}{\overline{\gamma}}} \left(1 - 2Q\left(\sqrt{\frac{2\gamma_{\text{th}}}{\overline{\gamma}}}\right)\right). \tag{3.49}$$

3.5.2 Selection Combining

In the EGC scheme, a considerable increase in SNR can be achieved by co-phasing the signals. However, in practice this is difficult to achieve as the phase of the channel varies rapidly over time. In such case, the signals cannot be necessarily perfectly co-phased and the addition of the signals may result in destructive interference and loss in diversity. An alternative approach is to adopt the SC technique where the combiner outputs the signal of the branch with the highest SNR. Since only one branch output is used, co-phasing of multiple branches is not required, so this scheme can be used with either coherent or differential modulation [68, 75]. In this scheme, the diversity combiner performs the following operation to select the branch with the maximum SNR

$$\gamma_{\text{SC}} = \max_{l,\ldots,N_r} \gamma_l. \tag{3.50}$$

Based on order statistics, the CDF of the SC can be expressed as

$$F_{\gamma_{\text{SC}}}(\gamma) = \Pr\{\gamma_{\text{SC}} \leq \gamma\} = \Pr\{\max_{l} \gamma_l \leq \gamma\} = \prod_{l=1}^{N_r} \Pr\{\gamma_l \leq \gamma\}. \tag{3.51}$$

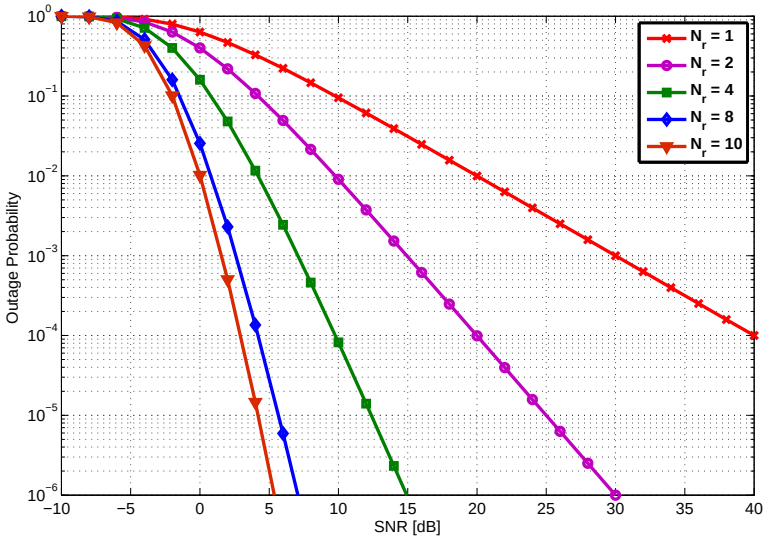

Figure 3.11 Outage probabilities of the selection combining scheme with i.i.d. Rayleigh fading.

Using the PDF for the exponential distribution in (3.12), the OP for identical $\overline{\gamma}$ in all diversity branches can be expressed as

$$\begin{aligned} P_{\text{out}}(\gamma_{\text{th}}) &= \prod_{l=1}^{N_r} \left(1 - e^{-\frac{\gamma_{\text{th}}}{\overline{\gamma}}}\right) \\ &= \left(1 - e^{-\frac{\gamma_{\text{th}}}{\overline{\gamma}}}\right)^{N_r}. \end{aligned} \tag{3.52}$$

At sufficiently high SNR, the above expression can be expressed [2, 68]

$$P_{\text{out}} \approx \left(\frac{\gamma_{\text{th}}}{\overline{\gamma}}\right)^{N_r}. \tag{3.53}$$

The SC scheme achieves diversity order of N_r which is the number of receive antennas. Fig. 3.11 shows the OP of SC versus SNR for $\gamma_{\text{th}} = 0$dB. It can be observed that the decaying rate of the OP increases with the number of receive antennas. The coding gain is more significant from $N_r = 1$ to $N_r = 2$ and this advantage is not increasing linearly as the number of diversity branches increases.

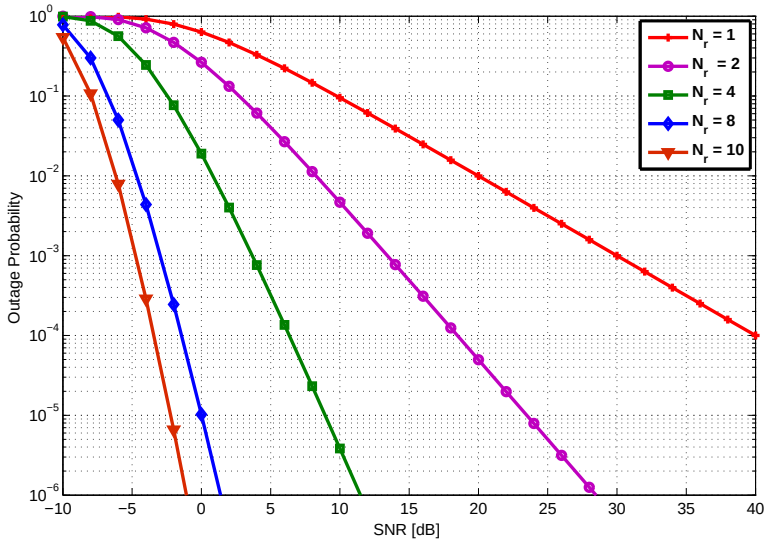

Figure 3.12 Outage probabilities of the maximal-ratio combining scheme with i.i.d. Rayleigh fading.

3.5.3 Maximal Ratio Combining

Both EGC and SC utilize the CSI to determine the weighting factors. However, the weighting factors applied in these schemes are not optimal in the sense of output SNR. To choose the weighting factors optimally, the MRC scheme is employed. MRC is an optimal linear combining technique that attains the highest SNR among any combining scheme regardless of the fading distribution [76]. In this scheme, the weighting factors that maximize the SNR, which minimizes the OP are given by [2]

$$v_l = \frac{\alpha_l^*}{N_0} = \frac{|\alpha_l| \exp(-j\theta_l)}{N_0}. \tag{3.54}$$

Here, the signals are weighted according to their local channel quality and are co-phased to achieve phase-coherent addition of signals at the receiver. Using (3.45) and (3.54), the output of the MRC combiner can be expressed as

$$\begin{aligned} z_{\text{MRC}} &= \sum_{l=1}^{N_r} v_l(\sqrt{P}\alpha_l x + n_l) \\ &= \sqrt{P}\left(\sum_{l=1}^{N_r} \frac{|\alpha_l|^2}{N_0}\right) x + \sum_{l=1}^{N_r} \frac{\alpha_l^*}{N_0} n_l. \end{aligned} \tag{3.55}$$

The resulting SNR is computed as [68, 75, 76]

$$\begin{aligned}\gamma_{\mathrm{MRC}} &= \frac{P\left(\sum_{l=1}^{N_r}|\alpha_l|^2/N_0\right)^2}{\sum_{l=1}^{N_r}|\alpha_l|^2/N_0} \\ &= \sum_{l=1}^{N_r}\gamma_l.\end{aligned} \tag{3.56}$$

Thus, the SNR of the combiner output is the sum of SNRs on each branch. It can be observed that the MRC scheme achieves the maximum SNR among all linear combining schemes.

Assuming i.i.d. Rayleigh fading on each branch with equal average branch SNR of $\bar{\gamma}$, the distribution of γ_{MRC} is chi-squared with $2N_r$ degrees of freedom, mean $N_r\bar{\gamma}$, variance $2N_r\bar{\gamma}$ and with the PDF given by [68]

$$f_{\gamma_{\mathrm{MRC}}}(\gamma) = \frac{\gamma^{N_r-1}e^{-\gamma/\bar{\gamma}}}{\bar{\gamma}^{N_r}(N_r-1)!}, \qquad \gamma \geq 0. \tag{3.57}$$

The corresponding OP can be computed as

$$P_{\mathrm{out}} = \Pr\{\gamma_{\mathrm{MRC}} \leq \gamma_{\mathrm{th}}\} = \int_0^{\gamma_{\mathrm{th}}} f_{\gamma_{\mathrm{MRC}}}(\gamma)\mathrm{d}\gamma = 1 - e^{-\gamma_{\mathrm{th}}/\bar{\gamma}}\sum_{l=1}^{N_r}\frac{(\gamma_{\mathrm{th}}/\bar{\gamma})^{l-1}}{(l-1)!}. \tag{3.58}$$

Furthermore, the OP at sufficiently high SNR regime can be approximated as [68, 75]

$$P_{\mathrm{out}} \approx \frac{1}{N_r!}\left(\frac{\gamma_{\mathrm{th}}}{\bar{\gamma}}\right)^{N_r}. \tag{3.59}$$

The above expression reveals that the MRC scheme achieves a full diversity order of N_r similar to that of SC scheme. However, an extra gain of $(10/N_r)\log_{10}(N_r!)$ dB can be obtained by using the optimal MRC scheme. Fig. 3.12 depicts the OP as a function of SNR of the MRC scheme for $\gamma_{\mathrm{th}} = 0$dB with different N_r. By comparing Fig. 3.11 and Fig. 3.12 at the same OP, we can observe that the MRC scheme achieves higher gain than the SC scheme. For instance, at $P_{\mathrm{out}} = 10^{-4}$ the MRC scheme outperforms the SC scheme by about 6.6 dB when $N_r = 10$. Extensive performance comparison between SC, EGC and MRC in terms of BER can be found in [76].

3.5.4 Diversity Combining at Destination Node in Cooperative Communications

It has already been mentioned that combining received signals at the receiver results to significant performance increase. To this effect, any of the combining methods discussed in Section 3.5 can be used to combine the direct and relayed signals over orthogonal channels in cooperative transmission schemes instead of across different antennas. For example, the received signals $y_{S,D}$ and $y_{R,D}$ can be combined across two time-slots in a time-based cooperative system that uses any of the relaying strategies discussed in Section 2.4. The MRC combining technique is considered the most effective as it attains the highest SNR among combining methods. To this effect, it can be employed in maximizing the received SNR at the destination in a cooperative system. In this context, the signals received in Phase I and Phase II are multiplied by the weighting coefficients v_1 and v_2 to obtain the received signal at the destination as [31]

$$y_D = v_1 y_{S,D} + v_2 y_{R,D} \tag{3.60}$$

where the factors v_1 and v_2 are determined such that the SNR of the MRC output is maximized. Here, the signals are weighted according to their local channel quality and are co-phased to achieve phase-coherent addition of signals at the destination.

In what follows, the MRC scheme will be used to optimally combine the direct and relayed signals at the destination in the single and multi-relay regenerative cooperative systems in Chapter 4 and Chapter 5, respectively.

Chapter 4

Error Analysis and Energy-Efficiency Optimization of Regenerative Relay Systems under Spatial Correlation

In this chapter, we investigate the error rate analysis and EE optimization of regenerative cooperative networks in the presence of multipath fading under spatial correlation. Exact and asymptotic expressions are, first, derived for the SER of $M-$QAM and $M-$PSK modulations assuming a dual-hop DF relay system, spatially correlated paths, Nakagami$-m$ multipath fading and MRC scheme. The derived expressions are subsequently employed in quantifying the energy consumption of the considered system, incorporating both transmit energy and the energy consumed by the transceiver circuits, as well as in deriving the OPA formulations for minimizing energy consumption under certain QoS requirements. A relatively harsh PL model that also accounts for realistic D2D communications is adopted in numerical evaluations and various useful insights are provided for the design of future low-energy wireless network deployments. All the results and analysis presented in this chapter are based on the author's published work in [113, 114].

4.1 Background and Overview of Contributions

Future wireless networks are expected to support high-speed data transmission, efficient wireless access, high QoS and reliable network coverage with reduced processing time and energy as well as widespread use of smart phones and other intelligent mobile devices. However, the currently witnessed scarcity of fundamental resources, such as power and bandwidth, constitutes a significant challenge to satisfy these demands while as mentioned in the previous chapter the wireless channel impairments such as multipath fading, shadowing and interference degrade information signals during wireless propagation. Furthermore, most wireless devices, such as terminals of mobile cellular, ad-hoc and wireless sensor networks, which are widely used in battlefield monitoring, environmental data collection, health care monitoring, disaster management and in other related devices, all the nodes cooperate with each other to execute the task are typically powered by small energy constrained batteries where replacement is rather difficult and costly [125, 126]. Therefore, finding a robust strategy for EE transmission and minimized energy consumption per successfully communicated information bit is essential in effective design and deployment of wireless systems. This accounts, for example, for cases such as low-energy sensor networks in ecological environment monitoring as well as energy consumption in infrastructure devices of cellular systems. In addition, it is in line with global policies and strategies on low energy consumption and awareness on environmental issues which, among others, has led to the rapid emerge of green communications with the objective of designing energy-efficient wireless systems without sacrificing the user QoS requirements [127, 128].

Multi-antenna communication system have shown their effectiveness in increasing network capacity by exploiting the spatial diversity with multiple antennas. However, this typically comes at a cost of complex transceiver circuitry and large amount of signal processing power that may lead to large power consumption at the circuit level. Furthermore, it is not currently feasible to embody large multi-antenna systems at hand held terminals due to spatial restrictions. As a result, cooperative communication systems have been proposed as an alternative solution. These systems improve coverage as well as performance under fading effects and have attracted significant attention due to their ability to overcome the limitations of the resource constrained wireless access networks, e.g., [6,8,118,129–138]. In addition, cooperative communication has shown its effectiveness in establishing the new emerging cellular technologies of D2D communication, which is a promising component of the LTE-Advanced systems for supporting peer-to-peer services, enhancing spectrum utilization, increasing cellular capacity, improving the user throughput, and for extending the battery life-

time of UEs [139,140]. The key feature of cooperative communications is that wireless agents, share and coordinate their resources for relaying messages to each other and for transmitting information signals over the numerous independent paths in the wireless network instead of competing for them, which ultimately enhances information transmission quality over the unreliable wireless channel. In this context, various resource allocation algorithms and techniques have been proposed for improving the EE of resource constrained wireless networks. Specifically, Cui *et al.* [141] analyzed energy-efficient DT adopting higher-level modulation for short distances, where circuit power is more dominant than transmission power. It was also suggested that high energy reduction can be achieved by optimizing the transmission time and the modulation parameters, particularly for short transmission distances. Devarajan *et al.* [142] addressed the OPA and throughput transmission strategy for minimizing the total energy consumption required to transmit a given number of bits. In [143], minimization of two-hop transmission energy with joint relay selection and power control was proposed for two policies: 1) for minimizing the energy consumption per data packet; and 2) for maximizing the network lifetime. In the same context, [144–148] addressed the modulation optimization for minimizing the total energy consumption for $M-$QAM, whereas energy-efficient cooperative communication in clustered sensor networks was investigated in [149]. EE in cooperative networks was also analyzed in [150–157] by optimizing the energy consumption. This was based on the involved relay decoding strategy, modulation parameters, number of relay nodes and their distance from the source and the destination nodes. Likewise, an energy-efficient scheme was proposed in [158] by exploiting the wireless broadcast nature and the node overhearing capability, whereas an optimal energy-efficient strategy based on the cooperative network parameters and transmission rate was reported in [159]. In the same context, the EE of cooperative and non-cooperative wireless sensor networks for given end-to-end throughput requirements was investigated in [160]. Finally, [161] analyzed realistic scenarios of energy-efficient infrastructure-to-vehicle communications.

It is also widely known that fading phenomena constitute a crucial factor of performance degradation in conventional and emerging wireless communication systems. Based on this, numerous investigations have addressed the effect of different types of fading conditions on the performance of cooperative communications, e.g., [26, 30, 39, 131, 135, 138, 166, 167]. However, the vast majority of the reported investigations assume that the involved communication paths are statistically independent to each-other. Nevertheless, this assumption is rather simplistic as in realistic cooperative communication scenarios the wireless channels may be spatially correlated, which should be taken into account particularly for deployments relating

to low-energy consumption requirements. Based on this, the spatial correlation in relay communications over fading channels was addressed in [168], whereas [169] investigated the performance of a DF system with $M-$PSK modulated signals in triple correlated branches over Nakagami$-m$ fading channels using selection combining. In the same context, [170] analyzed the performance of a DF system with orthogonal space time transmission over spatially correlated Nakagami$-m$ fading channels for integer values of m . The performance of a two hop AF relay network with beamforming and spatial correlation for the case that the source and destination are equipped with multiple antennas while the relay is equipped with a single antenna was investigated in [171]. Likewise, spatial correlation in the context of indoor office environments and multi-antenna AF relaying with keyhole effects was analyzed in [172] and [173], respectively. Furthermore, the authors in [174–178] analyzed the effects of spatial correlation on the performance of fixed relaying schemes. However, in the aforementioned investigations as well as in the related analysis that exists in literature, a comprehensive exact and asymptotic error rate analysis for regenerative systems over spatially correlated channels using MRC as well as a detailed EE analysis and optimization, have not been reported in the open technical literature.

Motivated by the above, the aim of this chapter is twofold. First, we derive exact analytic expressions for the SER of a two-hop DF relay system over spatially correlated Nakagami$-m$ fading channels for both $M-$QAM and $M-$PSK constellations along with simple and accurate asymptotic expressions for high SNR values. Second, we provide a comprehensive analysis of EE and the corresponding optimization in terms of power allocation between cooperating devices by minimizing the average total energy consumption under given constraints of target BER and total transmit power of the system.

In more details, the technical contributions of this chapter are as follows:

- Exact expressions are derived for the end-to-end SER of $M-$QAM and $M-$PSK based dual-hop regenerative relay network systems with MRC reception over Nakagami$-m$ multipath fading channels with arbitrary spatial correlation between source-destination (S-D) and relay-destination (R-D) links.

- Simple asymptotic expressions are derived for the above scenarios for high SNR values.

- The offered analytic results are employed in the comprehensive energy optimization analysis based on minimizing the average total energy consumption of the overall regenerative relay network under a given QoS target, in terms of BER, and maximum transmit power constraints.

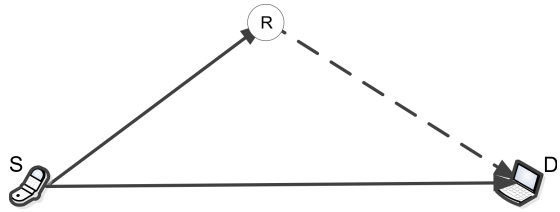

Figure 4.1 A dual-hop cooperative single relay model.

4.2 System and Channel Model

We consider a two-hop cooperative radio access system model consisting of source node (S), a relay node (R) and a destination node (D), where each node is equipped with a single antenna, as illustrated in Fig. 4.1. Without loss of generality, the system can represent both a conventional and emerging communication scenarios such as, for example, a mobile ad-hoc network or a V2V communication system. The cooperative strategy is based on a HD-DF relaying where transmission is performed using time division multiplexing. It is also assumed that the destination is equipped with MRC reception and that information signals are subject to multipath fading conditions that follow the Nakagami$-m$ distribution[1]

In phase I, the source broadcasts the signal to both destination and relay nodes and the corresponding received signals can be expressed as

$$y_{S,D} = \sqrt{\frac{P_S}{P_{L_{S,D}}}}\alpha_{S,D}x + n_{S,D} \tag{4.1}$$

and

$$y_{S,R} = \sqrt{\frac{P_S}{P_{L_{S,R}}}}\alpha_{S,R}x + n_{S,R} \tag{4.2}$$

respectively, where $P_{L_{S,D}}$ and $P_{L_{S,R}}$ denote the PL values in the S-D and S-R paths, respectively. The transmitted symbol, x, is normalized to unit energy in the first transmission phase. The relay checks whether the received signal can be decoded correctly which can be, for example, realized by examining the included cyclic-redundancy-check (CRC) digits or the received SNR levels [167, 168]. Based on this, if the signal is successfully decoded, the relay forwards it to the destination during phase II with power $\bar{P}_R = P_R$; otherwise, the relay does not transmit and remains idle with $\bar{P}_R = 0$.

[1]It is noted that the considered system requires the least resources in terms of bandwidth and power compared to multi-relay assisted transmission and thus, it can be adequate for low complexity and low-energy wireless networks.

Hence, the signal at the destination during phase II can be represented as follows:

$$y_{R,D} = \sqrt{\frac{\bar{P}_R}{P_{L_{R,D}}}}\,\alpha_{R,D}x + n_{R,D} \tag{4.3}$$

where $P_{L_{R,D}}$ is the PL of the R-D path. Finally, the destination combines the received direct and relayed signals based on MRC principle where the combined SNR can be expressed as follows [168, 179]:

$$\gamma_{\text{MRC}} = \frac{\left(\frac{P_S}{P_{L_{S,D}}}\right)|\alpha_{S,D}|^2 + \left(\frac{\bar{P}_R}{P_{L_{R,D}}}\right)|\alpha_{R,D}|^2}{N_0}. \tag{4.4}$$

The fading between the devices is assumed to follow the Nakagami$-m$ distribution. As explained in the previous chapter, the channel power gains $|\alpha_{S,D}|^2$, $|\alpha_{S,R}|^2$ and $|\alpha_{R,D}|^2$ follow the gamma distribution with different power parameters, $1/\Omega_{S,D}$, $1/\Omega_{S,R}$, $1/\Omega_{R,D}$, and fading parameters of $m_{S,D}$, $m_{S,R}$ and $m_{R,D}$, respectively.

In the considered regenerative system, arbitrary spatial correlation is assumed to exist between the S-D and R-D paths, as also adopted in the semi-analytical contribution of [168]. This assumption is an extension beyond classical totally uncorrelated fading scenarios, and can be considered realistic, particularly when the source and relay are relatively close to each other and when the relay is not necessarily aligned with the source and destination i.e. the S-R path is practically shorter than R-D and S-D paths. In addition, the relay forwards information signals to the destination only upon successful decoding and thus, it is realistic to quantify the effects of spatial correlation at the destination i.e. between S-D and R-D paths, as the final decoding result at D naturally depends on the reliability of both of these observations. To this effect, the corresponding MGF for the case of Nakagami$-m$ is given as follows: [76]

$$M(s) = \left(1 + \frac{\left(\frac{\overline{\gamma}_{S,D}}{P_{L_{S,D}}} + \frac{\overline{\gamma}_{R,D}}{P_{L_{R,D}}}\right)}{m}s + \frac{\frac{(1-\rho)\overline{\gamma}_{S,D}\overline{\gamma}_{R,D}}{(P_{L_{S,D}}P_{L_{R,D}})}}{m^2}s^2\right)^{-m} \tag{4.5}$$

where $\overline{\gamma}_{S,D}$ and $\overline{\gamma}_{R,D}$ are the corresponding average SNR values and

$$\rho = \frac{\text{Cov}(|\alpha_{S,D}|^2, |\alpha_{R,D}|^2)}{\sqrt{\text{Var}(|\alpha_{S,D}|^2)\text{Var}(|\alpha_{R,D}|^2)}} \tag{4.6}$$

represents the correlation coefficient [76, 90]. It is acknowledged that other practical impairments, such as co-channel interference, are not considered in this analysis.

4.3 SER for $M-$QAM Modulation over Nakagami$-m$ Fading with Spatial Correlation

This section is devoted to the error probability analysis of the dual-hop DF based cooperative network over Nakagami$-m$ fading channels with spatial correlation between the direct and the relay-destination paths. To this effect and assuming MRC reception, the average end-to-end SER at the destination terminal can be expressed as [168],

$$P_{\text{SER}}^{\text{C}} = F_{\text{QAM}}\left[\frac{1}{\left(1+\frac{P_S\Omega_{S,D}\,g_{\text{QAM}}}{N_0 m_c P_{L_{S,D}}\sin^2\theta}\right)^{m_c}}\right] F_{\text{QAM}}\left[\frac{1}{\left(1+\frac{P_S\,\Omega_{S,R}\,g_{\text{QAM}}}{N_0 m_{S,R} P_{L_{S,R}}\sin^2\theta}\right)^{m_{S,R}}}\right]$$
$$+F_{\text{QAM}}\left[\frac{1}{\left(1+\frac{[(P_S\Omega_{S,D}/P_{L_{S,D}})+(P_R\Omega_{R,D}/\,P_{L_{R,D}})]\;g_{\text{QAM}}}{N_0 m_c\sin^2\theta}+\frac{(1-\rho)P_S P_R\Omega_{S,D}\Omega_{R,D}g_{\text{QAM}}^2}{N_0^2 P_{L_{S,D}}P_{L_{R,D}}m_c^2\sin^4\theta}\right)^{m_c}}\right]$$
$$\times\left\{1-F_{\text{QAM}}\left[\frac{1}{\left(1+\frac{P_S\,\Omega_{S,R}\,g_{\text{QAM}}}{N_0 P_{L_{S,R}} m_{S,R}\sin^2\theta}\right)^{m_{S,R}}}\right]\right\} \tag{4.7}$$

where $m_c = m_{S,D} = m_{R,D}$, $g_{\text{QAM}} = 3/2(M-1)$ and

$$F_{\text{QAM}}\left[v(\theta)\right] = \frac{4}{\pi}\left(1-\frac{1}{\sqrt{M}}\right)\int_0^{\pi/2} v(\theta)\,\mathrm{d}\theta - \frac{4}{\pi}\left(1-\frac{1}{\sqrt{M}}\right)^2\int_0^{\pi/4} v(\theta)\,\mathrm{d}\theta. \tag{4.8}$$

The first term in (4.7) refers to the SER at the destination when the relay incorrectly decodes the received signal, whereas the second term denotes the SER at the destination when the relay decodes correctly. The integral representation in (4.8) is used for evaluating the average end-to-end SER of the system numerically. In what follows, we first derive an exact expression for the average SER in the case of direct communication mode. This expression is subsequently employed in the derivation of exact expressions for the average SER of $M-$QAM and $M-$PSK modulated regenerative systems over Nakagami$-m$ fading channels with spatial correlation. Furthermore, it is used in the analysis of the energy consumption model and energy minimization in Section 4.6 as it allows the derivation of an accurate expression for the energy consumption in the DT, which acts as a benchmark in the evaluation of the energy reduction of the cooperative system under certain QoS requirement and total maxi-

mum transmit power constraints.

4.3.1 Exact SER for the Direct Transmission

Here, we derive an exact expression for the average SER of the DT scheme for $M-$QAM constellations, which is particularly useful for the subsequent error and EE analysis of the considered system. [2]

Theorem 1. *For $P_S, P_{L_{S,D}}, \Omega_{S,D}, N_0, g_{\text{QAM}} \in \mathbb{R}^+$, $M \in \mathbb{N}$ and $m_{S,D} \geq \frac{1}{2}$, the SER of $M-QAM$ scheme for DT scheme can be expressed as*

$$P_{\text{SER}}^{\text{D}} = \frac{2(\sqrt{M}-1)N_0^{m_{S,D}} m_{S,D}^{m_{S,D}} P_{L_{S,D}}}{\sqrt{\pi} M (m_{S,D}\, N_0 P_{L_{S,D}} + P_S \Omega_{S,D} g_{\text{QAM}})^{m_{S,D}}} \times \left\{ \frac{\Gamma\left(m_{S,D}+\frac{1}{2}\right)}{\Gamma(m_{S,D}+1)}\, {}_2F_1\left(m_{S,D}, \frac{1}{2}; m_{S,D}+1; \frac{m_{S,D} N_0 P_{L_{S,D}}}{m_{S,D} N_0 P_{L_{S,D}} + P_S \Omega_{S,D} g_{\text{QAM}}}\right) + \frac{\sqrt{2}(\sqrt{M}-1)}{\sqrt{\pi}} F_1\left(\frac{1}{2}; \frac{1}{2}-m_{S,D}, m_{S,D}; \frac{3}{2}; \frac{1}{2}, \frac{m_{S,D} N_0 P_{L_{S,D}}}{2(m_{S,D} N_0 P_{L_{S,D}} + P_S \Omega_{S,D} g_{\text{QAM}})}\right) \right\} \tag{4.9}$$

where ${}_2F_1(.)$ and $F_1(.)$ denote the Gauss hypergeometric function and the Appell hypergeometric function of the first kind, respectively [104].

Proof. The average end-to-end SER for the direct transmission can be expressed as,

$$P_{\text{SER}}^{\text{D}} = F_{\text{QAM}}\left[\left(1 + \frac{P_S\, \Omega_{S,D}\, g_{\text{QAM}}}{N_0\, P_{L_{S,D}} m_{S,D} \sin^2(\theta)}\right)^{-m_{S,D}}\right]. \tag{4.10}$$

Evidently, a closed-form expression for (4.10) is subject to analytic evaluation of the following two definite integrals,

$$\mathcal{I}\left(a, m; 0, \frac{\pi}{2}\right) = \int_0^{\pi/2} \frac{1}{\left(1+\frac{a}{\sin^2(\theta)}\right)^m} d\theta \tag{4.11}$$

$$\mathcal{I}\left(a, m; 0, \frac{\pi}{4}\right) = \int_0^{\pi/4} \frac{1}{\left(1+\frac{a}{\sin^2(\theta)}\right)^m} d\theta. \tag{4.12}$$

[2] To differentiate notionally from the symbolic expression of the end-to-end average SER and BER of the cooperative system, we adopt $P_{\text{SER}}^{\text{D}}$ and BER^{D} for the DT case in this chapter.

By re-writing the indefinite form of the previous class of integrals as,

$$\mathcal{I}(a,m) = \int \frac{\sin^{2m}(\theta)}{\left(\sin^2(\theta)+a\right)^m} d\theta \tag{4.13}$$

and setting $u = \cos^2(\theta)$, one obtains,

$$\mathcal{I}(a,m) = -\int \frac{(1-u)^{m-\frac{1}{2}}}{2\sqrt{u}(1-u+a)^m} du. \tag{4.14}$$

The above integral can be expressed in closed-form in terms of the Appell hypergeometric function of the first kind, namely,

$$\mathcal{I}(a,m) = -\frac{\cos(\theta)}{(1+a)^m} F_1\left(\frac{1}{2}; \frac{1}{2}-m, m; \frac{3}{2}; \cos^2(\theta), \frac{\cos^2(\theta)}{1+a}\right). \tag{4.15}$$

Equation (4.15) reduces to zero when $\theta = \pi/2$. To this effect, it immediately follows that,

$$\mathcal{I}\left(a,m,0,\frac{\pi}{2}\right) = \frac{1}{(1+a)^m} F_1\left(\frac{1}{2}; \frac{1}{2}-m, m; \frac{3}{2}; 1, \frac{1}{1+a}\right) \tag{4.16}$$

which with the aid of the properties of $F_1(.)$ function can be equivalently expressed as,

$$\mathcal{I}\left(a,m,0,\frac{\pi}{2}\right) = \frac{\sqrt{\pi}\Gamma\left(m+\frac{1}{2}\right)}{2(1+a)^m\Gamma(m+1)} {}_2F_1\left(\frac{1}{2}, m; m+1; \frac{1}{1+a}\right). \tag{4.17}$$

In the same context,

$$\begin{aligned}&\mathcal{I}\left(a,m,0,\frac{\pi}{4}\right)\\ &= \frac{1}{(1+a)^m}\left\{F_1\left(\frac{1}{2}; \frac{1}{2}-m, m; \frac{3}{2}; 1, \frac{1}{1+a}\right) - \frac{1}{\sqrt{2}} F_1\left(\frac{1}{2}; \frac{1}{2}-m, m; \frac{3}{2}; \frac{1}{2}, \frac{1}{2(1+a)}\right)\right\}\end{aligned} \tag{4.18}$$

which can be alternatively expressed as,

$$\mathcal{I}\left(a,m,0,\frac{\pi}{4}\right) = \frac{\sqrt{\pi}\Gamma\left(m+\frac{1}{2}\right)\ {}_2F_1\left(\frac{1}{2}, m; m+1; \frac{1}{1+a}\right)}{2(1+a)^m\Gamma(m+1)} - \frac{F_1\left(\frac{1}{2}; \frac{1}{2}-m, m; \frac{3}{2}; \frac{1}{2}, \frac{1}{2(1+a)}\right)}{\sqrt{2}(1+a)^m}. \tag{4.19}$$

By performing the necessary change of variables in (4.17) and (4.19) and substituting in (4.10) yields (4.9), which completes the proof. □

4.3.2 Exact SER for the Cooperative-Transmission

Applying Theorem 1 and capitalizing on the proof of Lemma 1, this subsection is devoted on the derivation of a novel exact expression for the average end-to-end SER of the CT scenario when the involved relay node decodes and forwards successfully the decoded information signals to the destination. To this end, it is essential to derive first the exact expressions for two indefinite trigonometric integrals, which are generic and can be particularly useful in various applications relating to natural sciences and engineering, including in performance evaluation of wireless communications.

Lemma 1. *For $a, b, m \in \mathbb{R}^+$ and $2m - \frac{1}{2} \in \mathbb{N}$, the following closed-form expression is valid,*

$$\begin{aligned}\mathcal{J}(a,b,m) &= \int \frac{1}{\left(1+\frac{a}{\sin^2(\theta)}+\frac{b}{\sin^4(\theta)}\right)^m}\mathrm{d}\theta \\ &= -\sum_{l=0}^{2m-\frac{1}{2}} \binom{2m-\frac{1}{2}}{l} (-1)^l \frac{\left(a+2\sin^2(\theta)-\sqrt{a^2-4b}\right)^m \left(a+2\sin^2(\theta)+\sqrt{a^2-4b}\right)^m}{\left(2+a-\sqrt{a^2-4b}\right)^m \left(2+a+\sqrt{a^2-4b}\right)^m} \\ &\times \frac{\cos^{1+2l}(\theta)}{(1+2l)} \frac{F_1\left(l+\frac{1}{2}; m, m; l+\frac{3}{2}; \frac{2\cos^2(\theta)}{2+a-\sqrt{a^2-4b}}, \frac{2\cos^2(\theta)}{2+a+\sqrt{a^2-4b}}\right)}{\left(\sin^4(\theta)+a\sin^2(\theta)+b\right)^m} + C.\end{aligned} \tag{4.20}$$

Proof. The proof is provided in Appendix A. □

Lemma 2. *For $a, b, m, n \in \mathbb{R}^+$ and $m + n - \frac{1}{2} \in \mathbb{N}$, the following closed-form expression is valid,*

$$\begin{aligned}\mathcal{K}(a,b,m,n) &= \int \frac{1}{\left(1+\frac{a}{\sin^2(\theta)}\right)^m \left(1+\frac{b}{\sin^2(\theta)}\right)^n}\mathrm{d}\theta \\ &= -\sum_{l=0}^{m+n-\frac{1}{2}} \binom{m+n-\frac{1}{2}}{l} \frac{(-1)^l \cos^{1+2l}(\theta)\, F_1\left(l+\frac{1}{2}; m, n; l+\frac{3}{2}; \frac{\cos^2(\theta)}{1+a}, \frac{\cos^2(\theta)}{1+b}\right)}{(1+2l)(1+a)^m(1+b)^n} + C.\end{aligned} \tag{4.21}$$

Proof. The proof is provided in Appendix B. □

To the best of the authors' knowledge, the generic solutions in the above Lemmas have not been previously reported in the open technical literature. These results are employed in the subsequent sections for analyzing the performance of the considered system over fading channels.

Theorem 2. *For* $\{P_S, P_R, P_{L_{S,D}}, P_{L_{S,R}}, P_{L_{R,D}}, N_0\} \in \mathbb{R}^+$, $\{\Omega_{S,D}, \Omega_{S,R}, \Omega_{R,D}\} \in \mathbb{R}^+$, $M \in \mathbb{N}$, $m_{S,D} \geq \frac{1}{2}$, $m_{S,R} \geq \frac{1}{2}$, $m_{R,D} \geq \frac{1}{2}$, $2m_c - \frac{1}{2} \in \mathbb{N}$ *and* $0 \leq \rho < 1$, *the SER of* $M-QAM$ *based DF relaying over spatially correlated Nakagami−m fading channels, can be expressed as follows:*

$$
\begin{aligned}
P_{\mathrm{SER}}^{\mathrm{C}} = & \left\{ \frac{2\left(m_c - \frac{1}{2}\right)! \, {}_2F_1\left(m_c, \frac{1}{2}; m_c + 1; \frac{1}{1+a_1}\right)}{\sqrt{\pi}\, m_c!\, M(\sqrt{M}-1)^{-1}(1+a_1)^{m_c}} + \frac{2\sqrt{2}\, F_1\left(\frac{1}{2}; \frac{1}{2} - m_c, m_c; \frac{3}{2}; \frac{1}{2}, \frac{1}{2+2a_1}\right)}{\pi\, M(\sqrt{M}-1)^{-2}(1+a_1)^{m_c}} \right\} \\
& \times \left\{ \frac{2\left(m_{S,R} - \frac{1}{2}\right)! \, {}_2F_1\left(m_{S,R}, \frac{1}{2}; m_{S,R} + 1; \frac{1}{1+b_1}\right)}{\sqrt{\pi}\, m_{S,R}!\, M(\sqrt{M}-1)^{-1}(1+b_1)^{m_{S,R}}} + \frac{2\sqrt{2} F_1\left(\frac{1}{2}; \frac{1}{2} - m_{S,R}, m_{S,R}; \frac{3}{2}; \frac{1}{2}, \frac{1}{2+2b_1}\right)}{\pi\, M(\sqrt{M}-1)^{-2}(1+b_1)^{m_{S,R}}} \right\} \\
& + \left\{ 1 - \frac{2\left(m_{S,R} - \frac{1}{2}\right)! \, {}_2F_1\left(m_{S,R}, \frac{1}{2}; m_{S,R} + 1; \frac{1}{1+b_1}\right)}{\sqrt{\pi}\, m_{S,R}!\, M(\sqrt{M}-1)^{-1}(1+b_1)^{m_{S,R}}} \right. \\
& \qquad \left. - \frac{2\sqrt{2} F_1\left(\frac{1}{2}; \frac{1}{2} - m_{S,R}, m_{S,R}; \frac{3}{2}; \frac{1}{2}, \frac{1}{2+2b_1}\right)}{\pi\, M(\sqrt{M}-1)^{-2}(1+b_1)^{m_{S,R}}} \right\} \\
& \times \left\{ \sum_{l=0}^{2m_c - \frac{1}{2}} \binom{2m_c - \frac{1}{2}}{l} \frac{(-1)^l 4(\sqrt{M}-1)^2 2^{m_c - l - \frac{1}{2}} F_1\left(l + \frac{1}{2}; m_c, m_c; l + \frac{3}{2}; 2\mathcal{A}, 2\mathcal{B}\right)}{M\pi(1+2l)[1 + 2(a_1 + c_1) 4 a_1 d_1]^{m_c} \left[(1-2\mathcal{A})(1-2\mathcal{B})\right]^{-m_c}} \right. \\
& \left. + \sum_{l=0}^{2m_c - \frac{1}{2}} \binom{2m_c - \frac{1}{2}}{l} \frac{(-1)^l 4(\sqrt{M}-1) F_1\left(l + \frac{1}{2}; m_c, m_c; l + \frac{3}{2}; \mathcal{A}, \mathcal{B}\right)}{\pi M (1+2l)(a_1 d_1)^{m_c} (1-\mathcal{A})^{-m_c} (1-\mathcal{B})^{-m_c}} \right\}
\end{aligned}
\tag{4.22}
$$

where

$$
a_1 = \frac{P_S \Omega_{S,D} g_{\mathrm{QAM}}}{P_{L_{S,D}} m_c N_0}, \tag{4.23}
$$

$$
b_1 = \frac{P_S \Omega_{S,R} g_{\mathrm{QAM}}}{P_{L_{S,R}} N_0 m_{S,R}}, \tag{4.24}
$$

$$
c_1 = \frac{P_R \Omega_{R,D} g_{\mathrm{QAM}}}{P_{L_{R,D}} N_0 m_c}, \tag{4.25}
$$

$$
d_1 = \frac{(1-\rho) P_R \Omega_{R,D} g_{\mathrm{QAM}}}{P_{L_{R,D}} N_0 m_c} \tag{4.26}
$$

and

$$
\left\{ {\mathcal{A} \atop \mathcal{B}} \right\} = \frac{1}{2 + a_1 + c_1 \left\{ {- \atop +} \right\} \sqrt{(a_1 + c_1)^2 - 4 a_1 d_1}}. \tag{4.27}
$$

Proof. The first term in (4.7) corresponds to the direct transmission and thus, it can be expressed in closed-form based on Theorem 1. Likewise, the second and the fourth term in (4.7) have the same algebraic representation as (4.11) and (4.12).

Therefore, they can be readily expressed in closed-form by making the necessary change of variables and substituting in (4.17) and (4.19). As for the third term in (4.7), it is noticed that it has the same algebraic representation with (4.20). As a result, a closed-form expression is deduced by determining the following specific cases in (4.20), which practically evaluate (4.8), i.e.,

$$\mathcal{J}\left(a,b,m,0,\left\{\begin{smallmatrix}\pi/2\\ \pi/4\end{smallmatrix}\right\}\right)=\int_0^{\left\{\begin{smallmatrix}\pi/2\\ \pi/4\end{smallmatrix}\right\}}\frac{\mathrm{d}\theta}{\left(1+\frac{a}{\sin^2(\theta)}+\frac{b}{\sin^4(\theta)}\right)^m}. \tag{4.28}$$

Therefore, by carrying out some long but basic algebraic manipulations and substituting in (4.7) along with the aforementioned closed-form expressions, one obtains (4.22), which completes the proof. □

Remark 1. *Equation* (4.22) *reduces to the uncorrelated scenario by setting* $\rho=0$. *However, an alternative expression for this case which is valid for the case that* $\left\{2m_c-\frac{1}{2}\right\}\in\mathbb{N}$ *can also be deduced by applying the derived expressions in Theorem 1 and Lemma 2 in [168, Eq. (11)], namely*

$$\begin{aligned}
&P_{\mathrm{SER}}^{\mathrm{C}}\\
&=\left\{\frac{2\Gamma\left(m_c+\frac{1}{2}\right)\,{}_2F_1\left(m_c,\frac{1}{2};1+m_c;\frac{1}{1+a_1}\right)}{\sqrt{\pi}M(\sqrt{M}-1)^{-1}\Gamma(1+m_c)(1+a_1)^{m_c}}-\frac{2\sqrt{2}F_1\left(\frac{1}{2};\frac{1}{2}-m_c,m_c;\frac{3}{2};\frac{1}{2},\frac{1}{2+2a_1}\right)}{\pi(\sqrt{M}-1)^{-2}M(1+a_1)^{m_c}}\right\}\\
&\times\left\{\frac{2\Gamma\left(m_{S,R}+\frac{1}{2}\right)\,{}_2F_1\left(m_{S,R},\frac{1}{2};1+m_{S,R};\frac{1}{1+b_1}\right)}{\sqrt{\pi}M(\sqrt{M}-1)^{-1}\Gamma(1+m_{S,R})(1+b_1)^{m_{S,R}}}\right.\\
&\qquad\left.-\frac{2\sqrt{2}F_1\left(\frac{1}{2};\frac{1}{2}-m_{S,R},m_{S,R};\frac{3}{2};\frac{1}{2},\frac{1}{2+2b_1}\right)}{\pi(\sqrt{M}-1)^{-2}M(1+b_1)^{m_{S,R}}}\right\}\\
&+\left\{1-\frac{2\Gamma\left(m_{S,R}+\frac{1}{2}\right)\,{}_2F_1\left(m_{S,R},\frac{1}{2};1+m_{S,R};\frac{1}{1+b_1}\right)}{\sqrt{\pi}M(\sqrt{M}-1)^{-1}\Gamma(1+m_{S,R})(1+b_1)^{m_{S,R}}}\right.\\
&\qquad\left.+\frac{2\sqrt{2}F_1\left(\frac{1}{2};\frac{1}{2}-m_{S,R},m_{S,R};\frac{3}{2};\frac{1}{2},\frac{1}{2+2b_1}\right)}{\pi(\sqrt{M}-1)^{-2}M(1+b_1)^{m_{S,R}}}\right\}\\
&\times\left\{\sum_{l=0}^{2m_c-\frac{1}{2}}\frac{4(-1)^l(\sqrt{M}-1)F_1\left(l+\frac{1}{2};m_c,m_c;l+\frac{3}{2};\frac{1}{1+a_1},\frac{1}{1+c_1}\right)}{l!\pi M(1+a_1)^{m_c}(1+c_1)^{m_c}(1+2l)\left(2m_c+\frac{1}{2}\right)_{-l}}\right.
\end{aligned}$$

$$+\sum_{l=0}^{2m_c-\frac{1}{2}} \frac{(-1)^l 2^{\frac{3}{2}-l}(\sqrt{M}-1)^2 F_1\left(l+\frac{1}{2}; m_c, m_c; l+\frac{3}{2}; \frac{1}{2+2a_1}, \frac{1}{2+2c_1}\right)}{l!\pi M(1+a_1)^{m_c}(1+c_1)^{m_c}(1+2l)\left(m_c+m_c+\frac{1}{2}\right)_{-l}}\Bigg\}. \quad (4.29)$$

4.3.3 Asymptotic SER for the Cooperative-Transmission

Simple asymptotic expressions can be derived for the case of high SNR at the three paths of the system. To this end, it is essential to first derive exact expression for another trigonometric integral.

Lemma 3. *For $m \in \mathbb{R}$, the following generic exact expression holds,*

$$\int \sin^{2m} \mathrm{d}\theta = -\cos(\theta)\, {}_2F_1\left(\frac{1}{2}, \frac{1}{2}-m; \frac{3}{2}; \cos^2(\theta)\right) + C. \quad (4.30)$$

Proof. The proof is provided in Appendix C. □

Lemma 3 is subsequently employed in the derivation of the following proposition.

Proposition 1. *For $\{P_S, P_R, P_{L_{S,D}}, P_{L_{S,R}}, P_{L_{R,D}}, \Omega_{S,D}, \Omega_{S,R}, \Omega_{R,D}, N_0\} \in \mathbb{R}^+$, $M \in \mathbb{N}$, $m_{S,D} \geq \frac{1}{2}$, $m_{S,R} \geq \frac{1}{2}$, $m_{R,D} \geq \frac{1}{2}$, $2m_c - \frac{1}{2} \in \mathbb{N}$ and $0 \leq \rho < 1$, the SER of M−QAM based DF relaying over spatially correlated Nakagami−m fading channels in the high SNR regime can be expressed as follows:*

$$\begin{aligned}
P_{\mathrm{SER}}^{\mathrm{C}} \simeq & \left(\frac{P_{L_{S,D}} N_0 m_c}{P_S \Omega_{S,D} g_{\mathrm{QAM}}}\right)^{m_c} \left(1-\frac{1}{\sqrt{M}}\right) \\
& \times \left\{\frac{2\Gamma\left(m_c+\frac{1}{2}\right)}{\sqrt{\pi}\Gamma(1+m_c)} - \left(1-\frac{1}{\sqrt{M}}\right)\frac{{}_2F_1\left(\frac{1}{2}, 1; m_c+\frac{3}{2}; -1\right)}{\pi 2^{m_c-2}\left(1+2m_c\right)}\right\} \\
& \times \left(\frac{P_{L_{S,R}} N_0 m_{S,R}}{P_S \Omega_{S,R} g_{\mathrm{QAM}}}\right)^{m_{S,R}} \left(1-\frac{1}{\sqrt{M}}\right) \\
& \times \left\{\frac{2\Gamma\left(m_{S,R}+\frac{1}{2}\right)}{\sqrt{\pi}\,\Gamma(1+m_{S,R})} - \left(1-\frac{1}{\sqrt{M}}\right)\frac{{}_2F_1\left(\frac{1}{2}, 1; m_{S,R}+\frac{3}{2}; -1\right)}{\pi\, 2^{m_{S,R}-2}(1+2m_{S,R})}\right\} \\
& + \left(\frac{P_{L_{S,D}} P_{L_{R,D}} N_0^2 m_c^2}{(1-\rho)\, P_S P_R \Omega_{S,D} \Omega_{R,D} g_{\mathrm{QAM}}^2}\right)^{m_c} \left(1-\frac{1}{\sqrt{M}}\right) \\
& \times \left\{\frac{2\Gamma\left(2m_c+\frac{1}{2}\right)}{\sqrt{\pi}\,\Gamma(1+2m_c)} - \left(1-\frac{1}{\sqrt{M}}\right)\frac{{}_2F_1\left(\frac{1}{2}, 1; 2m_c+\frac{3}{2}; -1\right)}{\pi\, 2^{2m_c-2}(1+4m_c)}\right\}.
\end{aligned} \quad (4.31)$$

Proof. In the high SNR regime, it is realistic to assume that $P_S\Omega_{S,D} >> P_{L_{S,D}}N_0$, $P_S\Omega_{S,R} >> P_{L_{S,R}}N_0$ and $P_R\Omega_{R,D} >> P_{L_{R,D}}N_0$. Based on this, an integral represen-

tation was formulated in [168, Eq. (28)], i.e.,

$$P_{\mathrm{SER}}^{\mathrm{C}} \simeq A_c A_{S,R} \left(\frac{N_0 m_c P_{L_{S,D}}}{P_S \Omega_{S,D} g_{\mathrm{QAM}}} \right)^{m_c} \left(\frac{N_0 m_{S,R} P_{L_{S,R}}}{P_S \Omega_{S,R} g_{\mathrm{QAM}}} \right)^{m_{S,R}} + A_{2c} \left(\frac{N_0^2 m_c^2 P_{L_{S,D}} P_{L_{R,D}}}{(1-\rho) P_S P_R \Omega_{S,D} \Omega_{R,D} g_{\mathrm{QAM}}^2} \right)^{m_c} \tag{4.32}$$

where

$$\left\{ \begin{matrix} A_c \\ A_{2c} \end{matrix} \right\} = \frac{4}{\pi} \left(1 - \frac{1}{\sqrt{M}} \right) \int_0^{\pi/2} \sin^{\left\{ \begin{matrix} 2m_c \\ 4m_c \end{matrix} \right\}} \mathrm{d}\theta - \frac{4}{\pi} \left(1 - \frac{1}{\sqrt{M}} \right)^2 \int_0^{\pi/4} \sin^{\left\{ \begin{matrix} 2m_c \\ 4m_c \end{matrix} \right\}} \mathrm{d}\theta \tag{4.33}$$

and

$$A_{S,R} = \frac{4}{\pi} \left(1 - \frac{1}{\sqrt{M}} \right) \int_0^{\pi/2} \sin^{2m_{S,R}} \mathrm{d}\theta - \frac{4}{\pi} \left(1 - \frac{1}{\sqrt{M}} \right)^2 \int_0^{\pi/4} \sin^{2m_{S,R}} \mathrm{d}\theta. \tag{4.34}$$

Evidently, the terms A_c, A_{2c} and $A_{S,R}$ can be expressed in closed-form with the aid of Lemma 3. Based on this, by performing the necessary change of variables in (4.30) and substituting in (4.32), (4.31) is deduced, which completes the proof. □

Remark 2. *Using* (4.31)*, the correlation coefficient for the case of M−QAM modulation can be expressed in terms of the corresponding source and relay powers, fading parameters and average SER as*

$$\rho = 1 - \frac{K_3 \left\{ \frac{2C\Gamma\left(2m_c+\frac{1}{2}\right)}{\sqrt{\pi}\,\Gamma(1+2m_c)} - \frac{C^2\, {}_2F_1\left(\frac{1}{2},1;2m_c+\frac{3}{2};-1\right)}{\pi\, 2^{2m_c-2}(1+4m_c)} \right\}^{\frac{1}{m_c}}}{\left(P_{\mathrm{SER}}^{\mathrm{C}} - \frac{\left\{ \frac{2C\Gamma\left(m_c+\frac{1}{2}\right)}{\sqrt{\pi}\Gamma(1+m_c)} - \frac{C^2\, {}_2F_1\left(\frac{1}{2},1;m_c+\frac{3}{2};-1\right)}{\pi 2^{m_c-2}\,(1+2m_c)} \right\} \left\{ \frac{2C\Gamma\left(m_{S,R}+\frac{1}{2}\right)}{\sqrt{\pi}\,\Gamma(1+m_{S,R})} - \frac{C^2\, {}_2F_1\left(\frac{1}{2},1;m_{S,R}+\frac{3}{2};-1\right)}{\pi\, 2^{m_{S,R}-2}(1+2m_{S,R})} \right\}}{K_1^{-m_c} K_2^{-m_{S,R}}} \right)^{\frac{1}{m_c}}} \tag{4.35}$$

where

$$g = g_{\mathrm{QAM}}, \tag{4.36}$$

$$C = \left(1 - 1/\sqrt{M} \right), \tag{4.37}$$

$$K_1 = \frac{N_0 m_c P_{L_{S,D}}}{P_S \Omega_{S,D} g}, \tag{4.38}$$

$$K_2 = \frac{N_0 m_{S,R} P_{L_{S,R}}}{P_S \Omega_{S,R} g} \tag{4.39}$$

and

$$K_3 = \frac{N_0^2 m_c^2 P_{L_{S,D}} P_{L_{R,D}}}{P_S P_R \Omega_{S,D} \Omega_{R,D} g^2}. \tag{4.40}$$

4.4 SER for $M-$PSK Modulation in Nakagami$-m$ Fading with Spatial Correlation

Having derived novel analytic expressions for the case of $M-$QAM modulation, this section is devoted to the derivation of exact and asymptotic expressions for the case of $M-$PSK constellations.

4.4.1 Exact SER for the Cooperative-Transmission

Here, we derive exact expression for the average end-to-end SER of the CT scheme for $M-$PSK constellations. Similar to the previous derived expressions, this result is also useful for the error and EE analysis of the considered system.

Theorem 3. *For* $\{P_S, P_R, P_{L_{S,D}}, P_{L_{S,R}}, P_{L_{R,D}}\} \in \mathbb{R}^+$, $\{\Omega_{S,D}, \Omega_{S,R}, \Omega_{R,D}, N_0\} \in \mathbb{R}^+$, $M \in \mathbb{N}$, $m_{S,D} \geq \frac{1}{2}$, $m_{S,R} \geq \frac{1}{2}$, $m_{R,D} \geq \frac{1}{2}$, $2m_c - \frac{1}{2} \in \mathbb{N}$ *and* $0 \leq \rho < 1$, *the SER of* $M-$*PSK based DF relaying over spatially correlated Nakagami*$-m$ *fading channels, can be expressed as follows:*

$$\begin{aligned}
P_{\text{SER}}^{\text{C}} = {} & \frac{F_1\left(m_c + \frac{1}{2}; \frac{1}{2}, m_c; m_c + \frac{3}{2}; \sin^2\left(\frac{(M-1)\pi}{M}\right), \frac{\sin^2\left(\frac{(M-1)\pi}{M}\right)}{a_2}\right)}{\left(\sin^{2m_c+1}\left(\frac{(M-1)\pi}{M}\right)\right)^{-1}(1+2m_c)\pi a_2^{m_c}} \\
& \times \frac{F_1\left(m_{S,R} + \frac{1}{2}; \frac{1}{2}, m_{S,R}; m_{S,R} + \frac{3}{2}; \sin^2\left(\frac{(M-1)\pi}{M}\right), \frac{\sin^2\left(\frac{(M-1)\pi}{M}\right)}{b_2}\right)}{\left(\sin^{2m_{S,R}+1}\left(\frac{(M-1)\pi}{M}\right)\right)^{-1}(1+2m_{S,R})\pi b_2^{m_{S,R}}} \\
& + \left\{1 - \frac{F_1\left(m_{S,R} + \frac{1}{2}; \frac{1}{2}, m_{S,R}; m_{S,R} + \frac{3}{2}; \sin^2\left(\frac{(M-1)\pi}{M}\right), \frac{\sin^2\left(\frac{(M-1)\pi}{M}\right)}{b_2}\right)}{\left(\sin^{2m_{S,R}+1}\left(\frac{(M-1)\pi}{M}\right)\right)^{-1}(1+2m_{S,R})\pi b_2^{m_{S,R}}}\right\} \\
& \times \left\{\sum_{l=0}^{2m_c-\frac{1}{2}} \binom{2m_c - \frac{1}{2}}{l} \frac{(-1)^l F_1\left(l + \frac{1}{2}; m_c, m_c; l + \frac{3}{2}; \frac{2}{2+c_2-\sqrt{c_2^2-4d_2}}, \frac{2}{2+c_2+\sqrt{c_2^2-4d_2}}\right)}{(1+2l)\pi d_2^{m_c}\left[\left(1 - \frac{2}{2+c_2-\sqrt{c_2^2-4d_2}}\right)\left(1 - \frac{2}{2+c_2+\sqrt{c_2^2-4d_2}}\right)\right]^{-m_c}}\right.
\end{aligned}$$

$$- \sum_{l=0}^{2m_c-\frac{1}{2}} \binom{2m_c-\frac{1}{2}}{l} \frac{(-1)^l \cos^{1+2l}\left(\frac{(M-1)\pi}{M}\right)}{(1+2l)\pi \left(d_2 \sin^4\left(\frac{(M-1)\pi}{M}\right) + c_2 \cos^2\left(\frac{(M-1)\pi}{M}\right) + c_2\right)^{m_c}}$$
$$\times F_1\left(l+\frac{1}{2}; m_c, m_c; l+\frac{3}{2}; \frac{2\cos^2\left(\frac{(M-1)\pi}{M}\right)}{2+c_2-\sqrt{c_2^2-4d_2}}, \frac{\cos^2\left(\frac{(M-1)\pi}{M}\right)}{2+c_2+\sqrt{c_2^2-4d_2}}\right)$$
$$\times \left(1 - \frac{2\cos^2\left(\frac{(M-1)\pi}{M}\right)}{2+c_2-\sqrt{c_2^2-4d_2}}\right)^{m_c} \left(1 - \frac{2\cos^2\left(\frac{(M-1)\pi}{M}\right)}{2+c_2+\sqrt{c_2^2-4d_2}}\right)^{m_c} \Bigg\} \tag{4.41}$$

where

$$a_2 = \frac{P_S \Omega_{S,D} g_{\mathrm{PSK}}}{P_{L_{S,D}} m_c N_0}, \tag{4.42}$$

$$b_2 = \frac{P_S \Omega_{S,R} g_{\mathrm{PSK}}}{P_{L_{S,R}} N_0 m_{S,R}}, \tag{4.43}$$

$$c_2 = \frac{P_R \Omega_{R,D} g_{\mathrm{PSK}}}{P_{L_{R,D}} N_0 m_c}, \tag{4.44}$$

and

$$d_2 = \frac{(1-\rho) P_R \Omega_{R,D} g_{\mathrm{PSK}}}{P_{L_{R,D}} N_0 m_c}. \tag{4.45}$$

Proof. As a starting point, the average SER of $M-$PSK modulated DF systems over Nakagami$-m$ fading channels with spatial correlation can be formulated according to [168, Eq. (23)] as follows

$$P_{\mathrm{SER}}^{\mathrm{C}} = F_{\mathrm{PSK}}\left[\frac{1}{\left(1+\frac{P_S\Omega_{S,D}g_{\mathrm{PSK}}}{N_0 m_c P_{L_{S,D}} \sin^2(\theta)}\right)^{m_c}}\right] F_{\mathrm{PSK}}\left[\frac{1}{\left(1+\frac{P_S\Omega_{S,R}g_{\mathrm{PSK}}}{N_0 m_{S,R} P_{L_{S,R}} \sin^2(\theta)}\right)^{m_{S,R}}}\right]$$
$$+ F_{\mathrm{PSK}}\left[\frac{1}{\left(1+\frac{(P_S\Omega_{S,D}/P_{L_{S,D}}+P_R\Omega_{R,D}/P_{L_{R,D}})g_{\mathrm{PSK}}}{N_0 m_c \sin^2(\theta)} + \frac{(1-\rho)P_S P_R \Omega_{S,D}\Omega_{R,D} g_{\mathrm{PSK}}^2}{N_0^2 m_c^2 P_{L_{S,D}} P_{L_{R,D}} \sin^4(\theta)}\right)^{m_c}}\right]$$
$$\times \left\{1 - F_{\mathrm{PSK}}\left[\frac{1}{\left(1+\frac{P_S\Omega_{S,R}g_{\mathrm{PSK}}}{N_0 m_{S,R} P_{L_{S,R}} \sin^2(\theta)}\right)^{m_{S,R}}}\right]\right\} \tag{4.46}$$

$$F_{\mathrm{PSK}}[u(\theta)] = \frac{1}{\pi}\int_0^{\frac{(M-1)\pi}{M}} u(\theta)\mathrm{d}\theta. \tag{4.47}$$

The involved four integrals have the same algebraic form as the integrals in Theorem

1 and Lemma 1. Thus, the proof follows by performing the same necessary change of variables and substituting in (4.46). □

4.4.2 Asymptotic SER for the Cooperative-Transmission

Proposition 2. *For* $\{P_S, P_R, P_{L_{S,D}}, P_{L_{S,R}}, P_{L_{R,D}}\} \in \mathbb{R}^+$, $\{\Omega_{S,D}, \Omega_{S,R}, \Omega_{R,D}, N_0\} \in \mathbb{R}^+$ $M \in \mathbb{N}$, $m_{S,D} \geq \frac{1}{2}$, $m_{S,R} \geq \frac{1}{2}$, $m_{R,D} \geq \frac{1}{2}$, $2m_c - \frac{1}{2} \in \mathbb{N}$ *and* $0 \leq \rho < 1$, *the SER of* $M-$*PSK based DF relaying over spatially correlated Nakagami*$-m$ *channels in the high SNR regime is given by*

$$\begin{aligned} P_{\text{SER}}^{\text{C}} \simeq & \left(\frac{N_0 m_c P_{L_{S,D}}}{P_S \Omega_{S,D} g_{\text{PSK}}}\right)^{m_c} \left\{\frac{\Gamma\left(m_c+\frac{1}{2}\right)}{2\sqrt{\pi}\, m_c!} + \frac{\cos\left(\frac{\pi}{M}\right)\, {}_2F_1\left(\frac{1}{2}, \frac{1}{2}-m_c; \frac{3}{2}; \cos^2\left(\frac{\pi}{M}\right)\right)}{\pi}\right\} \\ & \times \left(\frac{N_0 m_{S,R} P_{L_{S,R}}}{P_S \Omega_{S,R} g_{\text{PSK}}}\right)^{m_{S,R}} \\ & \times \left\{\frac{\Gamma\left(m_{S,R}+\frac{1}{2}\right)}{2\sqrt{\pi}\, m_{S,R}!} + \frac{\cos\left(\frac{\pi}{M}\right)\, {}_2F_1\left(\frac{1}{2}, \frac{1}{2}-m_{S,R}; \frac{3}{2}; \cos^2\left(\frac{\pi}{M}\right)\right)}{\pi}\right\} \\ & + \left(\frac{N_0^2 m_c^2 P_{L_{S,D}} P_{L_{R,D}}}{(1-\rho) P_S P_R \Omega_{S,D} \Omega_{R,D} g_{\text{PSK}}^2}\right)^{m_c} \\ & \times \left\{\frac{\Gamma\left(2m_c+\frac{1}{2}\right)}{2\sqrt{\pi}(2m_c)!} + \frac{\cos\left(\frac{\pi}{M}\right)\, {}_2F_1\left(\frac{1}{2}, \frac{1}{2}-2m_c; \frac{3}{2}; \cos^2\left(\frac{\pi}{M}\right)\right)}{\pi}\right\}. \end{aligned} \tag{4.48}$$

Proof. The asymptotic SER for high SNR values was formulated in [168, Eq. (27)]

$$\begin{aligned} P_{\text{SER}}^{\text{C}} \simeq & \tilde{A}_c \tilde{A}_{S,R} \left(\frac{N_0 m_c P_{L_{S,D}}}{P_S \Omega_{S,D} g_{\text{PSK}}}\right)^{m_c} \left(\frac{N_0 m_{S,R} P_{L_{S,R}}}{P_S \Omega_{S,R} g_{\text{PSK}}}\right)^{m_{S,R}} \\ & + \tilde{A}_{2c} \left(\frac{N_0^2 m_c^2 P_{L_{S,D}} P_{L_{R,D}}}{(1-\rho) P_S P_R \Omega_{S,D} \Omega_{R,D} g_{\text{PSK}}^2}\right)^{m_c} \end{aligned} \tag{4.49}$$

where

$$\left\{\begin{matrix}\tilde{A}_c \\ \tilde{A}_{2c}\end{matrix}\right\} = \frac{1}{\pi} \int_0^{\frac{(M-1)\pi}{M}} \sin^{\left\{\begin{matrix}2m_c \\ 4m_c\end{matrix}\right\}} \mathrm{d}\theta \tag{4.50}$$

and

$$\tilde{A}_{S,R} = \frac{1}{\pi} \int_0^{\frac{(M-1)\pi}{M}} \sin^{2m_{S,R}} \mathrm{d}\theta. \tag{4.51}$$

Notably, the above two integrals have the same algebraic representation as the integral in Lemma 3. As a result, by performing the necessary change of variables and substituting in (4.49), one obtains (4.48), which completes the proof. □

Remark 3. *Based on* (4.48)*, the corresponding correlation coefficient can be ex-*

pressed in terms of the involved source and relay powers, fading parameters and average SER as

$$\rho = 1 - \frac{K_3 \left\{ \frac{\Gamma\left(2m_c+\frac{1}{2}\right)}{2\sqrt{\pi}(2m_c)!} + \frac{\cos\left(\frac{\pi}{M}\right) {}_2F_1\left(\frac{1}{2},\frac{1}{2}-2m_c;\frac{3}{2};\cos^2\left(\frac{\pi}{M}\right)\right)}{\pi} \right\}^{\frac{1}{m_c}}}{\left(P_{\text{SER}}^{\text{C}} - K_4\right)^{\frac{1}{m_c}}} \tag{4.52}$$

where $g = g_{PSK}$ is set in the K_1, K_2 and K_3 terms, which are given in Remark 2 and K_4 is given as

$$K_4 = K_1^{m_c} K_2^{m_{S,R}} \left\{ \frac{\Gamma\left(m_c+\frac{1}{2}\right)}{2\sqrt{\pi}\, m_c!} + \frac{\cos\left(\frac{\pi}{M}\right) {}_2F_1\left(\frac{1}{2},\frac{1}{2}-m_c;\frac{3}{2};\cos^2\left(\frac{\pi}{M}\right)\right)}{\pi} \right\} \times \left\{ \frac{\Gamma\left(m_{S,R}+\frac{1}{2}\right)}{2\sqrt{\pi}\, m_{S,R}!} + \frac{\cos\left(\frac{\pi}{M}\right) {}_2F_1\left(\frac{1}{2},\frac{1}{2}-m_{S,R};\frac{3}{2};\cos^2\left(\frac{\pi}{M}\right)\right)}{\pi} \right\}.$$

4.4.3 Diversity and Cooperation Gains

In the previous subsections, asymptotic SER expressions for CT with DF protocol were derived for both $M-$QAM and $M-$PSK constellations. These expressions are useful to determine the diversity and coding gains of the considered cooperative scheme. As already mentioned in Subsection 3.4.3, the asymptotic SER can be expressed in the form:

$$P_{\text{SER}}^{C} \approx (G_c \text{SNR})^{-G_d}. \tag{4.53}$$

In the considered CT scheme, since the relay is simply remodulating and retransmitting the decoded information, the constant term that multiples the SNR, G_c, can be denoted as the cooperation gain [197]. For simplicity, hereafter, we denote $P_S = a_0 P$ and $P_R = a_R P$ where a_0 and a_R are the power ratios, whereas P denotes the sum-power of the system. Using these notations, both expressions in (4.32) and (4.49) can be rewritten as:

$$\begin{aligned} P_{\text{SER}}^{\text{C}} \simeq \bar{A}_c \bar{A}_{S,R} \left(\frac{m_c P_{L_{S,D}}}{a_0 \Omega_{S,D} g}\right)^{m_c} \left(\frac{m_{S,R} P_{L_{S,R}}}{a_0 \Omega_{S,R} g}\right)^{m_{S,R}} \left(\frac{N_0}{P}\right)^{m_c+m_{S,R}} \\ + \bar{A}_{2c} \left(\frac{m_c^2 P_{L_{S,D}} P_{L_{R,D}}}{(1-\rho) a_0 a_R \Omega_{S,D} \Omega_{R,D} g^2}\right)^{m_c} \left(\frac{N_0}{P}\right)^{2m_c}. \end{aligned} \tag{4.54}$$

In the above expression, $\{\bar{A}_c, \bar{A}_{S,R}, \bar{A}_{2c}\} = \{A_c, A_{S,R}, A_{2c}\}$ for $M-$QAM modulation, whereas $\{\bar{A}_c, \bar{A}_{S,R}, \bar{A}_{2c}\} = \{\tilde{A}_c, \tilde{A}_{S,R}, \tilde{A}_{2c}\}$ for $M-$PSK modulation, respectively. Moreover, $g = g_{QAM}$ for $M-$QAM and $g = g_{PSK}$ for $M-$PSK constellations, respectively.

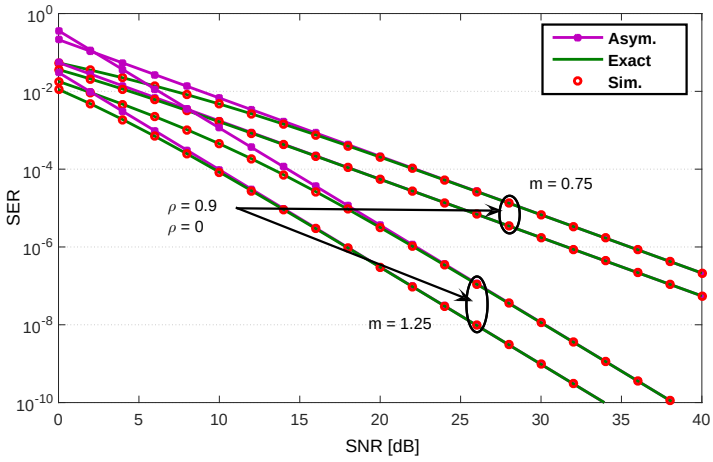

Figure 4.2 Example SER performance over Nakagami−m fading channels with $m_{S,D} = m_{S,R} = m_{R,D} = m = \{0.75, 1.25\}$, $\Omega_{S,D} = \Omega_{S,R} = \Omega_{R,D} = 0$dB for 4−QAM/QPSK constellations and different values of spatial correlation.

Using the expressions in (4.53), (4.54) and with the aid of [198, Eq. (13)], the diversity and cooperation gains of the considered system can be expressed as:

$$G_d = m_c + \min\{m_{S,R}, m_c\} \tag{4.55}$$

and

$$\begin{aligned} G_c = \Bigg(& \bar{A}_c \bar{A}_{S,R} \left(\frac{m_c P_{L_{S,D}}}{a_0 \Omega_{S,D} g} \right)^{m_c} \left(\frac{m_{S,R} P_{L_{S,R}}}{a_0 \Omega_{S,R} g} \right)^{m_{S,R}} \\ & + \bar{A}_{2c} \left(\frac{m_c^2 P_{L_{S,D}} P_{L_{R,D}}}{(1-\rho) a_0 a_R \Omega_{S,D} \Omega_{R,D} g^2} \right)^{m_c} \Bigg)^{-\frac{1}{G_d}}, \end{aligned} \tag{4.56}$$

respectively. The expression in (4.56) reveals that the spatial correlation between the direct and relayed paths impacts the cooperation gain of the system. This phenomenon agrees well with the results in [168] and we further illustrate this in the next figure.

Fig. 4.2 illustrates the SER performance as a function of SNR for 4−QAM/QPSK modulations. The S-D transmission distance is indicatively considered at 600m while the relay is assumed to be located in the middle where the transmit power is shared equally to the source and the relay. The corresponding PL effects are considered by

adopting the PL model in [180], namely

$$PL_{i,j}[dB] = 148 + 40\log_{10}(d_{i,j}[km]) \tag{4.57}$$

which has been shown to characterize adequately harsh communication scenarios and is particularly applicable to mobile relaying and D2D communications. It is clearly observed that the empirical simulated results are in excellent agreement with the respective analytical results. Furthermore, the simple asymptotic results are also highly accurate at higher SNR regime. It is also shown that the curves are shifted to the right as ρ increases from 0 to 0.9, which implies the correlation has an impact on the cooperation gain of the system.

4.5 System Power Consumption Model Analysis

Here, motivated by the general interests towards green communications and increasing incentives to save energy, we quantify the total energy consumption required to transmit information from the source to the destination. We assume that the transceiver circuitry operates on multi-mode basis: 1) When there is a signal to transmit, the circuits are in active mode; 2) when there is no signal to transmit, the circuits operate on a sleep mode; and 3) the circuits are in transient mode during the switching process from sleep mode to active mode. The elementary block diagrams of the assumed transmitter and receiver are illustrated in Figs. 4.3 and 4.4, respectively. This model is based on direct-conversion architecture which is commonly used in wireless transceivers. It is also assumed that all nodes are equipped with similar transmitter and receiver circuit blocks and that the power consumption of the active filters at the transmitter and receiver is similar.

Considering a node that transmits L bits and total transmission period T, the transient duration from active mode to sleep mode is short enough to be neglected. However, the start-up process from sleep mode to active mode may be slower due to the finite phase-locked loop (PLL) settling time in the frequency synthesizer. By denoting the duration of the sleep, transient and active modes as T_{sp}, T_{tr} and T_{on}, respectively, the total transmission period is defined as

$$T = T_{sp} + T_{tr} + T_{on} \tag{4.58}$$

with T_{tr} being equal to the frequency synthesizer settling time. Based on this, the total energy required to transmit and receive L information bits is expressed as

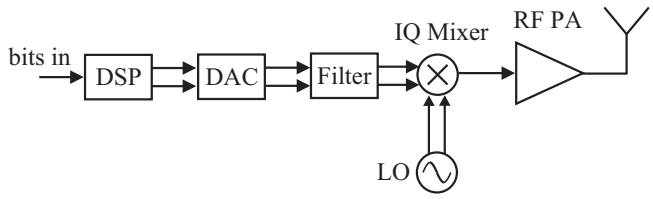

Figure 4.3 Elementary direct-conversion transmitter.

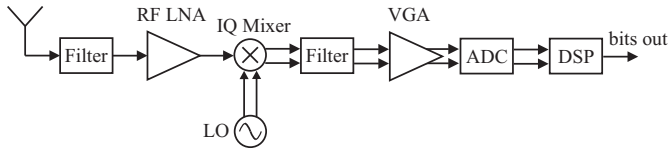

Figure 4.4 Elementary direct-conversion receiver.

$$E = P_{on}T_{on} + P_{sp}T_{sp} + P_{tr}T_{tr} \tag{4.59}$$

where P_{on}, P_{sp} and P_{tr} denote the power consumption values during the active, sleep and transient modes, respectively. In realistic circuit designs, the power consumption in the sleep mode, referring mostly to the ability of an idle node to wake up as quickly as necessary, can be considered negligible compared with the active mode power [141]; thus, $P_{sp} \simeq 0$. It is also noted that power consumption during the transient mode practically refers to the power consumption of the frequency synthesizers. Based on this, it is assumed that $P_{tr} = 2P_{LO}$; as a result, using the power consumption values at both transmitter and receiver sides during the active mode one obtains:

$$P_{on} = P_{ont} + P_{onr} \tag{4.60}$$

where P_{ont} is the total transmitter power consumption that accounts for the sum of signal transmission and transmitter circuit powers and P_{onr} is the total receiver power consumption. Hence, it follows that,

$$P_{ont} = P_t + P_{amp} + P_{CT_x} \tag{4.61}$$

and

$$P_{onr} = P_{CR_x} \tag{4.62}$$

where P_t refers to the transmission power of the source or the relay, P_{amp} is the power consumption of the RF power amplifier and P_{CT_x} and P_{CR_x} denote the total

transmitter circuit power and the total receiver circuit powers, i.e.,

$$P_{CT_x} = P_{DSP_{Tx}} + P_{DAC} + P_{Fil} + P_{Mix} + P_{LO} \tag{4.63}$$

and

$$P_{CR_x} = P_{ADC} + P_{VGA} + 2P_{Fil} + P_{Mix} + P_{LO} + P_{LNA} + P_{DSP_{Rx}} \tag{4.64}$$

respectively. The P_{CT_x} measure consists of the following power consumption entities: digital signal processor (DSP), $P_{DSP_{Tx}}$; digital to analog converter (DAC), P_{DAC}; active filter, P_{Fil}; IQ Mixer, P_{Mix} and synthesizer, P_{LO}. Likewise, the active power consumption at the receiver comprises the power consumption values for DSP, $P_{DSP_{Rx}}$; analog to digital converter (ADC), P_{ADC}; variable gain amplifier (VGA), P_{VGA}; active filter, P_{Fil}; IQ Mixer, P_{Mix}; synthesizer, P_{LO}; LNA, P_{LNA} [181]. Based on this, the total required circuit power consumption is given by

$$P_{TC} = P_{CT_x} + P_{CR_x}. \tag{4.65}$$

It is also noted that for signal transmission power P_t, the power consumption of the RF-power amplifier can be modeled by

$$P_{amp} = \omega P_t \tag{4.66}$$

where

$$\omega = \frac{\xi}{\eta_d} - 1 \tag{4.67}$$

with η_d and ξ denoting the respective drain efficiency of the amplifier and the peak-to-average power ratio, which depends on the modulation order and the associated constellation size. Based on this, for the case of square uncoded $M-$QAM modulation,

$$\xi = 3\frac{\sqrt{M}-1}{\sqrt{M}+1} \tag{4.68}$$

and

$$T_{on} = \frac{LT_s}{b} = \frac{L}{bB} \tag{4.69}$$

where $b = \log_2 M$ is the constellation size, L is the transmission block length in bits and T_s is the symbol duration that relates to the bandwidth B as $T_s \approx 1/B$ [145].

4.6 Energy Optimization and Power Allocation

By combining the results of the previous sections, we analyze the total energy required to transmit information efficiently from the source to the destination. To this end, we first quantify the total energy consumption in the direct communication scenario. Hence, by applying (4.59)−(4.62) and recalling that $P_{sp} \approx 0$ and $P_{tr} = 2P_{LO}$, the average energy consumption per information bit is given by [182]

$$\overline{E}_T^D = \frac{\left((1+\omega)P_S + P_{CT_x} + P_{CR_x}\right) T_{on} + 2P_{LO}T_{tr}}{L}. \tag{4.70}$$

In order to determine the average total energy consumption in the corresponding CT system deploying the DF protocol, we formulate the total average power consumption, which is a discrete random variable that can be represented as follows:

$$P_T^C = \begin{cases} P_{CT_x} + (1+\omega)\, P_S + 2P_{CR_x}, & \text{with } \Pr = 1 \\ P_{CT_x} + (1+\omega)\, P_R + P_{CR_x}, & \text{with } \Pr = 1 - P_{\mathrm{SER_{S,R}}}. \end{cases} \tag{4.71}$$

The first line of the above expression refers to the absolute total power consumption by the nodes in the first transmission phase, whereas the second line represents the power consumption in the second phase, subject to correct decoding of the received signal by the relay, which is indicated by the probabilistic term $\left(1 - P_{\mathrm{SER_{S,R}}}\right)$. Hence, the average total power consumption in the CT mode can be expressed as

$$\overline{P}_T^C = \left(P_{CT_x} + (1+\omega)P_R + P_{CR_x}\right)\left(1 - P_{\mathrm{SER_{S,R}}}\right) + P_{CT_x} + (1+\omega)P_S + 2P_{CR_x}. \tag{4.72}$$

Based on this, the corresponding average energy consumption per information bit is given by

$$\overline{E}_T^C = \frac{\overline{P}_T^C T_{on} + 2P_{LO}T_{tr}}{L}. \tag{4.73}$$

The achieved EE enhancement by the CT is determined with the aid of the cooperation gain (CG), which is the ratio of the EE of CT over the EE of the DT, per successfully delivered bit, namely

$$\mathrm{CG} = \frac{\overline{E}_T^D \left(1 - P_{\mathrm{BER}}^{\mathrm{C}}\right)}{\overline{E}_T^C \left(1 - P_{\mathrm{BER}}^{\mathrm{D}}\right)}. \tag{4.74}$$

Evidently, when the resulting ratio is smaller than one, it indicates that DT is more energy efficient; thus, the extra energy consumption induced by cooperation out-

weighs its gain in decreasing the average BER of the system. In what follows, the given expressions are employed in analyzing energy optimization problems aiming to guarantee certain QoS requirements, namely, target destination average BER. In this context, we also provide the OPA formulation for the CT scenario under the maximum total transmit power constraint.

4.6.1 Direct Transmission

We first consider the energy optimization problem for minimizing the average total energy consumption in the DT scenario with the maximum transmission power and target BER, p^*, as constraints. We assume that the power consumption of the circuit components are fixed and independent of the optimization. Thus, the only variable in the optimization is the transmit power of the source. To this effect and with the aid of (4.70), the optimization problem for the DT mode can be formulated as follows:

$$\begin{gathered}\min_{P_S} \overline{E}_T^D \\ \text{subject to: } P_S \leq P_{maxt},\ \ P_S \geq 0 \\ P_{\text{BER}}^{\text{D}} = p^*.\end{gathered} \tag{4.75}$$

Deriving the minimum average total energy required in the direct communication scenario, requires prior computation of the corresponding symbol error probability. This is realized with the aid of (4.9) which is expressed in an exact form in terms of ${}_2F_1\left(m, \frac{1}{2}; m+1; \frac{1}{1+a_1}\right)$ and $F_1\left(\frac{1}{2}; \frac{1}{2}-m, m; \frac{3}{2}; \frac{1}{2}, \frac{1}{2+2a_1}\right)$ functions[3]. It is recalled that these functions are widely employed in natural sciences and engineering and their computational implementation is rather straightforward as they are built-in functions in popular software packages, such as MATLAB, MAPLE and MATHEMATICA. It is also noted that the representation of these functions in the present analysis allows the following useful approximation expressions: ${}_2F_1\left(m, \frac{1}{2}; m+1; \frac{1}{1+a_1}\right) \simeq 1$ and $F_1\left(\frac{1}{2}; \frac{1}{2}-m, m; \frac{3}{2}; \frac{1}{2}, \frac{1}{2+2a_1}\right) \simeq F_1\left(\frac{1}{2}; \frac{1}{2}-m, m; \frac{3}{2}; \frac{1}{2}, 0\right)$ [86]. The accuracy of these approximations is validated through extensive numerical and simulation results, which indicate their tightness for random values of m and moderate and large values of a_1. To this effect, one obtains the following accurate closed-form average BER

[3]For the sake of simplicity, we assume that $m = m_{S,D}$.

approximation for $M-$QAM constellations as

$$P_{\mathrm{BER}}^{\mathrm{D}} \simeq \frac{2\,(\sqrt{M}-1)\Gamma(m+\frac{1}{2})}{\sqrt{\pi}Mm!(1+a_1)^m \log_2 M} + \frac{4\,F_1(\frac{1}{2};\frac{1}{2}-m,m;\frac{3}{2};\frac{1}{2},0)}{\sqrt{2}\pi(1+a_1)^m \log_2 M}\left(1-\frac{1}{\sqrt{M}}\right)^2. \tag{4.76}$$

Importantly, the Appell function in (4.76) can be expressed in terms of the Gauss hypergeometric function, namely

$$F_1\left(\frac{1}{2};\frac{1}{2}-m,m;\frac{3}{2};\frac{1}{2},0\right) = {}_2F_1\left(\frac{1}{2},\frac{1}{2}-m;\frac{3}{2};\frac{1}{2}\right). \tag{4.77}$$

As a result, equation (4.76) becomes

$$P_{\mathrm{BER}}^{\mathrm{D}} \simeq \frac{2\,(\sqrt{M}-1)\Gamma(m+\frac{1}{2})}{\sqrt{\pi}Mm!(1+a_1)^m \log_2 M} + \frac{4\;{}_2F_1\left(\frac{1}{2},\frac{1}{2}-m;\frac{3}{2};\frac{1}{2}\right)}{\sqrt{2}\pi(1+a_1)^m \log_2 M}\left(1-\frac{1}{\sqrt{M}}\right)^2. \tag{4.78}$$

It is evident that (4.78) is a function of the modulation order, the severity of multipath fading and a_1. Therefore, by substituting the targeted QoS p^* in (4.78), recalling that

$$a_1 = \frac{P_S\;\Omega_{S,D}\,g_{QAM}}{N_0 P_{L_{S,D}}} \tag{4.79}$$

and carrying out some algebraic manipulations, one obtains

$$P_S \simeq \frac{mN_0P_{L_{S,D}}}{\Omega_{S,D}g_{QAM}}\left[\left(\frac{C}{p^*}\right)^{\frac{1}{m}} - 1\right] \tag{4.80}$$

where

$$C = \frac{4(\sqrt{M}-1)^2\,{}_2F_1\left(\frac{1}{2},\frac{1}{2}-m;\frac{3}{2};\frac{1}{2}\right)}{\sqrt{2}M\,\pi\log_2 M} + \frac{2(\sqrt{M}-1)\Gamma(m+\frac{1}{2})}{\sqrt{\pi}m!M\log_2 M}. \tag{4.81}$$

To this effect and with the aid of (4.70) and (4.80), it follows that the minimum total energy per information bit required for DT for meeting the required QoS can be expressed in a closed-form as follows:

$$\overline{E}_T^{D*} = \frac{(P_{CT_x}+P_{CR_x})\,T_{on}}{L} + \frac{2P_{LO}T_{tr}}{L} + \frac{(1+\omega)N_0mT_{on}P_{L_{S,D}}}{L\,\Omega_{S,D}g_{QAM}}\left[\left(\frac{C}{p^*}\right)^{\frac{1}{m}} - 1\right] \tag{4.82}$$

Based on the total energy consumption in (4.82) and given the constellation size, i.e.,

$$b = \frac{L}{BT_{on}} \tag{4.83}$$

it is shown that the proposed energy expression comprises the transmission energy E_t and circuit energy E_C, namely

$$E_t = P_S T_{on} = \frac{N_0 m P L_{S,D}}{\Omega_{S,D} g_{QAM}} \left[\left(\frac{C}{p^*} \right)^{\frac{1}{m}} - 1 \right] \frac{T_{on}}{L} \tag{4.84}$$

where C can be expressed as a function of the transmission time T_{on} as follows

$$C = \frac{BT_{on} \left(2^{\frac{L}{2BT_{on}}} - 1 \right)^2}{L\pi 2^{\frac{L}{BT_{on}} - \frac{3}{2}}} \, {}_2F_1 \left(\frac{1}{2}, \frac{1}{2} - m; \frac{3}{2}; \frac{1}{2} \right) + \frac{2BT_{on}}{2^{\frac{L}{BT_{on}}} mL\sqrt{\pi}} \left(\frac{1}{2} \right)_m \left(2^{\frac{L}{2BT_{on}}} - 1 \right). \tag{4.85}$$

Hence, by inserting (4.85) in (4.84), an analytic expression for the transmission energy per information bit is deduced as

$$E_t = \frac{N_0 m P L_{S,D} T_{on}}{L \, \Omega_{S,D} g_{QAM}} \times$$

$$\left\{ \left[\frac{BT_{on} \left(2^{\frac{L}{2BT_{on}}} - 1 \right)^2}{p^* L\pi 2^{\frac{L}{BT_{on}} - \frac{3}{2}}} \, {}_2F_1 \left(\frac{1}{2}, \frac{1}{2} - m; \frac{3}{2}; \frac{1}{2} \right) + \frac{BT_{on} \left(2^{\frac{L}{2BT_{on}}} - 1 \right)}{p^* mL\sqrt{\pi} \, 2^{\frac{L}{BT_{on}} - 1}} \left(\frac{1}{2} \right)_m \right]^{\frac{1}{m}} - 1 \right\}. \tag{4.86}$$

Likewise, the total circuit energy of the system, E_C, can be expressed as

$$E_C = \left(P_{CT_x} + P_{CR_x} \right) T_{on}. \tag{4.87}$$

Notably, (4.86) indicates that for a fixed bandwidth B and packet length L, the transmission energy is a decreasing function with respect to the product $T_{on}B$, whereas the circuit energy increases monotonically with respect to T_{on}. In addition, it is shown that the transmission energy depends upon the transmission distance $d_{S,D}$ and the severity of fading m, whereas the corresponding circuit energy remains fixed regardless of the transmission distance, $d_{S,D}$ and fading severity m.

4.6.2 Cooperative Transmission

Here, we present the energy optimization and power allocation problem when the involved relay forwards successfully decoded signals, generally at different power than the power of the source. Evidently, the respective optimization model is a two dimensional problem; thus, we formulate the energy minimization problem with two optimization variables, namely, the source transmit power P_S and the relay transmit power P_R. In this context, the aim is to minimize the total energy consumption of the overall network instead of minimizing the energy consumption at individual nodes. Based on this and with the aid of (4.73), the optimization problem can be formulated as follows:

$$\begin{aligned} &\min_{P_S,P_R} \overline{E}_T^C(P_S,P_R) \\ &\text{subject to: } (P_S+P_R) \leq P_{maxt},\ P_S \geq 0,\ P_R \geq 0 \\ &P_{\mathrm{BER}}^{\mathrm{C}}(P_S,P_R) = p^*. \end{aligned} \tag{4.88}$$

The above optimization task is a non-linear programming (NLP) problem since the objective function and the constraint BER are both non-linear functions of P_S and P_R. It is also recalled that Karush Kuhn Tucker (KKT) conditions that handle both equality and inequality constraints are in general the first-order sufficient and necessary conditions for optimum solutions in non-linear optimization problems provided that certain regularity conditions are satisfied. To this end, using the Lagrange multipliers λ_1 and λ_2, λ_3 and λ_4, for the equality and inequality constraints, we set the corresponding Lagrangian equation that depends on the optimization variables and multipliers while meeting the KKT conditions in [183] for the non-linear convex optimization problem, namely

$$L_P = \overline{E}_T^C + \lambda_1 \left(P_{\mathrm{BER}}^{\mathrm{C}} - p^*\right) - \lambda_2 P_S - \lambda_3 P_R + \lambda_4 \left((P_S+P_R) - P_{maxt}\right). \tag{4.89}$$

The proof for the convexity of the optimization problem is provided in Appendix D.

Based on (4.89), the KKT conditions for the problem can be expressed as follows:

$$\nabla \overline{E}_T^C + \lambda_1 \nabla P_{\mathrm{BER}}^{\mathrm{C}} - \lambda_2 \nabla P_S - \lambda_3 \nabla P_R + \lambda_4 \nabla \left(P_S+P_R\right) = 0, \tag{4.90}$$

whereas the associated complementary conditions are given by

$$\begin{aligned} P_{\mathrm{BER}}^{\mathrm{C}} &= p^*, \\ P_S + P_R &\leq P_{maxt}, \end{aligned}$$

$$\begin{aligned} \lambda_1 \left(P_{\mathrm{BER}}^{\mathrm{C}} - p^*\right) &= 0, \\ \lambda_2 P_S &= 0, \\ \lambda_3 P_R &= 0, \\ \lambda_4 \left(P_S + P_R - P_{maxt}\right) &= 0, \\ \lambda_1, \lambda_2, \lambda_3, \lambda_4 &\geq 0. \end{aligned} \tag{4.91}$$

In the set of complementary KKT conditions of (4.91) both λ_2 and λ_3 represent inactive constraints; therefore, they can be assumed zero. To this effect, by applying (4.90) and setting the derivatives w.r.t P_S and P_R to zero, the following useful set of equations is deduced:

$$\frac{\partial \overline{E}_T^C}{\partial P_S} + \lambda_1 \frac{\partial P_{\mathrm{BER}}^{\mathrm{C}}}{\partial P_S} + \lambda_4 = 0 \tag{4.92}$$

and

$$\frac{\partial \overline{E}_T^C}{\partial P_R} + \lambda_1 \frac{\partial P_{\mathrm{BER}}^{\mathrm{C}}}{\partial P_R} + \lambda_4 = 0. \tag{4.93}$$

Solving for λ_4 from (4.92) and substituting in (4.93) yield the following relationship, which depends only on one of the Lagrangian multipliers:

$$\frac{\partial \overline{E}_T^C}{\partial P_S} - \frac{\partial \overline{E}_T^C}{\partial P_R} + \lambda_1 \left(\frac{\partial P_{\mathrm{BER}}^{\mathrm{C}}}{\partial P_S} - \frac{\partial P_{\mathrm{BER}}^{\mathrm{C}}}{\partial P_R} \right) = 0 \tag{4.94}$$

and

$$\lambda_1 = \frac{\frac{\partial \overline{E}_T^C}{\partial P_S} - \frac{\partial \overline{E}_T^C}{\partial P_R}}{\left(\frac{\partial P_{\mathrm{BER}}^{\mathrm{C}}}{\partial P_R} - \frac{\partial P_{\mathrm{BER}}^{\mathrm{C}}}{\partial P_S} \right)}. \tag{4.95}$$

Based on this and using the fact that $\lambda_1 \geq 0$, one obtains the following necessary condition for minimizing the total average energy consumption of the CT mode at the optimal power values:

$$\frac{\partial \overline{E}_T^C(P_S^*, P_R^*)}{\partial P_S} \geq \frac{\partial \overline{E}_T^C(P_S^*, P_R^*)}{\partial P_R}. \tag{4.96}$$

For a feasible set of optimal powers, the $P_{\mathrm{BER}}^{\mathrm{C}} = p^*$ and $P_S + P_R \leq P_{maxt}$ constraints must be satisfied.

Analytic solution for the optimal powers in (4.96) is intractable to derive in a closed-form. However, this can be alternatively realized with the aid of numerical optimization techniques, which can determine the optimal powers at the source and relay nodes that minimize the average total energy consumption. To this end, we employ the MATLAB optimization tool box and its function *fmincon*. This function

is generally applicable in minimizing nonlinear functions subject to linear or nonlinear constraints with both equalities and inequalities [183], and thus, it is used in the respective numerical calculations for allocating the available power optimally under the given constraints. Thus, the derived expressions and the offered results provide tools to understand, quantify and analyze how much energy can in general be saved, per successfully communicated bit in the system, if transmit power allocation and optimization beyond classical EPA is pursued in the cooperative system on one side and how much energy can be saved against the classical non-cooperative (DT) system on the other side. Furthermore, the considered values in this chapter are indicative and are selected in the context of demonstrating the validity of the proposed method. Therefore, the derived optimization flow can be readily extended to arbitrary design constraints for the total network power consumption and target destination error rate in the presence of Nakagami$-m$ multipath fading conditions.

4.7 Numerical Results and Analysis

Here, we demonstrate and evaluate the average total energy consumption of the considered regenerative system assuming that the S-D and S-R links are statistically independent, whereas the S-D and R-D paths are spatially correlated. As a realistic example, we assume $M-$QAM modulation scheme over the S-D, S-R and R-D links, in case of cooperative transmission mode, and over the S-D link in the case of only direct communication. For the sake of simplicity, it is also assumed that all wireless channels are subject to Nakagami$-m$ multipath fading conditions with $\Omega_{S,D} = \Omega_{S,R} = \Omega_{R,D} = 0$dB. The involved PL effects are modeled by an example model of $P_{L_{i,j}}\,[\text{dB}] = 148{+}40\log_{10}(d_{i,j}[\text{km}])$, which is also used in D2D based communications [180]; thus, applies to mobile relaying as well. Furthermore, to simplify the geometry-related calculations, we assume that all nodes are located along a straight line, which satisfies the distance relationship $d_{S,D} = d_{S,R} + d_{R,D}$. However, it is recalled here that the PL and distance assumptions are only indicative in the context of the considered examples, whereas the provided analysis and optimization frameworks are valid more generally. In this context, we further assume the following system parameters: $N_0 = -174$dBm/Hz; $T_{tr} = 5\mu s$; $L = 2$kbits, and $P_{LO} = 50$mW [141, 145]. We also use the constant circuit powers as $P_{CT_x} = 100$mW, $P_{CR_x} = 150$mW and the maximum transmission power $P_{maxt} = 1000$mW. The bandwidth of the system is assumed to be $B = 200$kHz and the noise figure $N_f = 6$dB. Due to the linearity requirement of the $M-$QAM signals, the value of the drain efficiency is assumed $\eta_d = 0.35$, which is a practical value for class-A and AB RF power amplifiers. The

Table 4.1 Assumed system parameters

N_0 = -174dBm/Hz	N_f = 6dB
B = 200kHz	L = 2kbits
P_{CT_x} = 100mW	P_{CR_x} = 150mW
P_{LO} = 50mW	P_{maxt} = 1000mW
$\eta_d = 0.35$	$T_{tr} = 5\mu s.$

considered system parameters are depicted in Table 4.1 and are used unless otherwise stated.

We commence by analyzing the minimum energy per information bit required for the direct and cooperative transmissions when the relay node is taken into account and placed in different locations. The location of the relay node is represented with parameter $f = d_{S,R}/d_{S,D}$. Fig. 4.5 shows the total energy consumption per information bit as a function of the transmission distance from source to destination for $4-$QAM/QPSK with fading parameter of $m = 1.25$, destination target BER of 10^{-2} and zero spatial correlation under the maximum transmit power constraint. The BER of 10^{-2} is chosen, as an example, since a relatively harsh PL model with PL constant of 4 is considered. Furthermore, such levels of BER are generally considered realistic, since our analysis measures reflect the uncoded system performance. The transmit power allocation is carried out by the derived OPA scheme resulting to the indicative values in Table 4.2. It is observed that distance thresholds separate the regions where DT performs better than CT and *vice-versa*. Furthermore, it is shown that when the relay is located in the middle, i.e., the S-R distance equals the R-D distance ($f = 0.5$), renders the best EE among all relay locations. This indicates that the configuration is almost symmetric in the S-R and R-D distances, which assists the system to operate robustly in transmission over severe fading conditions. However, it is shown that at relatively small distances (here $0 \leq d_{S,D} \leq 170m$), the exact location of the relay does not affect substantially the performance of the cooperative system as it appears to remain almost the same in all considered scenarios. This renders the relay positioning and planning rather simple when the relay falls within this range, whereas it additionally provides insights e.g., for relay selection algorithms in the case of randomly distributed relays in emerging relay-based wireless networks. The results also reveal that at relatively high S-D distances the CT scheme outperforms the DT scheme in terms of EE when the relay is placed in any of the three example locations.

The corresponding EE is also analyzed for target BERs of 10^{-2} and 10^{-3}. Fig. 4.6 shows the average total energy consumption per information bit for $4-$QAM/QPSK in both DT and CT in Nakagami-1.25 fading conditions under the maximum trans-

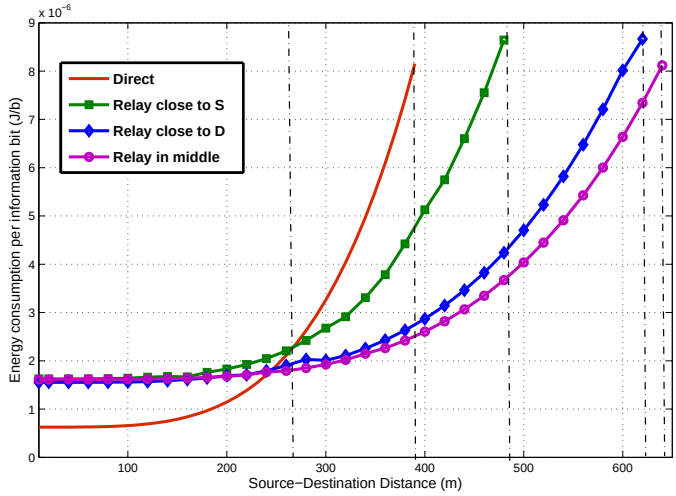

Figure 4.5 Energy consumption per information bit versus source-destination distance for different relay locations over uncorrelated Nakagami−1.25 at target BER of 10^{-2} for 4−QAM / QPSK constellation.

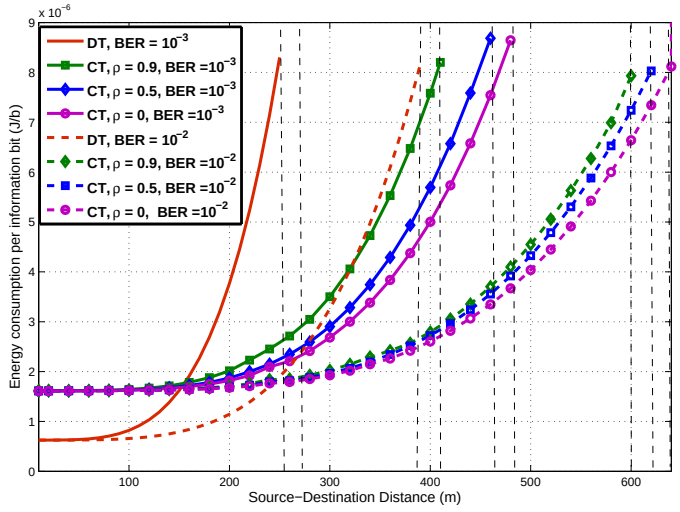

Figure 4.6 Energy consumption per information bit versus source-destination distance when the relay is located in the middle over spatially correlated Nakagami−1.25 for 4−QAM/QPSK constellations with different target BERs.

Table 4.2 Optimal transmit power values for source and relay for different relay locations over uncorrelated Nakagami−1.25 links at target BER of 10^{-2} for 4−QAM / QPSK Modulation.

	Relay close to S ($f = 0.1$)		Relay in middle ($f = 0.5$)		Relay close to D ($f = 0.9$)	
D(m)	P_S(W)	P_R(W)	P_S(W)	P_R(W)	P_S(W)	P_R(W)
100	0.00063	0.0006	0.000372	0.000197	0.000651	0.00049
200	0.016	0.0127	0.0057	0.0033	0.0104	0.0101
300	0.0877	0.0595	0.0228	0.0223	0.0527	0.0525
400	0.3366	0.1537	0.0706	0.0703	0.1666	0.0198
480	0.6225	0.3601	0.1466	0.1455	0.3455	0.0342
620	-	-	0.4107	0.402	0.9627	0.0373
650	-	-	0.4970	0.483	-	-

mit power constraint and the following spatial correlation scenarios: $\rho = \{0, 0.5, 0.9\}$. Moreover, the relay node is located in the middle and the transmit power is allocated optimally to the source and relay nodes in all cases. It is observed that for the fixed target BERs of 10^{-2} and 10^{-3}, the direct scheme outperforms the CT only at average S-D distances below 240m and 150m, respectively. On the contrary, for average distances greater than 240m and 150m, CT becomes more energy efficient as the transmit power constitutes a significant share of the average total energy consumption even under the worst spatial correlation scenario. Furthermore, it is shown that, for the given target BERs the DT schemes attain maximum transmission distances of 390m and 250m, respectively, under the given maximum transmission power constraint, whereas in both cases the CT schemes extend to substantially longer distances. However, these advantages vary according to the level of the involved spatial correlation where the improvement in EE is inversely proportional to ρ, in both scenarios. The reason is that for every step of transmission distance, greater proportion of power is assigned to the source and relay nodes in order to overcome performance losses incurred by the spatial correlation, within the given resource constraints. Concrete examples are shown in Tables 4.3 and 4.4 for some indicative transmission distances and the two target BERs; there, the energy savings using CT scheme, defined as $1 - \overline{E}_T^C / \overline{E}_T^D$ for $\rho = 0.9$, $\rho = 0.5$ and $\rho = 0$ for the target BER of 10^{-2} at $d_{S,D} = 390$m are 65%, 67% and 69.3%, respectively, whereas for a target BER of 10^{-3} at $d_{S,D} = 250$m the energy reduction is 69%, 72% and 73.8%, respectively. Interestingly, beyond a critical distance of 320m, even the highly spatially correlated CT mode at target BER of 10^{-3} exhibits better EE than the DT scheme with target BER of 10^{-2}.

In the same context, Fig. 4.7 shows the average total energy per information bit for both DT and CT for $m = 0.75$, which corresponds to severe fading conditions. The target BER is set to 10^{-2} under the given transmit power constraint while $\rho =$

Table 4.3 Optimal transmit power values for source and relay for relay located in the middle over correlated Nakagami−1.25 Links with target BER of 10^{-2} using 4−QAM / QPSK Modulation.

Corr.	$\rho = 0$		$\rho = 0.5$		$\rho = 0.9$	
D(m)	P_S(W)	P_R(W)	P_S(W)	P_R(W)	P_S(W)	P_R(W)
100	0.000372	0.000197	0.000424	0.000233	0.000514	0.000296
200	0.0057	0.0033	0.0064	0.0039	0.0077	0.0049
300	0.0225	0.0223	0.0249	0.0249	0.0290	0.0290
400	0.0706	0.0703	0.0788	0.0785	0.0918	0.0915
500	0.1728	0.1712	0.1929	0.1912	0.2249	0.2228
600	0.3598	0.3530	0.4021	0.3944	0.4692	0.4602
630	0.4381	0.4281	0.4897	0.4785	-	-
650	0.4970	0.4843	-	-	-	-

Table 4.4 Optimal transmit power values for source when the relay is located in the middle over correlated Nakagami−1.25 links with target BER of 10^{-3} using 4−QAM / QPSK constellations.

Corr.	$\rho = 0$		$\rho = 0.5$		$\rho = 0.9$	
D(m)	P_S(W)	P_R(W)	P_S(W)	P_R(W)	P_S(W)	P_R(W)
100	0.00012	0.0007	0.00014	0.0009	0.00022	0.00014
200	0.0179	0.0116	0.0218	0.0147	0.0331	0.0233
300	0.0762	0.0762	0.0914	0.0914	0.1332	0.1332
410	0.2662	0.2651	0.3196	0.3183	0.4660	0.4641
440	0.3533	0.3513	0.4242	0.4218	-	-
480	0.5009	0.4969	-	-	-	-

$\{0, 0.5, 0.9\}$. The transmit power is again allocated optimally to the source and relay with the latter positioned in the center of the network as shown in Table 4.5. It is shown that DT outperforms CT only when $d_{S,D} \leq 170m$. However, as the distance increases beyond this point, the corresponding overall benefits by CT are significant even under the worst spatial correlation scenario. Indicatively, at a transmission distance of 280m, which is the maximum distance that DT can operate with the available maximum transmission power, the energy gains by CT from the high to the low correlation values are 68%, 72% and 74%, respectively. In addition, it is shown that the advantage of the cooperation is more significant in severe fading conditions.

Fig. 4.8 shows the average total energy consumption per information bit required for CT and DT as a function of S-D distance for fading parameters, $m = \{0.75, 1.25, 1.75, 2.25\}$ for CT and $m = 2.25$ for DT. The target BER is set to 10^{-3}, the transmit power is allocated optimally, the relay is located in the middle and

Table 4.5 Optimal transmit power values for source and relay when the relay is located in the middle over spatially correlated Nakagami−0.75 links with target BER of 10^{-2} using 4−QAM / QPSK Modulations.

Corr.	$\rho = 0$		$\rho = 0.5$		$\rho = 0.9$	
D(m)	P_S(W)	P_R(W)	P_S(W)	P_R(W)	P_S(W)	P_R(W)
100	0.000754	0.0004635	0.0009112	0.0005811	0.00013	0.0009
200	0.0119	0.0076	0.0143	0.0093	0.0386	0.0097
300	0.0509	0.0509	0.0608	0.0608	0.0873	0.0873
400	0.1612	0.1606	0.1926	0.1918	0.2765	0.2753
460	0.2823	0.2802	0.3373	0.3348	0.4845	0.4808
500	0.3945	0.3905	0.4714	0.4666	-	-
530	0.4985	0.4921	-	-	-	-

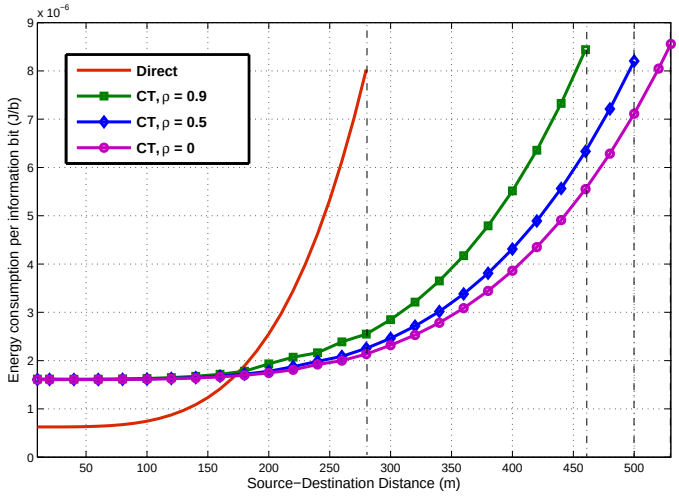

Figure 4.7 Energy consumption per information bit versus source-destination distance when the relay is located in the middle over spatially correlated Nakagami−0.75 fading channels at target BER of 10^{-2} for 4−QAM/QPSK constellation and different spatial correlation values.

a zero spatial correlation is assumed. It is observed that the critical distances below which DT outperforms the CT in terms of EE are 250m, 230m and 220m for $m = 1.25, m = 1.75,$ and $m = 2.25$, respectively. Moreover, the analysis indicates that DT with non-severe multipath fading condition (Nakagami−2.25) can operate only up to 360m before utilizing the maximum transmit power, whereas the CT extends significantly even for moderate fading conditions, except for the worst case scenario

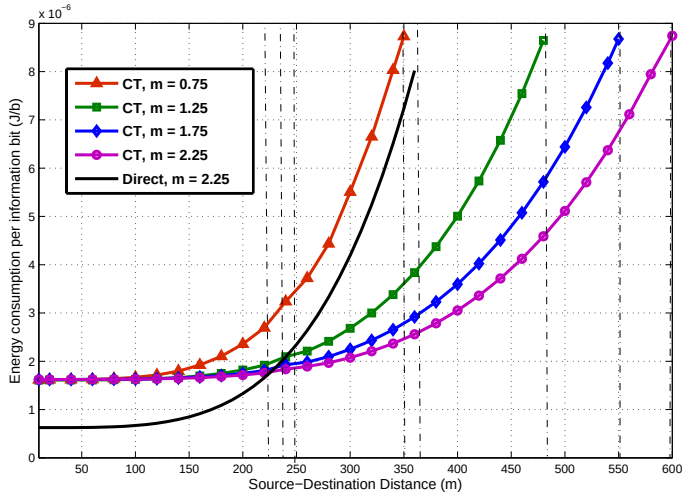

Figure 4.8 Energy consumption per information bit versus source-destination distance when the relay is located in the middle over uncorrelated Nakagami$-m$ fading conditions at target BER of 10^{-3} for 4$-$QAM / QPSK constellation.

($m = 0.75$). It is also shown that the gain from the cooperation is not uniform as the Nakagami parameter increases from $m = 0.75$ to $m = 1.25$, from $m = 1.25$ to $m = 1.75$ and then from $m = 1.75$ to $m = 2.25$.

Fig. 4.9 shows the CG, defined in (4.74), when the relay is located in the middle of the source and destination. The power allocation is again carried out by using the derived OPA scheme for target BER of 10^{-2} under the maximum transmission power constraint with $\rho = \{0, 0.5, 0.9\}$ for $m = 1.25$. The transmission distance is limited to 390m since beyond this limit it is only the CT mode that can transmit until its maximum transmission distance, depending on the spatial correlation between S-D and R-D paths. When the cooperation gain is below unity, the DT is actually more energy efficient than CT. As already mentioned, the reason behind this is that when CG ≤ 1, which corresponds to relatively small transmission distances, the actual transmit power constitutes only a small fraction of the total average power consumption. However, when CG > 1, the system benefits significantly from cooperation, and in general, CG increases proportionally as the transmission distance increases for all scenarios of spatial correlation between the S-D and R-D paths. Interestingly, the existence of such efficiency threshold distance also implies that a hybrid system, where cooperation is only sought and deployed beyond certain minimum distance, can provide the most comprehensive solution to the EE optimization. The analysis and

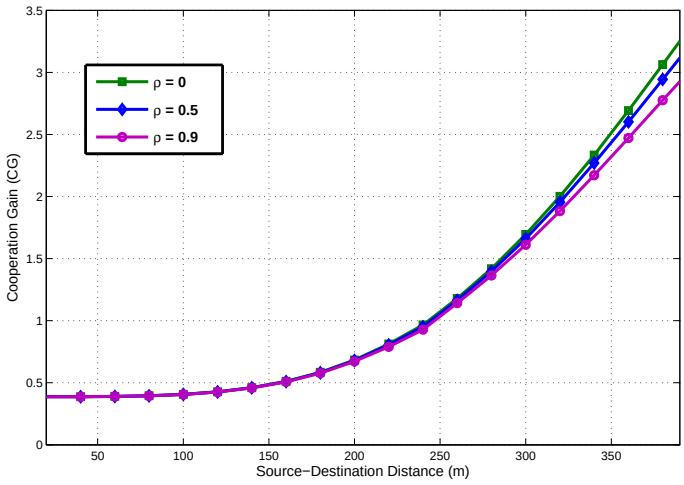

Figure 4.9 Cooperation gain versus source-destination distance when the relay is located in the middle over spatially correlated Nakagami−1.25 fading environment at target BER of 10^{-2} for 4−QAM / QPSK constellations. After source-destination distance of 390m, DT runs out of power and cannot anymore reach the target BER.

Table 4.6 System parameters.

$N_0 = $ -174dBm/Hz	$N_f = 9$dB
$B = 1$MHz	$L = 2$kbits
$P_{CT_x} = 98$mW	$P_{CR_x} = 112$mW
$P_{LO} = 50$mW	$P_{maxt} = 1500$mW
$\eta_d = 0.35$	$T_{tr} = 5\mu s.$

modeling results and tools provided in this chapter form directly the basis for further development of such schemes in different communication scenarios, which forms an important topic of future work.

As an additional numerical analysis, the average total energy consumption of the radio access system for different system parameters other than that shown in Table 4.1 is analyzed. The summary of the system parameters is given in Table 4.6 where N_0, P_{LO}, T_{tr} and η_d are given in [141], whereas the circuit powers are listed in [184].

Fig. 4.10, shows the total energy consumption per information bit as a function of S-D distance, for 4−QAM with fading parameter of $m = 1.25$, destination target BER of 10^{-2} and zero correlation under the maximum transmit power constraint when the relay is located in different locations for the case of OPA. It is observed that distance thresholds separate the regions where DT performs better than CT and

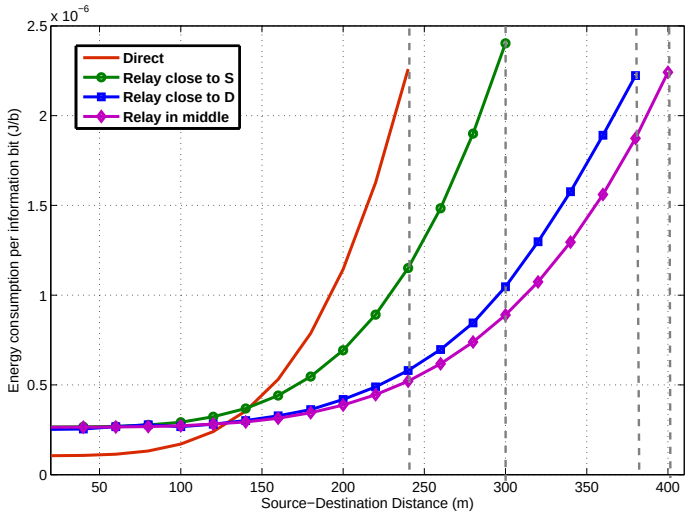

Figure 4.10 Energy consumption per information bit versus source-destination distance for relay in different locations over uncorrelated Nakagami−1.25 at target BER of 10^{-2} for 4−QAM Modulation.

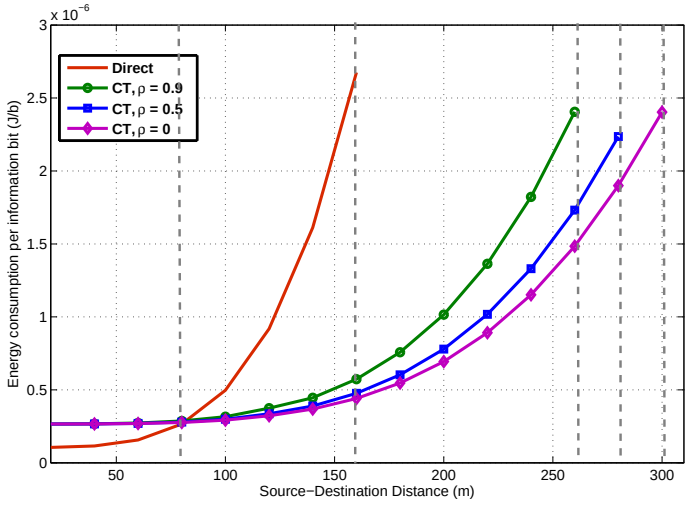

Figure 4.11 Energy consumption per information bit versus source-destination distance for relay located in the middle over correlated Nakagami−1.25 at target BER of 10^{-3} for 4−QAM Modulation.

vice-versa. Furthermore, it is shown that when the relay is located in the middle renders the best EE among all relay locations. This outcome is already shown in the previous analysis of Fig. 4.5 for different system parameter. However, it is shown that at relatively small distances (e.g., $0 \leq d_{S,D} \leq 100m$), the exact location of the relay does not affect substantially the performance of the cooperative system as it appears to remain almost the same in all considered scenarios.

Finally, Fig. 4.11 shows the total energy consumption per information bit required for CT and DT as a function of S-D distance over Nakagami-1.25 fading environment at target BER of 10^{-3}. The relay is placed in the middle and the power is allocated optimally to the source and relay to guarantee minimum energy per information bit. It is observed that at relatively small distance (e.g., $0 \leq d_{S,D} \leq 80m$) the DT scheme outperforms CT, while the system benefits substantially from CT beyond this range. Moreover, under the given QoS and maximum transmission power constraints, the DT reaches a maximum distance of 160m whereas the cooperative system extends beyond this limit even under high spatial correlation conditions. At this threshold transmission distance, the energy savings by CT are $78.6\%, 82.2\%$ and 83.5% for $\rho = 0.9$, $\rho = 0.5$ and $\rho = 0$, respectively.

4.8 Summary

In this chapter, we analyzed the end-to-end SER as well as the EE analysis and optimization of both direct and regenerative cooperative transmissions over Nakagami$-m$ fading conditions in the presence of spatial correlation. Novel closed-form expressions were first derived for the SER of both $M-$QAM and $M-$PSK constellations, which were subsequently employed in formulating the constrained energy analysis and optimization problems under destination BER target and maximum transmit power constraints considering both transmit energy as well as the energy consumed by the transceiver circuits. The corresponding results indicate that depending on the severity of multipath fading, spatial correlation between the S-D and R-D paths and the location of the relay node, the DT can be more energy-efficient than CT but only for rather short transmission distances and up to a certain threshold value. Beyond this value, the system, as expected, benefits substantially from relaying and the corresponding CG increases proportionally to the transmission distance. It is expected that the offered results can be useful in the design and deployment of low-cost and energy-efficient cooperative communication systems in the future, particularly towards the green communications era where the requirements and incentives towards energy consumption optimization are considered critical. Moreover, the EE analysis

in the considered model can be, in general, extended to multi-relay networks by considering spatial correlation effects between the direct and relayed paths of the system as well as different relay locations.

Chapter 5

Error Rate and Power Allocation Analysis of Multi-Relay Networks over $\eta-\mu$ Fading Channels

In this chapter, we investigate the end-to-end performance and power allocation of MRC based regenerative multi-relay cooperative network over non-homogeneous scattering environment, which is the case in realistic wireless communication scenarios. Novel analytic expressions are derived for the end-to-end SER of both $M-$PSK and $M-$QAM Modulations over independent and non-identically distributed (i.n.i.d) generalized fading channels. The offered results are expressed in exact analytic expressions involving Lauricella function and can be readily evaluated with the aid of the proposed computational algorithm. Simple expressions are also derived for the corresponding SER at asymptotically high SNRs. The derived expressions are employed in formulating the power optimization problem that enhances the system performance under total power constraints. It is shown that OPA provides substantial performance gains over the traditional EPA, particularly, when the S-R and R-D paths are highly unbalanced. The analysis and results presented in this chapter are mainly based on the author's published work in [117, 121].

5.1 Background and Overview of Contributions

As mentioned in the previous chapters, CT is one of the emerging technologies that promises significantly higher reliability and SE in wireless networks. Unlike conventional point-to-point communications, cooperative communication is a new form of

diversity scheme that allows users or nodes to share resources to create collaboration via distributed transmission and processing of messages. This scheme is applicable in size, power, hardware and price constrained devices, such as cellular mobile devices, wireless sensors, ad-hoc networks and military communications [9, 185–190].

The performance of cooperative systems can be substantially improved by optimally allocating the limited overall power to the source and relays of the network in order to minimize the end-to-end SER under a given total transmit power constraint. Among others, this can be efficiently achieved by accurately accounting for the detrimental effects of multipath fading. Based on this, Huang *et al.* [191] derived upper and lower bounds for the OP of multi-relay DF networks over i.n.i.d Nakagami$-m$ fading channels. In the same context, Duong *et al.* [163] derived the SER and OP of DF systems with relay selection over i.n.i.d Nakagami$-m$ fading channels for integer values of m, whereas a comprehensive analytical framework for a dual-hop multi-antenna DF system under multipath fading was derived in [192]. Likewise, the authors in [166, 193–195] investigated the performance of DF systems over different fading environments, whereas analysis for the SER of dual-hop DF relaying for $M-$PSK and $M-$QAM over Nakagami$-m$ fading channels was reported in [168]. In addition, [168] and [196] analyzed OPA in dual-hop regenerative relaying with respect to end-to-end SER and OP. This problem was also addressed in [197] for multi-node DF relaying based on asymptotic SER for a given network topology over Rayleigh fading channel. In the same context, [167] analyzed the power allocation schemes for the case of multi-relay DF communications in the high-SNR regime over Nakagami$-m$ fading channels.

Nevertheless, all reported investigations in performance as well as in OPA analysis have been carried out over Rayleigh or Nakagami$-m$ fading channels. However, as mentioned in Chapter 3, these fading models are based on the underlying concept of homogeneous scattering environments, which is not practically realistic since surfaces in most radio propagation environments are spatially correlated [77]. This issue was addressed in [78] by proposing the $\eta-\mu$ distribution, which is a generalized fading model that has been shown to provide particularly accurate fitting to realistic measurement results, while it includes as special cases the well known Rayleigh, Nakagami$-m$ and Hoyt distributions [78, 109, 199, 200]. Based on this, several contributions have been devoted to the analysis of various communication scenarios over generalized fading channels that follow the $\eta-\mu$ distribution, e.g., [107, 199–203]. Motivated by this, this chapter is devoted to the evaluation of the end-to-end SER in regenerative cooperative communication systems with multiple relays for $M-$PSK and $M-$QAM constellations over generalized fading channels as well as the corre-

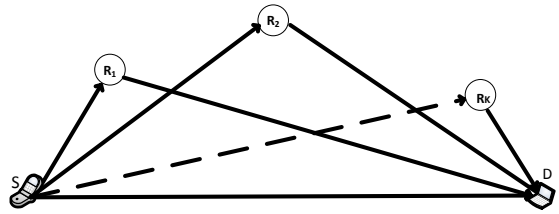

Figure 5.1 Multi-node dual hop cooperative relay system.

sponding OPA analysis.

In more detail, the technical contributions of this chapter are as follows:

- Exact expressions are derived for the end-to-end SER of $M-$PSK and $M-$QAM based multi-relay regenerative networks over generalized multipath fading environments for both i.n.i.d and i.i.d scenarios using MRC at the destination.
- Simple asymptotic expressions are derived for the above scenarios for high SNR values.
- The corresponding amount of fading is derived for quantifying the respective fading severity.
- OPA based on the convexity of the derived asymptotic expressions is formulated, to minimize the corresponding SER under sum-power constraint of the network.
- The derived expressions are employed in evaluating the performance of the considered system for extracting useful insights.
- Simple MATLAB algorithm is proposed for the computation of the generalized Lauricella function.
- It is shown that a maximum gain of 21dB occurs, compared to the ordinary DT, even if only few nodes are employed. This renders the resource constrained communication system a meaningful alternative for increasing the QoS of the demanding emerging wireless systems.

5.2 System and Channel Models

We consider a multi-node cooperative radio access system consisting of a source node S, intermediate relay nodes R_k, with $k = \{1, 2, \cdots, K\}$, and a destination node D, as shown in Fig. 5.1. Each node in the system is equipped with a single antenna while a

HD-DF protocol is adopted. Furthermore, it is assumed that the transmission channels for all relays are orthogonal, such that the transmitted signals from each relay can be separately processed at the destination without any interference from other relays, and finally combined in order to obtain the corresponding cooperation gain. The most common approach to compose such orthogonal channels is the time-based model, where $K+1$ different time slots are adopted and allocated properly. In this case, the first slot is used for broadcasting from the source to the destination and to all K relays, whereas the following K slots are subsequently used, one relay at a time, to transmit re-encoded and modulated signals from relays to the destination, e.g., [6, 167, 196, 197]. Alternative effective approaches can be obtained through frequency division multiplexing (FDM) and code division multiplexing (CDM), primarily orthogonal frequency division multiple-access (OFDMA) and code division multiple access (CDMA). In the OFDMA scenario, different subsets or sub-bands of subcarriers can provide the orthogonal channels while in the CDMA case, this can be realized by $K+1$ different orthogonal spreading codes [1]. Based on this and without loss of generality, the received signals in the first time slot can be represented as follows:

$$y_{S,D} = \sqrt{P_S}\alpha_{S,D}x + n_{S,D} \tag{5.1}$$

and

$$y_{S,R_k} = \sqrt{P_S}\alpha_{S,R_k}x + n_{S,R_k} \tag{5.2}$$

where x is the transmitted symbol with normalized unit energy in the first transmission phase, α_{S,R_k} is the complex fading coefficients from the source to the k^{th} relay, whereas n_{S,R_k} represents the corresponding AWGN with zero mean and variance N_0. In the next time-slots, if the k^{th} relay decodes correctly, then it forwards the decoded and re-encoded signal to the destination over the k^{th} orthogonal channel with power P_{R_k}; otherwise, it remains silent. To this effect, the received signal at the destination can be expressed as follows:

$$y_{R_k,D} = \sqrt{C(k)P_{R_k}}\alpha_{R_k,D}x + n_{R_k,D} \tag{5.3}$$

where $C(k) = 1$ if the k^{th} relay decodes successfully; otherwise, $C(k) = 0$. Also, $\alpha_{R_k,D}$ denotes the complex fading coefficient from the k^{th} relay to the destination and $n_{R_k,D}$ is the corresponding AWGN. Here, MRC diversity scheme is employed at the destination. Based on this, the corresponding combined output received signal

[1] In this chapter, we do not explicitly assume any of the above models but instead emphasize on the availability of the orthogonal resources, which ensure that the inter-relay interference at the destination node is ultimately avoided

can be expressed as follows:

$$y_D = w_S y_{S,D} + \sum_{k=1}^{K} w_k y_{R_k,D} \tag{5.4}$$

where $w_S = \sqrt{P_S}\alpha^*_{S,D}/N_0$ and $w_k = \sqrt{C(k)P_{R_k}}\alpha^*_{R_k,D}/N_0$ denote the optimal MRC coefficients for $y_{S,D}$ and $y_{R_k,D}$, respectively.

It is noted that in any considered strategy of assigning orthogonal channels, if the mapping of the physical resources i.e. time slots, frequencies, or codes is practically fixed and a particular relay node fails to decode correctly, the corresponding physical resource is momentarily left unused. On the other hand, if a centralized but dynamic resource management is available in the system, the physical resources can be allocated or re-allocated dynamically for e.g. always to those nodes that are able to decode correctly. This, however, requires additional control signaling between the relay nodes and the central control unit, which in turn reduces relatively the efficiency of the overall resource use on its own[2].

In the considered system, each path is assumed to experience narrowband multipath fading that follows the $\eta-\mu$ distribution. This distribution has been shown to account accurately for small-scale variations of the signal in NLOS communication scenarios where it is described by the two named parameters, η and μ, and it is valid for two different formats that correspond to two physical models as described in Subsection 3.3.3. The PDF of the instantaneous SNR γ is also given in (3.36).

5.3 Exact end-to-end Symbol Error Rate Analysis

The end-to-end SER for the considered cooperative system can be expressed as follows [167], [197]:

$$P_{\text{SER}} = \sum_{z=0}^{2^K-1} P(e|\mathbf{A} = \mathbf{C}_z)P(\mathbf{A} = \mathbf{C}_z) \tag{5.5}$$

where the binary vector $\mathbf{A} = [A(1), A(2), A(3), ..., A(K)]$ of dimension $(1 \times K)$ denotes the state of the relay nodes in the system, with $A(k)$ taking the binary values of 1 and 0 for successful and unsuccessful decoding, respectively. Furthermore, $\mathbf{C}_z = [C(1), C(2), C(3), \cdots, C(K)]$ denotes different possible decoding combinations of the relays with $z \in \{0, 2^K - 1\}$, where $C(k)$ takes the value of either 0 or 1. To this effect, for the case of statistically independent channels the joint probability of the possible

[2]These aspects are not addressed further in this chapter, but they form an important topic for the future work

state outcomes can be represented as follows:

$$P(\mathbf{A}=\mathbf{C}_z)=\prod_{k=1}^{K}P(A(k)=C(k)). \tag{5.6}$$

Notably, the conditional error probability $P(e|\mathbf{A}=\mathbf{C}_z)$ is the error probability conditioned on particular decoding results at relays, whereas $P(\mathbf{A}=\mathbf{C}_z)$ is the corresponding joint probability of the decoding outcomes. Based on the MRC method, the instantaneous SNR at the destination for a given decoding combination, $\mathbf{C}_z$, can be expressed as follows [167]:

$$\gamma_{\mathrm{MRC}}(\mathbf{C}_z)=|\alpha_{S,D}|^2\frac{P_0}{N_0}+\sum_{k=1}^{K}C(k)|\alpha_{R_k,D}|^2\frac{P_{R_k}}{N_0}. \tag{5.7}$$

Furthermore, the MGF for independent fading channels in DF scheme is given by [204]

$$\mathrm{M}_{\gamma_{\mathrm{MRC}}}(s)=M_{\gamma_{S,D}}(s)\prod_{k=1}^{K}M_{\gamma_{R_k,D}}(s) \tag{5.8}$$

which in the present analysis can be expressed in terms of the modulation scheme employed as follows [107]:

$$M_{\gamma_{\eta-\mu}}\left(\frac{g}{\sin^2\theta}\right)=\left(\frac{4\mu^2h}{(2(h-H)\mu+\frac{g}{\sin^2\theta}\bar{\gamma})(2(h+H)\mu+\frac{g}{\sin^2\theta}\bar{\gamma})}\right)^{\mu}. \tag{5.9}$$

It is noted that the expression in (5.9) is particularly useful in the subsequent end-to-end SER analysis of the considered cooperative network system for different modulation schemes.

5.3.1 End-to-End SER for $M-$PSK Constellations

The case of i.n.i.d $\eta-\mu$ fading channels

The end-to-end error probability for $M-$PSK constellations over individual $\eta-\mu$ fading link when η, μ and $\bar{\gamma}$ in each path are not necessarily equal can be expressed as follows [76, Eq. (5.78)]:

$$\bar{P}_{M-\mathrm{PSK}}=\underbrace{\frac{1}{\pi}\int_0^{\pi/2}M_\gamma\left(\frac{g_{\mathrm{PSK}}}{\sin^2\theta}\right)\mathrm{d}\theta}_{\triangleq\mathcal{I}_1}+\underbrace{\frac{1}{\pi}\int_{\pi/2}^{\frac{(M-1)\pi}{M}}M_\gamma\left(\frac{g_{\mathrm{PSK}}}{\sin^2\theta}\right)\mathrm{d}\theta}_{\triangleq\mathcal{I}_{11}}. \tag{5.10}$$

In order to evaluate (5.5), we first need to determine the error probability for decoding at the destination terminal, using MRC, under given decoding outcomes at nodes, i.e., for a given $\mathbf{C}_z$ [205]. To this end and based on the MGF approach it follows that

$$P(e|\mathbf{A}=\mathbf{C}_z)=\frac{1}{\pi}\int_0^{\pi/2}\left(\frac{4\mu_{S,D}^2 h_{S,D}(2(h_{S,D}+H_{S,D})\mu_{S,D}+\frac{g_{\mathrm{PSK}}}{\sin^2\theta}\bar{\gamma}_{S,D})^{-1}}{(2(h_{S,D}-H_{S,D})\mu_{S,D}+\frac{g_{\mathrm{PSK}}}{\sin^2\theta}\bar{\gamma}_{S,D})}\right)^{\mu_{S,D}}$$
$$\times\prod_{k=1}^{K}\left(\frac{4\mu_{R_k,D}^2 h_{R_k,D}\,(2(h_{R_k,D}-H_{R_k,D})\mu_{R_k,D}+\frac{g_{\mathrm{PSK}}}{\sin^2\theta}\bar{\gamma}_{R_k,D})^{-1}}{2(h_{R_k,D}+H_{R_k,D})\mu_{R_k,D}+\frac{g_{\mathrm{PSK}}}{\sin^2\theta}\bar{\gamma}_{R_k,D}}\right)^{\mu_{R_k,D}}\mathrm{d}\theta$$
$$+\frac{1}{\pi}\int_{\pi/2}^{\frac{(M-1)\pi}{M}}\left(\frac{4\mu_{S,D}^2 h_{S,D}(2(h_{S,D}+H_{S,D})\mu_{S,D}+\frac{g_{\mathrm{PSK}}}{\sin^2\theta}\bar{\gamma}_{S,D})^{-1}}{(2(h_{S,D}-H_{S,D})\mu_{S,D}+\frac{g_{\mathrm{PSK}}}{\sin^2\theta}\bar{\gamma}_{S,D})}\right)^{\mu_{S,D}}$$
$$\times\prod_{k=1}^{K}\left(\frac{4\mu_{R_k,D}^2 h_{R_k,D}\,(2(h_{R_k,D}-H_{R_k,D})\mu_{R_k,D}+\frac{g_{\mathrm{PSK}}}{\sin^2\theta}\bar{\gamma}_{R_k,D})^{-1}}{(2(h_{R_k,D}+H_{R_k,D})\mu_{R_k,D}+\frac{g_{\mathrm{PSK}}}{\sin^2\theta}\bar{\gamma}_{R_k,D})}\right)^{\mu_{R_k,D}}\mathrm{d}\theta. \tag{5.11}$$

Evidently, the derivation of an analytic solution for (5.11) is subject to analytic evaluation of the integrals $\mathcal{I}_1$ and $\mathcal{I}_{11}$ in closed-form. To this end, for the case of non-identical fading parameters, i.e, $\mu_{S,D}\neq\mu_{R_1,D}\neq\cdots\neq\mu_{R_K,D}$, $\eta_{S,D}\neq\eta_{R_1,D}\neq\cdots\neq\eta_{R_K,D}$ and $\overline{\gamma}_{S,D}\neq\overline{\gamma}_{R_1,D}\neq\cdots\neq\overline{\gamma}_{R_k,D}$, the $\mathcal{I}_1$ term can be alternatively expressed as follows

$$\mathcal{I}_1=\frac{1}{\pi}\int_0^{\pi/2}\frac{1}{\left(1+\frac{A_1}{\sin^2\theta}\right)^{\mu_{S,D}}\left(1+\frac{A_2}{\sin^2\theta}\right)^{\mu_{S,D}}}\prod_{k=1}^{K}\frac{\mathrm{d}\theta}{\left(1+\frac{B_{1k}}{\sin^2\theta}\right)^{\mu_{R_k,D}}\left(1+\frac{B_{2k}}{\sin^2\theta}\right)^{\mu_{R_k,D}}} \tag{5.12}$$

where

$$\left\{\begin{matrix}A_1\\A_2\end{matrix}\right\}=\frac{\overline{\gamma}_{S,D}g_{\mathrm{PSK}}}{2(h_{S,D}\left\{\mp\right\}H_{S,D})\mu_{S,D}} \tag{5.13}$$

and

$$\left\{\begin{matrix}B_{1k}\\B_{2k}\end{matrix}\right\}=\frac{\overline{\gamma}_{R_k,D}g_{\mathrm{PSK}}}{2(h_{R_k,D}\{\mp\}H_{R_k,D})\mu_{R_k,D}}. \tag{5.14}$$

By also setting $u=\sin^2(\theta)$ and carrying out tedious but basic algebraic manipulations, (5.12) can be expressed as follows:

$$\mathcal{I}_1=\frac{\beta_{\gamma_{\mathrm{MRC}}}(g_{\mathrm{PSK}})}{2\pi} \times\int_0^1 \frac{(1-u)^{-\frac{1}{2}}u^{2(\mu_{S,D}+\sum_{k=1}^{K}C(k)\mu_{R_k,D})-\frac{1}{2}}}{\left(1+\frac{u}{A_1}\right)^{\mu_{S,D}}\left(1+\frac{u}{A_2}\right)^{\mu_{S,D}}}\prod_{k=1}^{K}\frac{\mathrm{d}u}{\left(1+\frac{u}{B_{1k}}\right)^{\mu_{R_k,D}}\left(1+\frac{u}{B_{2k}}\right)^{\mu_{R_k,D}}} \tag{5.15}$$

where

$$\beta_{\gamma_{\mathrm{MRC}}}(g_{\mathrm{PSK}})=\left(\frac{4\mu_{S,D}^2(h_{S,D}^2-H_{S,D}^2)}{\overline{\gamma}_{S,D}^2 g_{\mathrm{PSK}}^2}\right)^{\mu_{S,D}}\prod_{k=1}^{K}\left(\frac{4\mu_{R_k,D}^2(h_{R_k,D}^2-H_{R_k,D}^2)}{\overline{\gamma}_{R_k,D}^2 g_{\mathrm{PSK}}^2}\right)^{\mu_{R_k,D}} \tag{5.16}$$

Importantly, (5.15) can be expressed explicitly in terms of [104, Eq. (7.2.4.57)], yielding

$$\mathcal{I}_1=\frac{\beta_{\gamma_{\mathrm{MRC}}}(g_{\mathrm{PSK}})\Gamma(2\mu_{S,D}+2\sum_{k=1}^{K}C(k)\mu_{R_k,D}+\frac{1}{2})}{2\sqrt{\pi}\Gamma(2\mu_{S,D}+2\sum_{k=1}^{K}C(k)\mu_{R_k,D}+1)} \tag{5.17}$$

$$\times F_D^{(2K+2)}\left(2\mu_{S,D}+2\sum_{k=1}^{K}C(k)\mu_{R_k,D}+\frac{1}{2};\mu_{S,D},\mu_{S,D},\mu_{R_1,D},\cdots,\mu_{R_K,D},\mu_{R_1,D},\cdots,\right.$$

$$\left.\mu_{R_K,D};2\mu_{S,D}+2\sum_{k=1}^{K}C(k)\mu_{R_k,D}+1;-\frac{1}{A_1},-\frac{1}{A_2},-\frac{1}{B_{11}},\cdots,-\frac{1}{B_{1K}},-\frac{1}{B_{21}},\cdots,-\frac{1}{B_{2,K}}\right)$$

where $F_D^{(n)}(\cdot)$ denotes the generalized Lauricella hypergeometric function of n variables [104].

In the same context, for the $\mathcal{I}_{11}$ integral we set $u=\cos^2(\theta)/\cos^2(\pi/M)$ in (5.11) yield

$$\mathcal{I}_{11}=\frac{M_{\gamma_{\mathrm{MRC}}}(g_{\mathrm{PSK}})\cos(\pi/M)}{2\pi}$$

$$\times\int_0^1 \frac{u^{-\frac{1}{2}}(1-\cos^2(\pi/M)u)^{2(\mu_{S,D}+\sum_{k=1}^{K}C(k)\mu_{R_k,D})-\frac{1}{2}}}{\left(1-\frac{\cos^2(\pi/M)}{1+A_1}u\right)^{\mu_{S,D}}\left(1-\frac{\cos^2(\pi/M)}{1+A_2}u\right)^{\mu_{S,D}}}\prod_{k=1}^{K}\frac{\left(1-\frac{\cos^2(\pi/M)}{1+B_{2k}}u\right)^{-\mu_{R_k,D}}}{\left(1-\frac{\cos^2(\pi/M)}{1+B_{1k}}u\right)^{\mu_{R_k,D}}}\mathrm{d}u. \tag{5.18}$$

Evidently, the involved integral can be also expressed in an exact-form in terms of the $F_D^{(n)}(\cdot)$ function; therefore, by performing the necessary change of variables and

substituting in (5.18), one obtains

$$\mathcal{I}_{11} = \frac{M_{\gamma_{\mathrm{MRC}}}(g_{\mathrm{PSK}})}{\pi} F_D^{(2K+3)}\left(\frac{1}{2}; \mu_{S,D}, \mu_{S,D}, \mu_{R_1,D}, \cdots, \mu_{R_K,D}, \mu_{R_1,D}, \cdots, \mu_{R_K,D}, \right.$$
$$\frac{1}{2} - 2\mu_{S,D} - 2\sum_{k=1}^{K} C(k)\mu_{R_K,D}; \frac{3}{2}; \frac{\cos^2(\pi/M)}{1+A_1}, \frac{\cos^2(\pi/M)}{1+A_2}, \frac{\cos^2(\pi/M)}{1+B_{11}}, \cdots,$$
$$\left.\frac{\cos^2(\pi/M)}{1+B_{1K}}, \frac{\cos^2(\pi/M)}{1+B_{21}}, \cdots, \frac{\cos^2(\pi/M)}{1+B_{2K}}, \cos^2(\pi/M)\right). \tag{5.19}$$

It is noted here that the $F_D^{(n)}(\cdot)$ function has been studied extensively over the past decades. Nevertheless, despite its importance it is not unfortunately included as built-in function in popular software packages such as MATLAB, MATHEMATICA and MAPLE. Based on this, a simple MATLAB algorithm for computing this function straightforwardly is proposed in Appendix E.

The case of i.i.d $\eta-\mu$ fading channels

For the special case of identical relay to destination paths i.e., $\mu_{R_1,D} = \cdots = \mu_{R_K,D} = \mu_{R,D}, \eta_{R_1,D} = \cdots = \eta_{R_K,D} = \eta_{R,D}$, $\overline{\gamma}_{R_1,D} = \cdots = \overline{\gamma}_{R_K,D} = \overline{\gamma}_{R,D}$ and thus, $B_{11} = \cdots = B_{1K} = B_1$, and $B_{21} = \cdots = B_{2K} = B_2$, equations (5.17) and (5.19) can be readily simplified to the following representations

$$\mathcal{I}_{1\mathrm{i.i.d}} = \frac{\beta_{\gamma_{\mathrm{MRC}}}(g_{\mathrm{PSK}})\Gamma\left(2\mu_{S,D} + 2\mu_{R,D}\sum_{k=1}^{K} C(k) + \frac{1}{2}\right)}{2\sqrt{\pi}\Gamma\left(2\mu_{S,D} + 2\mu_{R,D}\sum_{k=1}^{K} C(k) + 1\right)} F_D^{(4)}\left(2\mu_{S,D} + 2\mu_{R,D}\sum_{k=1}^{K} C(k)\right.$$
$$\left.+\frac{1}{2}; \mu_{S,D}, \mu_{S,D}, K\mu_{R,D}, K\mu_{R,D}; 2\mu_{S,D} + 2\mu_{R,D}\sum_{k=1}^{K} C(k) + 1; -\frac{1}{A_1}, -\frac{1}{A_2}, -\frac{1}{B_1}, -\frac{1}{B_2}\right) \tag{5.20}$$

and

$$\mathcal{I}_{11\mathrm{i.i.d}} = \frac{M_{\gamma_{\mathrm{MRC}}}(g_{\mathrm{PSK}})}{\pi} F_D^{(5)}\left(\frac{1}{2}; \mu_{S,D}, \mu_{S,D}, K\mu_{R,D}, K\mu_{R,D}, \frac{1}{2} - 2\mu_{S,D} - 2\mu_{R,D}\sum_{k=1}^{K} C(k)\right.$$
$$\left.; \frac{3}{2}; \frac{\cos^2(\pi/M)}{1+A_1}, \frac{\cos^2(\pi/M)}{1+A_2}, \frac{\cos^2(\pi/M)}{1+B_1}, \frac{\cos^2(\pi/M)}{1+B_2}, \cos^2(\pi/M)\right), \tag{5.21}$$

respectively. As a result, with the aid of the derived expressions for $\mathcal{I}_1$ and $\mathcal{I}_{11}$, the corresponding error probability for $M-$PSK constellations can be determined by $P(e|\mathbf{A}=\mathbf{C}_z)=\mathcal{I}_1+\mathcal{I}_{11}$.

It is recalled that the derivation of the overall SER also requires the determination of the decoding probability of the relay nodes $P(\mathbf{A}=\mathbf{C}_z)$. This is in fact a direct product of the terms $P(\bar{\gamma}_{S,R_k})=P(A(k)=C(k)=0)$, i.e., decoding error at the relays and $(1-P(\bar{\gamma}_{S,R_k}))=P(A(k)=C(k)=1)$, i.e., successful decoding at the relays, which, as already mentioned, is a pre-requisite for forwarding re-encoded signals to the destination. Importantly, this can be also determined in closed-form with the aid of the commonly used MGF approach, namely

$$P(\bar{\gamma}_{S,R_k})=\underbrace{\frac{1}{\pi}\int_0^{\pi/2}M_{\gamma_{S,R_k}}\left(\frac{g_{\mathrm{PSK}}}{\sin^2\theta}\right)\mathrm{d}\theta}_{\triangleq\mathcal{I}_2}+\underbrace{\frac{1}{\pi}\int_{\pi/2}^{\frac{(M-1)\pi}{M}}M_{\gamma_{S,R_k}}\left(\frac{g_{\mathrm{PSK}}}{\sin^2\theta}\right)\mathrm{d}\theta}_{\triangleq\mathcal{I}_{22}} \quad (5.22)$$

which with the aid of (5.9) can be equivalently re-written as follows:

$$\begin{aligned}&P(A(k)=C(k)=0)\\&=\frac{1}{\pi}\int_0^{\pi/2}\left(\frac{4\mu_{S,R_k}^2h_{S,R_k}\left(2(h_{S,R_k}+H_{S,R_k})\mu_{S,R_k}+\frac{g_{\mathrm{PSK}}}{\sin^2\theta}\bar{\gamma}_{S,R_k}\right)^{-1}}{\left(2(h_{S,R_k}-H_{S,R_k})\mu_{S,R_k}+\frac{g_{\mathrm{PSK}}}{\sin^2\theta}\bar{\gamma}_{S,R_k}\right)}\right)^{\mu_{S,R_k}}\mathrm{d}\theta\\&+\frac{1}{\pi}\int_{\pi/2}^{\frac{(M-1)\pi}{M}}\left(\frac{4\mu_{S,R_k}^2h_{S,R_k}\left(2(h_{S,R_k}+H_{S,R_k})\mu_{S,R_k}+\frac{g_{\mathrm{PSK}}}{\sin^2\theta}\bar{\gamma}_{S,R_k}\right)^{-1}}{\left(2(h_{S,R_k}-H_{S,R_k})\mu_{S,R_k}+\frac{g_{\mathrm{PSK}}}{\sin^2\theta}\bar{\gamma}_{S,R_k}\right)}\right)^{\mu_{S,R_k}}\mathrm{d}\theta.\end{aligned} \quad (5.23)$$

Notably, the integrals in (5.23) have similar algebraic form to $\mathcal{I}_1$ and $\mathcal{I}_{11}$ since the difference is the absence of $\mu_{R_k,D}$ terms. As a result, the following exact analytic expressions are deduced:

$$\begin{aligned}\mathcal{I}_2=&\frac{\beta_{\gamma_{S,R_k}}(g_{\mathrm{PSK}})\Gamma(2\mu_{S,R_k}+\frac{1}{2})}{2\sqrt{\pi}\Gamma(2\mu_{S,R_k}+1)}\\&\times F_D^{(2)}\left(2\mu_{S,R_k}+\frac{1}{2};\ \mu_{S,R_k},\mu_{S,R_k};2\mu_{S,R_k}+1;-\frac{1}{C_1},-\frac{1}{C_2}\right)\end{aligned} \quad (5.24)$$

and

$$\begin{aligned}\mathcal{I}_{22}=&\frac{M_{\gamma_{S,R_k}}(g_{\mathrm{PSK}})}{\pi}\\&\times F_D^{(3)}\left(\frac{1}{2};\mu_{S,R_k},\mu_{S,R_k},\frac{1}{2}-2\mu_{S,R_k};\frac{3}{2};\frac{\cos^2(\pi/M)}{1+C_1},\frac{\cos^2(\pi/M)}{1+C_2},\cos^2(\pi/M)\right)\end{aligned} \quad (5.25)$$

where

$$\left\{\begin{matrix} C_1 \\ C_2 \end{matrix}\right\} = \frac{\overline{\gamma}_{S,R_k} g_{\mathrm{PSK}}}{2(h_{S,R_k}\{\mp\}H_{S,R_k})} \tag{5.26}$$

and

$$\beta_{S,R_k}(g_{\mathrm{PSK}}) = \left(\frac{4\mu_{S,R_k}^2(h_{S,R_k}^2 - H_{S,R_k}^2)}{\overline{\gamma}_{S,R_k}^2 g_{\mathrm{PSK}}^2}\right)^{\mu_{S,R_k}}. \tag{5.27}$$

Therefore, the P_{SER} for $M-$PSK is deduced by inserting the corresponding results of $P(e|\mathbf{A}=\mathbf{C}_z)$ and $P(\mathbf{A}=\mathbf{C}_z)$ in (5.5).

5.3.2 End-to-End SER for $M-$QAM Constellations

Having derived the SER over i.n.i.d and i.i.d $\eta-\mu$ fading channels for the case of $M-$PSK modulations, we can readily derived the respective SER for the case of $M-$QAM constellations.

The case of i.n.i.d $\eta-\mu$ fading channels

In the case of independent but not necessarily identically distributed $\eta-\mu$ fading channels and based on [76, Eq. (9.21)], it follows that

$$\bar{P}_{M-\mathrm{QAM}} = \frac{4C}{\pi}\underbrace{\int_0^{\pi/2} M_{\gamma_{\mathrm{MRC}}}\left(\frac{g_{\mathrm{QAM}}}{\sin^2\theta}\right)\mathrm{d}\theta}_{\triangleq\mathcal{I}_3} - \frac{4C^2}{\pi}\underbrace{\int_0^{\pi/4} M_{\gamma_{\mathrm{MRC}}}\left(\frac{g_{\mathrm{QAM}}}{\sin^2\theta}\right)\mathrm{d}\theta}_{\triangleq\mathcal{I}_4} \tag{5.28}$$

In this case, the probability of decoding error using the MRC scheme under given decoding results at the relays can be expressed as follows:

$$\begin{aligned} P(e|\mathbf{A}=\mathbf{C}_z) = \frac{4C}{\pi}\int_0^{\pi/2}&\left(\frac{4\mu_{S,D}^2 h_{S,D}(2(h_{S,D}+H_{S,D})\mu_{S,D}+\frac{g_{\mathrm{QAM}}}{\sin^2\theta}\bar{\gamma}_{S,D})^{-1}}{(2(h_{S,D}-H_{S,D})\mu_{S,D}+\frac{g_{\mathrm{QAM}}}{\sin^2\theta}\bar{\gamma}_{S,D})}\right)^{\mu_{S,D}} \\ &\times\prod_{k=1}^{K}\left(\frac{4\mu_{R_k,D}^2 h_{R,k,D}\,(2(h_{R_k,D}+H_{R_k,D})\mu_{R_k,D}+\frac{g_{\mathrm{QAM}}}{\sin^2\theta}\bar{\gamma}_{R_k,D})^{-1}}{(2(h_{R_k,D}-H_{R_k,D})\mu_{R_k,D}+\frac{g_{\mathrm{QAM}}}{\sin^2\theta}\bar{\gamma}_{R_k,D})}\right)^{\mu_{R_k,D}}\mathrm{d}\theta \\ &-\frac{4C^2}{\pi}\int_0^{\pi/4}\left(\frac{4\mu_{S,D}^2 h_{S,D}(2(h_{S,D}+H_{S,D})\mu_{S,D}+\frac{g_{\mathrm{QAM}}}{\sin^2\theta}\bar{\gamma}_{S,D})^{-1}}{(2(h_{S,D}-H_{S,D})\mu_{S,D}+\frac{g_{\mathrm{QAM}}}{\sin^2\theta}\bar{\gamma}_{S,D})}\right)^{\mu_{S,D}} \\ &\times\prod_{k=1}^{K}\left(\frac{4\mu_{R_k,D}^2 h_{R_k,D}\,(2(h_{R_k,D}+H_{R_k,D})\mu_{R_k,D}+\frac{g_{\mathrm{QAM}}}{\sin^2\theta}\bar{\gamma}_{R_k,D})^{-1}}{(2(h_{R_k,D}-H_{R_k,D})\mu_{R_k,D}+\frac{g_{\mathrm{QAM}}}{\sin^2\theta}\bar{\gamma}_{R_k,D})}\right)^{\mu_{R_k,D}}\mathrm{d}\theta. \end{aligned} \tag{5.29}$$

Evidently, the derivation of an exact expression for (5.29) is subject to analytic evaluation of the above two integrals that correspond to $\mathcal{I}_3$ and $\mathcal{I}_4$. Following the same methodology as in the case of $M-$PSK constellations and using the change of variable of $u = \sin^2\theta$, one obtains

$$\mathcal{I}_3 = \frac{\beta_{\gamma_{\mathrm{MRC}}}(g_{\mathrm{QAM}})}{2} \times \int_0^1 \frac{(1-u)^{-\frac{1}{2}} u^{2(\mu_{S,D}+\sum_{k=1}^{K} C(k)\mu_{R_k,D})-\frac{1}{2}}}{\left(1+\frac{u}{A_1}\right)^{\mu_{S,D}} \left(1+\frac{u}{A_2}\right)^{\mu_{S,D}}} \prod_{k=1}^{K} \frac{\mathrm{d}u}{\left(1+\frac{u}{B_{1k}}\right)^{\mu_{R_k,D}} \left(1+\frac{u}{B_{2k}}\right)^{\mu_{R_k,D}}} \tag{5.30}$$

where the parameters A_1, A_2, B_{1k} and B_{2k} are determined by substituting g_{PSK} with g_{QAM} in (5.13) and (5.14), respectively. To this effect and after some algebraic manipulations, the following analytic expression is deduced:

$$\mathcal{I}_3 = \frac{\beta_{\gamma_{\mathrm{MRC}}}(g_{\mathrm{QAM}})\sqrt{\pi}\Gamma\left(2\mu_{S,D}+2\sum_{k=1}^{K} C(k)\mu_{R_k,D}+\frac{1}{2}\right)}{2\Gamma\left(2\mu_{S,D}+2\sum_{k=1}^{K} C(k)\mu_{R_k,D}+1\right)} \times F_D^{(2K+2)}\left(2\mu_{S,D}+2\sum_{k=1}^{K} C(k)\mu_{R_k,D}+\frac{1}{2}; \mu_{S,D}, \mu_{S,D}, \mu_{R_1,D}, \cdots, \mu_{R_K,D}, \mu_{R_1,D}, \cdots, \mu_{R_K,D}; 2\mu_{S,D}+2\sum_{k=1}^{K} C(k)\mu_{R_k,D}+1; -\frac{1}{A_1}, -\frac{1}{A_2}, -\frac{1}{B_{11}}, \cdots, -\frac{1}{B_{1K}}, -\frac{1}{B_{21}}, \cdots, -\frac{1}{B_{2,K}}\right) \tag{5.31}$$

Likewise, the $\mathcal{I}_4$ integral has the same integrand but a different upper limit of integration. Thus, by following the same methodology and setting $y = 2u$, yields the following exact expression

$$\mathcal{I}_4 = \frac{\beta_{\gamma_{\mathrm{MRC}}}(g_{\mathrm{QAM}})\Gamma(2\mu_{S,D}+2\sum_{k=1}^{K} C(k)\mu_{R_k,D}+\frac{1}{2})}{\Gamma(2\mu_{S,D}+2\sum_{k=1}^{K} C(k)\mu_{R_k,D}+\frac{3}{2})2^{2(\mu_{S,D}+\sum_{k=1}^{K} C(k)\mu_{R_k,D})+\frac{3}{2}}} \times F_D^{(2K+3)}\left(2\mu_{S,D}+2\sum_{k=1}^{K} C(k)\mu_{R_k,D}+\frac{1}{2}; \mu_{S,D}, \mu_{S,D}, \mu_{R_1,D}, \cdots, \mu_{R_K,D}, \mu_{R_1,D}, \cdots, \mu_{R_K,D}, \frac{1}{2}; 2\mu_{S,D}+2\sum_{k=1}^{K} C(k)\mu_{R_k,D}+\frac{3}{2}; -\frac{1}{2A_1}, -\frac{1}{2A_2}, -\frac{1}{2B_{11}}, \cdots, -\frac{1}{2B_{1K}}, -\frac{1}{2B_{21}}, \cdots, -\frac{1}{2B_{2K}}, \frac{1}{2}\right) \tag{5.32}$$

where

$$\beta_{\gamma_{\mathrm{MRC}}}(g_{\mathrm{QAM}}) = \left(\frac{4\mu_{S,D}^2 h_{S,D}}{\overline{\gamma}_{S,D}^2 g_{\mathrm{QAM}}^2}\right)^{\mu_{S,D}} \prod_{k=1}^{K} \left(\frac{4\mu_{R_k,D}^2 (h_{R_k,D}^2 - H_{R_k,D}^2)}{\overline{\gamma}_{R_k,D}^2 g_{\mathrm{QAM}}^2}\right)^{\mu_{R_k,D}} . \quad (5.33)$$

Notably, the $\mathcal{I}_3$ and $\mathcal{I}_4$ terms are also expressed in terms of the generalized Lauricella function.

The case of i.i.d $\eta-\mu$ fading channels

In this simplified scenario, the corresponding solutions for $\mathcal{I}_3$ and $\mathcal{I}_4$ for the case of $M-$QAM constellations can be derived by following the same methodology as in the case of $M-$PSK modulations. To this end, after performing the necessary change of variables and long but basic algebraic manipulations, it immediately follows that:

$$\mathcal{I}_{3\mathrm{i.i.d}} = \frac{\beta_{\gamma_{\mathrm{MRC}}}(g_{\mathrm{QAM}})\sqrt{\pi}\Gamma\left(2\mu_{S,D} + 2\mu_{R,D}\sum_{k=1}^{K} C(k) + \frac{1}{2}\right)}{2\Gamma\left(2\mu_{S,D} + 2\mu_{R,D}\sum_{k=1}^{K} C(k) + 1\right)} \times F_D^{(4)}\left(2\mu_{S,D} + 2\mu_{R,D}\sum_{k=1}^{K} C(k) + \frac{1}{2};\ \mu_{S,D}, \mu_{S,D}, K\mu_{R,D}, K\mu_{R,D}; 2\mu_{S,D} + 2\mu_{R,D}\sum_{k=1}^{K} C(k) + 1; -\frac{1}{A_1}, -\frac{1}{A_2}, -\frac{1}{B_1}, -\frac{1}{B_2}\right) \quad (5.34)$$

and

$$\mathcal{I}_{4\mathrm{i.i.d}} = \frac{\beta_{\gamma_{\mathrm{MRC}}}(g_{\mathrm{QAM}})\Gamma(2\mu_{S,D} + 2\mu_{R,D}\sum_{k=1}^{K} C(k) + \frac{1}{2})}{\Gamma(2\mu_{S,D} + 2\mu_{R,D}\sum_{k=1}^{K} C(k) + \frac{3}{2})2^{2\mu_{S,D}+2\mu_{R,D}\sum_{k=1}^{K} C(k)+\frac{3}{2}}} \times F_D^{(5)}\left(2\mu_{S,D} + 2\mu_{R,D}\sum_{k=1}^{K} C(k) + \frac{1}{2};\ \mu_{S,D}, \mu_{S,D}, K\mu_{R,D}, K\mu_{R,D}, \frac{1}{2}; 2\mu_{S,D} + 2\mu_{R_k,D}\sum_{k=1}^{K} C(k) + \frac{3}{2}; -\frac{1}{2A_1}, -\frac{1}{2A_2}, -\frac{1}{2B_1}, -\frac{1}{2B_2}, \frac{1}{2}\right), \quad (5.35)$$

respectively. Hence, the error probability is determined by $P(e|\mathbf{A} = \mathbf{C}_z) = 4C\mathcal{I}_3/\pi - 4C^2\mathcal{I}_4/\pi$.

Likewise, the corresponding decoding error probability at the relay nodes can be

expressed as

$$P(\bar{\gamma}_{S,R_k}) = \frac{4C}{\pi}\underbrace{\int_0^{\pi/2} M_{\gamma_{S,R_k}}\left(\frac{g_{\mathrm{QAM}}}{\sin^2\theta}\right)\mathrm{d}\theta}_{\triangleq\,\mathcal{I}_5} - \frac{4C^2}{\pi}\underbrace{\int_0^{\pi/4} M_{\gamma_{S,R_k}}\left(\frac{g_{\mathrm{QAM}}}{\sin^2\theta}\right)\mathrm{d}\theta}_{\triangleq\,\mathcal{I}_6}. \quad (5.36)$$

Based on the approach in (5.23) and given the non-arbitrary limits of integration, the following exact expressions are deduced for the integrals $\mathcal{I}_5$ and $\mathcal{I}_6$:

$$\begin{aligned}\mathcal{I}_5 =& \frac{\beta_{\gamma_{S,R_k}}(g_{\mathrm{QAM}})\sqrt{\pi}\Gamma(2\mu_{S,R_k}+\frac{1}{2})}{2\Gamma(2\mu_{S,R_k}+1)} \\ &\times F_D^{(2)}\left(2\mu_{S,R_k}+\frac{1}{2};\mu_{S,R_k},\mu_{S,R_k};2\mu_{S,R_k}+1;-\frac{1}{C_1},-\frac{1}{C_2}\right)\end{aligned} \quad (5.37)$$

and

$$\begin{aligned}\mathcal{I}_6 =& \frac{\beta_{\gamma_{S,R_k}}(g_{\mathrm{QAM}})\Gamma(2\mu_{S,R_k}+\frac{1}{2})}{\Gamma(2\mu_{S,R_k}+\frac{3}{2})2^{2\mu_{S,R_k}+\frac{3}{2}}} \\ &\times F_D^{(3)}\left(2\mu_{S,R_k}+\frac{1}{2};\mu_{S,R_k},\mu_{S,R_k},\frac{1}{2};2\mu_{S,R_k}+\frac{3}{2};-\frac{1}{2C_1},-\frac{1}{2C_2},\frac{1}{2}\right)\end{aligned} \quad (5.38)$$

respectively, where

$$\beta_{\gamma_{S,R_k}}(g_{\mathrm{QAM}}) = \left(\frac{4\mu_{S,R_k}^2(h_{S,R_k}^2 - H_{S,R_k}^2)}{\overline{\gamma}_{S,R_k}^2 g_{\mathrm{QAM}}^2}\right)^{\mu_{S,R_k}}, \quad (5.39)$$

whereas C_1 and C_2 are obtained by substituting g_{PSK} with g_{QAM} in (5.26). Therefore, using (5.37) and (5.38), the corresponding decoding error probability can be readily expressed as

$$P(\bar{\gamma}_{S,R_k}) = P(A(k)=C(k)=0) = \frac{4C}{\pi}\mathcal{I}_5 - \frac{4C^2}{\pi}\mathcal{I}_6. \quad (5.40)$$

To this effect, an exact analytic expression for the SER is deduced by substituting $P(\mathbf{A}=\mathbf{C}_z)$ in (5.5) along with the corresponding $P(e|\mathbf{A}=\mathbf{C}_z)$. Notably, the expression can be computed using the proposed MATLAB algorithm in Appendix E.

5.3.3 Simple Asymptotic Expressions

The derivation of asymptotic expressions typically leads to useful insights on the impact of the involved parameters on the system performance. This is also the case in

the present analysis as simple exact asymptotic expressions are derived for high SNR values. To this end, the MGF of $\eta-\mu$ distribution can be accurately approximated as follows:

$$\begin{aligned} M_{\gamma_{\eta-\mu}}\left(\frac{g}{\sin^2\theta}\right) &= \left(\frac{4\mu^2 h}{(2(h-H)\mu+\frac{g}{\sin^2\theta}\bar{\gamma})(2(h+H)\mu+\frac{g}{\sin^2\theta}\bar{\gamma})}\right)^{\mu} \\ &\approx \left(\frac{4\mu^2 h}{g^2\bar{\gamma}^2}\right)^{\mu}\sin^{4\mu}(\theta). \end{aligned} \tag{5.41}$$

Based on this, the conditional error probability $P(e|\mathbf{A}=\mathbf{C}_z)$ can be approximated as follows:

$$P(e|\mathbf{A}=\mathbf{C}_z) \approx \left(\frac{4\mu_{S,D}^2 h_{S,D}}{g^2\overline{\gamma}_{S,D}^2}\right)^{\mu_{S,D}} \prod_{k=1}^{K} A_{R_K,D}(\mathbf{C}_z)\left(\frac{4\mu_{R_k,D}^2 h_{R_k,D}}{g^2\overline{\gamma}_{R_k,D}^2}\right)^{\mu_{R_k,D}} \tag{5.42}$$

where $A_{R_K,D}(\mathbf{C}_z)$ for $M-$PSK constellations is given by

$$A_{R_K,D}(\mathbf{C}_z) = \frac{1}{\pi}\int_0^{\frac{(M-1)\pi}{\pi}} [\sin(\theta)]^{4(\mu_{S,D}+\sum_{k=1}^{K} C(k)\mu_{R_k,D})}\mathrm{d}\theta \tag{5.43}$$

which can be equivalently re-written as follows:

$$\begin{aligned} A_{R_K,D}(\mathbf{C}_z) = \frac{1}{\pi}\underbrace{\int_0^{\pi/2}[\sin(\theta)]^{4(\mu_{S,D}+\sum_{k=1}^{K} C(k)\mu_{R_k,D})}\mathrm{d}\theta}_{\mathcal{I}_7} \\ +\frac{1}{\pi}\underbrace{\int_{\pi/2}^{\frac{(M-1)\pi}{M}}[\sin(\theta)]^{4(\mu_{S,D}+\sum_{k=1}^{K} C(k)\mu_{R_k,D})}\mathrm{d}\theta}_{\mathcal{I}_8}. \end{aligned} \tag{5.44}$$

The derivation of an exact expression for (5.42) is subject to analytic evaluation of the above trigonometric integrals. Hence, setting $u=\sin^2(\theta)$ and $a=2(\mu_{S,D}+\sum_{k=1}^{K} C(k)\mu_{R_k,D})$ yield

$$\mathcal{I}_7 = \frac{1}{2}\int_0^1 \frac{u^{a-\frac{1}{2}}}{(1-u)^{\frac{1}{2}}}\mathrm{d}u \tag{5.45}$$

which can be expressed in an exact expression according to [86, Eq. (3.191.1)]. To this end, by performing the necessary variable transformation and after basic algebraic manipulations one obtains

$$\mathcal{I}_7 = \frac{\sqrt{\pi}\Gamma(2\mu_{S,D}+2\sum_{k=1}^{K} C(k)\mu_{R_k,D}+\frac{1}{2})}{2\Gamma(2\mu_{S,D}+2\sum_{k=1}^{K} C(k)\mu_{R_k,D}+1)}. \tag{5.46}$$

Likewise, by setting $u = \cos^2(\theta)/\cos^2(\pi/M)$ to the second integral in (5.44), it follows that

$$\mathcal{I}_8 = \frac{\cos(\pi/M)}{2}\int_0^1 \frac{u^{-\frac{1}{2}}}{\left(1-u\cos^2\left(\frac{\pi}{M}\right)\right)^{\frac{1}{2}-a}}\mathrm{d}u \tag{5.47}$$

which can be expressed in terms of the Gauss hypergeometric function as follows:

$$\mathcal{I}_8 = \cos\left(\frac{\pi}{M}\right)\ {}_2F_1\left(\frac{1}{2}-2\mu_{S,D}+2\sum_{k=1}^{K}C(k)\mu_{R_k,D},\frac{1}{2};\frac{3}{2};\cos^2\left(\frac{\pi}{M}\right)\right). \tag{5.48}$$

To this effect, $A_{R_K,D}(\mathbf{C}_z)$ can be readily expressed as $A_{R_K,D}(\mathbf{C}_z) = \mathcal{I}_7/\pi + \mathcal{I}_8/\pi$.

In the same context, for the case of $M-$QAM constellations one obtains

$$\begin{aligned} A_{R_K,D}(\mathbf{C}_z) = \frac{4C}{\pi}\underbrace{\int_0^{\pi/2}[\sin(\theta)]^{4(\mu_{S,D}+\sum_{k=1}^{K}C(k)\mu_{R_k,D})}\mathrm{d}\theta}_{\mathcal{I}_9} \\ -\frac{4C^2}{\pi}\underbrace{\int_0^{\pi/4}[\sin(\theta)]^{4(\mu_{S,D}+\sum_{k=1}^{K}C(k)\mu_{R_k,D})}\mathrm{d}\theta}_{\mathcal{I}_{10}}. \end{aligned} \tag{5.49}$$

It is evident that the integrals $\mathcal{I}_7$ and $\mathcal{I}_9$ have the same algebraic forms. Hence, it follows that

$$\mathcal{I}_9 = \frac{\sqrt{\pi}\Gamma(2(\mu_{S,D}+\sum_{k=1}^{K}C(k)\mu_{R_k,D})+\frac{1}{2})}{2\Gamma(2(\mu_{S,D}+\sum_{k=1}^{K}C(k)\mu_{R_k,D})+1)} \tag{5.50}$$

for the first integral, while and upon setting $u = 2\sin^2(\theta)$ in the second integral, one obtains

$$\begin{aligned} \mathcal{I}_{10} = \frac{2^{-(2\mu_{S,D}+\frac{3}{2})}}{2^{2\sum_{k=1}^{K}C(k)\mu_{R_k,D}}} \\ \times\frac{{}_2F_1\left(\frac{1}{2},2\mu_{S,D}+2\sum_{k=1}^{K}C(k)\mu_{R_k,D}+\frac{1}{2};2\mu_{S,D}+2\sum_{k=1}^{K}C(k)\mu_{R_k,D}+\frac{3}{2};\frac{1}{2}\right)}{\Gamma(2\mu_{S,D}+2\sum_{k=1}^{K}C(k)\mu_{R_k,D}+\frac{3}{2})[\Gamma(2\mu_{S,D}+2\sum_{k=1}^{K}C(k)\mu_{R_k,D}+\frac{1}{2})]^{-1}}. \end{aligned} \tag{5.51}$$

Therefore, with the aid of (5.50) and (5.51), the $A_{R_K,D}(\mathbf{C}_z)$ for the case of square $M-$QAM constellations is given by $A_{R_K,D}(\mathbf{C}_z) = 4C\mathcal{I}_9/\pi - 4C^2\mathcal{I}_{10}/\pi$.

The decoding error probability of the relays also in the high SNR regime can be expressed as

$$P(A(k)=C(k)=0) \approx A_{S,R_k}\left(\frac{4\mu_{S,R_k}^2 h_{S,R_k}}{g^2\overline{\gamma}_{S,R_k}^2}\right)^{\mu_{S,R_k}} \tag{5.52}$$

and

$$P(A(k)=C(k)=1) \approx 1 - A_{S,R_k}\left(\frac{4\mu_{S,R_k}^2 h_{S,R_k}}{g^2\overline{\gamma}_{S,R_k}^2}\right)^{\mu_{S,R_k}} \tag{5.53}$$

where A_{S,R_k} for $M-$PSK and $M-$QAM constellations is given by

$$A_{S,R_k} = \frac{1}{\pi}\int_0^{\frac{(M-1)\pi}{M}} \sin^{4\mu_{S,R_k}}(\theta)\mathrm{d}\theta \tag{5.54}$$

and

$$A_{S,R_k} = \frac{4C}{\pi}\int_0^{\pi/2} \sin^{4\mu_{S,R_k}}(\theta)\mathrm{d}\theta - \frac{4C^2}{\pi}\int_0^{\pi/4} \sin^{4\mu_{S,R_k}}(\theta)\mathrm{d}\theta \tag{5.55}$$

respectively. It is evident that exact expressions for A_{S,R_k} for both modulation schemes can be obtained by following the same methodology and procedure as in the previous case yielding

$$A_{S,R_k} = \frac{\Gamma(2\mu_{S,R_k}+\frac{1}{2})}{2\sqrt{\pi}\Gamma(2\mu_{S,R_k}+1)} + \frac{\cos(\pi/M)}{\pi}\,{}_2F_1\left(\frac{1}{2}-2\mu_{S,R_k},\frac{1}{2};\frac{3}{2};\cos^2(\pi/M)\right) \tag{5.56}$$

for the case of $M-$PSK and

$$A_{S,R_k} = \frac{2C\Gamma(2\mu_{S,R_k}+\frac{1}{2})}{\sqrt{\pi}\Gamma(2\mu_{S,R_k}+1)} - \frac{C^2\Gamma(2\mu_{S,R_k}+\frac{1}{2})\,{}_2F_1\left(\frac{1}{2},2\mu_{S,R_k}+\frac{1}{2};2\mu_{S,R_k}+\frac{3}{2};\frac{1}{2}\right)}{\pi 2^{2\mu_{S,R_k}+\frac{1}{2}}\,\Gamma(2\mu_{S,R_k}+\frac{3}{2})} \tag{5.57}$$

for the case of $M-$QAM. It is noted here that at sufficiently high SNR, the probability $P(A(k)=C(k)=0)$ is very small and thus, it is resealable to approximate $1 - A_{S,R_k}((4\mu_{S,R_k}^2 h_{S,R_k})/(g^2\overline{\gamma}_{S,R_k}^2))^{\mu_{S,R_k}} \simeq 1$. To this effect and by substituting (5.42) and (5.52) into (5.5), the SER of the multi-relay regenerative system over generalized fading channels at the high SNR regime can be expressed as follows:

$$P_{\mathrm{SER}} \approx \left(\frac{4\mu_{S,D}^2 h_{S,D}}{g^2\overline{\gamma}_{S,D}^2}\right)^{\mu_{S,D}} \sum_{z=0}^{2^K-1}\prod_{k=1}^{K} A_{R_K,D}(\mathbf{C}_z)\left(\frac{4\mu_{R_k,D}^2 h_{R_k,D}}{g^2\overline{\gamma}_{R_k,D}^2}\right)^{\mu_{R_k,D}}$$
$$\times \prod_{k=1}^{K} A_{S,R_k}\left(\frac{4\mu_{S,R_k}^2 h_{S,R_k}}{g^2\overline{\gamma}_{S,R_k}^2}\right)^{\mu_{S,R_k}} \tag{5.58}$$

where g corresponds to $g_{\mathrm{PSK}} = \sin^2(\pi/M)$ or $g_{\mathrm{QAM}} = 3/(2(M-1))$ according to (5.10) and (5.28), respectively, depending on the selected modulation scheme.

Employing the expressions in (4.53), (5.58) and after performing some algebraic manipulations with the aid of [198, Eq. (13)], the diversity and cooperation gains of

the considered scenario can be expressed as:

$$G_d = 2\mu_{S,D} + 2\sum_{k=1}^{K} \min\{\mu_{S,R_k}, \mu_{R_k,D}\} \tag{5.59}$$

and

$$\begin{aligned} G_c = \Bigg(\left(\frac{4\mu_{S,D}^2 h_{S,D}}{g^2 a_0^2 \Omega_{S,D}^2} \right)^{\mu_{S,D}} \sum_{z=0}^{2^K-1} \prod_{k=1}^{K} A_{R_K,D}(\mathbf{C}_z) \left(\frac{4\mu_{R_k,D}^2 h_{R_k,D}}{g^2 a_{R_k}^2 \Omega_{R_k,D}^2} \right)^{\mu_{R_k,D}} \\ \times \prod_{k=1}^{K} A_{S,R_k} \left(\frac{4\mu_{S,R_k}^2 h_{S,R_k}}{g^2 a_0^2 \Omega_{S,R_k}^2} \right)^{\mu_{S,R_k}} \Bigg)^{-\frac{1}{G_d}}, \end{aligned} \tag{5.60}$$

respectively. The power ratios a_0 and a_{R_k} are explained in Section 5.4. It is noticed that the fading parameter η has no impact on the diversity order while it influences the cooperation gain of the system. For Rayleigh fading case, i.e., for $\mu_{S,D} = \mu_{S,R_k} = \mu_{R_k,D} = 0.5$, (5.59) reduces to $G_d = 1 + K$, which agrees with the results in [197].

5.3.4 Amount of Fading

It is recalled that the amount of fading (AoF) is a useful metric for quantifying the fading severity in the communication scenarios and is defined according to [76, Eq. (1.27)], namely

$$\text{AoF} = \frac{\text{Var}(\gamma_{\text{MRC}})}{(\text{E}(\gamma_{\text{MRC}}))^2} = \frac{\text{E}(\gamma_{\text{MRC}}^2) - (\text{E}(\gamma_{\text{MRC}}))^2}{(\text{E}(\gamma_{\text{MRC}}))^2}. \tag{5.61}$$

The n^{th} moment of the γ_{MRC} in the considered set up can be determined by [76,204], yielding

$$\mu_n = (-1)^n \left[\frac{d^n}{ds^n} \left(M_{\gamma_{S,D}}(s) \prod_{k=1}^{K} M_{R_k,D}(s) \right) \right]_{s=0}. \tag{5.62}$$

Based on this, the first two moments in (5.62) are obtained for $n = 1$ and $n = 2$, namely

$$\text{E}(\gamma_{\text{MRC}}) = \frac{\partial \text{M}_{\gamma_{\text{MRC}}}(s)}{\partial s}|_{s=0} \tag{5.63}$$

and

$$\text{E}(\gamma_{\text{MRC}}^2) = \frac{\partial^2 \text{M}_{\gamma_{\text{MRC}}}(s)}{\partial^2 s}|_{s=0}. \tag{5.64}$$

To this effect and recalling (5.7)−(5.9) as well as carrying out long but basic algebraic manipulations, the corresponding minimum AoF, if all relays decode correctly in i.i.d

fading condition, can be represented as follows:

$$\begin{aligned}\text{AoF} = &\frac{\mu_{S,D}(\mu_{S,D}+1)\delta_1^2 - 2\delta_2\mu_{S,D} - 2\delta_3 K\mu_{R,D}}{(\mu_{S,D}\delta_1 + K\mu_{R,D}\delta_4)^2} \\ &+\frac{K\mu_{R,D}(K\mu_{R,D}+1)\delta_4^2 + 2K\mu_{S,D}\mu_{R,D}\delta_1\delta_4}{(\mu_{S,D}\delta_1 + K\mu_{R,D}\delta_4)^2} - 1\end{aligned} \tag{5.65}$$

where

$$\delta_1 = \frac{\overline{\gamma}_{S,D} h_{S,D}}{\mu_{S,D}(h_{S,D}^2 - H_{S,D}^2)} \tag{5.66}$$

$$\delta_2 = \frac{\overline{\gamma}_{S,D}^2}{4\mu_{S,D}^2(h_{S,D}^2 - H_{S,D}^2)} \tag{5.67}$$

$$\delta_3 = \frac{\overline{\gamma}_{R,D}^2}{4\mu_{R,D}^2(h_{R,D}^2 - H_{R,D}^2)} \tag{5.68}$$

and

$$\delta_4 = \frac{\overline{\gamma}_{R,D} h_{R,D}}{\mu_{R,D}(h_{R,D}^2 - H_{R,D}^2)}. \tag{5.69}$$

By recalling that the $\eta - \mu$ model includes the Nakagami$-m$, Hoyt and Rayleigh distributions, the AoF for these cases can be readily deduced accordingly.

5.4 Optimum Power Allocation

EPA is not an optimal power allocation scheme for distributing the available total transmission power between the source and relay nodes, especially when the channel conditions are highly unbalanced. Hence, the main aim of this section is to analyze and compare the performance of the considered cooperative system under generalized fading channels, with EPA and OPA, under the assumption of total sum-power constraint. Opposed to single-device implementation perspective and the corresponding per node power constraint, the considered approach is more of a network or system view from the optimization perspective, seeking to understand and quantify the potential gain in the end-to-end BER/SER performance if the total power is allocated more efficiently compared to the baseline EPA scheme. To this effect, we derive the OPA strategy that minimizes the derived asymptotic SER of the considered regenerative system subject to the sum-power constraint of a power budget P. It is noted here that only partial knowledge of the CSI is required for employing the OPA scheme [38,167,168]. The derived SER expression in (5.58) is a function of the power allocated at the source and the K relays of the system, the available power should be

allocated optimally in order to enhance the end-to-end quality of the transmission [3]. Based on this, the corresponding non-linear optimization problem can be formulated as follows:

$$\begin{aligned} \mathbf{a_{opt}} &= \arg\min_{\mathbf{a}} P_{\mathrm{SER}} \\ \text{Subject to: } & a_0 + \sum_{k=1}^{K} a_{R_k} = 1, \quad a_0 \geq 0, a_{R_k} \geq 0 \end{aligned} \tag{5.70}$$

where $\mathbf{a} = [a_0, a_{R_1}, a_{R_2}, \ldots, a_{R_k}]$ denotes the relative power allocation vector. Importantly, the cost function in (5.70) is convex in the parameters a_0 and a_{R_k} over the feasible set defined by linear power ratio constraints. The corresponding proof is provided in Appendix F. To this effect and following the definitions in [183], the Lagrangian of this optimization problem is given by

$$L = P_{\mathrm{SER}} + \lambda \left(a_0 + \sum_{k=1}^{K} a_{R_k} - 1 \right) - \mu_0 a_0 - \sum_{k=1}^{K} \mu_k a_{R_k} \tag{5.71}$$

where λ denotes the Lagrange multiplier satisfying the power constraint, whereas μ_0 and μ_k parameters serve as slack variables. The nonlinear optimization problem in (5.70) can be solved using e.g. a line search method. However, to develop some insights for the power allocation policy we apply the KKT conditions for minimizing the corresponding SER [183]. To this end, it follows that all μ_k and μ_0 parameters are zero while the following first derivatives form the necessary condition for maximizing the performance of the system

$$\frac{\partial P_{\mathrm{SER}}}{\partial a_0} = \frac{\partial P_{\mathrm{SER}}}{\partial a_{R_k}} \qquad (1 \leq k \leq K). \tag{5.72}$$

In order to obtain feasible relations between optimal powers of the cooperating nodes, we employ the asymptotic SER in (5.58). By re-writing this in terms of the power ratios allocated at the transmitting nodes it follows that

$$\begin{aligned} P_{\mathrm{SER}} \approx & \left(\frac{4\mu_{S,D}^2 h_{S,D} N_0^2}{g^2 a_0^2 \Omega_{S,D}^2 P^2} \right)^{\mu_{S,D}} \sum_{z=0}^{2^K-1} \prod_{k=1}^{K} A_{R_K,D}(\mathbf{C}_z) \left(\frac{4\mu_{R_k,D}^2 h_{R_k,D} N_0^2}{a_{R_k}^2 g^2 \Omega_{R_k,D}^2 P^2} \right)^{\mu_{R_k,D}} \\ & \times \prod_{k=1}^{K} A_{S,R_k} \left(\frac{4\mu_{S,R_k}^2 h_{S,R_k} N_0^2}{a_0^2 g^2 \Omega_{S,R_k}^2 P^2} \right)^{\mu_{S,R_k}} . \end{aligned} \tag{5.73}$$

[3] Without loss of generality, the considered OPA can be practically controlled by a centralized management or power allocation unit

To develop an optimal power allocation policy for the considered cooperative network system, we initially restrict our scenario to $K = 1$ and $K = 2$ relay nodes, while we also comment on the power allocation optimization in the generalized case with $K > 2$ relays.

K = 1 Scenario

The possible decoding sets in this case are $C_0 = 0$, i.e., the relay is unable to decode correctly, and $C_1 = 1$, i.e., the relay decodes successfully. Thus, using (5.73) and neglecting the constant term outside the summation after factoring out a_0, it follows that

$$\min \left[\frac{K_1}{a_0^{2(\mu_{S,D}+\mu_{S,R_1})}} + \frac{K_2}{a_0^{2\mu_{S,D}} a_{R_1}^{2\mu_{R_1,D}}} \right] \quad \text{Subject to: } a_0 + a_{R_1} = 1 \tag{5.74}$$

where

$$K_1 = A_{S,D} A_{S,R_1} \left(\frac{4\mu_{S,R_1}^2 h_{S,R_1} N_0^2}{g^2 \Omega_{S,R_1}^2 P^2} \right)^{\mu_{S,R_1}} \tag{5.75}$$

$$K_2 = A_{R_1,D}(C_1) \left(\frac{4\mu_{R_1,D}^2 h_{R_1,D} N_0^2}{g^2 \Omega_{R_1,D}^2 P^2} \right)^{\mu_{R_1,D}}. \tag{5.76}$$

Next, we apply the necessary condition in (5.72) to determine the relation between optimal power allocations in the two nodes. Thus, the first derivative of P_{SER} with respect to a_0 is given by

$$\frac{\partial P_{\text{SER}}}{\partial a_0} = -\frac{2(\mu_{S,D}+\mu_{S,R_1})K_1}{a_0^{2(\mu_{S,D}+\mu_{S,R_1})+1}} - \frac{2\mu_{S,D}K_2}{a_0^{2\mu_{S,D}+1} a_{R_1}^{2\mu_{R_1,D}}}, \tag{5.77}$$

whereas the first derivative with respect to a_{R_1} is given by

$$\frac{\partial P_{\text{SER}}}{\partial a_{R_1}} = -\frac{2\mu_{R_1,D}K_2}{a_0^{2\mu_{S,D}} a_{R_1}^{2\mu_{R_1,D}+1}}. \tag{5.78}$$

Equating the above two relations and after some long but basic rearrangements, it follows that

$$\frac{(\mu_{S,D}+\mu_{S,R_1})K_1}{K_2} = \frac{a_0^{2\mu_{S,R_1}+1}}{a_{R_1}^{2\mu_{R_1,D}}} \left(\frac{\mu_{R_1,D}}{a_{R_1}} - \frac{\mu_{S,D}}{a_0} \right). \tag{5.79}$$

It is noticed that the left-hand side of (5.79) depends only on the channel parameters. As a result, this term is always positive which implies directly a power policy of

$$a_0\mu_{R_1,D} \geq a_{R_1,D}\mu_{S,D}. \tag{5.80}$$

Furthermore, using the power constraint $a_0 + a_{R_1} = 1$ the following conditions are also justified.

$$\frac{\mu_{S,D}}{\mu_{S,D}+\mu_{R_1,D}}P < P_S < P \tag{5.81}$$

and

$$0 < P_{R_1} < \frac{\mu_{R_1,D}}{\mu_{S,D}+\mu_{R_1,D}}P, \tag{5.82}$$

respectively. These relation are also in agreement with the power allocation over Rayleigh, Nakagami$-m$, and Hoyt (Nakagami$-q$) fading distributions under the special cases given in Subsection 3.3.3. Closed-form expressions for the power ratios for arbitrary values of μ_{S,R_1} and $\mu_{R_1,D}$ are mathematically intractable. However, for $\mu_{S,R_1} = \mu_{R_1,D} = \mu$ and assigning $\zeta = a_0/a_{R_1}$ (5.79) can be written as follows:

$$\zeta^{2\mu+1} - \frac{\mu_{S,D}}{\mu}\zeta^{2\mu} - \left(1+\frac{\mu_{S,D}}{\mu}\right)\frac{K_1}{K_2} = 0. \tag{5.83}$$

The above polynomial equation can be solved for $2\mu \in \mathbb{Z}^+$. Specifically, for $2\mu = 1$ using the power constraint closed-form expressions for the optimal powers transmitted at the source and relay nodes can be expressed as

$$P_S = \frac{\mu_{S,D} + \sqrt{\mu_{S,D}^2 + (1+2\mu_{S,D})K_1/K_2}}{1+\mu_{S,D}+\sqrt{\mu_{S,D}^2 + (1+2\mu_{S,D})K_1/K_2}}P \tag{5.84}$$

and

$$P_{R_1} = \frac{1}{1+\mu_{S,D}+\sqrt{\mu_{S,D}^2 + (1+2\mu_{S,D})K_1/K_2}}P, \tag{5.85}$$

respectively. Closed-form expressions for the optimal powers for higher values of 2μ can be obtained by evaluating (5.83) using mathematical software, such as MATLAB, MATHEMATICA and MAPLE.

$K = 2$ Scenario

In this case, the following four scenarios are valid: $\mathbf{C}_0 = (0,0)$ when the two relays decode incorrectly; $\mathbf{C}_1 = (0,1)$ when the first relay decodes incorrectly and the second relay decodes successfully; $\mathbf{C}_2 = (1,0)$ when the first relay decodes successfully and the second relay decodes incorrectly; and $\mathbf{C}_3 = (1,1)$ when both relays decode successfully. Based on this, the corresponding optimization problem can be expressed

as follows:

$$\min \left[\frac{K_3}{a_0^{2(\mu_{S,D}+\mu_{S,R_1}+\mu_{S,R_2})}} + \frac{K_4}{a_0^{2(\mu_{S,D}+\mu_{S,R_1})} a_{R_2}^{2\mu_{R_2,D}}} + \frac{K_5}{a_0^{2(\mu_{S,D}+\mu_{S,R_2})} a_{R_1}^{2\mu_{R_1,D}}} + \frac{K_6}{a_0^{2\mu_{S,D}} a_{R_2}^{2\mu_{R_2,D}} a_{R_1}^{2\mu_{R_1,D}}} \right] \tag{5.86}$$

$$\text{Subject to: } a_0 + a_{R_1} + a_{R_2} = 1$$

where K_3, K_4, K_5 and K_6 relate to the channel parameters, which are not affecting the sign of the derivatives in any case. To this effect, the derivative of P_{SER} with respect to a_{R_1} is given by

$$\frac{\partial P_{\text{SER}}}{\partial a_{R_1}} = -\frac{2K_5\mu_{R_1,D}}{a_0^{2(\mu_{S,D}+\mu_{S,R_2})} a_{R_1}^{2\mu_{R_1,D}+1}} - \frac{2K_6\mu_{R_1,D}}{a_0^{2\mu_{S,D}} a_{R_2}^{2\mu_{R_2,D}} a_{R_1}^{2\mu_{R_1,D}+1}}, \tag{5.87}$$

whereas the derivative of P_{SER} with respect to a_{R_2} is given by

$$\frac{\partial P_{\text{SER}}}{\partial a_{R_2}} = -\frac{2K_4\mu_{R_2,D}}{a_0^{2(\mu_{S,D}+\mu_{S,R_1})} a_{R_2}^{2\mu_{R_2,D}+1}} - \frac{2K_6\mu_{R_2,D}}{a_0^{2\mu_{S,D}} a_{R_2}^{2\mu_{R_2,D}+1} a_{R_1}^{2\mu_{R_1,D}}}. \tag{5.88}$$

With the aid of the above two representations, and assuming that the channel conditions for the relays are all the same, i.e. $\mu_{S,R_1} = \mu_{S,R_2}, \eta_{S,R_1} = \eta_{S,R_2}, \Omega_{S,R_1} = \Omega_{S,R_2}, \mu_{R_1,D} = \mu_{R_2,D}, \eta_{R_1,D} = \eta_{R_2,D},$ and $\Omega_{R_1,D} = \Omega_{R_2,D}$ a power allocation strategy can be proposed as

$$a_{R_1} = a_{R_2}. \tag{5.89}$$

Likewise, applying $\partial P_{\text{SER}}/\partial a_{R_k} = \partial P_{\text{SER}}/\partial a_{R_k+1}$ for $(1 \leq k \leq K)$ it is straightforwardly shown that

$$a_{R_k} = a_{R_k+1}. \tag{5.90}$$

The power assignment indicates that under the total power constraint and the assumed channel conditions for the regenerative network, power control mechanism with the relays is not essential, but the remaining power left from the total power budget after the source can be simply allocated uniformly between the nodes. This is further elaborated and largely verified in the following section.

5.5 Numerical Results and Analysis

In this section, the offered analytic results are employed in evaluating the performance of the multi-relay regenerative system over the realistic generalized fading model for different communication scenarios. The SER expressions presented in this chapter are used for analyzing the performance of the system. To this end, we plot the performance curves in terms of the end-to-end average SER versus SNR for $M-$PSK and $M-$QAM modulations where the overall transmit power is equally or optimally allocated to the source and the relays following the power policy derived in Section 5.4. It is also noted that the presented results are limited to Format-1 of the $\eta-\mu$ distribution, but they can be readily extended to scenarios that correspond to Format-2 as described in Subsection 3.3.3.

Fig. 5.2 shows the SER performance as a function of SNR for one, two and three relays using EPA, i.e., $P_S = P_{R_k} = P/(K+1)$ over symmetric and balanced $\eta-\mu$ fading channels for $4-$PSK/$4-$QAM constellations. Moreover, the $\eta-\mu$ fading parameters are $\mu = 0.5$ and $\eta = 1$ while Ω parameters are equal to unity. It is evident that the results from the exact analytic expressions are in excellent agreement with the respective results from computer simulations, which verifies their validity. It is also shown that the exact results are bounded tightly by the corresponding asymptotic curves in the range from moderate SNR values to the high SNR regime while a full diversity order i.e., 2, 3 and 4, can be respectively achieved. Table 5.1 shows the corresponding diversity gains computed from the slopes for the exact and asymptotic curves along with the DT scenario, for reference, where it is assumed that $P_S = P$. It is observed that at a target SER of 10^{-4} the single relay system exhibits a gain of 15dB over the DT, whereas the two and three relay systems outperform the direct scenario by about 19.5dB and 21.5dB, respectively. In the same context, Fig. 5.3 shows the SER performance as a function of SNR for $4-$QAM/$4-$PSK and $16-$QAM constellations for the case of two relays with EPA over symmetric $\eta-\mu$ fading channels with $\mu = 0.5$ and $\eta = 1$ as well as balanced links, i.e., $\Omega_{S,D} = \Omega_{S,R_k} = \Omega_{R_k,D} = \Omega = 0$dB. It is also shown that the exact results are again in tight agreement with the respective simulation results and that the asymptotic curves are tending to be practically identical to the exact ones for SERs lower than 10^{-3}. Therefore, it becomes evident that in practical system designs of DF relaying at the high SNR regime, the offered asymptotic expressions can provide useful insights on the system performance.

Fig. 5.4 shows the cooperation performance of $4-$QAM/QPSK system in a two relay scenario for $\mu = \{0.5, 1, 1.5\}$ and identical channel variance of $\Omega_{S,D} = \Omega_{S,R_k} =$

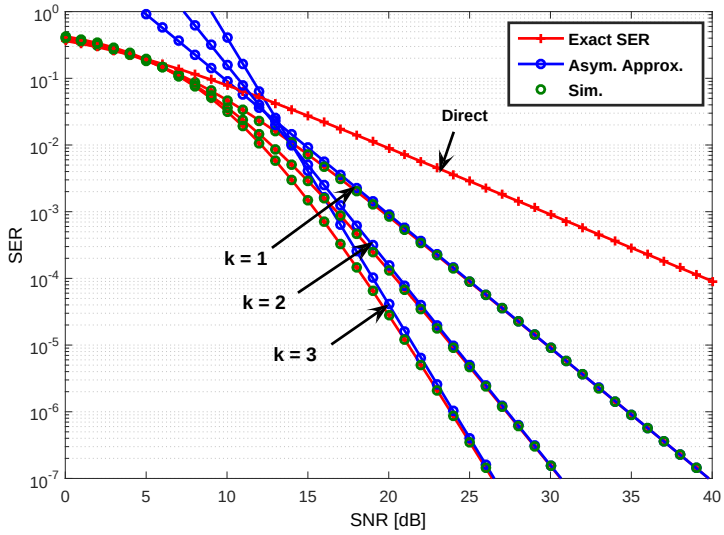

Figure 5.2 SER in $\eta - \mu$ fading with $\mu = 0.5, \eta = 1$ and $\Omega_{S,D} = \Omega_{S,R_k} = \Omega_{R_k,D} =$ 0dB for 4−PSK/4−QAM constellations with different number of relays and EPA.

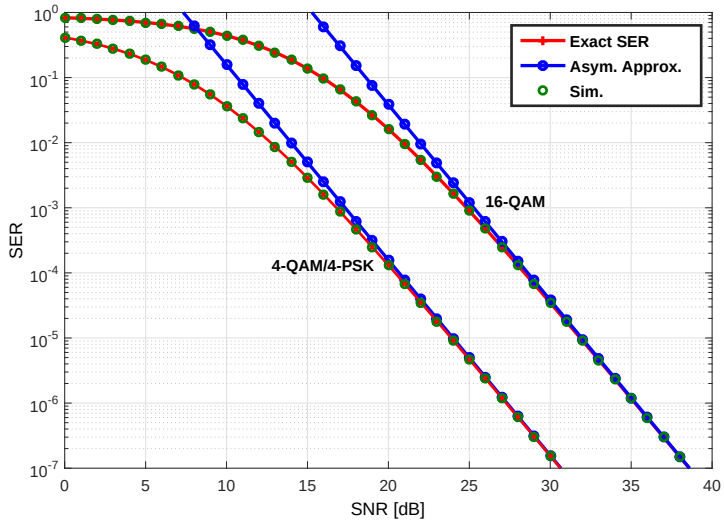

Figure 5.3 SER in $\eta - \mu$ fading with $\mu = 0.5, \eta = 1$ and $\Omega_{S,D} = \Omega_{S,R_k} = \Omega_{R_k,D} =$ 0dB for 4−QAM/4−PSK and 16−QAM, $K = 2$ and EPA.

Table 5.1 Diversity gains for one, two and three relays using 4−PSK/4−QAM for $\mu = 0.5$ and $\eta = 1$.

K	Diversity gain(Exact)	Diversity gain (Asymp.)	Diversity gain (Eq.(5.59))
1	1.96	2	2
2	2.91	3	3
3	3.85	4	4

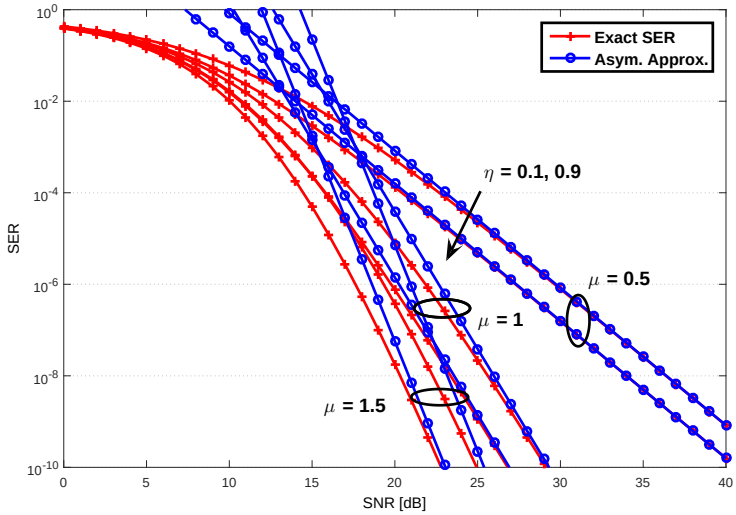

Figure 5.4 SER vs SNR with $\mu = \{0.5, 1, 1.5\}$, $\eta = \{0.1, 0.9\}$ and $\Omega_{S,D} = \Omega_{S,R_k} = \Omega_{R_k,D} = 0$dB for 4−PSK/4−QAM, $K = 2$ and EPA.

$\Omega_{R_k,D} = 0$dB with EPA. It is also recalled that the case of $\mu = 0.5$ corresponds to the Nakagami−q (Hoyt) distribution with $q^2 = \eta$. By varying the value of η, we observe the effect of the scattered-wave power ratio on the average SER of the considered regenerative system. This verifies that the SER is inversely proportional to η since for an indicative SER of 10^{-4}, an average gain of 2dB is observed when η increases from 0.1 to 0.9 for all values of μ. Furthermore, average gains of 4dB and 1.75dB are obtained as μ increases from 0.5 to 1 and from 1 to 1.5, respectively.

In the same context, Fig. 5.5 shows the SER performance in i.n.i.d $\eta-\mu$ fading channels for 4−QAM/4−PSK constellations for the case of two relays with EPA. It is assumed that $\eta_{S,D} = 0.9$, $\Omega_{S,D} = \Omega_{S,R_k} = 0$dB, $\Omega_{R_k,D} = \{0, 10\}$dB, $\mu_{S,D} = \mu_{S,R_k} = \mu_{R_k,D} = \mu = \{0.5, 1\}$ with different values of η_{S,R_k} and $\eta_{R_1,D}$ set as $\{\eta_{S,R_k}, \eta_{R_1,D}, \eta_{R_2,D}\} = \{0.1, 0.1, 0.9\}$ and $\{0.9, 0.8, 0.9\}$, respectively. It is observed that the performance of the system improves substantially as η_{S,R_k} and $\eta_{R_1,D}$ in-

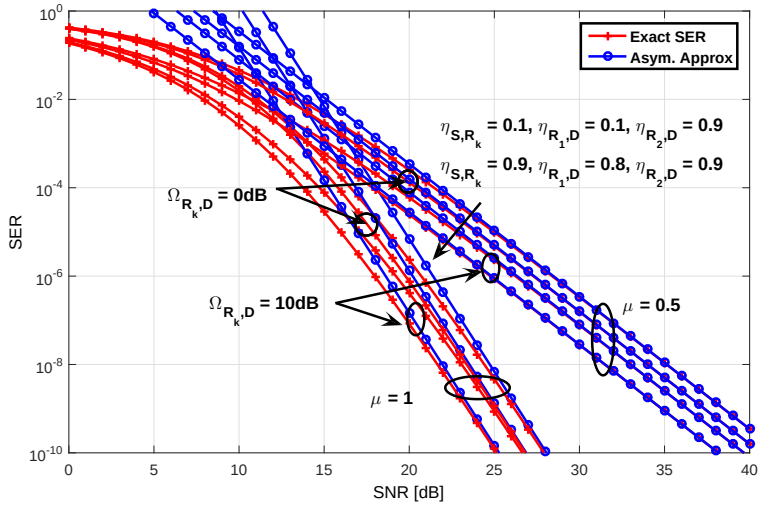

Figure 5.5 SER vs SNR with $\mu = \{0.5, 1\}$, $\eta_{S,D} = 0.9$, $\Omega_{S,D} = \Omega_{S,R_k} = 0$dB, $\Omega_{R_k,D} = \{0, 10\}$dB with different η_{S,R_k} and $\eta_{R_1,D}$ for $4-$PSK/$4-$QAM, $K = 2$ and EPA.

crease as at a SER of 10^{-4} almost 1.25dB and 1.75dB gains are achieved when the values of $\{\eta_{S,R_k}, \eta_{R_1,D}, \eta_{R_2,D}\}$ changes from $\{0.1, 0.1, 0.9\}$ to $\{0.9, 0.8, 0.9\}$ for $\Omega_{R_k,D} = \{0, 10\}$dB, for the considered values of μ.

Fig. 5.6 shows the SER performance in $\eta - \mu$ fading conditions with $\mu_{S,D} = 0.5$ and $\eta = 0.1$ for $4-$QAM/$4-$PSK constellations and balanced links of relative channel variance 0dB for the case of two relays using EPA with different μ_{S,R_k} and non-identical values of $\mu_{R_k,D}$. The figure shows that increasing at least one of $\mu_{R_k,D}$'s value at a fixed μ_{S,R_k} or increasing both μ_{S,R_k} and $\mu_{R_k,D}$ simultaneously can improve the cooperation performance. Indicatively, at SER of 10^{-4} nearly 1.25dB and 1.75dB gains are observed when $\{\mu_{S,R_k}, \mu_{R_1,D}, \mu_{R_2,D}\}$ changes from $\{0.5, 0.5, 0.5\}$ to $\{0.5, 0.5, 1\}$ and from $\{0.5, 0.5, 1\}$ to $\{0.5, 1, 1.5\}$, respectively. Moreover, nearly 0.75dB and 1dB gains are achieved when $\{\mu_{R_1,D}, \mu_{R_2,D}\}$ varies from $\{1, 1\}$ to $\{1, 1.5\}$ and then to $\{1.5, 2\}$ when $\mu_{S,R_k} = 1$, whereas a gain of 4dB is shown when both μ_{S,R_k} and $\mu_{R_k,D}$ increase at the same time, for instance, from $\{0.5, 0.5, 1\}$ to $\{1, 1, 1.5\}$.

Similarly, Fig. 5.7 shows the SER performance for $4-$QAM/$4-$PSK constellations for $\mu = 0.5$ and 1, $\eta = 0.5$ and unbalanced channel links employing two relays with EPA. It is shown that increasing either Ω_{S,R_k} or $\Omega_{R_k,D}$ can improve the SER and that the performance for the case of $\Omega_{S,R_k} = 0$dB and $\Omega_{R_k,D} = 10$dB is better than the reverse scenario, i.e., $\Omega_{S,R_k} = 10$dB and $\Omega_{R_k,D} = 0$dB. For example, almost

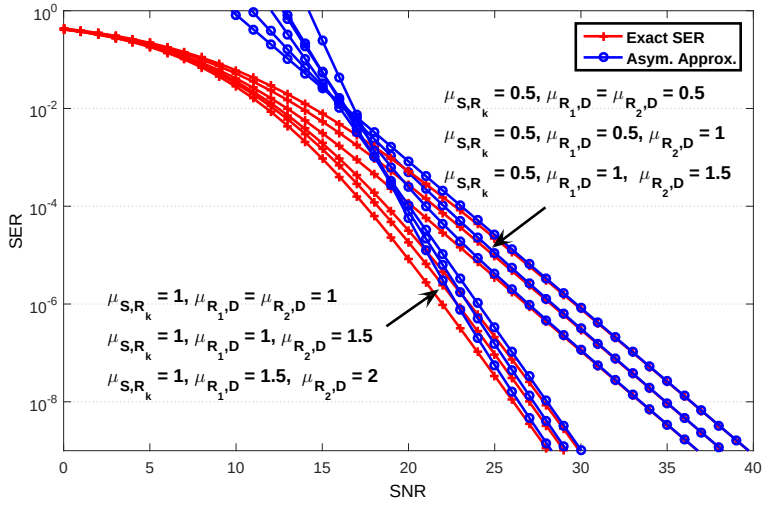

Figure 5.6 SER in $\eta-\mu$ fading with $\mu_{S,D}=0.5$ and $\eta=0.1$, $\Omega_{S,D}=\Omega_{S,R_k}=\Omega_{R_k,D}=0$dB for different μ_{S,R_k} and $\mu_{R_k,D}$ for 4−QAM/4−PSK signals for $K=2$ with EPA.

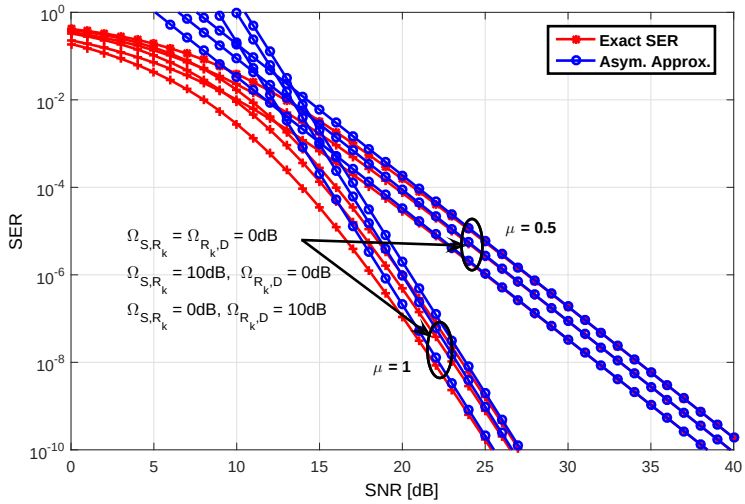

Figure 5.7 SER in $\eta-\mu$ fading with $\mu=\{0.5,1\}$, $\eta=0.5$, and $\Omega_{S,D}=0$dB for different Ω_{S,R_k} and $\Omega_{R_k,D}$ for 4−QAM/4−PSK for $K=2$ and EPA.

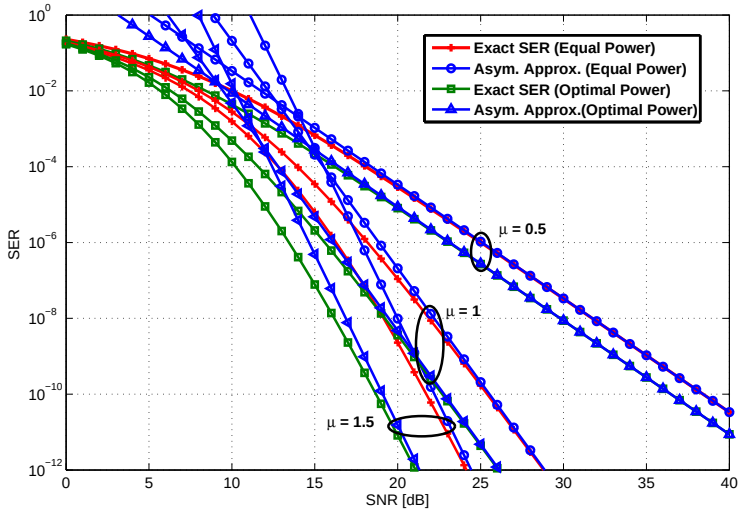

Figure 5.8 SER with OPA in $\eta - \mu$ fading with $\eta = 0.5$, $\Omega_{S,D} = \Omega_{S,R_k} = 0$dB and $\Omega_{R_k,D} = 10$dB for different μ and 4−QAM/4−PSK and $K = 2$.

constant gains of 1dB and 1.75dB are achieved when $\Omega_{S,R_k} = 0$dB and $\Omega_{R_k,D} = 0$dB increase to Ω_{S,R_k} =10dB and $\Omega_{R_k,D} = 0$dB and from Ω_{S,R_k} =0dB and $\Omega_{R_k,D} = 0$dB to Ω_{S,R_k} =0dB and $\Omega_{R_k,D} = 10$dB, respectively. This verifies that in the considered regenerative protocol, the overall performance improves more when increasing average fading power from the relays to the destination than from the source to the relays.

Fig. 5.8 then shows the SER performance of the proposed OPA scheme for different values of the fading parameter μ, and assuming stronger channel variance from the relay nodes to the destination node with constant scattered-wave power ratio for the case of two relays and 4−QAM/4−PSK constellations. It is also assumed that $\mu_{S,D} = \mu_{S,R_k} = \mu_{R_k,D} = \mu$, $\Omega_{S,D} = \Omega_{S,R_k} = 0$dB, $\Omega_{R_k,D} = 10$dB and $\eta = 0.5$. It is shown that when μ is small, for example $\mu = 0.5$, the OPA provides small gain to the cooperation system, which, however, increases as μ increases. Indicatively, for a SER of 10^{-4} the optimal system outperforms the EPA scenario by at least 1.5dB when $\mu = 0.5$ and by 2.5dB and 3dB when $\mu = 1$ and $\mu = 1.5$, respectively. In addition, Fig. 5.9 depicts the corresponding SER for the case that $\mu_{S,D} = \mu_{S,R_k} = \mu_{R_k,D} = \mu$, $\eta = 0.5$, $\Omega_{S,D} = \Omega_{S,R_k} = 0$dB and $\Omega_{R_k,D} = \{0, 10\}$dB. It is observed that when $\Omega_{S,R_k} = \Omega_{R_k,D} = 0$dB, OPA does not provide significant performance improvement for the considered DF network. On the contrary, the SER improves as the difference between Ω_{S,R_k} and $\Omega_{R_k,D}$ increases. For example, it is noticed that for a SER of

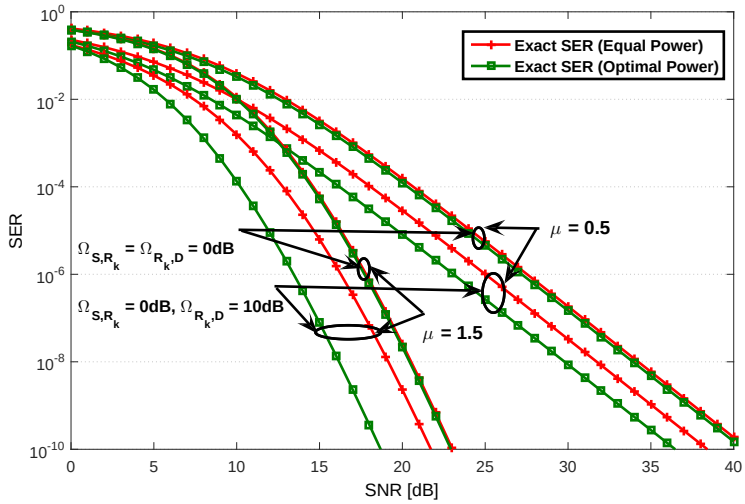

Figure 5.9 SER with OPA over $\eta-\mu$ fading for $\mu_{S,D} = \mu_{S,R_k} = \mu_{R_k,D} = \mu, \eta = 0.5, \Omega_{S,D} = \Omega_{S,R_k} = 0$dB with different $\Omega_{R_k,D}$ for $4-$QAM/$4-$PSK and $K = 2$.

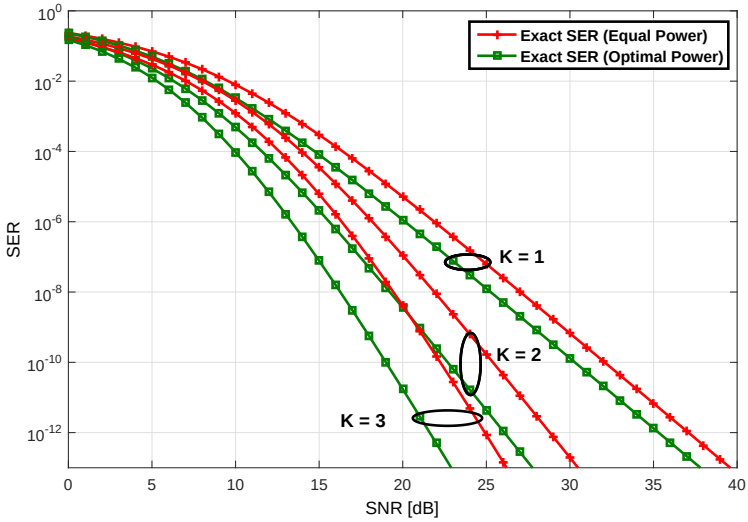

Figure 5.10 SER with OPA over $\eta-\mu$ fading for $\mu = 1$, $\eta = 0.5$, $\Omega_{S,D} = \Omega_{S,R_k} = 0$dB and $\Omega_{R_k,D} = 10$dB for $4-$PSK/$4-$QAM and different number of relays.

Table 5.2 Optimal transmit power allocations with different μ_{S,R_k} and $\mu_{R_k,D}$ for $\mu_{S,D} = 0.5$, $\eta = 0.5, \Omega_{S,D} = \Omega_{S,R_k} = \Omega_{R_k,D} = 0$dB using 4−QAM/4−PSK signals at SNR = 20 dB.

μ_{S,R_k}	$\mu_{R_k,D}$	$P_S/P \mid P_{R_1}/P$	$P_S/P \mid P_{R_1,R_2}/P$
0.5	0.5	0.6270 | 0.3730	0.4832 | 0.2584
	1	0.6572 | 0.3428	0.4914 | 0.2543
	1.5	0.6871 | 0.3129	0.5048 | 0.2476
1	0.5	0.5415 | 0.4585	0.4006 | 0.2997
	1	0.5302 | 0.4698	0.3842 | 0.3079
	1.5	0.5725 | 0.4275	0.3971 | 0.3014
1.5	0.5	0.5160 | 0.4840	0.3724 | 0.3138
	1	0.4652 | 0.5348	0.3443 | 0.3278
	1.5	0.5008 | 0.4992	0.3424 | 0.3288

10^{-4} and $\mu = 0.5$, gains of 0.5dB and 2dB are achieved by OPA over the EPA scheme when $\Omega_{R_k,D} = \{0, 10\}$dB, respectively. Similarly, gains of 0.5dB and 3dBs are obtained when μ is increased to $\mu = 1.5$ while it is generally noticed that OPA is typically more effective than EPA, even in the low-SNR regime.

In the same context, Fig. 5.10 shows the SER performance of the proposed OPA and EPA scenarios for single, two and three relays over symmetric $\eta - \mu$ fading scenario, i.e., with constant μ and constant scattered-power ratios η and unbalanced channel variances from source-to-relay and from relay-to-destination. It is assumed that $\mu_{S,D} = \mu_{S,R_k} = \mu_{R_k,D} = 1, \eta = 0.5$, whereas $\Omega_{S,D} = \Omega_{S,R_k} = 0$dB and $\Omega_{R_k,D} =$ 10dB. It is shown that the OPA strategy clearly outperforms its EPA counterpart since the gain for a SER of 10^{-4} is 2dB, 2.5dB and 2.75dB for one, two and three relays, respectively. Evidently, the analysis shows that as the number of relay nodes increases the additional advantage of saving extra dBs through adding more and more relay nodes becomes gradually smaller. This result is due to the fact that as the number of relay nodes increases, the source is assigned with a small fraction of the total available transmit power.

The characteristics of the OPA strategy are further analyzed with the aid of Tables 5.2, 5.3 and 5.4, which depict the optimal power ratios allocated to the source and the relay-nodes in terms of P_S/P and P_{R_k}/P which are evaluated numerically. In case of multiple relays, the relays are assigned with equal powers ($P_{R_k}/P = P_{R_{k+1}}/P$). The power ratios allocated to the source and relay nodes for asymmetric and balanced channel conditions are tabulated in Table 5.2. The result indicates that the numerical values are in tight agreement with the power strategy proposed in Section 5.4. The tabulated values also indicate that as the difference between $\mu_{S,R}$ and $\mu_{R,D}$ becomes

Table 5.3 Optimal transmit power allocations with different $\Omega_{R_k,D}$ and $\mu_{S,D} = \mu_{S,R_k} = \mu_{R_k,D} = \mu$ for $\eta = 0.5, \Omega_{S,D} = \Omega_{S,R_k} = 0$dB and 4− QAM/4−PSK signals at SNR = 20 dB.

μ	$\Omega_{R_k,D}$	$P_S/P \mid P_{R_1}/P$	$P_S/P \mid P_{R_1,R_2}/P$	$P_S/P \mid P_{R_1,R_2,R_3}/P$
0.5	1	0.6270 | 0.3730	0.4832 | 0.2584	0.4036 | 0.1988
	10	0.7968 | 0.2032	0.6974 | 0.1513	0.6328 | 0.1224
	100	0.9181 | 0.0819	0.8712 | 0.0644	0.8371 | 0.0543
1	1	0.5925 | 0.4075	0.4368 | 0.2816	0.3520 | 0.2160
	10	0.8316 | 0.1684	0.7343 | 0.1328	0.6658 | 0.1114
	100	0.9557 | 0.0443	0.9247 | 0.0376	0.8995 | 0.0335
1.5	1	0.5735 | 0.4265	0.4131 | 0.2935	0.3274 | 0.2242
	10	0.8496 | 0.1504	0.7549 | 0.1226	0.6850 | 0.1050
	100	0.9683 | 0.0317	0.9439 | 0.0280	0.9232 | 0.0256

Table 5.4 Optimal transmit power allocations with different modulations and $\mu_{S,D} = \mu_{S,R_k} = \mu_{R_k,D} = \mu, \eta = 0.5, \Omega_{S,D} = \Omega_{S,R_k} = \Omega_{R_k,D} = 0$dB for two relays at SNR = 20 dB.

	4−PSK	16−PSK	16−QAM
μ	$P_S/P \mid P_{R_1,R_2}/P$	$P_S/P \mid P_{R_1,R_2}/P$	$P_S/P \mid P_{R_1,R_2}/P$
0.5	0.4832 | 0.2584	0.4932 | 0.2534	0.5113 | 0.2443
1	0.4368 | 0.2816	0.4392 | 0.2804	0.4572 | 0.2714
1.5	0.4130 | 0.2935	0.4138 | 0.2931	0.4287 | 0.2857

large, in most cases, more proportion of power is assigned to the source. Table 5.3 also corresponds to the case that the source is assigned with high proportion of power when $\Omega_{R_k,D}$ is larger than Ω_{S,R_k}, i.e., unbalanced channel links. Finally, Table 5.4 verifies that the OPA strategy is dependent upon the considered modulation scheme.

5.6 Summary

In this chapter, we analyzed the end-to-end performance and OPA of regenerative cooperative systems over generalized fading channels. Novel exact and asymptotic expressions for the end-to-end SER assuming $M-$PSK and $M-$QAM modulated signals were derived over i.i.d and i.n.i.d channels. The derived analytic expressions were then used to draw insights of the different fading parameters in the generalized $\eta-\mu$ fading conditions and their impact on the end-to-end system performance. The offered results were subsequently employed in developing an asymptotically optimum power allocation scheme under a total sum-power constraint, which was shown to outperform significantly the conventional EPA strategy. It was also shown that the

OPA scheme is practically independent of the scattered-waves power ratio parameter from source-to-destination, while it depends upon the number of multipath clusters as well as the selected modulation scheme and that it overall provides significant performance enhancement.

Chapter 6

Full-Duplex Regenerative Relaying and Energy Optimization Over Generalized Fading Channels

In this chapter, we investigate the performance, OPA and energy optimization analysis under given constraints for FDR system with different relay SI levels over asymmetric generalized fading conditions. As mentioned in Chapter 2, relay transmission can adopt either HDR or FDR modes. The FDR scheme allows the relay node to transmit and receive signals over the same frequency band at the same time-slot. The FDR has the potential to enhance the SE and shorten the latency of the relay communication system in comparison with the traditional HDR scheme which receives and transmits on orthogonal channels. Unlike the previous works that considered the scenario of signal transmission over symmetric fading channels, here we consider asymmetric fading scenarios. Specifically, we consider the case where the S→R link is subject to the generalized LOS small-scale fading model of $\kappa-\mu$, whereas the R→D link is subject to the generalized NLOS small-scale fading model of $\eta-\mu$. Furthermore, the direct link is subject to three different conditions: To the NLOS communication scenario of the $\eta-\mu$ fading, to the LOS case of $\kappa-\mu$ and to the IG fading model. To this end, novel analytic expressions are derived for the OPs of the FDR system based on the asymmetric fading models. The analysis and results presented in this chapter are based on the author's published work in [115,116] and extended to OPA and EE optimization analysis in [122].

6.1 Background and Overview of Contributions

Traditionally, relay transmission assumes HD mode where the relays operate in either transmission or reception mode. In this mode, the S→R and R→D links, which are operated in two-time slots, are orthogonal to each other [65, 208, 209]. The HD mode avoids relay SI at the cost of sacrificing the limited resources (e.g. time-slots and frequency). However, recently, the FD relaying concept with a capability to allow the relay(s) to receive and transmit signals simultaneously over the same frequency band has been introduced. This has constituted it to be an effective alternative scheme to overcome the limitations imposed by the HD systems, e.g., [210, 211]. Based on this, Kwon *et al.* [212] derived closed-form expressions for the OP over Rayleigh fading channels by considering the relay SI. Likewise, Baranwal *et al.* [213] derived the OP of multi-hop FDR system by considering the relay SI and interference from the adjacent terminals over Rayleigh fading channel. In a similar context, Day *et al.* [214] derived tight upper and lower bounds on the end-to-end achievable rate of DF-based FD-MIMO relay systems. Altieri *et al.* [215] analyzed the outage performance of interference-limited FDR system using DF and CF schemes, whereas Suraweera *et al.* [216] proposed and analyzed low complexity end-to-end performance for MIMO-FD relay systems using AF relaying scheme. In [217], the performance of FD block Markov relaying with SI at the relay over Nakagami$-m$ fading channels was analyzed. Riihonen *et al.* [218] also proposed hybrid techniques that switch opportunistically between FD and HD relaying modes in both DF and AF systems with power adaptation to maximize the instantaneous and average SE, whereas in [219] the outage performance and power allocation problem of FD relay channel with DF protocol were investigated. Huang *et al.* [220] investigated an OPA scheme for multi-carrier secure communication in DF-FD relay networks. Likewise, Alves *et al.* [221] investigated the performance of DF based secure FD cooperative network over composite fading channels. Sohaib *et al.* [222], on the other hand, proposed and analyzed asynchronous cooperative relaying for V2V communications by employing dual polarized antennas at the relay node to achieve AF-FD communication. [223] investigated OPA under individual and total power constraints that maximizes the capacity of FDR with AF protocol neglecting the impact of the direct link, whereas Yu *et al.* [224] studied the impact of the direct link over the transmit power optimization for FD with DF protocol. Also, [225] studied energy-efficient cooperative network for FDR system with loop back interference using the DF relaying protocol over Rayleigh fading channels.

However, the aforementioned investigations as well as most of the related literature are limited to the scenario of information transmission over symmetric multipath

fading channels, i.e., the S→R and R→D links undergo the same fading conditions. In practice, asymmetric channels are frequently encountered due to terminal and relay locations and fading conditions. For example, the link between a fixed relay and BS might experience LOS radio propagation, whereas the link between a mobile terminal and relay might experience NLOS communications because of random location and mobility of the mobile terminal [226]. Based on this, Suraweera *et al.* [227] investigated the end-to-end performance of a dual-hop fixed gain relaying system when the S→R and the R→D channels experience Rayleigh/Rician and Rician/Rayleigh fading scenarios respectively and in [228] for the Nakagami−m and Rician case. Likewise, Jayasinghe *et al.* [229] analyzed the performance of dual-hop transmissions for optimal beamforming in fixed gain AF-MIMO relaying over asymmetric fading conditions, whereas Majhi *et al.* [230] investigated the performance of a repetition-based two hop HD-DF system over asymmetric Rayleigh and Rician fading channels. Likewise, [231] investigated the end-to-end performance of dual-hop AF relaying communication over generalized small-scale NLOS and LOS asymmetric fading conditions.

Most of the above analyses over asymmetric fading conditions are limited to HD relaying mechanism. Motivated by this, in this Chapter, we analyze the OP, OPA and energy optimization over generalized asymmetric fading channels. To this end, novel analytic expressions for the overall OP of the FDR system are first derived with Rayleigh distributed relay SI envelope.

In more detail, the technical contributions of this chapter are as follows:

- We investigate the outage performance of the FDR system under the effects of relay SI and the interference from the direct link for $\kappa-\mu$ and $\eta-\mu$ fading conditions when the direct link is subject to $\eta-\mu$, $\kappa-\mu$ and IG fading conditions.

- We investigate power optimization with DF protocol under asymmetric fading conditions. The optimization problem for the power constrained systems is conducted by minimizing the overall OP of the system under a given end-to-end SE constraint.

- We compare the FD and the reference HD relaying architectures under the same asymmetric fading conditions for both equal power and OPA schemes. The results of the comparison can provide valuable insights for system designing and network planning in practical communication scenarios.

- EE optimization analysis is performed by minimizing the average total energy consumption of the FDR and HDR systems under a given target OP, end-to-end SE, and maximum total transmit power constraints.

6.2 System and Channel Model

6.2.1 System Model with Full-Duplex Relay Node

We consider a two-hop three-node relay network consisting of one source, S, a single relay, R, and a destination, D. The source and destination nodes are equipped with a single antenna, whereas the relay has two antennas, one for receiving and one for transmitting, to better facilitate FD mode operation as shown in Fig. 6.1. The relay uses DF relaying protocol to re-transmit the received signal to the destination where reception and re-transmission occur simultaneously at the same frequency band, which ultimately induces relay SI. The received signals at the relay and destination nodes can be expressed as follows:

$$y_R = \sqrt{P_S}\alpha_{S,R}x_S + \sqrt{P_R}\alpha_{R,R}x_R + n_R \tag{6.1}$$

and

$$y_D = \sqrt{P_R}\alpha_{R,D}x_R + \sqrt{P_S}\alpha_{S,D}x_S + n_D, \tag{6.2}$$

respectively, where x_S and x_R denote the transmitted signals from the source and relay nodes with normalized unit energy, whereas $\alpha_{R,R}$ is the fading coefficient of the R $\rightarrow$ R SI link. n_R and n_D also denote the AWGN at the relay and destination nodes, respectively. We assume that the CSI is known to the receiving nodes while each path experiences narrow band multipath fading.

6.2.2 Asymmetric Channel Model

As already mentioned, fading conditions in asymmetric channels differ between at least two paths of the system. Based on this, in the present analysis we assume that the S$\rightarrow$R path experiences κ–μ fading conditions, whereas R$\rightarrow$D path is subject to η–μ fading scenarios. It is noted that the κ–μ and η–μ distributions have been shown to accurately model small-scale fading conditions of various LOS and NLOS communications scenarios [78]. Furthermore, the relay SI that cannot be perfectly canceled in practice using the existing antenna and interference cancellation (IC) techniques is assumed to be Rayleigh distributed [211–213, 218], whereas the direct, S$\rightarrow$D, link is subject to either the NLOS model of η–μ, the LOS model of κ–μ or the IG distribution model. The PDFs of the instantaneous SNR, γ, for the Rayleigh, κ–μ, η–μ and IG distributions are given in (3.12), (3.33), (3.36) and (3.38), respectively.

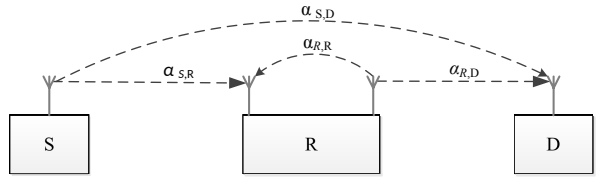

Figure 6.1 Two-hop full-duplex relay system.

6.3 Outage Probability Analysis

6.3.1 Full-Duplex Relaying

In the DF-FD relay system, the relay is subject to SI, whereas the destination is subject to interference from the direct S→D signal propagation. The direct signal, if it exists, is here treated as interference from the destination point of view, since it occurs simultaneously at the same frequency with the signal transmitted by the relay node. To this effect, the instantaneous signal-to-interference-and-noise-ratios (SINRs) at the relay and destination nodes are expressed as follows [212]:

$$\Gamma_R = \frac{|\alpha_{S,R}|^2 P_S}{|\alpha_{R,R}|^2 P_R + N_0} \tag{6.3}$$

and

$$\Gamma_D = \frac{|\alpha_{R,D}|^2 P_R}{|\alpha_{S,D}|^2 P_S + N_0}, \tag{6.4}$$

respectively. An outage of the end-to-end communication system occurs if the S→R link fails to support the required SINR or if the R→D link cannot meet the required SINR. Accordingly, similar to the work in [212] and [213] the overall OP of the considered system in terms of the instantaneous SINRs can be expressed as follows:

$$\begin{aligned} P_{\text{out}} &= \Pr\{\min(\Gamma_{\text{R}}, \Gamma_{\text{D}}) < \Gamma_{\text{T}}\} \\ &= \Pr\{\Gamma_R < \Gamma_T\} + (1 - \Pr\{\Gamma_R < \Gamma_T\})\Pr\{\Gamma_D < \Gamma_T\} \end{aligned} \tag{6.5}$$

where $\Gamma_T = 2^R - 1$ is the required SINR for successful transmission with end-to-end SE of R in bits/sec/Hz. To derive the overall OP of the system, we first represent (6.3) and (6.4) in terms of the equivalent SNRs of the respective links as in the following expressions

$$\Gamma_R = \frac{\gamma_{S,R}}{(\gamma_{R,R} + 1)} \tag{6.6}$$

and

$$\Gamma_D = \frac{\gamma_{R,D}}{(\gamma_{S,D}+1)}, \tag{6.7}$$

respectively, where $\gamma_{S,R} = |\alpha_{S,R}|^2(P_S/N_0)$ is the SNR of the S→R link, $\gamma_{R,R} = |\alpha_{R,R}|^2(P_R/N_0)$ is the SNR of the relay SI which is exponentially distributed with mean value of $\overline{\gamma}_{R,R}$, $\gamma_{R,D} = |\alpha_{R,D}|^2(P_R/N_0)$ is the SNR of the R→D link and $\gamma_{S,D} = |\alpha_{S,D}|^2(P_S/N_0)$ is the SNR of the direct-interference with mean value of $\overline{\gamma}_{S,D}$. Furthermore, Γ_R and Γ_D can be equivalently expressed in terms of the common RVs X and Y as $Z = X/(Y+1)$. Based on this and foundations of probability theory in [233], the CDF of Z for independently distributed X and Y can be written as

$$F_Z(z) = \int_0^\infty F_X(z(y+1))f_Y(y)\mathrm{d}y. \tag{6.8}$$

Asymmetric Channel I

Here, we assume that S→R link is subject to the generalized κ−μ fading model, whereas the R→D and S→D links are subject to η−μ fading model. In this communication scenario, the S→R link can be considered as the link between two closely located nodes where there exists LOS in between, whereas the R→D link can be considered as the communication between a relay node and a mobile terminal where there is no LOS between them because of the random location and mobility of the destination terminal [226, 230].

In order to evaluate the OP of the system over the asymmetric fading environment, we first determine the CDF of η−μ distribution in a simple form. To this effect, using the CDF for a continuous distribution as $F_\gamma(z) \triangleq \int_0^z f_\gamma(x)\mathrm{d}x$ and by expressing the $I_n(\cdot)$ term in (3.36) according to [86, Eq. (8.467)], as well as using [86, Eq. (8.350.1)] and carrying out long but basic algebraic manipulations, it follows that

$$\begin{aligned} F_\gamma(z) =& \sum_{l=0}^{\mu-1} \frac{(-1)^l h^\mu \Gamma(\mu+l)(h-H)^{l-\mu}\gamma\left(\mu-l, \frac{2(h-H)\mu z}{\overline{\gamma}}\right)}{l!2^{\mu+l}\Gamma(\mu)H^{\mu+l}\Gamma(\mu-l)} \\ &+ \sum_{l=0}^{\mu-1} \frac{(-1)^\mu h^\mu \Gamma(\mu+l)(h+H)^{l-\mu}\gamma\left(\mu-l, \frac{2(h+H)\mu z}{\overline{\gamma}}\right)}{l!2^{\mu+l}\Gamma(\mu)H^{\mu+l}\Gamma(\mu-l)} \end{aligned} \tag{6.9}$$

To this effect and by also using [86, Eq. (8.352.6)], the CDF of $\eta-\mu$ distribution for integer values of μ can be equivalently expressed as follows:

$$F_{\gamma}(z) = \sum_{l=0}^{\mu-1} \frac{h^{\mu}\Gamma(\mu+l)((-1)^{l}(h-H)^{l-\mu}+(-1)^{\mu}(h+H)^{l-\mu})}{l!2^{\mu+l}\Gamma(\mu)H^{\mu+l}} - \sum_{l=0}^{\mu-1}\sum_{i=0}^{\mu-l-1} \frac{h^{\mu}\Gamma(\mu+l)\mu^{i}z^{i}}{l!i!2^{\mu+l-i}\overline{\gamma}^{i}\Gamma(\mu)H^{\mu+l}} \left\{ \frac{(-1)^{l}(h-H)^{l+i-\mu}}{\exp\left(\frac{2(h-H)\mu z}{\overline{\gamma}}\right)} + \frac{(-1)^{\mu}(h+H)^{l+i-\mu}}{\exp\left(\frac{2(h+H)\mu z}{\overline{\gamma}}\right)} \right\}. \tag{6.10}$$

Theorem 4. *For $\{\overline{\gamma}_{S,R}, \overline{\gamma}_{R,R}, \kappa_{S,R}, z\} \in \mathbb{R}^{+}$ and $\mu_{S,R} \in \mathbb{N}$, the following closed form expression is valid for the CDF of Γ_R for a FDR system when the $S \to R$ link is subject to $\kappa-\mu$ fading while the instantaneous SNR of the relay SI $\gamma_{R,R}$ is exponentially distributed*

$$F_{Z}(z) = 1 - Q_{\mu_{S,R}}\left(\sqrt{b}, \sqrt{a}\right) + \left(\frac{a\overline{\gamma}_{S,R}}{a\overline{\gamma}_{S,R}+2}\right)^{\mu_{S,R}} \frac{Q_{\mu_{S,R}}\left(\sqrt{\frac{ab}{a+\frac{2}{\overline{\gamma}_{R,R}}}}, \sqrt{\frac{2}{\overline{\gamma}_{R,R}}+a}\right)}{e^{-\frac{1}{\overline{\gamma}_{R,R}}+\frac{b}{2+a\overline{\gamma}_{R,R}}}} \tag{6.11}$$

where $b = 2\kappa_{S,R}\mu_{S,R}$ and $a = 2\mu_{S,R}(1+\kappa_{S,R})z/\overline{\gamma}_{S,R}$.

Proof. We substitute the CDF and PDF of X and Y which correspond to the CDF of $\kappa-\mu$ distribution in [78, Eq.(3)] and the PDF of the exponential distribution into (6.8) which after some simple mathematical manipulations yield

$$F_{Z}(z) = 1 - \int_{0}^{\infty} \frac{Q_{\mu_{S,R}}\left(\sqrt{2\kappa\mu_{S,R}}, \sqrt{\frac{2\mu_{S,R}(1+\kappa_{S,R})z(y+1)}{\overline{\gamma}_{S,R}}}\right)}{\overline{\gamma}_{R,R}\exp\left(\frac{y}{\overline{\gamma}_{R,R}}\right)} \mathrm{d}y. \tag{6.12}$$

By setting $u = \sqrt{y+1}$ and with the aid of [234, Eq. (13)], the closed-form expression in (6.11) is deduced, which completes the proof. □

Theorem 5. *For $\{\overline{\gamma}_{R,D}, \overline{\gamma}_{S,D}, z\} \in \mathbb{R}^{+}$, $\{\eta_{R,D}, \eta_{S,D}\} \in \mathbb{R}^{+}$ in Format-1 and $-1 < \{\eta_{R,D}, \eta_{S,D}\} < 1$ in Format-2 and $\{\mu_{R,D}, \mu_{S,D}\} \in \mathbb{N}$ the following closed form expression is valid for the CDF of Γ_D for the FDR system when $S \to R$ link is subject to $\kappa-\mu$ fading, whereas $R \to D$ and $S \to D$ links are subject to $\eta-\mu$ fading,*

$$
\begin{aligned}
&F_Z(z)\\
&= \sum_{l=0}^{\mu_{R,D}-1} \frac{\Gamma(\mu_{R,D}+l)((-1)^l(h_{R,D}-H_{R,D})^{l-\mu_{R,D}}+(-1)^{\mu_{R,D}}(h_{R,D}+H_{R,D})^{l-\mu_{R,D}})}{l!h_{R,D}^{-\mu_{R,D}}h_{S,D}^{-\mu_{S,D}}2^{\mu_{R,D}+l}\Gamma(\mu_{R,D})H_{R,D}^{\mu_{R,D}+l}(h_{S,D}^2-H_{S,D}^2)^{\mu_{S,D}}}\\
&- \sum_{l=0}^{\mu_{R,D}-1}\sum_{i=0}^{\mu_{R,D}-l-1}\sum_{j=0}^{i}\binom{i}{j}\frac{\mu_{R,D}^i\Gamma(\mu_{R,D}+l)\sqrt{\pi}\mu_{S,D}^{2\mu_{S,D}}h_{S,D}^{\mu_{S,D}}\Gamma(2\mu_{S,D}+j)z^i\overline{\gamma}_{R,D}^{2\mu_{S,D}+j-i}}{l!i!2^{\mu_{R,D}+2\mu_{S,D}+l+j-i-1}\Gamma(\mu_{R,D})H_{R,D}^{\mu_{R,D}+l}\Gamma(\mu_{S,D}+\frac{1}{2})\overline{\gamma}_{S,D}^{-j}}\\
&\times\left\{\frac{(-1)^l h_{R,D}^{\mu_{R,D}}(h_{R,D}-H_{R,D})^{(l+i-\mu_{R,D})}\ {}_2F_1\left(\mu_{S,D}+\frac{j}{2},\mu_{S,D}+\frac{1+j}{2};\mu_{S,D}+\frac{1}{2};D_3\right)}{\Gamma(\mu_{S,D})(\overline{\gamma}_{S,D}\mu_{R,D}z(h_{R,D}-H_{R,D})+\overline{\gamma}_{R,D}\mu_{S,D}h_{S,D})^{2\mu_{S,D}+j}\exp(D_1z)}\right.\\
&\left.+\frac{(-1)^{\mu_{R,D}}\ h_{R,D}^{\mu_{R,D}}(h_{R,D}+H_{R,D})^{(l+i-\mu_{R,D})}\ {}_2F_1\left(\mu_{S,D}+\frac{j}{2},\mu_{S,D}+\frac{1+j}{2};\mu_{S,D}+\frac{1}{2};D_4\right)}{\Gamma(\mu_{S,D})(\overline{\gamma}_{S,D}\mu_{R,D}z(h_{R,D}+H_{R,D})+\overline{\gamma}_{R,D}\mu_{S,D}h_{S,D})^{2\mu_{S,D}+j}\exp(D_2z)}\right\}.
\end{aligned}
\tag{6.13}
$$

where

$$
\left\{\begin{matrix}D_1\\D_2\end{matrix}\right\} = \frac{2(h_{R,D}\mp H_{R,D})\mu_{R,D}}{\overline{\gamma}_{R,D}} \tag{6.14}
$$

$$
\left\{\begin{matrix}D_3\\D_4\end{matrix}\right\} = \frac{\overline{\gamma}_{R,D}^2\mu_{S,D}^2H_{S,D}^2}{(\overline{\gamma}_{S,D}\mu_{R,D}z(h_{R,D}\mp H_{R,D})+\mu_{S,D}\overline{\gamma}_{R,D}h_{S,D})^2}. \tag{6.15}
$$

Proof. The proof is provided in appendix G. □

Asymmetric Channel II

For asymmetric channel of scenario II, the S→R and S→D links are subject to the $\kappa-\mu$ fading models, whereas the R→D link is subject to $\eta-\mu$ fading conditions. Unlike the first transmission condition, the S→D link in this case is subject to the LOS communication scenario.

Theorem 6. *For* $\{\overline{\gamma}_{R,D},\overline{\gamma}_{S,D},\kappa_{S,D},z\}\in\mathbb{R}^+$, $\eta_{R,D}\in\mathbb{R}^+$ *in Format-1 and* $-1<\eta_{R,D}<1$ *in Format-2 and* $\mu_{R,D}\in\mathbb{N}$ *the following closed form expression is valid for the CDF of* Γ_D *for the FDR system when* $S\to R$ *and* $S\to D$ *links are subject to* $\kappa-\mu$

fading, whereas $R \to D$ link is subject to $\eta-\mu$ fading conditions.

$$F_Z(z) = \sum_{l=0}^{\mu_{R,D}-1} \frac{h_{R,D}^{\mu_{R,D}} \left((-1)^l (h_{R,D} - H_{R,D})^{l-\mu_{R,D}} + (-1)^{\mu_{R,D}} (h_{R,D} + H_{R,D})^{l-\mu_{R,D}}\right)}{(\Gamma(\mu_{R,D}+l))^{-1} l! 2^{\mu_{R,D}+l} \Gamma(\mu_{R,D}) H_{R,D}^{\mu_{R,D}+l}}$$
$$- \sum_{l=0}^{\mu_{R,D}-1} \sum_{i=0}^{\mu_{R,D}-l-1} \sum_{j=0}^{i} \binom{i}{j} \frac{z^i h_{R,D}^{\mu_{R,D}} \Gamma(\mu_{R,D}+l) \mu_{R,D}^i \mu_{S,D}^{\mu_{S,D}} \overline{\gamma}_{R,D}^{\mu_{S,D}+j-i} \overline{\gamma}_{S,D}^{j} \Gamma(\mu_{S,D}+j)}{\exp(\kappa_{S,D}\mu_{S,D}) \Gamma(\mu_{S,D}) l! i! 2^{\mu_{R,D}+l-i} \Gamma(\mu_{R,D}) H_{R,D}^{\mu_{R,D}+l}}$$
$$\times \left\{ \frac{\left((-1)^l (h_{R,D} - H_{R,D})^{l+i-\mu_{R,D}} (1+\kappa_{S,D})^{\mu_{S,D}} {}_1F_1\left(\mu_{S,D}+j; \mu_{S,D}; E_1\right)\right)}{\exp\left(D_1 z\right) \left(\mu_{S,D} \overline{\gamma}_{R,D} (1+\kappa_{S,D}) + 2(h_{R,D} - H_{R,D}) \overline{\gamma}_{S,D} z \mu_{R,D}\right)^{\mu_{S,D}+j}} \right.$$
$$\left. + \frac{\left((-1)^{\mu_{R,D}} (h_{R,D} + H_{R,D})^{l+i-\mu_{R,D}} (1+\kappa_{S,D}) {}_1F_1\left(\mu_{S,D}+j; \mu_{S,D}; E_2\right)\right)}{\exp\left(D_2 z\right) \left(\mu_{S,D} \overline{\gamma}_{R,D} (1+\kappa_{S,D}) + 2(h_{R,D} + H_{R,D}) \overline{\gamma}_{S,D} z \mu_{R,D}\right)^{\mu_{S,D}+j}} \right\}. \tag{6.16}$$

where ${}_1F_1(\cdot;\cdot;\cdot)$ is the confluent hypergeometric function [104] and

$$\left\{ {E_1 \atop E_2} \right\} = \frac{\mu_{S,D}^2 \overline{\gamma}_{R,D} \kappa_{S,D} (1+\kappa_{S,D})}{\mu_{S,D} \overline{\gamma}_{R,D} (1+\kappa_{S,D}) + 2\overline{\gamma}_{S,D} (h_{R,D} \mp H_{R,D}) z \mu_{R,D}}. \tag{6.17}$$

Proof. The proof is provided in Appendix H. □

The expression in (6.16) is long but relatively convenient to handle both analytically and numerically since it involves elementary and special functions that are built-in in most popular scientific software packages, such as MATLAB, MAPLE and MATHEMATICA. Furthermore, the derived expression can be readily substituted in (6.5) for deriving a novel exact expression for the OP of the considered DF-FDR system over generalized asymmetric fading conditions.

Asymmetric Channel III

In this final scenario, the S→R and R→D links are subject to the $\kappa-\mu$ and $\eta-\mu$ fading models, respectively, whereas the direct S→D link is subject to the IG fading condition. As mentioned in Chapter 3, the IG distribution has been shown to provide accurate characterization and modeling of shadowing effects.

Theorem 7. *For $\{\overline{\gamma}_{R,D}, \overline{\gamma}_{S,D}, \lambda, z\} \in \mathbb{R}^+$, $\eta_{R,D} \in \mathbb{R}^+$ in Format-1 and $-1 < \eta_{R,D} < 1$ in Format-2 and $\mu_{R,D} \in \mathbb{N}$ the following closed form expression is valid for the CDF of Γ_D for the FDR system when $S \to R$ and $R \to D$ links are subject to $\kappa-\mu$ and $\eta-\mu$*

fading scenarios while $S \to D$ link is subject to the IG fading condition.

$$F_Z(z) = \sum_{l=0}^{\mu_{R,D}-1} \frac{((-1)^l (h_{R,D} - H_{R,D})^{l-\mu_{R,D}} + (-1)^{\mu_{R,D}} (h_{R,D} + H_{R,D})^{l-\mu_{R,D}})}{(h_{R,D}^{\mu_{R,D}}\, \Gamma(\mu_{R,D}+l))^{-1} H_{R,D}^{\mu_{R,D}+l} \Gamma(\mu_{R,D})\, l!\, 2^{\mu_{R,D}+l}}$$

$$- \sum_{l=0}^{\mu_{R,D}-1} \sum_{i=0}^{\mu_{R,D}-l-1} \sum_{j=0}^{i} \binom{i}{j} \frac{((-1)^i (h_{R,D} - H_{R,D})^{l+i-\mu_{R,D}} h_{R,D}^{\mu_{R,D}} \Gamma(\mu_{R,D}+l) \mu_{R,D}^i z^i)}{l! i! 2^{\mu_{R,D}+l-i} \sqrt{2\pi} \overline{\gamma}_{R,D}^i H_{R,D}^{\mu_{R,D}+l} \exp(D_1 z) \exp\left(-\frac{\lambda_{S,D}}{\overline{\gamma}_{S,D}}\right)}$$

$$\times \frac{\sqrt{\lambda_{S,D}}}{\Gamma(\mu_{R,D})} 2^{\frac{5}{4}-\frac{j}{2}} \left(\frac{1}{2\overline{\gamma}_{S,D}^2} + \frac{D_1 z}{\lambda_{S,D}}\right)^{\frac{1}{4}-\frac{j}{2}} K_{(\frac{1}{2}-j)} \left(\sqrt{\frac{\lambda_{S,D}^2}{\overline{\gamma}_{S,D}^2} + 2\lambda_{S,D} D_1 z}\right)$$

$$- \sum_{l=0}^{\mu_{R,D}-1} \sum_{i=0}^{\mu_{R,D}-l-1} \sum_{j=0}^{i} \frac{((-1)^{\mu_{R,D}} (h_{R,D} + H_{R,D})^{l+i-\mu_{R,D}} h_{R,D}^{\mu_{R,D}} \Gamma(\mu_{R,D}+l) \mu_{R,D}^i z^i)}{l! i! 2^{\mu_{R,D}+l-i} \sqrt{2\pi} \overline{\gamma}_{R,D}^i H_{R,D}^{\mu_{R,D}+l} \exp(D_2 z) \exp\left(-\frac{\lambda_{S,D}}{\overline{\gamma}_{S,D}}\right)}$$

$$\times \frac{\sqrt{\lambda_{S,D}}}{\Gamma(\mu_{R,D})} 2^{\frac{5}{4}-\frac{j}{2}} \left(\frac{1}{2\overline{\gamma}_{S,D}^2} + \frac{D_2 z}{\lambda_{S,D}}\right)^{\frac{1}{4}-\frac{j}{2}} K_{(\frac{1}{2}-j)} \left(\sqrt{\frac{\lambda_{S,D}^2}{\overline{\gamma}_{S,D}^2} + 2\lambda_{S,D} D_2 z}\right) \tag{6.18}$$

where $K_n(\cdot)$ denotes the modified Bessel function of the second kind [86].

Proof. The proof is provided in Appendix I. □

6.3.2 Half-Duplex Mode

As already mentioned, the conventional HD regenerative relaying assumes that a signal is transmitted within two orthogonal channels since a HD relay cannot transmit and receive simultaneously in the same frequency band. As a result, the SI issue in the relay is eliminated i.e. $h_{R,R} = 0$ and the corresponding OP without the direct link can be expressed as follows:

$$P_{\text{out}} = \Pr(\gamma_{S,R} < \gamma_T) + (1 - \Pr(\gamma_{S,R} < \gamma_T))\Pr(\gamma_{R,D} < \gamma_T) \tag{6.19}$$

where $\gamma_T = 2^{2R} - 1$ is the required SNR threshold value for successful transmission. Note that for an end-to-end SE of R, the individual links in the HD system need to provide a SE of $2R$, due to the orthogonal time slots based operation. Furthermore, for an asymmetric channel where fading effects in the S→R link are $\kappa-\mu$ distributed and R→D link experiences $\eta-\mu$ fading conditions, the $\Pr(\gamma_{S,R} < \gamma_T)$ and $\Pr(\gamma_{R,D} < \gamma_T)$ can be readily deduced with the aid of [78, Eq. (3)] and (6.10), respectively. The HDR scheme used here is serving as a baseline for comparisons with the FDR scheme in energy and other performance analyses.

6.4 Power Allocation and Energy-Efficiency Optimization

6.4.1 Optimal Power Allocation

Here, we investigate and develop power allocation schemes for both FDR and HDR systems. The target is to minimize the overall OP through proper optimization of the transmit powers of the source and relay nodes under total transmit power constraint over asymmetric fading scenarios. Specifically, we analyze the impact of the relay SI on the OPA scheme in the FDR case. Thus, for power constrained networks, we formulate a non-linear optimization problem as

$$\begin{aligned} \mathbf{a_{opt}} &= \arg\min_{\mathbf{a}} P_{\text{out}} \\ \text{Subject to}: \; & a_0 + a_R = 1, \quad a_0 \geq 0, \quad a_R \geq 0 \end{aligned} \tag{6.20}$$

where $a_0 = P_S/P$ and $a_R = P_R/P$ are the relative transmit power ratios at the source and relay nodes, respectively, whereas $P = P_S + P_R$ denotes the total power budget of the system. This approach is widely adopted in power constrained cooperative communications to facilitate the delivery of a given amount of data from the source to the destination. The OP for different asymmetric fading scenarios is determined by using the expressions stated in the previous theorems where the purpose of the OPA scheme is to decrease the impact of the relay SI.

In general, closed-form expressions for the optimal values of a_0 and a_R are not tractable analytically. However, they can be efficiently computed with the help of standard numerical tools, which is the approach that we also take here. We also compare the obtained results with the traditional EPA scheme to acquire insights about the OPA scheme under the impact of different relay SI levels.

6.4.2 Energy Optimization Analysis

Here, we quantify the average total energy consumption required to transmit L information bits from the source to the destination efficiently for FDR and HDR systems over the generalized asymmetric fading models. Similar to the energy modeling in Chapter 4, we assume here also that the transceiver circuitry operates on multi-mode basis, i.e., on active mode, on a sleep mode and on switching mode. To this end, the total energy required to transmit and receive L information bits can be expressed as

$$E = P_{on}T_{on} + P_{sp}T_{sp} + P_{tr}T_{tr}. \tag{6.21}$$

where T_{on} refers to the time period of active transmission and/or reception. In the above expression, T_{on} for the FDR system in terms of the packet size L and the bandwidth B for end-to-end SE of R can be expressed as

$$T_{\text{on}} = \frac{L}{BR} \tag{6.22}$$

which is the period of active transmission and reception of the source and the relay, respectively. Furthermore, due to the FD principle, this is then also the period of active transmission and reception of the relay and the destination, respectively, in the case of successful decoding at relay. In the HDR system, on the other hand, assuming the same end-to-end SE of R, T_{on} can be expressed as

$$T_{\text{on}} = \frac{L}{2BR}. \tag{6.23}$$

To determine then the average total energy consumption in the DF strategy of the HDR and FDR systems, we first formulate the average total power consumption for the HDR scheme, without the direct link for simplicity, which is a discrete random variable that can be represented as follows:

$$P_T^{HD} = \begin{cases} P_{CT_x} + (1+\omega_{HD})\, P_S + P_{CR_x}, & \text{with } \Pr = 1 \\ P_{CT_x} + (1+\omega_{HD})\, P_R + P_{CR_x}, & \text{with } \Pr = 1 - \Pr(\gamma_{S,R} < 2^{2R} - 1) \end{cases} \tag{6.24}$$

By recalling the expressions in (4.67), (4.68) and using $M = 2^{2R}$ for evaluating the power consumption of the RF-power amplifier, ω_{HD} can be expressed in the HDR case as

$$\omega_{HD} = \frac{3}{\eta_d} \frac{\sqrt{2^{2R}} - 1}{\sqrt{2^{2R}} + 1} - 1. \tag{6.25}$$

The first line in (6.24) refers to the absolute total power consumption by the nodes in the first transmission phase, whereas the second line represents the power consumption in the second phase subject to correct decoding of the received signal by the relay. Based on this, the average total power consumption in the HDR transmission mode can be expressed as

$$\begin{aligned} \bar{P}_T^{HD} &= P_{CT_x} + (1+\omega_{HD}) P_S + P_{CR_x} \\ &\quad + \left(P_{CT_x} + (1+\omega_{HD}) P_R + P_{CR_x}\right) \left(1 - \Pr(\gamma_{S,R} < 2^{2R} - 1)\right). \end{aligned} \tag{6.26}$$

Similarly, the power consumption of the FDR scheme without the direct link can be expressed as follows:

$$P_T^{FD} = \begin{cases} P_{CT_x} + (1+\omega_{FD})\, P_S + P_{CR_x}, & \text{with } \Pr = 1 \\ P_{CT_x} + (1+\omega_{FD})\, P_R + P_{CR_x}, & \text{with } \Pr = 1 - \Pr(\Gamma_R < 2^R - 1). \end{cases} \tag{6.27}$$

To this end, the average total power consumption for the FDR transmission mode can be expressed as

$$\begin{aligned} \bar{P}_T^{FD} &= P_{CT_x} + (1+\omega_{FD}) P_S + P_{CR_x} \\ &\quad + \left(P_{CT_x} + (1+\omega_{FD}) P_R + P_{CR_x}\right) \left(1 - \Pr(\Gamma_R < 2^R - 1)\right). \end{aligned} \tag{6.28}$$

Applying $M = 2^R$ for computing the power consumption of the RF-power amplifier, ω_{FD} can be expressed in the FDR case as

$$\omega_{FD} = \frac{3}{\eta_d} \frac{\sqrt{2^R} - 1}{\sqrt{2^R} + 1} - 1. \tag{6.29}$$

Using (6.26) and (6.28), the corresponding average energy consumption per information bit is given by

$$\bar{E}_T = \frac{\bar{P}_T T_{\text{on}} + 2 P_{LO} T_{tr}}{L} \tag{6.30}$$

where in the case of HDR scheme $\bar{P}_T = \bar{P}_T^{HD}$, whereas for the case of FDR system $\bar{P}_T = \bar{P}_T^{FD}$. Moreover, T_{on} for the FDR mode is given in (6.22), whereas for the HDR mode is expressed in (6.23). Applying (6.30), the energy minimization problem with the two optimization variables, namely, P_S and P_R at target OP of p^* and maximum total transmission power constraint, P_{maxt}, can be formulated as follows:

$$\begin{aligned} &\min_{P_S, P_R} \bar{E}_T(P_S, P_R) \\ &\text{subject to: } (P_S + P_R) \le P_{maxt}, \quad P_S \ge 0, \quad P_R \ge 0 \\ &P_{\text{out}}(P_S, P_R) = p^*. \end{aligned} \tag{6.31}$$

For the above optimization problem, the optimal powers at the source and relay nodes that minimize the total energy consumption under the given constrains can be evaluated with the aid of numerical optimization techniques such as MATLAB optimization tool box and its *fmincon* function.

In general, the total average power consumption models and the energy consumption formulations, which are based on active, sleep and transmit/receive modes, in

Section 4.6 and in this Section are analytically similar. Specifically, in Section 4.6 the total average power consumption was evaluated where the direct link between the source and destination exists. This assumption was useful to compare the total energy consumption of the HD based regenerative cooperative system with the reference direct transmission scheme. Furthermore, the total average energy consumption was optimized for some given total transmit power under a given end-to-end BER requirement. On the other hand, for evaluating and comparing the total average energy consumption of HD and FD modes under the impact of different relay SI levels in the FDR case, the direct link is ignored in this Chapter. The total average energy consumption is also optimized under a given total maximum transmit power constraint for target OP of p^*.

6.5 Numerical Results and Discussion

In this section, we present numerical results to illustrate the theoretical analysis carried out in the previous sections. In all numerical studies, we assume that the system is operating over the generalized small-scale asymmetric fading channels. This is performed for different fading and interference scenarios assuming that the total transmit power is equally or optimally allocated to the source and relay nodes, following the power allocation scheme formulated in this chapter. Moreover, we use Format-1 to characterize the fading channels of the η−μ distribution. The analysis is also valid for Format-2 scenario.

Fig. 6.2 shows the outage performance of the FDR system where the total transmit power is equally allocated to the source and relay nodes. In particular, we assume that the S→R link is subject to the generalized LOS small-scale κ−μ fading channel, and therefore undergo fading with $\mu_{S,R} = 1$ and different values of $\kappa_{S,R}$, whereas the R→D link is subject to the NLOS η−μ fading with $\mu_{R,D} = 1, \eta_{R,D} = 1$. In addition, the S→D link, which is treated as an interference at the destination is modeled as η−μ fading with $\mu_{S,D} = 1$ and $\eta_{S,D} = 1$. In this communication scenario, the destination terminal can be considered as a mobile UE without LOS connection to the relay node due to the random location and mobility of the destination terminal [226, 230]. The mean values of the relay SI and the direct link interference are set to be $\overline{\gamma}_{R,R} = 5$dB and $\overline{\gamma}_{S,D} = 0$dB, respectively, for two different SINR thresholds $\Gamma_T = 0$dB and $\Gamma_T = 5$dB. As expected, and observed from the figure the outage performance of the asymmetric FDR improves with increasing $\kappa_{S,R}$. For example, at P_{out} of 10^{-3} average gains of almost 3dB and 8.5dB are observed when $\kappa_{S,R}$ changes from 2dB to 4dB and then to 8dB at $\Gamma_T = 0$dB. It is also noticed that the outage performance

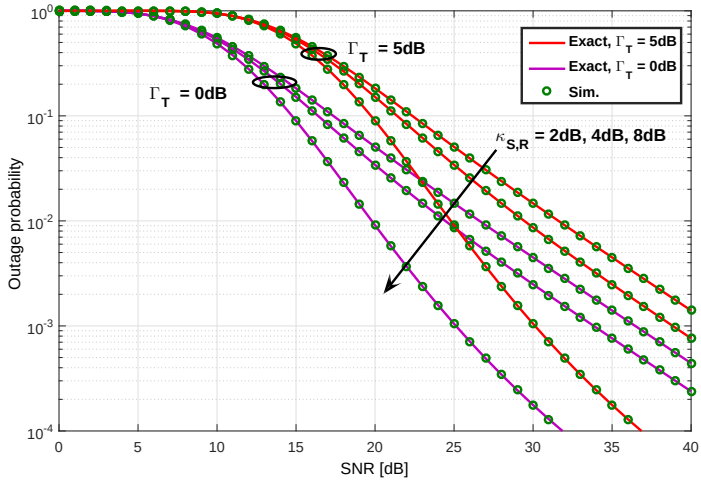

Figure 6.2 Outage probability of FDR vs. SNR with EPA over asymmetric $\kappa-\mu$ and $\eta-\mu$ fading channels for $\mu_{S,R} = \mu_{R,D} = \mu_{S,D} = 1, \eta_{R,D} = \eta_{S,D} = 1, \overline{\gamma}_{R,R} = 5\text{dB}, \overline{\gamma}_{S,D} = 0\text{dB}$ for different $\kappa_{S,R}$ and Γ_T.

degrades as the target Γ_T increases. This is because the system remains in complete outage until the threshold or target SINR is achieved for successful transmission. It is also evident that the results from the exact analytic expressions are in excellent agreement with the respective results from computer simulations, also shown in Fig. 6.2, which verifies their validity. Hence, from now on, we focus primarily on the numerical evaluations of the analytical results.

Likewise, Fig. 6.3 shows the outage performance of the FDR system with EPA for target SINRs of $\Gamma_T = 0\text{dB}$ and 5dB for $\kappa_{S,R} = 4.5\text{dB}$ and $\mu_{S,D} = 1, \eta_{S,D} = \eta_{R,D} = 1$, $\overline{\gamma}_{R,R} = 5\text{dB}$, $\overline{\gamma}_{S,D} = 0\text{dB}$ with different values of $\mu_{S,R}$ and $\mu_{R,D}$. It is shown that at relatively high SNR values the OP improves significantly when the values of the fading parameters $\mu_{S,R}$ and $\mu_{R,D}$ increase i.e. fading severity decreases and/or when the required threshold Γ_T decreases. Thus, when the fading parameters of S→R and R→D increase, the effects of the relay SI and the direct interference reduce and the corresponding errors tend to be negligible, and as a result, the performance of the system increases. For instance, at P_{out} of 10^{-3} nearly 9dB and 2.5dB gains are obtained when $\{\mu_{S,R}, \mu_{R,D}\}$ changes from $\{1,1\}$ to $\{2,2\}$ and then to $\{3,3\}$ when $\Gamma_T = 0\text{dB}$.

Fig. 6.4 shows the outage performance of the FDR system for relatively moderate values of the fading parameters from the source to relay node and from the relay to

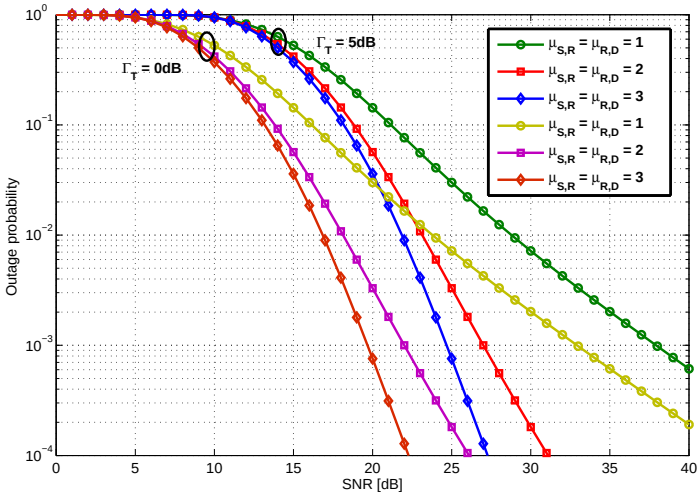

Figure 6.3 Outage probability of FDR vs. SNR with EPA over asymmetric $\kappa-\mu$ and $\eta-\mu$ fading channels for $\kappa_{S,R} = 4.5\text{dB}, \mu_{S,D} = 1, \eta_{S,D} = \eta_{R,D} = 1, \overline{\gamma}_{R,R} = 5\text{dB}, \overline{\gamma}_{S,D} = 0\text{dB}$ for different $\mu_{S,R} = \mu_{R,D}$ and Γ_T values.

the destination with EPA. Specifically, we set $\mu_{S,R} = \mu_{R,D} = 2, \mu_{S,D} = 1, \kappa_{S,R} = 4\text{dB}$ and $\eta_{R,D} = \eta_{S,D} = 1$ for $\overline{\gamma}_{S,D} = 0\text{dB}$ and $\overline{\gamma}_{R,R} = \{5, 0, -5\}\text{dB}$ with target SINR of $\Gamma_T = 0\text{dB}$ and $\Gamma_T = 5\text{dB}$, respectively. It is shown that the performance of the FDR system is significantly affected by the relay SI. This is because the relay SI is acting as additional noise to the received signal from source to relay node and thus it reduces the effective SINR and consequently the outage performance of the system. It is also evident that the curves are shifted to the right as the relay SI strength increases from -5dB to 0dB and then to 5dB. This infers that the relay SI has an impact on the cooperation gain of the system. However, the degradation in the cooperation gain is not linear as the relay SI reduces from 5dB to 0dB and then to -5dB. The considered relay SI levels also affect slightly the diversity gain of the system.

Fig. 6.5 then shows the OP versus R for asymmetric channel model of $\kappa-\mu$ and $\eta-\mu$ for HD and FD relay systems under similar fading conditions of $\mu_{S,R} = \mu_{R,D} = 2, \eta_{R,D} = 1, \kappa_{S,R} = 2$ dB with EPA for SNR of 25dB and different values of the relay SI levels in the case of FDR system. It is shown that the HDR system tends to be in complete outage, i.e., $P_{\text{out}} = 1$ when $R = 4.5$ bps/Hz, whereas the FDR mode performs relatively well for all considered signal strengths of the relay SI levels. In other words, the outage of HDR occurs faster than the FDR system as the SE increases. This is because, in order to support the same value of R, the instantaneous

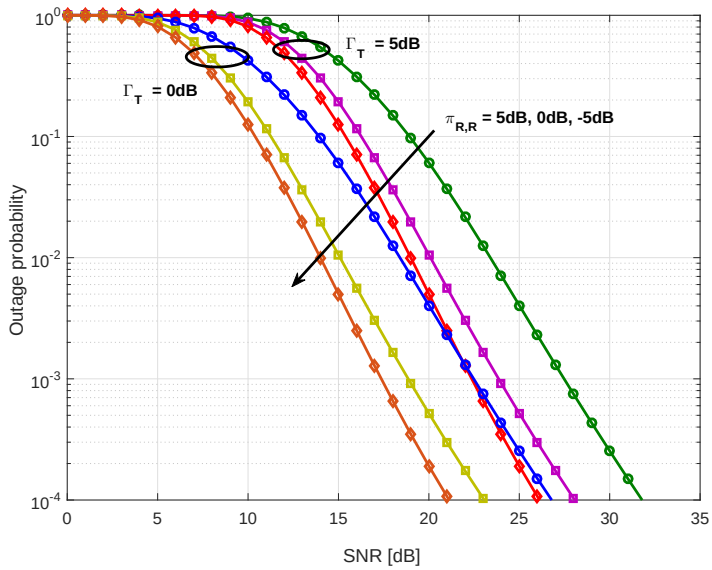

Figure 6.4 Outage probability of FDR vs. SNR with EPA over asymmetric $\kappa-\mu$ and $\eta-\mu$ fading channels for $\mu_{S,R} = \mu_{R,D} = 2$, $\kappa_{S,R} = 4\text{dB}, \mu_{S,D} = 1, \eta_{R,D} = \eta_{S,D} = 1, \overline{\gamma}_{S,D} = 0\text{dB}$ for different $\overline{\gamma}_{R,R} = \pi_{R,R}$ and Γ_T.

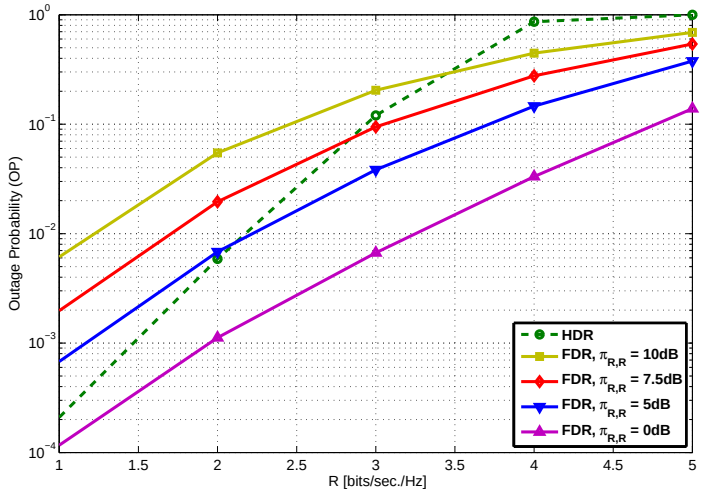

Figure 6.5 Outage probability of HDR and FDR vs. R with EPA over asymmetric $\kappa-\mu$ and $\eta-\mu$ fading channels for $\mu_{S,R} = \mu_{R,D} = 2, \eta_{R,D} = 1, \kappa_{S,R} = 2\text{dB}$ for different values of $\overline{\gamma}_{R,R} = \pi_{R,R}$ without the direct link.

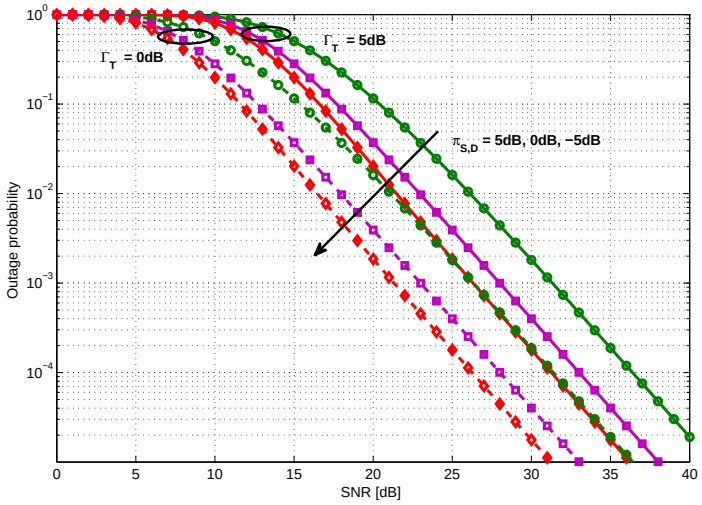

Figure 6.6 Outage probability of FDR vs. SNR with EPA over asymmetric $\kappa-\mu$ and $\eta-\mu$ fading channels for $\mu_{S,R} = 2, \mu_{R,D} = \mu_{S,D} = 1, \eta_{R,D} = 1$, $\kappa_{S,R} = 4\text{dB}, \kappa_{S,D} = 2\text{dB}, \overline{\gamma}_{R,R} = 0\text{dB}$ for different values of $\overline{\gamma}_{S,D} = \pi_{S,D}$ and Γ_T.

rate of HDR transmissions must be twice as high as the FD system. It is also noticed that at relatively high values of R e.g. for 3.5bps/Hz, the FDR mode outperforms its HDR counterpart even under the strong SI level of 10dB. However, it is also shown that the OP of the HDR system is lower, compared to the FDR system, if the SE requirement is relatively low and especially if the relative SI level in the FDR system is very high.

Assuming asymmetric channel model II, Fig. 6.6 shows the effect of the direct S→D interference on the behavior and performance of the OP with EPA scheme for fading parameters of $\mu_{S,R} = 2, \kappa_{S,R} = 4\text{dB}$, $\mu_{S,D} = 1, \kappa_{S,D} = 2\text{dB}$, $\mu_{R,D} = 1, \eta_{R,D} = 1$, $\overline{\gamma}_{R,R} = 0\text{dB}$ and different values of $\overline{\gamma}_{S,D}$ at target SINRs of $\Gamma_T = 0\text{dB}$ and 5dB, respectively. It is observed that the outage performance of the system is significantly affected by the interference from the S→D link. This is because as the direct interference increases, the equivalent SINR at the destination is reduced, which ultimately degrades the corresponding outage performance of the system.

In similar way, by assuming the asymmetric channel model III, Fig. 6.7 shows the outage performance of the FDR system with EPA scheme for fading parameters of $\mu_{S,R} = \mu_{R,D} = 2, \eta_{R,D} = 1$, $\overline{\gamma}_{R,R} = 0\text{dB}$, $\overline{\gamma}_{S,D} = 0\text{dB}$, $\lambda = 3.5$ and different values of $\kappa_{S,R}$ with target SINRs of $\Gamma_T = 0\text{dB}$ and 5dB, respectively. The shape

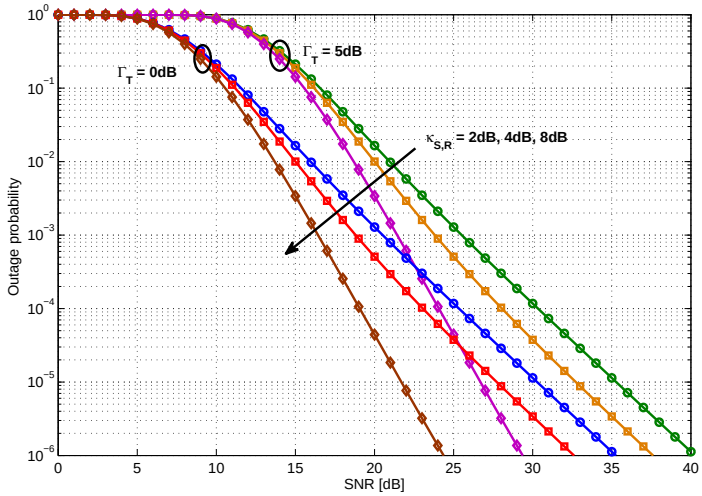

Figure 6.7 Outage probability of FDR vs. SNR with EPA over asymmetric fading channel III for $\mu_{S,R} = \mu_{R,D} = 2, \eta_{R,D} = 1, \overline{\gamma}_{R,R} = 0\text{dB}, \overline{\gamma}_{S,D} = 0\text{dB}, \lambda = 3.5$ for different values of $\kappa_{S,R}$ and Γ_T.

parameter $\lambda = 3.5$ corresponds to the shadowing effect in the urban areas. Similar to the asymmetric channel model I, the outage performance in this case also improves with increasing $\kappa_{S,R}$. This is because, as $\kappa_{S,R}$ increases the corresponding SINR tends to increase, which aids to decrease the overall OP of the considered system. Moreover, the outage performance increases as the target SINR reduces from 5dB to 0dB.

Fig. 6.8 shows the outage performance of the FDR system for EPA and OPA schemes for asymmetric I fading model with $\mu_{S,R} = \mu_{R,D} = 2, \eta_{R,D} = 1, \mu_{S,D} = 1, \eta_{S,D} = 1$ for mean values of direct interference and relay SI of -10dB and 5dB, respectively, at target SINR of $\Gamma_T = 5\text{dB}$ and different values of $\kappa_{S,R}$. As expected, the analysis shows that the OPA scheme outperforms its counterpart EPA scheme as $\kappa_{S,R}$ varies. Indicatively, at P_{out} of 10^{-3} about 2dB, 1.75dB and 1.25dB gains are achieved due to the OPA strategy when $\kappa_{S,R}$ is set at $\{0, 4, 8\}$dB, respectively.

Fig. 6.9 shows the outage performance of the FDR system for EPA and OPA schemes over asymmetric III fading model with fading parameters of $\mu_{S,R} = \mu_{R,D} = 2, \eta_{R,D} = 1, \kappa_{S,R} = 4\text{dB}$, $\lambda = 3.5$ and $\overline{\gamma}_{S,D} = -10\text{dB}$ for different relay SI levels at target SINR of $\Gamma_T = 5\text{dB}$. It is observed that the gain from the OPA scheme is significant when the relay SI is high. For example, a gain of 2dB is achieved at OP of 10^{-3} for relay SI level of 10dB. However, this gain is gradually decreasing as the relay SI becomes smaller and smaller and in particular when $\overline{\gamma}_{R,R} < 0\text{dB}$ the OPs for

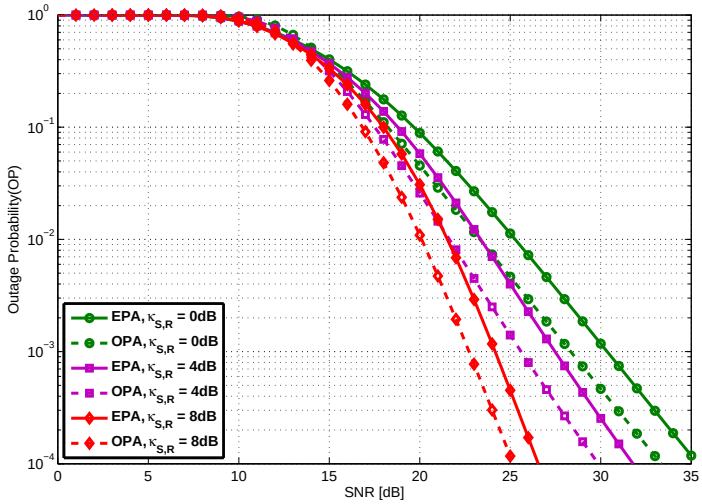

Figure 6.8 Outage probability of FDR vs. SNR over asymmetric I fading model for $\mu_{S,R} = \mu_{R,D} = 2, \mu_{S,D} = 1, \eta_{R,D} = \eta_{S,D} = 1, \Gamma_T = 5\text{dB}, \overline{\gamma}_{S,D} = -10\text{dB}, \overline{\gamma}_{R,R} = 5\text{dB}$ for different values of $\kappa_{S,R}$ using EPA and OPA schemes.

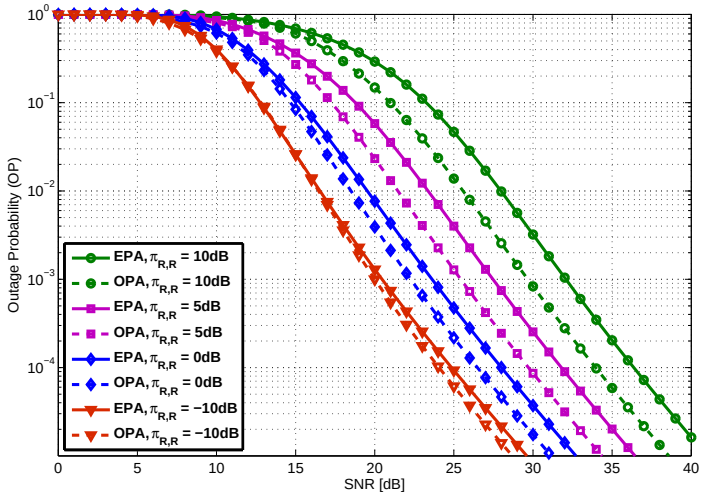

Figure 6.9 Outage probability of FDR vs. SNR over asymmetric channel model III for $\mu_{S,R} = \mu_{R,D} = 2, \kappa_{S,R} = 4\text{dB}, \eta_{R,D} = 1, \lambda = 3.5, \Gamma_T = 5\text{dB}, \overline{\gamma}_{S,D} = -10\text{dB}$ with different $\overline{\gamma}_{R,R}$ for EPA and OPA schemes.

Table 6.1 Optimal power ratio values for source and relay nodes over asymmetric III fading model with $\lambda = 3.5, \kappa_{S,R} = 4\text{dB}, \Gamma_{\text{T}} = 5\text{dB}, \overline{\gamma}_{\text{S,D}} = -10\text{dB}$ for different relay SI levels using FDR system at SNR = 20dB.

$\overline{\gamma}_{R,R}$(dB)	P_S/P	P_R/P
10	0.8710	0.129
5	0.8096	0.1904
0	0.7187	0.2813
-10	0.6201	0.3799

EPA and OPA schemes appear to be very close to each other. Indicatively, Table 6.1 shows the optimal power ratios allocated to the source and relay nodes, which shows that the proportion of the power allocated to the source node increases as the relay SI level increases. The results here indicate that the impact of the relay SI can be reduced by allocating the power optimally.

Likewise, Fig. 6.10 shows the OP versus R using EPA and OPA schemes for asymmetric channel model of $\kappa-\mu$ and $\eta-\mu$ for HD and FD relay systems under similar fading conditions of $\mu_{S,R} = \mu_{R,D} = 2, \eta_{R,D} = 1, \kappa_{S,R} = 4\text{dB}$, at SNR of 25dB and relay SI level of 5dB in the case of FDR without the direct link. It is shown that the OPA outperforms the EPA scheme in both HDR and FDR systems, but the benefit of the OPA scheme is more significant in FDR than the HDR system. This outcome is due to the existence of the SI in the relay, which makes the Γ_R and Γ_D highly unbalanced comparing with the respective SNRs of the HDR scheme. This verifies that the benefit of the OPA is significant when S→R and R→D links are highly unbalanced. Similar result was also observed in Chapter 5 for the generalized fading model.

In the next part of the numerical analysis, we demonstrate and evaluate the average total energy consumption per information bit required in the HDR and FDR systems over the generalized asymmetric fading conditions to guarantee certain QoS. To account the PL effects in both schemes, the PL is modeled by $P_{L_{i,j}}[\text{dB}] = 148 + 40\log_{10}(d_{i,j}[\text{km}])$, which is similar to the PL model in Chapter 4. Furthermore, it is assumed that all communicating nodes are located along a straight line, which satisfies the distance relationship $d_{S,D} = d_{S,R} + d_{R,D}$. The system parameters that are used to analyze the energy optimization are listed in Table 4.1.

Fig. 6.11 shows the average total energy consumption per information bit as a function of transmission distance, distance from source to destination, over asymmetric $\kappa-\mu$ and $\eta-\mu$ fading condition with $\kappa_{S,R} = 2\text{dB}$, $\mu_{S,R} = \mu_{R,D} = 2, \eta_{R,D} = 1$ and relay SI levels of -5dB, 0dB and 5dB in the case of FDR system for target P_{out} of

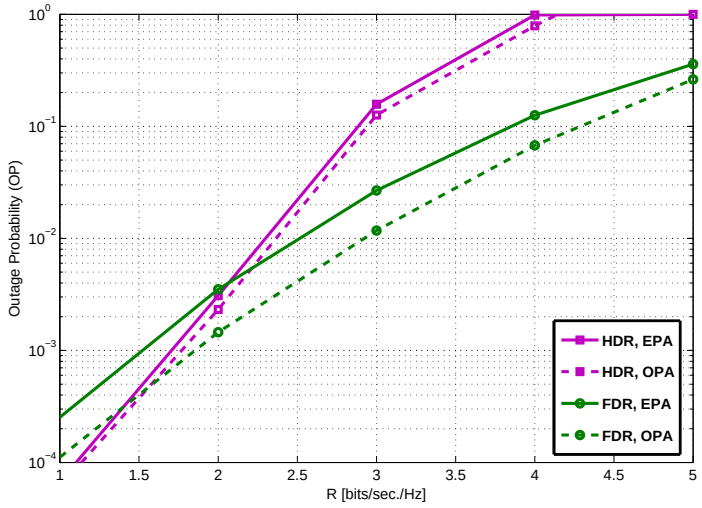

Figure 6.10 Outage probability of FDR and HDR vs. R over asymmetric $\kappa-\mu$ and $\eta-\mu$ fading channels for $\mu_{S,R} = \mu_{R,D} = 2, \kappa_{S,R} = 4\text{dB}, \eta_{R,D} = 1, \overline{\gamma}_{R,R} = 5\text{dB}$ without direct link for EPA and OPA schemes at SNR = 25dB.

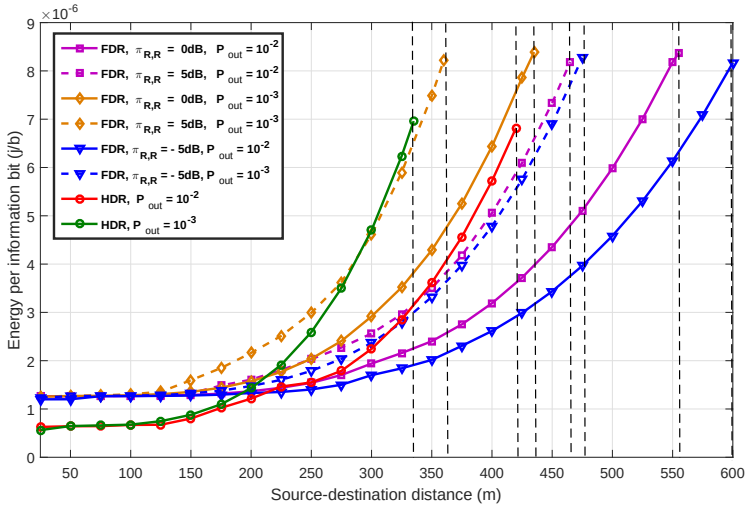

Figure 6.11 Energy consumption per information bit of FDR and HDR systems vs. source-destination distance over asymmetric $\kappa-\mu$ and $\eta-\mu$ fading channels for $\mu_{S,R} = \mu_{R,D} = 2, \kappa_{S,R} = 2\text{dB}, \eta_{R,D} = 1, R = 2\text{bps/Hz}$ without direct link using OPA for different relay SI levels and target P_{out} values.

Table 6.2 Optimal transmit power values for source and relay nodes over asymmetric $\kappa-\mu/\eta-\mu$ fading model for $\mu_{S,R} = \mu_{R,D} = 2, \kappa_{S,R} = 2\text{dB}, \eta_{\text{R,D}} = 1$ with relay SI level of 5dB for different values of P_{out} for FDR system at $R = 2\text{bps/Hz}$.

	$P_{\text{out}} = 10^{-3}$		$P_{\text{out}} = 10^{-2}$	
$d_{S,D}$(m)	P_S(W)	P_R(W)	P_S(W)	P_R(W)
100	0.0049	0.0038	0.0028	0.0018
200	0.0788	0.0409	0.0263	0.0147
300	0.4127	0.0578	0.134	0.054
360	0.852	0.124	0.2833	0.0693
400	-	-	0.4363	0.0983
465	-	-	0.8047	0.1685

10^{-2} and 10^{-3} at $R = 2\text{bps/Hz}$. Moreover, the relay is located in the middle and the transmit power of the system is optimally allocated to the source and relay nodes to minimize the average total energy consumption as shown in Table 6.2 for some indicative transmission distances. It is observed that distance thresholds separate the regions where HDR performs better, in terms of EE, than FDR system and vice-versa. For example, for the fixed OP of 10^{-2} the HDR scheme outperforms the FDR system only at average S−D distances below $220m$, $260m$ and $330m$ when the relay SI levels are -5dB, 0dB and 5dB, respectively. On the contrary, for average transmission distances greater than $220m$, $260m$ and $330m$, FDR becomes more energy efficient. Furthermore, for the given target OP of 10^{-2} the HDR scheme attains maximum transmission distance of $420m$ under the given maximum transmission power constraint, whereas the FDR scheme extends to substantially longer distances. In similar way, for the target OP of 10^{-3} the HDR scheme outperforms the FDR scheme at average transmission distances below $200m$, $210m$ and $300m$ for relay SI levels of -5dB, 0dB and 5dB, respectively. It also attains maximum transmission distance of $335m$, whereas the FDR scheme extends to some distance beyond this limit. The energy savings that can be defined as $1 - \bar{E}_T^{FD}/\bar{E}_T^{HD}$ for relay SI levels of 5dB, 0dB and -5dB at target P_{out} of 10^{-2} at the maximum transmission distance of the HDR, i.e., $d_{S,D} = 420\text{m}$ can be computed and are 14%, 46.4% and 58%, respectively, whereas for P_{out} of 10^{-3} and $d_{S,D} = 335\text{m}$ the corresponding figures are 9.4%, 42% and 52%, respectively.

In the same context, Fig. 6.12 shows the average total energy consumption per information bit versus transmission distance for HDR and FDR systems over asymmetric $\kappa-\mu$ and $\eta-\mu$ fading conditions with fading parameters of $\mu_{S,R} = \mu_{R,D} = 2, \eta_{R,D} = 1, \kappa_{S,R} = 4\text{dB}$, and relay SI level of 5dB. The target P_{out} is set at 10^{-2}

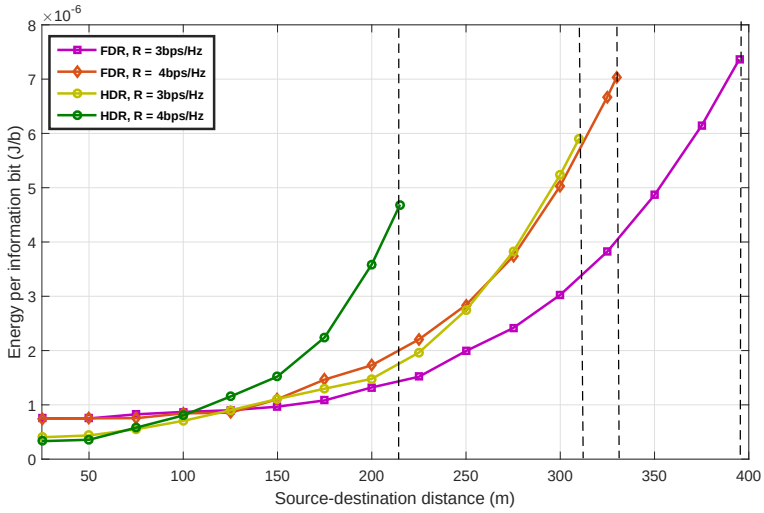

Figure 6.12 Energy consumption per information bit of FDR and HDR systems vs. source-destination distance over asymmetric $\kappa-\mu$ and $\eta-\mu$ fading channels for $\mu_{S,R} = \mu_{R,D} = 2, \kappa_{S,R} = 4\text{dB}, \eta_{R,D} = 1$ without direct link using OPA for relay SI level of 5dB at target P_{out} of 10^{-2} for different values of R.

for $R = 3$bps/Hz and $R = 4$bps/Hz, and the total transmit power is again optimally allocated to the source and relay nodes with the relay positioned in the middle of the network. It is observed that at relatively small transmission distances (e.g., $0 \leq d_{S,D} \leq 125$ m) and ($0 \leq d_{S,D} \leq 100$ m) for $R = 3$bps/Hz and $R = 4$bps/Hz, respectively, the HDR scheme outperforms the FDR scheme. However, as the transmission distances increase beyond the threshold points of 125m and 100m the corresponding overall benefits by the FDR scheme are significant despite the given considerable relay SI level. Indicatively, at transmission distance of 310m, which is the maximum distance that the HDR scheme can operate under the given system constraints at $R = 3$bps/Hz, the energy gain by the FDR system with the assumed relay SI level is 42%, whereas the energy gain by the FDR scheme at the distance limit of 215m for the HDR system at SE of 4bps/Hz is 58%. It is also shown in Table 6.3 that the values of the transmit powers allocated to the source and relay increases as the SE of the system increases.

Table 6.3 Optimal transmit power values for source and relay nodes over asymmetric $\kappa-\mu/\eta-\mu$ fading model for $\mu_{S,R} = \mu_{R,D} = 2, \kappa_{S,R} = 4\text{dB}, \eta_{\text{R,D}} = 1$ with different R for FDR system at $P_{\text{out}} = 10^{-2}$ and relay SI of 5dB.

	$R = 3$bps/Hz		$R = 4$bps/Hz	
$d_{S,D}$(m)	P_S(W)	P_R(W)	P_S(W)	P_R(W)
100	0.0030	0.0029	0.0065	0.0031
200	0.0681	0.0042	0.109	0.0661
300	0.2514	0.0712	0.5474	0.1452
330	0.479	0.097	0.8098	0.1902
395	0.773	0.1875	-	-

6.6 Summary

In this chapter, we analyzed the outage performance, OPA and energy optimization of the regenerative FD and HD relay systems over asymmetric generalized small-scale fading channels. It was shown that the performance of the FDR system is affected by the fading parameters of S→R, R→D links, the direct interference and relay SI levels. Compared to the HDR mode, which serves as a baseline, results showed that at relatively high target SE the FDR mode can provide better outage performance than the HDR system even under some considerable relay SI levels. Besides, OPA that minimizes the overall OP of the FDR system was formulated. Based on this, results revealed that significant outage performance enhancement is achieved by the OPA strategy over the traditional EPA scheme under the presence of relay SI levels. In addition, we proposed energy optimization scheme under certain target OP, and maximum transmit power constraint that incorporates both transmit energy as well as the energy consumed by the transceiver circuits for FDR and HDR systems. The corresponding results indicated that depending on the end-to-end SE and target OP, the HDR can be more energy-efficient than FDR but only for rather short transmission distances and up to a certain threshold value. On the other hand, beyond this value the FDR system is more energy-efficient than the HDR system for some moderate relay SI levels as the transmission distance increases. In general, the results and formulations in this chapter can be used to analyze the performance and average total energy consumption of FDR and HDR modes over the realistic small-scale asymmetric fading conditions.

Chapter 7

Conclusions

In this final chapter, we summarize the contributions of the work presented in this dissertation and suggest some direction for future work in the areas of cooperative communications.

7.1 Conclusion

In this thesis, we investigated the error-rate analysis and energy optimization of regenerative cooperative networks over multipath fading in the presence of spatial correlation effects, and the end-to-end performance and power allocation of regenerative multi-relay networks over non-homogeneous scattering environment, which is the case in realistic wireless communication scenarios. Furthermore, we evaluated the behavior and performance for OPA and energy optimization analysis of DF based FDR system under given system constraints over asymmetric generalized fading conditions. There are various contributions in the studied areas which are discussed in detail in Chapter 4 to 6 and are shortly summarized below.

The EE analysis of cooperative networks under the effects of spatial correlation between the direct and relayed paths and the conventional DT mode in Chapter 4 contributes to the analysis, design and deployment of low-cost and energy-efficient cooperation communication systems in the future, especially towards the green communications era where optimizing the energy consumption is considered critical. Analytic expressions are first derived for the end-to-end average SER of $M-$QAM and $M-$PSK modulations over Nakagami$-m$ fading channels using MRC at the destination. The derived expressions are subsequently employed in quantifying the total energy consumption of the system as well as in formulating OPA schemes for minimizing the energy consumption under given QoS requirements. To draw useful insights, a relatively harsh PL model that accounts for realistic D2D communications is also used. The corresponding analysis on the EE show that depending on the severity of

fading, spatial correlation between source-destination and relay-destination as well as the location of the relay node, it is verified that the DT can be more energy-efficient than CT only for rather short transmission distances and only up to a certain threshold value. Beyond this limit, the system benefits substantially from the CT with minimum total energy consumption where the CG increases proportionally to the transmission distance. The EE and power allocation conducted in this study can act as a bench mark for multi-relay cooperative network systems. Furthermore, the considered single relay system can be particularly useful in low-energy applications, including mobile-to-mobile communications.

The end-to-end performance and power allocation strategies for multi-relay regenerative cooperative networks over the realistic generalized $\eta - \mu$ fading channels is investigated in Chapter 5. In practical scenarios, the considered model represents better the small-scale variations of the fading signal in NLOS communication conditions in non-homogeneous scattering environment. Novel analytic expressions are derived first for the end-to-end average SER for $M-$QAM and $M-$PSK modulation schemes. The offered results are represented in exact analytic expressions involving Lauricella function and are readily evaluated with the aid of the proposed computational algorithm. Furthermore, to acquire useful insights simple expressions are derived for the corresponding SERs at asymptotically high SNRs. Based on these results, power allocation schemes are formulated for given overall transmit power constraints. The study indicated that the proposed power allocation scheme provides substantial performance gain over the conventional EPA, particularly, when the source-relay and relay-destination are highly unbalanced. It was also shown that the OPA is independent on the scattered-wave power ratio parameter from source-to-destination, while it depends on the number of multipath clusters as well as on the nature of modulation schemes. The theoretical results from the performance and power allocation analysis in this study can serve as guidelines and benchmark in the future practical cooperative network designs.

Finally, in Chapter 6 we extend our investigations to the scenario of information transmission using FDR systems. Unlike the previous works that considered the scenario of information transmission over symmetric fading conditions, here we considered the scenario of signal transmission over asymmetric generalized fading conditions. Particularly, it is considered that the source-relay link is subject to the small-scale LOS model of $\kappa - \mu$, whereas the relay-destination link is subject to the $\eta - \mu$ fading model. Analytic expressions are first derived for the overall OP of the FDR system under the effect of relay SI levels. Based on this, the performance, OPA and energy optimization under certain QoS requirement and total transmit power con-

straints are conducted. It is shown that the outage performance of the FDR system is highly dependent on the fading parameters and performs better than the reference HDR scheme for high SE regime even under relatively strong relay SI levels. It is also shown that the OPA provides substantial performance gains over the traditional EPA scheme, particularly when the relay SI level is strong. Furthermore, it is shown that for moderate values of the relay SI levels the FDR scheme performs better than the HDR system in terms of EE for relatively larger transmission distances.

7.2 Future Work

There is a variety of fruitful areas for future research on cooperative communications. We mentioned some issues in the previous chapters and in the following, we highlight some directions that can be included in the future work.

- Error-rate and EE optimization of the regenerative relay system was analyzed assuming spatial correlation effects between the direct and relayed paths with no interference effects. Since most wireless communication systems are not noise-limited, but interference limited future work should look into incorporating spatial correlation and interference effects. Furthermore, from performance and EE point of view, the study will be more comprehensive when the correlation effects between the source-relay and source-destination, and the effects between the source-relay and relay-destination are incorporated.

- It will be also more interesting to optimize the total energy consumption of the dual-hop regenerative system under the joint constraints of overall transmit power, constellation size and bandwidth for a given QoS requirement with both spatial correlation and interference effects.

- The performance and power allocation of the regenerative multi-relay cooperative communication system over the generalized fading model was based on one-way cooperation strategy. The use of the two-way cooperation scheme over generalized fading channels is an interesting area, e.g., [64, 65] for performance enhancement.

- Centralized, but dynamic resource management that allocates the physical resource dynamically can be one potential research area when a relay node fails to decode and the corresponding physical resource is left unused.

- In Chapter 6, we studied the performance, power allocation and energy optimization of the FDR system with SI levels over the generalized fading con-

ditions. For further improving the quality of the FD transceivers, especially over the asymmetric fading scenarios, additional interference cancellation techniques [47, 60, 211, 232] could be implemented for better feasibility and EE of the FDR system at high SI levels.

- Furthermore, hybrid full-duplex/half-duplex relaying [218] over the asymmetric generalized fading models with energy optimization and OPA could be another future research direction.The motivation for this mode stems from the fundamental trade-off determining the SE: The HDR avoids the SI at the cost of reducing the symbol rate by half while the FDR mode achieves the full symbol rate but suffers from residual interference even after cancellation. The opportunistic mode selection can balance these trade-offs to achieve better performance over the asymmetric generalized fading scenarios.

Finally, the thesis contributes in various different emerging areas of radio communications discipline, which enables better understanding and handling of cooperative communications. These contributions are expected to provide useful tools and guidelines for the design and implementation of size, price and resource-efficient cooperative networks in the coming green communication era.

Appendix A

Proof of Lemma 1

The $\mathcal{J}(a,b,m)$ integral can be re-written as,

$$\mathcal{J}(a,b,m) = \int \frac{\sin^{4m}(\theta)}{(\sin^4(\theta) + a\sin^2(\theta) + b)^m} \mathrm{d}\theta. \tag{A.1}$$

By setting $u = \cos^2(\theta)$ it follows that,

$$\mathcal{J}(a,b,m) = -\frac{1}{2}\int \frac{(1-u)^{2m}}{\sqrt{u}\sqrt{1-u}\,[(1-u)^2 + a(1-u) + b]^m} \mathrm{d}u. \tag{A.2}$$

With the aid of the binomial theorem in [86, eq. (1.111)], it follows that,

$$\mathcal{J}(a,b,m) = -\sum_{l=0}^{2m-\frac{1}{2}} \binom{2m-\frac{1}{2}}{l} \frac{(-1)^l}{2} \int \frac{u^{l-\frac{1}{2}}}{[1-u(a+2)+u^2+a+b]^m} \mathrm{d}u. \tag{A.3}$$

The above integral can be expressed in terms of the Appell function of the first kind yielding,

$$\begin{aligned}
&\mathcal{J}(a,b,m) \\
&= -\sum_{l=0}^{2m-\frac{1}{2}} \binom{2m-\frac{1}{2}}{l} \frac{(-1)^l u^{l+\frac{1}{2}}\, F_1\left(l+\tfrac{1}{2}; m, m; l+\tfrac{3}{2}; \tfrac{2u}{2+a-\sqrt{a^2-4b}}, \tfrac{2u}{2+a+\sqrt{a^2-4b}}\right)}{(1+2l)(a+b+(u-1)^2-au)^m} \\
&\times \left(1 - \frac{2u}{2+a-\sqrt{a^2-4b}}\right)^m \left(1 - \frac{2u}{2+a-\sqrt{a^2-4b}}\right)^m
\end{aligned} \tag{A.4}$$

which upon performing the necessary counter-substitution and algebraic manipulations yields (4.20).

Appendix B

Proof of Lemma 2

The $\mathcal{K}(a,b,m,n)$ integral can be alternatively re-written as,

$$\mathcal{K}(a,b,m,n) = \int \frac{\sin^{2m+2n}(\theta)}{(\sin^2(\theta)+a)^m\,(\sin^2(\theta)+b)^n}\mathrm{d}\theta \tag{B.1}$$

which by setting $u = \cos^2(\theta)$ can be expressed as,

$$\mathcal{K}(a,b,m,n) = \int \frac{(1-u)^{m+n-\frac{1}{2}}}{2(1-u+a)^m(1-u+b)^n\sqrt{u}}\mathrm{d}u. \tag{B.2}$$

By applying the binomial theorem in [86, eq. (1. 111)], it immediately follows that,

$$\mathcal{K}(a,b,m,n) = \sum_{l=0}^{m+n-\frac{1}{2}} \binom{m+n-\frac{1}{2}}{l} \frac{(-1)^l}{2} \int \frac{u^{l-\frac{1}{2}}}{(1-u+a)^m(1-u+b)^n}\mathrm{d}u. \tag{B.3}$$

The above integral can be expressed in closed-form in terms of the Appell function of the first kind. As a result, by making the necessary counter-substitution and performing some long but basic algebraic manipulations, equation (4.21) is deduced.

Appendix C

Proof of Lemma 3

By setting $u = \sin^2(\theta)$, it follows that,

$$\int \sin^{2m}(\theta)\mathrm{d}\theta = \int \frac{u^{m-\frac{1}{2}}}{2\sqrt{1-u}}\mathrm{d}u. \tag{C.1}$$

The above integral can be expressed in closed-form in terms of the hypergeometric function, namely,

$$\int \frac{u^{m-\frac{1}{2}}}{2\sqrt{1-u}}\mathrm{d}u = -\sqrt{1-u}\,{}_2F_1\left(\frac{1}{2}, \frac{1}{2}-m; \frac{3}{2}; 1-u\right). \tag{C.2}$$

Therefore, by performing the counter-substitution, equation (4.30) is straightforwardly deduced.

Appendix D

Proof of Convexity of the Optimization Problem

Below we prove the existence of optimal powers, which are subsequently employed in minimizing the overall energy consumption in the considered cooperative communication system. Based on (4.72), the average total power consumption can be re-written as follows:

$$\overline{P}_T^C = (C_1 + (1+\omega)P_S) + (C_2 + (1+\omega)P_R)\left(1 - P_{\mathrm{SER_{S,R}}}\right) \tag{D.1}$$

where

$$C_1 = P_{CT_x} + 2P_{CR_x} \tag{D.2}$$

and

$$C_2 = P_{CT_x} + P_{CR_x} \tag{D.3}$$

The symbol-error-rate $P_{\mathrm{SER_{S,R}}}$ can be expressed in closed-form with the aid of Theorem 1. This expression is a function of $1 + P_S\ \Omega_{S,R}\, g_{\mathrm{QAM}}/P_{L_{S,R}} N_0\, m_{S,R}$; therefore, for proving the existence of the optimum values, it is sufficient to show that

$$\frac{\partial^2 \overline{P}_T^C}{\partial^2 P_R^2} \geq 0 \tag{D.4}$$

and

$$\frac{\partial^2 \overline{P}_T^C}{\partial^2 P_S^2} \geq\ 0 \tag{D.5}$$

To this end, it is straightforward to show that $\partial^2 \overline{P}_T^C / \partial^2 P_R^2 = 0$. Likewise, based on the optimal condition in (4.96) and taking the second-order partial derivative w.r.t the variables P_S and P_R, one obtains

$$\frac{\partial^2 \overline{P}_T^C}{\partial^2 P_S^2} \geq \frac{\partial^2 \overline{P}_T^C}{\partial^2 P_S P_R} \tag{D.6}$$

where

$$\frac{\partial^2 \overline{P}_T^C}{\partial P_S P_R} = \frac{(1+\omega) m_{S,R} \Omega_{S,R} g_{\text{QAM}}}{(1+a_1) N_0 P_{L_{S,R}}} K_5 \tag{D.7}$$

and

$$K_5 = \frac{4C}{\pi} \mathcal{I}\left(\frac{P_S \Omega_{S,R}\, g_{\text{QAM}}}{N_0 P_{L_{S,R}}\, m_{S,R}}, m_{S,R}; 0, \frac{\pi}{2}\right) - \frac{4C^2}{\pi} \mathcal{I}\left(\frac{P_S \Omega_{S,R}\, g_{\text{QAM}}}{N_0\, P_{L_{S,R}} m_{S,R}}, m_{S,R}; 0, \frac{\pi}{4}\right) \tag{D.8}$$

where it is recalled that $C = 1 - 1/\sqrt{M}$ for the case of $M-$QAM whereas K_5 denotes the SER representation with values in the range $0 \leq P_{\text{SER}} \leq 1$ and with all other constants being positive. Based on this, the second-order partial derivatives w.r.t P_S and P_R are always greater than or equal to zero, which satisfies (D.5). Given the general second order conditions in [183], it immediately follows that (D.1) is convex w.r.t to P_S and P_R and possesses a unique minimum value.

Appendix E

A MATLAB Algorithm for Computing the Generalized Lauricella Function

The Generalized Lauricella function is defined by the following non-infinite single integral,

$$F_D^{(n)}(\mathrm{a}; b_1, \cdots, b_n; c; x_1, \cdots, x_n) \triangleq \frac{\Gamma(c)}{\Gamma(\mathrm{a})\Gamma(c-\mathrm{a})} \int_0^1 t^{\mathrm{a}-1} \frac{(1-t)^{c-\mathrm{a}-1}}{(1-x_1 t)^{b_1} \cdots (1-x_n t)^{b_n}} \mathrm{d}t \tag{E.1}$$

The numerical evaluation of the above representation was also discussed in [206, Appendix E] and can be straightforwardly evaluated with the aid of the following proposed MATLAB algorithm:

```
Function FD = Lauricella(a, b1, ... , bn, c, x1, ... , xn);
f = gamma(c)./(gamma(a).*gamma(c - a));
Q = @(t)  f.*t.^(a - 1).*(1 - t).^(c - a - 1).*...
(1 - x1.*t).^(-b1) ... (1 - xn.*t).^(-bn);
FD = quad(Q,0,1)
```

Appendix F

Proof of Convexity of the Optimization Problem for SER

We provide the proof for the convexity of the SER expression by using (5.58). For mathematical tractability, we consider the proof for three relay-nodes. Based on this, the proof for larger number of nodes scenario follows immediately. To this end, the asymptotic SER can be expressed as follows:

$$\begin{aligned} P_{\text{SER}} \approx & \frac{K_1}{a_0^{2(\mu_{S,D}+\mu_{S,R_1}+\mu_{S,R_2}+\mu_{S,R_3})}} + \frac{K_2}{a_0^{2(\mu_{S,D}+\mu_{S,R_1}+\mu_{S,R_2})} a_{R_3}^{2\mu_{R_3,D}}} \\ & + \frac{K_3}{a_0^{2(\mu_{S,D}+\mu_{S,R_1}+\mu_{S,R_3})} a_{R_2}^{2\mu_{R_2,D}}} + \frac{K_4}{a_0^{2(\mu_{S,D}+\mu_{S,R_1})} a_{R_2}^{2\mu_{R_2,D}} a_{R_3}^{2\mu_{R_3,D}}} \\ & + \frac{K_5}{a_0^{2(\mu_{S,D}+\mu_{S,R_2}+\mu_{S,R_3})} a_{R_1}^{2\mu_{R_1,D}}} + \frac{K_6}{a_0^{2(\mu_{S,D}+\mu_{S,R_2})} a_{R_1}^{2\mu_{R_1,D}} a_{R_3}^{2\mu_{R_3,D}}} \\ & + \frac{K_7}{a_0^{2(\mu_{S,D}+\mu_{S,R_3})} a_{R_1}^{2\mu_{R_1,D}} a_{R_2}^{2\mu_{R_2,D}}} + \frac{K_8}{a_0^{2\mu_{S,D}} a_{R_1}^{2\mu_{R_1,D}} a_{R_2}^{2\mu_{R_2,D}} a_{R_3}^{2\mu_{R_3,D}}} \end{aligned} \quad \text{(F.1)}$$

where $K_1, \cdots, K_8$ are related to the channel parameters. Let $f_1(a_0, \cdots, a_{R_3}), \cdots, f_8(a_0, \cdots, a_{R_3})$ be functions which represent each term of P_{SER}. For example, we assign

$$f_1(a_0) = \frac{K_1}{a_0^{2(\mu_{S,D}+\mu_{S,R_1}+\mu_{S,R_2}+\mu_{S,R_3})}},\ f_2(a_0, a_{R_3}) = \frac{K_2}{a_0^{2(\mu_{S,D}+\mu_{S,R_1}+\mu_{S,R_2})} a_{R_3}^{2\mu_{R_3,D}}}, \cdots \quad \text{(F.2)}$$

The second order derivative of $f_1(a_0)$ w.r.t a_0 is given by

$$\frac{\partial^2 f_1(a_0)}{\partial^2 a_0} = \frac{4K_1(\mu_{S,D}+\mu_{S,R_1}+\mu_{S,R_2}+\mu_{S,R_3})(\mu_{S,D}+\mu_{S,R_1}+\mu_{S,R_2}+\mu_{S,R_3}+\frac{1}{2})}{a_0^{2(\mu_{S,D}+\mu_{S,R_1}+\mu_{S,R_2}+\mu_{S,R_3}+1)}}. \tag{F.3}$$

The Hessian matrix of $f_2(a_0, a_{R_3})$, $\bigtriangledown^2 f_2(a_0, a_{R_3})$, can be determined as follows:

$$H(a_0, a_{R_3}) = \begin{bmatrix} \frac{4K_2(\mu_{S,D}+\mu_{S,R_1}+\mu_{S,R_2})(\mu_{S,D}+\mu_{S,R_1}+\mu_{S,R_2}+\frac{1}{2})}{a_0^{2(\mu_{S,D}+\mu_{S,R_1}+\mu_{S,R_2}+1)} a_{R_3}^{2\mu_{R_3,D}}} & \frac{4K_2\mu_{R_3,D}(\mu_{S,D}+\mu_{S,R_1}+\mu_{S,R_2})}{a_0^{2(\mu_{S,D}+\mu_{S,R_1}+\mu_{S,R_2}+\frac{1}{2})} a_{R_3}^{2\mu_{R_3,D}+1}} \\ \frac{4K_2\mu_{R_3,D}(\mu_{S,D}+\mu_{S,R_1}+\mu_{S,R_2})}{a_0^{2(\mu_{S,D}+\mu_{S,R_1}+\mu_{S,R_2}+\frac{1}{2})} a_{R_3}^{2\mu_{R_3,D}+1}} & \frac{4K_2\mu_{R_3,D}(\mu_{R_3,D}+\frac{1}{2})}{a_0^{2(\mu_{S,D}+\mu_{S,R_1}+\mu_{S,R_2})} a_{R_3}^{2(\mu_{R_3,D}+1)}} \end{bmatrix}. \tag{F.4}$$

The principal minors of the matrix $H(a_0, a_{R_3})$, $H_{11}(a_0, a_{R_3}) \geq 0$, $H_{22}(a_0, a_{R_3}) \geq 0$ and $H_{11}H_{22} \geq H_{12}H_{21}$. To this effect, the symmetric Hessian matrix $H(a_0, a_{R_3})$ is positive semi-definite (PSD). Since $\frac{\partial^2 f_1(a_0)}{\partial^2 a_0} \geq 0$ and then $H(a_0, a_{R_3})$ is PSD, i.e., $\bigtriangledown^2 f_2(a_0, a_{R_3}) \succeq 0$, by the second order test in [183] both $f_1(a_0)$ and $f_2(a_0, a_{R_3})$ functions are convex. Following the same methodology, it is shown that the functions $f_3, \cdots, f_8$ are also convex. Hence, by the sum rule of convexity [183, Section (3.2.1)] it follows that the total function P_{SER} is convex w.r.t a_0, a_{R_1}, a_{R_2} and a_{R_3}.

Appendix G

Proof of Theorem 5

Proof. By substituting the PDF and CDF of the $\eta-\mu$ distribution in (3.36) and in (6.10) into (6.8), respectively, one obtains $F_Z(z)$ as

$$
\begin{aligned}
F_Z(z) = \int_0^\infty \Bigg\{ & \sum_{l=0}^{\mu_{R,D}-1} \frac{h_{R,D}^{\mu_{R,D}}\Gamma(\mu_{R,D}+l)(-1)^l(h_{R,D}-H_{R,D})^{l-\mu_{R,D}}}{l!2^{\mu_{R,D}+l}\Gamma(\mu_{R,D})H_{R,D}^{\mu_{R,D}+l}} \\
& + \frac{h_{R,D}^{\mu_{R,D}}\Gamma(\mu_{R,D}+l)(-1)^{\mu_{R,D}}(h_{R,D}+H_{R,D})^{l-\mu_{R,D}}}{l!2^{\mu_{R,D}+l}\Gamma(\mu_{R,D})H_{R,D}^{\mu_{R,D}+l}} \\
& - \sum_{l=0}^{\mu_{R,D}-1}\sum_{i=0}^{\mu_{R,D}-l-1} \frac{(-1)^l h_{R,D}^{\mu_{R,D}}\Gamma(\mu_{R,D}+l)\mu_{R,D}^i(h_{R,D}-H_{R,D})^{l+i-\mu_{R,D}}(z(x+1))^i}{l!i!2^{\mu_{R,D}+l-i}\overline{\gamma}_{R,D}^i\Gamma(\mu_{R,D})H_{R,D}^{\mu_{R,D}+l}\exp\left(D_1 z(x+1)\right)} \\
& - \sum_{l=0}^{\mu_{R,D}-1}\sum_{i=0}^{\mu_{R,D}-l-1} \frac{(-1)^{\mu_{R,D}} h_{R,D}^{\mu_{R,D}}\Gamma(\mu_{R,D}+l)\mu_{R,D}^i(h_{R,D}+H_{R,D})^{l+i-\mu_{R,D}}(z(x+1))^i}{l!i!2^{\mu_{R,D}+l-i}\overline{\gamma}_{R,D}^i\Gamma(\mu_{R,D})H_{R,D}^{\mu_{R,D}+l}\exp\left(D_2 z(x+1)\right)} \Bigg\} \\
& \times \frac{2\sqrt{\pi}\,\mu_{S,D}^{\mu_{S,D}+\frac{1}{2}}\,h_{S,D}^{\mu_{S,D}}\,x^{\mu_{S,D}-\frac{1}{2}}}{\Gamma(\mu_{S,D})H_{S,D}^{\mu_{S,D}-\frac{1}{2}}\,\overline{\gamma}_{S,D}^{\mu_{S,D}+\frac{1}{2}}}\exp\left(-\frac{2\mu_{S,D}xh_{S,D}}{\overline{\gamma}_{S,D}}\right) I_{\mu_{S,D}-\frac{1}{2}}\left(\frac{2\mu_{S,D}H_{S,D}x}{\overline{\gamma}_{S,D}}\right)\mathrm{d}x.
\end{aligned}
\tag{G.1}
$$

Notably, with the aid of [86, Eq. (8.406.3)] and [86, Eq. (6.621.1)] the above expression can be expressed in closed-form . Therefore, by performing the necessary variable transformation and carrying out long but basic algebraic manipulations, the CDF of Γ_D can be expressed as in (6.13), which completes the proof. □

Appendix H

Proof of Theorem 6

Proof. By substituting the CDF of the $\eta-\mu$ distribution in (6.10) and the PDF of the $\kappa-\mu$ distribution in (3.33) into (6.8), the CDF of Γ_D, $F_Z(z)$ can be expressed as

$$\begin{aligned}
F_Z(z) = \int_0^\infty \Bigg(& \sum_{l=0}^{\mu_{R,D}-1} \frac{\Gamma(\mu_{R,D}+l) h_{R,D}^{\mu_{R,D}} (-1)^l (h_{R,D}-H_{R,D})^{l-\mu_{R,D}}}{l! 2^{\mu_{R,D}+l} \Gamma(\mu_{R,D}) H_{R,D}^{\mu_{R,D}+l}} \\
& + \frac{\Gamma(\mu_{R,D}+l) h_{R,D}^{\mu_{R,D}} (-1)^{\mu_{R,D}} (h_{R,D}+H_{R,D})^{l-\mu_{R,D}}}{l! 2^{\mu_{R,D}+l} \Gamma(\mu_{R,D}) H_{R,D}^{\mu_{R,D}+l}} \\
& - \sum_{l=0}^{\mu_{R,D}-1} \sum_{i=0}^{\mu_{R,D}-l-1} \frac{h_{R,D}^{\mu_{R,D}} \Gamma(\mu_{R,D}+l) \mu_{R,D}^i (z(x+1))^i}{l! i! 2^{\mu_{R,D}+l-i} \overline{\gamma}_{R,D}^i \Gamma(\mu_{R,D}) H_{R,D}^{\mu_{R,D}+l}} \\
& \times \left\{ \frac{(-1)^l (h_{R,D}-H_{R,D})^{l+i-\mu_{R,D}}}{\exp\left(D_1 z(x+1)\right)} + \frac{(-1)^{\mu_{R,D}} (h_{R,D}+H_{R,D})^{l+i-\mu_{R,D}}}{\exp\left(D_2 z(x+1)\right)} \right\} \Bigg) \\
& \times \frac{\mu_{S,D}(1+\kappa_{S,D})^{\frac{\mu_{S,D}+1}{2}} x^{\frac{(\mu_{S,D}-1)}{2}} I_{\mu_{S,D}-1}\left(2\mu_{S,D}\sqrt{\frac{\kappa_{S,D}(\kappa_{S,D}+1)x}{\overline{\gamma}_{S,D}}}\right)}{\kappa_{S,D}^{\frac{\mu_{S,D}-1}{2}} \overline{\gamma}_{S,D}^{\frac{\mu_{S,D}+1}{2}} \exp\left(\mu_{S,D}\kappa_{S,D} + \frac{\mu_{S,D}(\kappa_{S,D}+1)x}{\overline{\gamma}_{S,D}}\right)} \mathrm{d}x
\end{aligned} \tag{H.1}$$

By also applying [86, eq. (1.111)] and after long but basic algebraic manipulations, equation (H.1) can be expressed as

$$\begin{aligned}
F_Z(z) = & \sum_{l=0}^{\mu_{R,D}-1} \frac{E_3\left((-1)^l (h_{R,D}-H_{R,D})^{l-\mu_{R,D}} + (-1)^{\mu_{R,D}} (h_{R,D}+H_{R,D})^{l-\mu_{R,D}}\right)}{\left(\Gamma(\mu_{R,D}+l)\right)^{-1} l!\, 2^{\mu_{R,D}+l} H_{R,D}^{\mu_{R,D}+l}} \\
& \times \int_0^\infty I_{\mu_{S,D}-1}\left(2\mu_{S,D}\sqrt{\frac{\kappa_{S,D}(\kappa_{S,D}+1)x}{\overline{\gamma}_{S,D}}}\right) x^{\frac{\mu_{S,D}-1}{2}} \exp\left(-\frac{\mu_{S,D}(1+\kappa_{S,D})x}{\overline{\gamma}_{S,D}}\right) \mathrm{d}x \\
& - \sum_{l=0}^{\mu_{R,D}-1} \sum_{i=0}^{\mu_{R,D}-l-1} \sum_{j=0}^{i} \binom{i}{j} \frac{E_3 (-1)^l z^i \Gamma(\mu_{\mu_{R,D}}+l) \mu_{R,D}^i (h_{R,D}-H_{R,D})^{l+i-\mu_{R,D}}}{l! i! 2^{\mu_{R,D}+l-i} \overline{\gamma}_{R,D}^i H_{R,D}^{\mu_{R,D}+l} \exp\left(\frac{2(h_{R,D}-H_{R,D})z\mu_{R,D}}{\overline{\gamma}_{R,D}}\right)}
\end{aligned}$$

$$\times \int_0^{\infty} \frac{x^{\frac{\mu_{S,D}-1}{2}+j} I_{\mu_{S,D}-1}\left(2\mu_{S,D}\sqrt{\frac{\kappa_{S,D}(\kappa_{S,D}+1)x}{\overline{\gamma}_{S,D}}}\right)}{\exp\left(x\left(\frac{\mu_{S,D}(1+\kappa_{S,D})}{\overline{\gamma}_{S,D}}+\frac{2(h_{R,D}-H_{R,D})z\mu_{R,D}}{\overline{\gamma}_{R,D}}\right)\right)}\mathrm{d}x$$

$$- \sum_{l=0}^{\mu_{R,D}-1}\sum_{i=0}^{\mu_{R,D}-l-1}\sum_{j=0}^{i}\binom{i}{j}\frac{E_3(-1)^{\mu_{R,D}} z^i \Gamma(\mu_{\mu_{R,D}}+l)\mu_{R,D}^i (h_{R,D}+H_{R,D})^{l+i-\mu_{R,D}}}{l!i!2^{\mu_{R,D}+l-i}\,\overline{\gamma}_{R,D}^{\,i} H_{R,D}^{\mu_{R,D}+l}\exp\left(\frac{2(h_{R,D}+H_{R,D})z\mu_{R,D}}{\overline{\gamma}_{R,D}}\right)}$$

$$\times \int_0^{\infty} \frac{x^{\frac{\mu_{S,D}-1}{2}+j} I_{\mu_{S,D}-1}\left(2\mu_{S,D}\sqrt{\frac{\kappa_{S,D}(\kappa_{S,D}+1)x}{\overline{\gamma}_{S,D}}}\right)}{\exp\left(x\left(\frac{\mu_{S,D}(1+\kappa_{S,D})}{\overline{\gamma}_{S,D}}+\frac{2(h_{R,D}+H_{R,D})z\mu_{R,D}}{\overline{\gamma}_{R,D}}\right)\right)}\mathrm{d}x \tag{H.2}$$

where

$$E_3 = \frac{h_{R,D}^{\mu_{R,D}}\mu_{S,D}(1+\kappa_{S,D})^{\frac{\mu_{S,D}+1}{2}}}{\Gamma(\mu_{R,D})\kappa_{S,D}^{\frac{\mu_{S,D}-1}{2}}\exp(\kappa_{S,D}\mu_{S,D})\overline{\gamma}_{S,D}^{\frac{\mu_{S,D}+1}{2}}}. \tag{H.3}$$

Importantly, the involved integrals in (H.2) can be expressed in a closed form with the aid of [86, eq. (6.621.1)]. Therefore, by performing the necessary variable transformations and carrying out long but basic algebraic operations, the CDF of Γ_D can be expressed as (6.16), which completes the proof. □

Appendix I

Proof of Theorem 7

Proof. By properly substituting the CDF of the $\eta-\mu$ distribution in (6.10) and the PDF of the IG distribution in (3.38) into (6.8) and denoting $\gamma = x$, one obtains the CDF of the RV Z as

$$\begin{aligned}
F_Z(z) = & \sum_{l=0}^{\mu_{R,D}-1} \frac{h_{R,D}^{\mu_{R,D}}\left((-1)^l(h_{R,D}-H_{R,D})^{l-\mu_{R,D}}+(-1)^{\mu_{R,D}}(h_{R,D}+H_{R,D})^{l-\mu_{R,D}}\right)}{(\Gamma(\mu_{R,D}+l))^{-1}H_{R,D}^{\mu_{R,D}+l}\Gamma(\mu_{R,D})\,l!\,2^{\mu_{R,D}+l}} \\
& - \sum_{l=0}^{\mu_{R,D}-1}\sum_{i=0}^{\mu_{R,D}-l-1} \frac{\left((-1)^l(h_{R,D}-H_{R,D})^{l+i-\mu_{R,D}}h_{R,D}^{\mu_{R,D}}\Gamma(\mu_{R,D}+l)\mu_{R,D}^i\right)}{l!i!2^{\mu_{R,D}+l-i}\overline{\gamma}_{R,D}^i\Gamma(\mu_{R,D})H_{R,D}^{\mu_{R,D}+l}} \\
& \times \int_0^\infty \frac{(z(x+1))^i}{\exp\left(\frac{2(h_{R,D}-H_{R,D})\mu_{R,D}(z(x+1))}{\overline{\gamma}_{R,D}}\right)}\sqrt{\frac{\lambda_{S,D}}{2\pi x^3}}\exp\left(-\frac{\lambda_{S,D}(x-\overline{\gamma}_{S,D})^2}{2x\overline{\gamma}_{S,D}^2}\right)\mathrm{d}x \\
& - \sum_{l=0}^{\mu_{R,D}-1}\sum_{i=0}^{\mu_{R,D}-l-1} \frac{\left((-1)^{\mu_{R,D}}(h_{R,D}+H_{R,D})^{l+i-\mu_{R,D}}h_{R,D}^{\mu_{R,D}}\Gamma(\mu_{R,D}+l)\mu_{R,D}^i\right)}{l!i!2^{\mu_{R,D}+l-i}\overline{\gamma}_{R,D}^i\Gamma(\mu_{R,D})H_{R,D}^{\mu_{R,D}+l}} \\
& \times \int_0^\infty \frac{(z(x+1))^i}{\exp\left(\frac{2(h_{R,D}+H_{R,D})\mu_{R,D}(z(x+1))}{\overline{\gamma}_{R,D}}\right)}\sqrt{\frac{\lambda_{S,D}}{2\pi x^3}}\exp\left(-\frac{\lambda_{S,D}(x-\overline{\gamma}_{S,D})^2}{2x\overline{\gamma}_{S,D}^2}\right)\mathrm{d}x
\end{aligned} \tag{I.1}$$

The above expression can be equivalently re-written as follows:

$$\begin{aligned}
F_Z(z) = & \sum_{l=0}^{\mu_{R,D}-1} \frac{h_{R,D}^{\mu_{R,D}}\left((-1)^l(h_{R,D}-H_{R,D})^{l-\mu_{R,D}}+(-1)^{\mu_{R,D}}(h_{R,D}+H_{R,D})^{l-\mu_{R,D}}\right)}{(\Gamma(\mu_{R,D}+l))^{-1}H_{R,D}^{\mu_{R,D}+l}\Gamma(\mu_{R,D})\,l!\,2^{\mu_{R,D}+l}} \\
& - \sum_{l=0}^{\mu_{R,D}-1}\sum_{i=0}^{\mu_{R,D}-l-1} \frac{\left((-1)^l(h_{R,D}-H_{R,D})^{l+i-\mu_{R,D}}h_{R,D}^{\mu_{R,D}}\sqrt{\lambda_{S,D}}\Gamma(\mu_{R,D}+l)\mu_{R,D}^i\right)z^i}{l!i!2^{\mu_{R,D}+l-i}\sqrt{2\pi}\overline{\gamma}_{R,D}^i\Gamma(\mu_{R,D})H_{R,D}^{\mu_{R,D}+l}\exp\left(\frac{2(h_{R,D}-H_{R,D})\mu_{R,R}z}{\overline{\gamma}_{R,D}}\right)}
\end{aligned}$$

$$\times \exp\left(\frac{\lambda_{S,D}}{\overline{\gamma}_{S,D}}\right)\int_0^{\infty}\frac{(x+1)^i}{x\sqrt{x}\exp\left(\frac{2(h_{R,D}-H_{R,D})\mu_{R,D}zx}{\overline{\gamma}_{R,D}}\right)}\exp\left(-\frac{\lambda_{S,D}x}{2\overline{\gamma}_{S,D}^2}-\frac{\lambda_{S,D}}{2x}\right)\mathrm{d}x$$

$$-\sum_{l=0}^{\mu_{R,D}-1}\sum_{i=0}^{\mu_{R,D}-l-1}\frac{((-1)^{\mu_{R,D}}(h_{R,D}+H_{R,D})^{l+i-\mu_{R,D}}h_{R,D}^{\mu_{R,D}}\sqrt{\lambda_{S,D}}\Gamma(\mu_{R,D}+l)\mu_{R,D}^i)z^i}{l!i!2^{\mu_{R,D}+l-i}\sqrt{2\pi}\overline{\gamma}_{R,D}^i\Gamma(\mu_{R,D})H_{R,D}^{\mu_{R,D}+l}\exp\left(\frac{2(h_{R,D}+H_{R,D})\mu_{R,R}z}{\overline{\gamma}_{R,D}}\right)}$$

$$\times \exp\left(\frac{\lambda_{S,D}}{\overline{\gamma}_{S,D}}\right)\int_0^{\infty}\frac{(x+1)^i}{x\sqrt{x}\exp\left(\frac{2(h_{R,D}+H_{R,D})\mu_{R,D}zx}{\overline{\gamma}_{R,D}}\right)}\exp\left(-\frac{\lambda_{S,D}x}{2\overline{\gamma}_{S,D}^2}-\frac{\lambda_{S,D}}{2x}\right)\mathrm{d}x \tag{I.2}$$

By expanding the above power terms in terms of the binomial in [86, eq. (1. 111)] and with the aid of [86, eq. (3. 471.9)] after long but basic manipulations the closed-form expression in (6.18) is deduced, which completes the proof. □

Bibliography

[1] J. G. Proakis, *Digital Communications*. McGraw-Hill Inc., 4$^{\text{th}}$ edn., 2001.

[2] Y.-W. Hong, W.-J. Huang, and C.-C. Jay Kuo, *Cooperative Communication and Networking: Technologies and System Design*, New York: Springer, 2010.

[3] Y. Yang, H. Hu, J. Xu, and G. Mao, "Relay technologies for WiMax and LTE-advanced mobile systems," *IEEE Communications Magazine*, vol. 47, no. 10, pp. 100−105, Oct. 2009.

[4] "Further advancements for E-UTRA; Physical layer aspects," Sophia-Antipolis, France, 3GPP TR 36.814 V9.0.0, Release 9, Mar. 2010.

[5] A. Sendonaris, E. Erkip, and B. Aazhang, "User cooperation diversity — part I: System description," *IEEE Transactions on Communications*, vol. 51, no. 11, pp. 1927−1938, Nov. 2003.

[6] J. N. Laneman, D. N. C. Tse, and G. W. Wornell, "Cooperative diversity in wireless networks: Efficient protocols and outage behavior," *IEEE Transactions on Information Theory* , vol. 50, no. 12, pp. 3062−3082, Dec. 2004.

[7] T. Hunter and A. Nosratinia, "Diversity through coded cooperation," *IEEE Transactions on Wireless Communications*, vol.5, no. 2, pp. 283−289, Feb. 2006.

[8] Y.-Win Hong, W.-J. Huang, F.-H. Chiu, and C.-C. Jay Kuo, "Cooperative communications in resource-constrained wireless networks," *IEEE Signal Processing Magazine*, vol. 24. no. 3, pp. 47− 57, May 2007.

[9] A. Nosratinia, T. E. Hunter, and A. Hedayat, "Cooperative communication in wireless networks," *IEE Communications Magazine,* vol. 42, no. 10, pp. 74−80, 2004.

[10] Z. Liu, M. Uppal, V. Stankovic, and Z. Xiong, "Compress-forward coding with BPSK Modulation for the half-duplex Gaussian relay channel," in *Proc. IEEE International Symposium on Information Theory (ISIT)* , Jul. 2008, pp. 2395−2399.

[11] M. Uppal, Z. Liu, V. Stankovic, and Z. Xiong, "Compress-forward coding with BPSK Modulation for the half-duplex Gaussian relay channel," *IEEE Transactions on Signal Processing*, vol. 57, no. 11, pp. 4467 −4481, Nov. 2009.

[12] N.Zlatanov, R. Schober, and P. Popovski, "Buffer-aided relaying with adaptive link selection," *IEEE Journal on Selected Areas in Communications,* vol. 31, no. 8, 1530−1542 ,Aug. 2013.

[13] N. Zlatanov and R. Schober, "Buffer-aided half-duplex relaying can outperform ideal full-duplex relaying," *IEEE Communication Letters,* vol. 17, no. 3, 479−482, Mar. 2013.

[14] E. C. Van Der Meulen, "Three-terminal communication channels," *Advanced Applied Probability,* vol. 3, pp. 120−154, 1971.

[15] T. M. Cover and A. El Gamal, "Capacity theorems for the relay channel," *IEEE Transactions on Information Theory,* vol.5, no. 25, pp. 572–584, Sep. 1979.

[16] A. Sahebalam and G. A. Hodtani, "General and new inner bound for multiple-access relay channel and two certain capacity theorems," *IET Communications*, vol. 7, no. 13, pp. 1348−1359, Sep. 2013.

[17] D. Zahavi and R. Dabora, "Capacity theorems for the fading interference channel with a relay and feedback links," *IEEE Transactions on Information Theory,* vol. 58, no. 8, pp. 5185−5212, Aug. 2012.

[18] A.E. Gamal and S. Zahedi, "Capacity of a class of relay channels with orthogonal components," *IEEE Transactions on Information Theory* , vol. 51, no. 5, pp. 1815−1817, May 2005.

[19] A. Sendonaris, E. Erkip, and B. Aazhang, "User cooperation diversity-Part II: Implementation aspects and performance analysis," *IEEE Transactions on Communications*, vol. 51, no. 11, pp. 1939 −1948, Nov. 2003.

[20] Y.-W. Hong and A. Scaglione, "Energy-efficient broadcasting with cooperative transmissions in wireless sensor networks," *IEEE Transactions on Wireless Communications,* vol. 5, no. 10, 2844−2855, Oct. 2006.

[21] A. Scaglione and Y.-W. Hong, "Opportunistic large arrays: Cooperative transmission in wireless multihop ad hoc networks to reach far distances," *IEEE Transactions on Signal Processing*, vol. 51, no. 8, pp. 2082−2092, Aug. 2003.

[22] D. R. Brown, "Resource allocation for cooperative transmission in wireless networks with orthogonal users," in *Proc. 38th Asilomar conference on Signals, Systems and Computers*, Nov. 2004, vol. 2, pp.1473−1477.

[23] I. Maric and R. D. Yates, "Bandwidth and power allocation for cooperative strategies in Gaussian relay networks," *IEEE Transactions on Information Theory,* vo1. 56, no. 4, pp. 1880−1889, Apr. 2010.

[24] M. O. Hasna and M.-S. Alouini, "Optimal power allocation for relayed transmissions over Rayleigh-fading channels," *IEEE Transactions on Wireless Communications*, vol. 3, pp. 1999−2004, Nov. 2004.

[25] X. Deng and A. M. Haimovich, "Power allocation for cooperative relaying in wireless networks," *IEEE Communications Letter*, vol. 9, no. 11, pp. 994−996, Nov. 2005.

[26] J. Luo, R. S. Blum, L. J. Cimini, L. J. Greenstein, and A. M. Haimovich, "Decode-and-forward cooperative diversity with power allocation in wireless networks," *IEEE Transactions on Wireless Communications*, vol. 6, no. 3, pp. 793−799, Mar. 2007.

[27] M. Dohler, Y. Li, *Cooperative Communications: Hardware, Channel and PHy* John Wiley and Sons, 2010.

[28] J. N. Laneman and G. W. Wornell, "Energy-efficient antenna sharing and relaying for wireless networks," in *Proc. IEEE Wireless Communications and Networking Conference (WCNC),* Sep. 2000, pp. 7−12.

[29] M. Hasna and M. S. Alouini, "End-to-end performance of transmission systems with relays over Rayleigh-fading channels," *IEEE Transactions on Communications*, vol. 2, pp. 1126−1131, Nov. 2003.

[30] P. Anghel and M. Kaveh, "Exact symbol error probability of a cooperative network in a Rayleigh-fading environment," *IEEE Transactions on Communications*, vol. 3, pp. 1416−1421, Sep. 2004.

[31] W. Su, A. K. Sadek, and K. J. R. Liu, "Cooperative communication protocols in wireless networks: performance analysis and optimum power allocation," *Wireless Personal Communications*, vol. 44, pp. 181−217, Jan. 2008.

[32] M. K.Simon and M.-S. Alouini, "A unified approach to the performance analysis of digital communication over generalized fading channels ," in *Proc. of the IEEE*, Sep. 1998, vol. 86, no. 9, pp. 1860− 1877.

[33] J. Yang, P. Fan and Z. Ding, "Capacity of AF two-way relaying with multiuser scheduling in Nakagami−m fading communications," *IET Electronic Letter*, vol. 48, no. 22, pp. 1432−1434, Oct. 2012.

[34] V. Asghari, D. B. da Costa, and S. Aissa, "Performance analysis for multihop relaying channels with Nakagami−m fading: ergodic capacity upper-bounds and outage probability," *IEEE Transactions Communications,* vol. 60, no. 10, pp. 2761−2767, Oct. 2012.

[35] M. Elkashlan, P. L. Yeoh, N. Yang, T. Q. Duong, and C. Leung, "A comparison of two MIMO relaying protocols in Nakagami−m fading," *IEEE Transactions on Vehicular Technology,* vol. 61, no. 3, pp. 1416−1422, Mar. 2012.

[36] P. L. Yeoh, M. Elkashlan, Z. Chen, and I. B. Collings, "SER of multiple amplify-and-forward relays with selection diversity," *IEEE Transactions on Communications,* vol. 59, no. 8, pp. 2078−2083, Aug. 2011.

[37] M. M. Fareed and M. Uysal, "On relay selection for decode-and-forward relaying ,"*IEEE Transactions on Wireless Communications*, vol. 8, no. 7, pp. 3341−3346, Jul. 2009.

[38] W. Su, A. K. Sadek, and K. J. R. Liu, "SER performance analysis and optimum power allocation for decode-and-forward cooperation protocol in wireless networks," in *Proc. IEEE Wireless Communications and Networking Conference (WCNC)*, Mar. 2005, vol. 2, pp. 984−989.

[39] S. S. Ikki and M. H. Ahmed, "Performance analysis of cooperative diversity with incremental-best-relay technique over Rayleigh fading channels," *IEEE Transactions on Vehicular Technology,* vol. 59, no. 8, pp. 2152−2161, Aug. 2011.

[40] S.S. Ikki1 and M.H. Ahmed, "Performance analysis of incremental-relaying cooperative-diversity networks over Rayleigh fading channels," *IET Communications*, vol. 5, no. 3, pp. 337−349, 2011.

[41] M. Janani, A. Hedayat, T. E. Hunter, and A. Nosratinia, "Coded cooperation in wireless communications: Space-time transmission and iterative decoding," *IEEE Transactions on Signal Processing*, vol. 52, no. 2, pp.362−371, Feb. 2004.

[42] G. Kramer, M. Gastpar, and P. Gupta, "Cooperative strategies and capacity theorems for relay networks," *IEEE Transactions on Information Theory* , vol. 51, no. 9, pp. 3037−3063, Sep. 2005.

[43] V. Stankovic, A. Host-Madsen, and Z. Xiong, "Cooperative diversity for wireless ad-hoc networks: Capacity bounds and code designs," *IEEE Signal Processing Magazine*, vol. 22, pp. 37−49, Sep. 2006.

[44] A.Wyner and J. Ziv, "The rate-distortion function for source coding with side information at the decoder," *IEEE Transactions on Information Theory,* vol. 22, no. 1, pp. 1−10, Jan. 1976.

[45] M. Uppal, G. Yue, X. Wang, and Z. Xiong, "A rate less coded protocol for half-duplex wireless relay channels," *IEEE Transactions on Signal Processing,* vol. 59, no. 1, 209−222, Jan. 2011.

[46] R. Hu and J. Li, "Practical compress-forward in user cooperation: Wyner-Ziv cooperation," in *Proc. IEEE International Symposium on Information Theory (ISIT),* Jul. 2006, pp. 489−493.

[47] T. Riihonen, S. Werner, R. Wichman, and E. B. Zacarias, "On the feasibility of full-duplex relaying in the presence of loop interference," in *Proc. IEEE 10th Workshop on Signal Processing Advances in Wireless Communications (SPAWC),* June 2009, pp. 275−279.

[48] T. Riihonen, S. Werner, and R. Wichman, "Optimized gain control for single-frequency relaying with loop interference," *IEEE Transactions on Wireless Communications,* vol. 8, pp. 2801−2806, June 2009.

[49] T. Riihonen, "Recent advances in full-duplex relaying," *Finnish URSI convention on radio science and SMARAD seminar,* 2013, pp. 87−90.

[50] B. Rankov and A. Wittneben, "Spectral efficient protocols for half-duplex fading relay channels", *IEEE Journal on Selected Areas in Communication,* vol. 25, pp. 379−389, Feb. 2007.

[51] P. Liu and I.-M. Kim, "Performance analysis of bidirectional communication protocols based on decode-and-forward relaying", *IEEE Transactions on Communications*, vol. 58, no. 9, pp. 2683−2696, Sep. 2010.

[52] C.E. Shannon, "Two-way communication channels," in *Proc. 4th Berkeley Symposium on Mathematics, Statistics and Probability*, 1961, vol. 1, pp. 611−644.

[53] B. Rankov and A. Wittneben, "Achievable rate regions for the two-way relay channel," in *Proc. IEEE International Symposium on Information Theory (ISIT)*, Jul. 2006, pp. 1668−1672.

[54] S. J. Kim, P. Mitra, and V. Tarokh, "Performance bounds for bidirectional coded cooperation protocols," *IEEE Transactions on Information Theory*, vol. 54, no. 11, pp. 5235−5241, Nov. 2008.

[55] S.-Y. R. Li, R. W. Yeung, and N. Cai, "Linear network coding," *IEEE Transactions on Information Theory*, vol. 49, pp. 1204−1216, Feb. 2003.

[56] S. Zhang, S. Liew, and P. Lam, "Physical layer network coding," in *Proc. ACM MobiCom* Sep. 2006, pp. 358−365.

[57] Z. Yi, M. Ju, and I.-M. Kim, "Outage probability and optimum combining for time division broadcasting protocol", *IEEE Transaction Wireless Communications*, vol. 10, no. 5, pp. 1362−1367, May 2011.

[58] Z. Yi, M. Ju, and I.-M. Kim, "Outage probability and optimum power allocation for analog network coding", *IEEE Transactions on Wireless Communications,* vol. 10, no. 2, pp. 407−412, Feb. 2011.

[59] Z. Yi and I.-M. Kim, "An opportunistic-based protocol for bidirectional cooperative networks," *IEEE Transactions on Wireless Communications*, vol. 8, no. 9, pp. 4836−4847, Sep. 2009.

[60] Z. Zhang, X. Chai, K. Long, A. V. Vasilakos, and L. Hanzo, "Full duplex techniques for 5G networks: Self-interference cancellation, protocol design, and relay selection," *IEEE Communications Magazine*, vol. 53, no. 5, pp. 128−137, May 2015.

[61] D. Korpi, T. Riihonen, K. Haneda, K. Yamamoto, and M. Valkama, "Achievable transmission rates and self-interference channel estimation in hybrid full-duplex/half-duplex MIMO relaying," in *Proc. IEEE 82nd Vehicular Technology Conference (VTC) Fall*, Sep. 2015, pp. 1−5.

[62] T. Huusari, Y.-S. Choi, P. Liikkanen, D. Korpi, S. Talwar, and M. Valkama, "Wideband self-adaptive RF cancellation circuit for full-duplex radio: Operating principle and measurements," in *Proc. IEEE 81st Vehicular Technology Conference (VTC) Spring*, May 2015, pp. 1−7.

[63] M. Duarte, C. Dick, and A. Sabharwal, "Experiment-driven characterization of full-duplex wireless systems," *IEEE Transactions on Wireless Communications,* vol. 11, no. 12, pp. 4296−4307, Dec. 2012.

[64] X. Ji, B. Zheng, Y. Cai, and L. Zou, "On the study of half-duplex asymmetric Two-way relay transmission using an amplify-and-forward relay," *IEEE Transactions on Vehicular Technology*, vol. 61, no. 4, pp. 1649−1663, May 2012.

[65] M. Xia and S.Aissa, "Moments based framework for performance analysis of one-way/two-way CSI-assisted AF relaying," *IEEE Journal on Selected Areas in Communications*, vol. 30, no. 8, pp. 1464−1476, Sep. 2012.

[66] M. Ju and I.-M. Kim, "Relay selection with ANC and TDBC Protocols in bidirectional relay networks," *IEEE Transaction on Communications,* vol. 58, no. 12, pp. 3500−3511, Dec. 2010.

[67] J.D. Parsons, *The Mobile Radio Propagation Channel,* 2nd edn., Willey, 2002.

[68] A. Goldsmith, *Wireless Communications*, 1st ed. Cambridge University Press, 2005.

[69] S. Y. Seidel, T. S. Rappaport, S. Jain, M. L. Lord, and R. Singh, "Path loss, scattering, and multipath delay statistics in four European cities for digital cellular and microcellular radiotelephone," *IEEE Transactions on Vehicular Technology,* vol. 40, no. 4, pp. 721−730, Nov. 1991.

[70] A.F. de Toledo, A.M.D. Turkmani and J.D. Parsons, "Estimating coverage of radio transmission into and within buildings at 900, 1800, and 2300 MHz ," *IEEE Personal Communications Magazine*, vol. 5, no. 2, pp. 40−47, Apr. 1998.

[71] M. F. Iskander, and Z. Yun, "Propagation prediction models for wireless communication systems," *IEEE Transactions on Microwave Theory and Techniques,* vol. 50, no. 3, pp. 662−673, Mar. 2002.

[72] M. Chamchoy, W. Doungdeun, and S. Promwong, "Measurement and modeling of UWB path loss for single-band and multi-band propagation channel," in *Proc. IEEE International Symposium on Communications and Information Technology (ISCIT)*, Oct. 2005, vol. 2, pp. 991−995.

[73] V. Erceg, L. J. Greenstein, S. Y. Tjandra, S. R. Parkoff, A. Gupta, B. Kulic, A. A. Julius, and R. Bianchi, "An empirically based path loss model for wireless channels in suburban environments," *IEEE Journal on Selected Areas in Communications*, vo. 17, no. 7, pp. 1205−1211, Jul. 1999.

[74] P. S. Bithas, A.S. Lioumpas, and A. Alexiou, "Mitigating shadowing effects through cluster-head cooperation techniques," *IET Networks*, vol. 2, no. 2, pp. 71−80, 2013.

[75] G. L. Stuber, *Principles of Mobile Communication*, 3^{rd} edn., New York: Springer, 2012.

[76] M. K. Simon and M.-S. Alouni, *Digital Communication over Fading Channels*, 2^{nd}edn., New York: Wiley, 2005.

[77] W. Braun and U. Dersch, "A physical mobile radio channel model," *IEEE Transactions on Vehicular Technology*, vol. 40, no. 2, pp. 472−482, May 1991.

[78] M. D. Yacoub, "The $\kappa-\mu$ distribution and the $\eta-\mu$ distribution," *IEEE Antenna and Propagation Magazine*, vol. 49, no. 1, pp. 68−81, Feb. 2007.

[79] G. R. Sugar, "Some fading characteristics of regular VHF ionospheric propagation," in *Proc. IRE*, Oct. 1955, pp. 1432−1436.

[80] S. Basu, E. M. MacKenzie, S. Basu, E. Costa, P. F. Fougere, H. C. Carlson, and H. E. Whitney, "250 MHz/GHz scintillation parameters in the equatorial, polar, and aural environments," *IEE Journal on Selected Areas in Communications,* vol. 5, no. 2, pp. 102−115, Feb. 1987.

[81] H. B. James and P. I. Wells, "Some tropospheric scatter propagation measurements near the radio-horizon," in *Proc. IRE*, Oct. 1955, pp. 1336−1340.

[82] T. L. Staley, R. C. North, W. H. Ku, and J. R. Zeidler, "Performance of coherent $M-$PSK on frequency selective slowly fading channels," in *Proc. IEEE 46th Vehicular Technology Conference (VTC)*, Apr. 1996, vol. 2, pp. 784−788.

[83] K. A. Stewart, G. P. Labedz, and K. Sohrabi, "Wideband channel measurements at 900 MHz," in *Proc. IEEE 45th Vehicular Technology Conference (VTC)*, Jul. 1995, pp. 236−240.

[84] R. J. C. Bultitude, S. A. Mahmoud, and W. A. Sullivan, "A comparison of indoor radio propagation characteristics at 910 MHz and 1.75 GHz," *IEEE Journal on Selected Areas in Communications*, vol.7, no.1, pp. 20−30, Jan. 1989.

[85] T. S. Rappaport and C. D. McGillem, "UHF fading in factories," *IEEE Journal on Selected Areas in Communications*, vol. 7,no.1, pp. 40−48, Jan. 1989.

[86] I. S. Gradshteyn and I. M. Ryzhik, *Tables of Integrals, Series, and Products* -7$^{\text{th}}$ edn. Academic Press, 2007.

[87] B. Chytil, "The distribution of amplitude scintillation and the conversion of scintillation indices," *Journal on Atmospheric and Territorial Physics,* vol. 29, no. 9, PP. 1175−1177, Sep. 1967.

[88] K. Bischoff and B. Chytil, "A note on scintillation indices," *Planet. Space Sci.*, vol. 17, no.5, pp. 1059−1066, 1969.

[89] N. Youssef, C.-X. Wang, and M. Patzold, "A study on the second order statistics of Nakagami-Hoyt mobile Fading channels," *IEEE Transactions on Vehicular Technology*, vol. 54, no. 4, pp. 1259−1265, Jul. 2005.

[90] M. Nakagami, "The m-distribution−A general formula of intensity distribution of rapid fading," in *Statistical Methods in Radio Wave Propagation*, W. C. Hoffmann, Ed. Elmsford, NY, USA: Pergamon, 1960.

[91] T. Aulin, "Characteristics of a digital mobile radio channel," *IEEE Transactions on Vehicular Technology,* vol. 30 no.2, pp. 45−53, May 1981.

[92] P. K. Banerjee, R. S. Dabas, and B. M. Reddy, "C-band and L-band transionospheric scintillation experiment—some results for applications to satellite radio systems," *Radio Sci.*, vol. 27, pp. 955−969, June 1992.

[93] A. Lakhzouri, E. S. Lohan, J. Saastamoinen, and M. Renfors, "On second order statistics of the satellite-to-indoor channel based on field measurements," in *Proc. IEEE 16th International Symposium on Personal Indoor and Mobile Radio Communications (PIMRC)*, Sep. 2005, vol. 4, pp. 2632−2636.

[94] A. Lakhzouri, E. S. Lohan, I. Saastamoinen, and M. Renfors, "Interference and indoor channel propagation modeling based on GPS satellite signal measurements," in *Proc. of ION GPS*, pp. 1−6.

[95] H. Hashemi, M. M. Guire, T. Vlasschaert, and D. Tholl, "Measurements and modeling of temporal variations of the indoor radio propagation channel," *IEEE Transactions on Vehicular Technology,* vol. 43. no. 3, pp. 733−737, Aug. 1994.

[96] H. Bertoni, "Coverage prediction for mobile radio systems operating in the 800/900 MHz frequency range received signal fading distributions," *IEEE Transactions on Vehicular Technology,* vol. 37, no. 1, pp. 57−60, Feb. 1988.

[97] C.-C. Chong and S. K. Yong, "A generic statistical-based UWB channel model for high-rise apartments," *IEEE Transactions on Antennas Propagation,* vol. 53, no. 8, pp. 2389−2399, Aug. 2005.

[98] Q. Wu, D. W. Matolak, and I. Sen, "5-GHz-band vehicle-to-vehicle channels: Models for multiple values of channel bandwidth," *IEEE Transactions on Vehicular Technology*, vol. 59, no. 5, pp. 2620−2625, Jun. 2010.

[99] N. C. Sagias, and G. K. Karagiannidis, "Gaussian class multivariate Weibull distributions: Theory and applications in fading channels," *IEEE Transactions on Information Theory*, vol. 51, no. 10, 3608−3619, Oct. 2005.

[100] M. D. Yacoub "The $\alpha-\mu$ distribution: A physical fading model for the Stacy distribution," *IEEE Transactions on Vehicular Technology*, vol. 56, no. 1, pp. 27−34, Jan. 2007.

[101] Y.Jeong, H. Shin, and M. Z. Win, "H-Transforms for wireless communication," *IEEE Transactions on Information Theory*, vol. 61, no. 7, pp. 3773−3809, Jul. 2015.

[102] U. S. Dias and M. D. Yacoub, "On the $\alpha-\mu$ auto correlation and power spectrum functions: Field trials and validation," in *Proc. IEEE Global Telecommunications Conference (GLOBECOM),* Nov. 30-Dec.4, 2009, pp. 1−6.

[103] A. M. Magableh and M. M. Matalgah, "Moment generating function of the generalized $\alpha-\mu$ distribution with applications," *IEEE Communications Letter,* vol. 13, no. 6, pp. 411−413, June 2009.

[104] A. P. Prudnikov, Y. A. Brychkov, and O. I. Marichev, *Integrals and Series, vol. 3: More Special Functions*, Oxford University Press US, 1986.

[105] S. Stein, "Fading channel issues in system engineering," *IEEE Journal on Selected Areas in Communications,* vol. 5, no. 2, pp. 68−69, Feb. 1987.

[106] S. L. Cotton, and W. G. Scanlon, "High-order statistics for distribution," *IEEE Electronics Letter,* vol. 43, no. 22, pp. 1215−1217, Oct. 2007.

[107] N. Y. Ermolova, "Moment generating functions of the generalized $\eta-\mu$ and $\kappa-\mu$ distributions and their applications to performance evaluations of communication systems," *IEEE Communications Letter*, vol. 12, no. 7, pp. 502−504, Jul. 2008.

[108] D. B. da Costa and M. D. Yacoub, "The $\eta-\mu$ joint phase-envelope distribution," *IEEE Antenna and Wireless Propagation Letter*, vol. 6, 195−198, 2007.

[109] J. C. S. S. Filho and M. D. Yacoub, "Highly accurate $\eta-\mu$ approximation to sum of M independent non-identical Hoyt variates," *IEEE Antenna and Wireless Propagation Letter*, vol. 4, pp. 436−438, Apr. 2005.

[110] N. D. Chatzidiamantis, H. G. Sandalidis, G.K. Karagiannidis, and S. A. Kotsopoulos, "On the Inverse-Gaussian shadowing," in *Proc. IEEE International Conference on Communications and Information Technology (ICCIT)*, Mar. 2011, pp. 142−146.

[111] P. C. Sofotasios, S. Freear, "The $\eta-\mu$/gamma composite fading model," in *Proc. IEEE International Conference in Wireless Information Technology and Systems (ICWITS)*, Aug/Sep. 2010. pp. 1−4.

[112] P. C. Sofotasios, S. Freear, "The $\alpha-\kappa-\mu$/gamma composite distribution: A generalized non-Linear multipath/Shadowing fading model," in *Proc. IEEE India International Conference (INDICON),* Dec. 2011, pp. 1−6.

[113] M. K. Fikadu, P. C. Sofotasios, M. Valkama, Q. Cui, and G. K. Karagiannidis. "Exact error analysis and energy-efficiency optimization of regenerative relay systems under spatial correlation," *IEEE Transactions on Vehicular Technology*, 2015, doi: 10.1109/TVT.2015.2464211.

[114] M. K. Fikadu, P. C. Sofotasios, M. Valkama, Q. Cui, and G. K. Karagiannidis, "Energy-efficiency analysis of regenerative cooperative systems under spatial correlation," in *Proc. IEEE 26th International Symposium on Personal Indoor and Mobile Radio Communications (PIMRC)*, Aug. 30−Sep. 2, 2015, pp. 217−222.

[115] M. K. Fikadu, P. C. Sofotasios, M. Valkama, Q. Cui, S. Muhaidat, and G. K. Karagiannidis, "Outage probability analysis of full-duplex regenerative relaying over generalized asymmetric fading channels," in *Proc. IEEE Global Communications (GLOBECOM)*, Dec. 2015.

[116] M. K. Fikadu, P. C. Sofotasios, M. Valkama, Q. Cui, S. Muhaidat, and G. K. Karagiannidis, "Outage probability analysis of dual-hop full-duplex decode-and-forward relaying over generalized multipath fading conditions," in *Proc. IEEE 11th International Conference on Wireless and Mobile Computing, Networking and Communications (WiMob)*, Oct. 2015, pp. 414−421.

[117] M. K. Fikadu, P. C. Sofotasios, M. Valkama, Q. Cui, S. Muhaidat, and G. K. Karagiannidis, "Analytic symbol error rate evaluation of $M-$PSK based regenerative cooperative networks over generalized fading channels," in *Proc. IEEE*

11th International Conference on Wireless and Mobile Computing, Networking and Communications (WiMob), Oct. 2015, 704−711.

[118] M. K. Fikadu, P. C. Sofotasios, M. Valkama, and Q. Cui, "Analytic performance evaluation of $M-$QAM based decode-and-forward relay networks over enriched multipath fading channels," in *Proc. IEEE 10th International Conference on Wireless and Mobile Computing, Networking and Communications (WiMob)*, Oct. 2014, pp. 194−199.

[119] M. K. Fikadu and M. Valkama, "Error probability and power allocation analysis of cooperative relay networks over Nakagami$-q$ (Hoyt) fading channels," in *Proc. IEEE 78th International Vehicular Technology Conference (VTC) Fall*, Sept. 2013, pp. 1−7.

[120] M. K. Fikadu, M. Elmusrati, and R. Virrankoski, "Power allocation in multinode cooperative networks in Rician fading channels," in *Proc. IEEE 8th International Conference on Wireless and Mobile Computing, Networking and Communications (WiMob)*, Oct. 2012, pp. 496−501.

[121] M. K. Fikadu, P. C. Sofotasios, M. Valkama, Q. Cui, S. Muhaidat, and G. K. Karagiannidis, "Error rate and power allocation analysis of regenerative networks over generalized fading channels," *IEEE Transactions on Communications*, pp. 1751−1768, Apr. 2016.

[122] M. K. Fikadu, P. C. Sofotasios, S. Muhaidat, Q. Cui, G. K. Karagiannidis, and M. Valkama, "Full-duplex regenerative relaying and energy optimization over generalized asymmetric fading channels," *IEEE Transactions on Wireless Communications*. Manuscript submitted for publication, 2016.

[123] J.Abate and W. Whitt, "Numerical inversion of Laplace transforms of probability distributions," *ORSA Journal on Computing* , vol. 17, no. 1, pp. 36−43, 1995.

[124] Z. Wang and G. B. Giannakis, "A simple and general parameterization quantifying performance in fading channels," *IEEE Transactions on Communications*, vol. 51, no. 8, pp. 1389−1398, Aug. 2003.

[125] I.F. Akyildiz, W. Su, Y. Sankarasubramaniam, and E. Cayirci, "A survey on sensor networks," *IEEE Communications Magazine*, vol. 40, no. 8, pp. 102−114, Aug. 2002.

[126] G. U. Li, S. Xu, A. Swami, N. Himayat, and G. Fettweis, "Guest-editorial energy-efficient wireless communications," *IEEE Journal on Selected Areas in Communications*, vol. 29, no. 8, pp. 1505−1507, Sep. 2011.

[127] Feng, C. Jiang, G. Lim, L. J. Cimini, G. Feng, and G.Y. Li, "A survey of energy-efficient wireless communications," *IEEE Communications Surveys and Tutorials*, vol. 15, no. 1, pp. 167−178, 1st Quart. 2013.

[128] T. Ma, M. Hempel, D. Peng, and H. Sharif, "A survey of energy-efficient compression and communication techniques for multimedia in resource constrained systems," *IEEE Communications Surveys and Tutorials*, vol. 15, no. 3, pp. 963−972, 3rd Quart., 2013.

[129] P. C. Sofotasios, T. A. Tsiftsis, Yu. A. Brychkov, S. Freear, M. Valkama, and G. K. Karagiannidis, "Analytic expressions and bounds for special functions and applications in communication theory," *IEEE Transactions on Information Theory*, vol. 60, no. 12, pp. 7798−7823, Dec. 2014.

[130] G. K. Karagiannidis, "On the symbol error probability of general order rectangular QAM in Nakagami−m fading," *IEEE Communications Letter*, vol. 10, no. 11, pp. 745−747, Oct. 2006.

[131] K. Ho-Van and P. C. Sofotasios, "Outage behavior of cooperative underlay cognitive networks with inaccurate channel estimation," in *Proc. 5th International Conference on Ubiquitous and Future Networks (ICUFN)*, Jul. 2013, pp. 501−505.

[132] K. Ho-Van and P. C. Sofotasios, "Bit error rate of underlay multi-hop cognitive networks in the presence of multipath fading," in *Proc. 5th International Conference on Ubiquitous and Future Networks (ICUFN)*, Jul. 2013, pp. 620−624.

[133] D. A. Zogas, G. K. Karagiannidis, and S. A. Kotsopoulos, "Equal gain combining over Nakagami−n (Rice) and Nakagami−q (Hoyt) generalized fading channels," *IEEE Transactions on Wireless Communications*, vol. 4, no. 2, pp. 374−379, Apr. 2005.

[134] K. Ho-Van and P. C. Sofotasios, "Exact BER analysis of underlay decode-and-forward multi-hop cognitive networks with estimation errors," *IET Communications*, vol. 7, no. 18, pp. 2122−2132, Dec. 2013.

[135] K. Ho-Van, P. C. Sofotasios, and S. Freear, "Underlay cooperative cognitive networks, with imperfect Nakagami−m fading channel information and strict

transmit power constraint," *Journal of of Communications and Networks*, vol. 16. no. 1, pp. 10−17, Feb. 2014.

[136] D. S. Michalopoulos and G. K. Karagiannidis, "Distributed switch and stay combining (DSSC) with a single decode and forward relay," *IEEE Communications Letter*, vol. 11, no. 5, pp. 408−410, Nov. 2007.

[137] D. S Michalopoulos, G. K Karagiannidis, T. A. Tsiftsis, and R. K. Mallik, "An optimized user selection method for cooperative diversity systems," ìn *Proc. IEEE Global Communications (GLOBECOM)*, Nov. 27-Dec. 1 2006, pp. 1−6.

[138] D. S. Michalopoulos, A. S. Lioumpas, G. K. Karagiannidis, and R. Schober, "Selective cooperative relaying over time-varying channels," *IEEE Transactions on Communications*, vol. 58, no. 8, pp. 2402−2412, Aug. 2008.

[139] P. Li, S. Guo, and J. Hu, "Energy-efficient cooperative communications for multimedia applications in multi-channel wireless networks," *IEEE Transactions on Computer*, vol. 64, no. 6, pp. 1670−1679, June 2015.

[140] Nokia Siemens Networks, *The Advanced LTE Toolbox for More Efficient Delivery of Better User Experience,* technical white paper, 2011.

[141] S. Cui, A. Goldsmith, and A. Bahai, "Energy-constrained modulation optimization for coded systems," in *Proc IEEE Global Communications (GLOBECOM)* Dec. 2003, pp. 372−376.

[142] R. Devarajan, S. C. Jha, U. Phuyal, and V. K. Bhargava, "Energy-aware user selection and power allocation for cooperative communication system with guaranteed quality-of-service," in *Proc. 12th Canadian Workshop on Information Theory (CWIT)*, May 2011, pp. 216−220.

[143] Z. Zhou, S. Zhou, J.-H. Cui, and S. Cui, "Energy-efficient cooperative communication based on power control and selective single-relay in wireless sensor networks," *IEEE Transactions on Wireless Communications*, vol. 7, no. 8, pp. 3066−3078, Aug. 2008.

[144] C. Schurgers, O. Aberthorne, and M. B. Srivastava, "Modulation scaling for energy aware communication systems," in *Proc. IEEE International Symposium on Low Power Electronics and Design*, Aug. 2001, pp. 96−99.

[145] S. Cui, A. Goldsmith and A. Bahai, "Modulation optimization under energy constraints," in *Proc. IEEE International Conference on Communications (ICC)*, May 2003, vol. 4, pp. 2805−2811.

[146] J. Wu, G.Wang, and Y. R. Zheng,"Energy efficiency and spectral efficiency trade-off in type-I ARQ systems," *IEEE Journal on Selected Areas in Communication,* vol. 32, no. 2, 356−366, Frb. 2014

[147] Q. Chen and M.C. Gursoy, "Energy efficiency analysis in amplify-and-forward and decode-and-forward cooperative networks," in *Proc. IEEE Wireless Communications and Networking Conference(WCNC)*, Apr. 2010, pp. 1−6.

[148] S Cui, A. Goldsmith, and A. Bahai, "Joint modulation and multiple access optimization under energy constraints, " in *Proc. IEEE Global Telecommunications Conference (GLOBECOM)*, Nov. 2004, pp. 151−155.

[149] S. Cui, A. J. Goldsmith, and A. Bahai, "Energy-efficiency of MIMO and cooperative MIMO techniques in sensor networks," *IEEE Journal on Selected Areas in Communications*, vol. 22, no. 6, pp. 1089−1098, Aug. 2004.

[150] C-C. Kao, J. Wu, and S-C. Chen, "Energy efficient clustering communication protocol for wireless sensor network," in *Proc. IEEE 12th International Conference on Advanced Communication Technology (ICACT)*, Feb. 2010, pp. 830−833.

[151] M.T. Kakitani, G. Brante, S.R. Demo, and A. Munaretto, "Comparing the energy efficiency of single-hop, multi-hop and incremental decode-and-forward in multi-relay wireless sensor networks," in *Proc. IEEE 22nd International Symposium on Personal Indoor and Mobile Radio Communications (PIMRC)*, Sep. 2011, pp. 970−974.

[152] M.T. Kakitani, S.R. Demo, and M.A. Imran, "Energy efficiency contours for amplify-and-forward and decode-and-forward cooperative protocols," in *Proc. IEEE 8th International Symposium on Communication Systems, Networks and Digital Signal Processing (CSNDSD)* Jul. 2012, pp. 1−5.

[153] Z. Sheng, B. J. Ko, and K. K. Leung, "Power efficient decode-and-forward cooperative relaying," *IEEE Wirelless Communications Letter*, vol. 1, no. 5, pp. 444−447, Oct. 2012.

[154] G. Lim and L.J. Cimini, "Energy-efficient cooperative beamforming in clustered wireless networks," *IEEE Transactions on Wireless Communications*, vol. 12, no. 3, pp. 1376−1385, Mar. 2013.

[155] Y. Zhou, H. Liu, Z. Pan, L. Tian, J. Shi, and G. Yang, "Two-stage cooperative multicast transmission with optimized power consumption and guaranteed cov-

erage," *IEEE Journal on Selected Areas in Communications*, vol. 32, no. 2, pp. 274−284, Feb. 2014.

[156] Y. Xu1, Z. Bai, B.Wang, P. Gong, and K. Kwak, "Energy-efficient power allocation scheme for multi-relay cooperative communications," in *Proc. IEEE 16th International Conference on Advanced Communication Technology (ICACT)*, Feb. 2014, pp. 260−264.

[157] W. Ji and B. Zheng, "Energy efficiency based cooperative communication in wireless sensor networks," in *Proc. IEEE 12th International Conference on Communication Technology (ICCT)* , Nov. 2010, pp. 938−941.

[158] W. Fang, F. Liu, F. Yang, L. Shu, and S. Nishio, "Energy-efficient cooperative communication for data transmission in wireless sensor networks," *IEEE Transactions on Consumer Electronics*, vol. 56, no. 4, pp. 2185−2192, Nov. 2010.

[159] E. Kurniawan, S. Rinit, and A. Goldsmith, "Energy efficient cooperation for two-hop relay networks," in *Proc. IEEE Asia-Pacific Signal and Information Processing Association Annual Summit and Conference (APSIPAASC)*, Dec. 2012, pp. 1−10.

[160] G. Brante, M. T. Kakitani, and R. D. Souza, "Energy efficiency analysis of some cooperative and non-cooperative transmission schemes in wireless sensor networks", *IEEE Transaction Communication,* vol. 59, no. 10, pp. 2671−2677, Oct. 2011.

[161] T.-D. Nguyen, O. Berder, and O. Sentieys, "Energy-efficient cooperative techniques for infrastructure-to-vehicle communications," *IEEE Transactions on Intelligent Transportation Systems*, vol. 12, no. 3, pp. 659−668, Sep. 2011.

[162] D. B. da Costa and S. Aissa, "Capacity analysis of cooperative systems with relay selection in Nakagami−m fading," *IEEE Communication Letter*, vol. 13, no. 9, pp. 637−639, Sep. 2009.

[163] T. Q. Duong, V. N.Q. Bao, and H. J. Zepernick, "On the performance of selection decode-and-forward relay networks over Nakagami−m fading channels," *IEEE Communication Letter*, vol. 13, no. 3, pp. 172−174, Mar. 2009.

[164] T. Q. Duong, G. C. Alexandropoulos, T. A. Tsiftsis, and H. Zepernick, "Outage probability of MIMO AF relay networks over Nakagami−m fading channels," *Electronics Letter,* vol. 46, no. 17, pp. 1229−1231, Aug. 2010.

[165] Q. Shi and Y. Karasawa, "Error probability of opportunistic decode-and-forward relaying in Nakagami−m fading channels with arbitrary m," *IEEE Wireless Communication Letter*, vol. 2, no. 1, pp. 86−89, Feb. 2013.

[166] S. S. Ikki and M. H. Ahmed, "Multi-branch decode-and-forward cooperative diversity networks performance analysis over Nakagami−m fading channels," *IET Communication*, vol. 5, no. 6, pp. 872−878, June 2011.

[167] Y. Lee, M. H. Tsai, and S. I. Sou, "Performance of decode-and-forward cooperative communications with multiple dual-hop Relays over Nakagami−m fading channels," *IEEE Transactions on Wireless Communications*, vol. 8, no. 6, pp. 2853−2859, June 2009.

[168] Y. Lee and M-H. Tsai, "Performance of decode-and-forward cooperative communications over Nakagami−m fading channels," *IEEE Transactions on Vehicular Technology*, vol. 58, no. 3, pp. 1218−1228, Mar. 2009.

[169] R. Swaminathan, R. Roy, and M.D.Selvaraj, "Performance analysis of triple correlated selection combining for cooperative diversity systems," in *Proc. IEEE international Conference on Communications (ICC)*, June 2013, pp. 5483−5488.

[170] K. Yang, J. Yang, J. Wu, C. Xing, and Y. Zhou, "Performance analysis of DF cooperative diversity system with OSTBC over spatially correlated Nakagami−m fading channels, *IEEE Transactions on Vehicular Technology*, vol. 63, no. 3, pp. 1270−1281, Mar. 2014.

[171] R. H. Y. Louie, Y. Li, H. A. Suraweera, and B. Vucetic, "Performance analysis of beamforming in two hop AF relay networks with antenna correlation," *IEEE Transactions on Wireless Communications*, vol. 8, no.6, pp. 3132−3141, June 2009.

[172] D. Liqin, W. Yang, Z. Jiliang, L. Limei, Li Xi, and Y. Dayong, "Investigation of spatial correlation for two-user cooperative communication in indoor office environment," in *Proc. IEEE 12th International Conference on Communication Technology (ICCT)*, Nov. 2010, pp. 420−423.

[173] T. Q. Duong, H. A. Suraweera, T. A. Tsiftsis, H. J. Zepernick, and A. Nallanathan, "OSTBC transmission in MIMO AF relay systems with keyhole and spatial correlation effects," in *Proc. IEEE International Conference on Communications (ICC)*, June 2011, pp. 1−6.

[174] Y. A. Chau, and K. Y-Ta. Huang, "Performance of cooperative diversity on correlated dual-hop channels with an amplify-and-forward relay over Rayleigh fading environments," in *Proc. IEEE TENCON*, Nov. 2011, pp. 563−567.

[175] H. Katiyar and R. Bhattacharjee, "Performance of two-hop regenerative relay network under correlated Nakagami−m fading at multi-antenna relay," *IEEE Communications Letter*, vol. 13, no. 11, pp. 820− 822, Nov. 2009.

[176] K. Yang, J. Yang, J. Wu, and C. Xing, "Performance analysis of cooperative DF relaying over correlated Nakagami−m fading channels," in *Proc. IEEE International Conference on Communications (ICC)*, June 2013, pp. 4973−4977.

[177] Y. Chen, R. Shi, and M. Long, "Performance analysis of amplify-and forward relaying with correlated links," *IEEE Transactions on Vehicular Technology*, vol. 62, no. 5, pp. 2344 − 2349, June 2013.

[178] T. Q. Duong, G. C. Alexandropoulos, H. Zepernick, and T. A. Tsiftsis, "Orthogonal space-time block codes with CSI-assisted amplify-and-forward relaying in correlated Nakagami−m fading channels," *IEEE Transactions on Vehicular Technology*, vol. 60, no. 3, pp. 882−889, Mar. 2011.

[179] H. A. Suraweera, D. S. Michalopoulos, and G. K. Karagiannidis, "Performance of distributed diversity systems with a single amplify-and-forward relay," *IEEE Transactions on Vehicular Technology*, vol. 58, pp. 2603-2608, June 2009.

[180] "Selection procedures for the choice of radio transmission technologies of the UMTS," *3GPP TR 30.03U,* ver. 3.2.0, 1998.

[181] A. Mezghani and J. A. Nossek, "Modeling and minimization of transceiver power consumption in wireless networks," in *Proc. IEEE International ITG Workshop on Smart Antennas (WSA)*, Feb. 2011. pp. 1−8.

[182] S. Cui, A. J. Goldsmith, and A. Bahai, "Energy-constrained modulation optimization," *IEEE Transactions on Wireless Communications*, vol. 4, no. 5, pp. 2349−2360, Sep. 2005.

[183] S. Boyd and L. Vandenberghe, *Convex Optimization*, Cambridge University Press, 1994.

[184] O. Amin, and L. Lampe, "Opportunistic energy efficient cooperative communication," *IEEE Wireless Communications Letter*, vol. 1, no. 5, pp. 412−415, Oct.2012.

[185] J. N. Laneman and G. W. Wornell, "Distributed space-time coded protocols for exploiting cooperative diversity in wireless networks," *IEEE Transactions on Information Theory*, vol. 49, no. 10, pp. 2415−2425, Nov. 2003.

[186] J. Boyer, D. D. Falconer, and H. Yanikomeroglu, "Multihop diversity in wireless relaying channels," *IEEE Transactions on Communications*, vol. 52, no. 10, pp. 1820−1830, Oct. 2004.

[187] Z. Zhao, M. Peng, Z. Ding, W. Wang, and H. H. Chen, "Decode-and-Forward Network Coding for Two-Way Relay MIMO Systems," *IEEE Transactions on Vehicular Technology*, vol. 63, no. 2, pp. 775−788, Feb. 2014.

[188] Y. Zou, B. Zheng, and J Zhu, "Outage analysis of opportunistic cooperation over Rayleigh fading channels," *IEEE Transactions on Wireless Communications*, vol. 8, no. 6, pp. 3077−3085, June 2009.

[189] M. Di Renzo, F. Graziosi, and F. Santucci, "A unified framework for performance analysis of CSI-assisted cooperative communications over fading channels," *IEEE Transactions on Communications*, vol. 57, no. 9, pp. 2551−2557, Sep. 2009.

[190] Y. Zou, B. Zheng, and W. P. Zhu, "An opportunistic cooperation scheme and its BER analysis," *IEEE Transactions on Wireless Communications*, vol. 8, no. 9, pp. 4492−4497, Sep. 2009.

[191] S.-Q. Huang, H.-H. Chen, and M.-Y. Lee, "Performance bounds of multi-relay decode-and-forward cooperative networks over Nakagami−m fading channels," in *Proc. IEEE International Conference on Communications (ICC)*, June 2011, pp. 1−5.

[192] S. N. Datta, S. Chakrabarti, and R. Roy, "Comprehensive error analysis of multi-antenna decode-and-forward relay in fading channels," *IEEE Communications Letter*, vol. 16, no. 1, pp. 47−49, Jan. 2012.

[193] S. N. Datta and S. Chakrabarti, "Unified error analysis of dual-hop relay link in Nakagami−m fading channels," *IEEE Communications Letter*, vol. 14, no. 10, pp. 897−899, Oct. 2010.

[194] S.S. Ikki and M.H. Ahmed, "Performance analysis of adaptive decode-and-forward cooperative diversity networks with best-relay selection," *IEEE Transactions on Communications*, vol. 58, no. 1, pp. 68−72, Jan. 2010.

[195] K. J. Kim, T. Q. Duong, H. V. Poor, and M. H. Lee, "Performance analysis of adaptive decode-and-forward cooperative single-carrier systems," *IEEE Transactions on Vehicular Technology*, vol. 61, no. 7, pp. 3332−3337, Jul. 2012.

[196] Y.-R. Tsai and L.-C. Lin, "Optimal power allocation for decode-and forward cooperative diversity under an outage performance constraint," *IEEE Communications Letter*, vol. 14, no. 10, pp. 945−947, Oct. 2010.

[197] A. K. Sadek, W. Su, and K.J. Ray Liu, "Multi-node cooperative communications in wireless networks," *IEEE Transactions on Signal Processing*, vol. 55, no. 1, pp. 341−355, Jan. 2007.

[198] P. Kumar and P. R. Sahu, "Analysis of M−PSK with MRC receiver over $\kappa-\mu$ fading channels with outdated CSI," *IEEE Wireless Communications Letter*, vol. 3, no. 6, pp. 557−560, Dec. 2014.

[199] V. Asghari, D. B. da Costa, and S. Aissa, "Symbol error probability of rectangular QAM in MRC systems with correlated $\eta - \mu$ fading channels," *IEEE Transactions on Vehicular Technology*, vol. 59, no. 3, pp. 1497−1503, Mar. 2010.

[200] K. Peppas, F. Lazarakis, A. Alexandridis, and K. Dangakis, "Error performance of digital modulation schemes with MRC diversity reception over $\eta-\mu$ fading channels," *IEEE Transactions on Wireless Communications*, vol. 8, no. 10, pp. 4974−4980, Oct. 2009.

[201] H. Yu, G. Wei, F. Ji, and X. Zhang, "On the error probability of cross−QAM with MRC reception over generalized $\eta-\mu$ fading channels," *IEEE Transactions on Vehicular Technology*, vol. 60, no. 6, pp. 2631−2643 Jul. 2011.

[202] D. M. Jimenez and J.F. Paris, "Outage probability analysis for $\eta-\mu$ fading channels," *IEEE Communications Letter*, vol. 14, no. 6, pp. 521−523, June 2010.

[203] W.-G. Li, H.-M. Chen, and M. Chen, "Outage probability of dual-hop decode-and-forward relaying systems over generalized fading channels," *European Transactions on Telecommunications*, vol. 21, no. 1, pp. 86−89, Jan. 2010.

[204] S.S. Ikki, and M.H. Ahmed, "Performance analysis of decode-and-forward cooperative diversity using differential EGC over Nakagami−m fading channels," in *Proc. IEEE 69th Vehicular Technology Conference (VTC)Spring*, April 2009, pp. 1−6.

[205] G. P. Efthymoglou, T. Piboongungon, and V. A. Aalo, "Error rates of $M-$ary signals with multichannel reception in Nakagami$-m$ fading channels," *IEEE Communications Letter*, vol. 10, no. 2, pp. 100−102, Feb. 2006.

[206] J. F. Paris, "Statistical characterization of $\kappa-\mu$ shadowed fading," *IEEE Transactions on Vehicular. Technology.*, vol. 63, no. 2, pp. 518−526, Feb. 2014.

[207] P. Sofotasios, "On special functions and composite statistical distributions and their applications in digital communications over fading channels," *PhD Thesis*, University of Leeds, Jul. 2010.

[208] Z. Mo, W. Su, S. Batalama,and J. D. Matyjas, "Cooperative communication protocol designs based on optimum power and time allocation," *IEEE Transactions on Wireless Communications*, vol. 13, no. 8, pp. 4283−4296, Aug. 2014.

[209] M. R. Bhatnagar, "Decode-and-forward-based differential modulation for cooperative communication system with unitary and non unitary constellations," *IEEE Transactions on Vehicular. Technology*, vol. 61, no. 1, pp. 152−165, Jan. 2012.

[210] T. Riihonen, S. Werner, and R. Wichman, "Comparison of full-duplex and half-duplex modes with a fixed amplify-and-forward relay," in *Proc. IEEE Wireless Communications and Networking Conference (WCNC)*, Apr. 2009, pp. 1−5.

[211] L. J. Rodríguez, N. H. Tran, and T. Le-Ngoc, "Performance of full-duplex AF relaying in the presence of residual self-interference," *IEEE Journal on Selected Areas in Communications,* vol. 32, no. 9, pp. 1752−1764, Sep. 2014.

[212] T. Kwon, S. Lim, S. Choi, and D. Hong, "Optimal duplex mode for DF relay in terms of the outage probability," *IEEE Transactions on Vehicular. Technology*, vol. 59, no. 7, pp. 3628 − 3634, Sep. 2010.

[213] T. Baranwal, D. S. Michalopoulos, and R. Schober, "Outage analysis of multihop full duplex relaying," *IEEE Communications Letter*, vol. 17, no. 1, pp. 63−66, Jan. 2013.

[214] B. P. Day, A. R. Margetts, D. W. Bliss, and P. Schniter, "Full-duplex MIMO relaying: Achievable rates under limited dynamic range," *IEEE Journal on Selected Areas in Communications*, vol. 30, no. 8, pp. 1541−1553, Sep. 2012.

[215] A. Altieri, L. R. Vega, P. Piantanida, and C. G. Galarza, "On the outage probability of the full-duplex interference-limited relay channel," *IEEE Journal on Selected Areas in Communications,* vol. 32, no. 9, pp. 1765−1777, Sep. 2014.

[216] H. A. Suraweera, I. Krikidis, G. Zheng, C. Yuen, and P. J. Smith, "Low-complexity end-to-end performance optimization in MIMO full-duplex relay systems," *IEEE Transactions on Wireless Communications*, vol. 13, no. 2, pp. 913−927, Feb. 2014.

[217] H. Alves, D.B. da Costa, R. D. Souza, and M. Latva-aho, "Performance of block-Markov full duplex relaying with self interference in Nakagami $-m$ fading," *IEEE Wireless Communications Letter*, vol. 2, no. 3, pp. 311−314, June 2013.

[218] T. Riihonen, S. Werner, and R. Wichman, "Hybrid full-duplex/half-duplex relaying with transmit power adaptation," *IEEE Transactions on Wireless Communications,* vol. 10, no. 9, pp. 3074−3085, Sep.2011.

[219] M. Khafagy, A. Ismail, M.-S. Alouini, and S. Aissa, "On the outage performance of full-duplex selective decode-and-forward relaying," *IEEE Communications Letter,* vol. 17, no. 6, pp. 1180−1183, June 2013.

[220] X. Huang, J. He, Q. Li, Q. Zhang, and J. Qin, "Optimal power allocation for multicarrier secure communications in full-duplex decode-and-forward relay networks," *IEEE Communications Letter,* vol. 18, no. 12, pp. 2169−2172, Dec. 2014.

[221] H. Alves, G. Brante, R. D. Souza, D.B. da Costa, and M. Latva-aho, "On the performance of secure full-duplex relaying under composite fading channels," *IEEE Signal Processing Letters*, vol. 22, no. 7, pp. 867−870, Jul. 2015.

[222] S. Sohaib, and D. K. C. So, "Asynchronous cooperative relaying for vehicle-to-vehicle communications, " *Transactions on Communications,* vol. 61, no. 5, pp. 1732−1738, May 2013.

[223] L. J. Rodriguez, N. H. Tran, and T. L. Ngoc, "Optimal power allocation and capacity of full-duplex AF relaying under residual self-interference," *IEEE Wireless Communications Letter,* vol. 3, no. 2, pp. 233−236, Apr. 2014.

[224] B. Yu, L. Yang, X. Cheng, and R. Cao, "Transmit power optimization for full duplex decode and forward relaying," in *Proc. IEEE Global Communications Conference (GLOBECOM),* Dec. 2013, pp. 3347−3352.

[225] M. Khafagy, A. Ismail, M-S. Alouini, and S. Aissa, "Energy-Efficient Cooperative Protocols for Full-Duplex Relay Channels," in *Proc. IEEE Global Commun. Workshop,* Dec. 2013, pp. 362−367.

[226] Y. Kim and H. Liu, "Infrastructure relay transmission with cooperative MIMO," *IEEE Transactions on Vehicular Technology*, vol. 57, pp. 2180−2188, Jul. 2008.

[227] H. A. Suraweera, G. K. Karagiannidis, and P. J. Smith, "Performance analysis of the dual-hop asymmetric fading channel," *IEEE Transactions on Wireless Communications,* vol. 8, no. 6, pp. 2783−2788, June 2009.

[228] W. Xu, J. Zhang and P. Zhang, "Performance analysis of dual-hop amplify-and-forward relay system in mixed Nakagami−m and Rician fading channels," *Electronics Letter*, vol. 46, no. 17, pp. 1231−1232, Aug. 2010.

[229] P. Jayasinghe, L. K. S. Jayasinghe, M. Juntti, and M. Latva-Aho, "Performance analysis of optimal beamforming in fixed-gain AF MIMO relaying over asymmetric fading channels," *IEEE Transactions on Communications,* vol. 62, no. 4, pp. 1201−1217, Apr. 2014.

[230] S. Majhi, Y. Nasser, J. F. Helard, and M. Helard, "Performance analysis of repetition-based decode-and-forward relaying over asymmetric fading channels," in *Proc. IEEE 21st International Symposium on Personal Indoor and Mobile Radio Communications (PIMRC)* Sep. 2010, pp. 362−367.

[231] K. P. Peppas, G. C. Alexandropoulos, and P. T. Mathiopoulos, "Performance analysis of dual-hop AF relaying systems over mixed $\eta-\mu$ and $\kappa-\mu$ fading channels," *IEEE Transactions on Vehicular Technology*, vol. 62, no. 7, pp. 3149−3163, Sep. 2013.

[232] T. P. Do and T. V. T. Le, "Power allocation and performance comparison of full duplex dual hop relaying protocols, "*IEEE Communications Letter*, vol. 19, no. 5, pp. 791−794, May 2015.

[233] A. Papoulis, S.U. Pillai, *Probability, Random Variables and Stochastic Processes,* -4$^{\text{th}}$ edn. McGraw-Hill, 2002.

[234] A. H. Nuttall, "Some Integrals Involving the Q_M Function," *IEEE Transactions on Information Theory*, vol. 21, no. 1, pp. 95−96, 1975.

Tampereen teknillinen yliopisto
PL 527
33101 Tampere

Tampere University of Technology
P.O.B. 527
FI-33101 Tampere, Finland

ISBN 978-952-15-3767-7
ISSN 1459-2045